frontiers | Research Topics

Advances in brain tumor therapy

Edited by
Tanmay Abhay Kulkarni, Ramcharan Singh Angom
and Joubert Banjop Kharlyngdoh

Published in
Frontiers in Oncology
Frontiers in Neurology

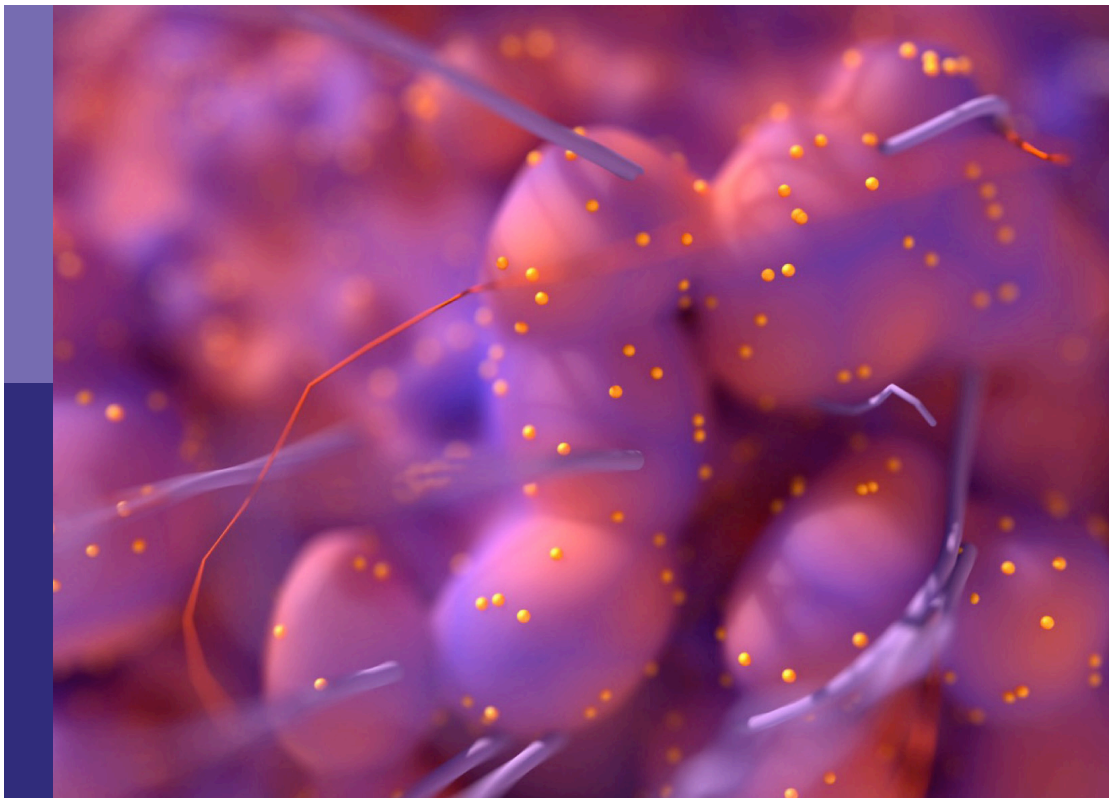

ISSN 1664-8714
ISBN 978-2-8325-6603-9
DOI 10.3389/978-2-8325-6603-9

Generative AI statement
Any alternative text (Alt text) provided alongside figures in the articles in this ebook has been generated by Frontiers with the support of artificial intelligence and reasonable efforts have been made to ensure accuracy, including review by the authors wherever possible. If you identify any issues, please contact us.

About Frontiers

Frontiers is more than just an open access publisher of scholarly articles: it is a pioneering approach to the world of academia, radically improving the way scholarly research is managed. The grand vision of Frontiers is a world where all people have an equal opportunity to seek, share and generate knowledge. Frontiers provides immediate and permanent online open access to all its publications, but this alone is not enough to realize our grand goals.

Frontiers journal series

The Frontiers journal series is a multi-tier and interdisciplinary set of open-access, online journals, promising a paradigm shift from the current review, selection and dissemination processes in academic publishing. All Frontiers journals are driven by researchers for researchers; therefore, they constitute a service to the scholarly community. At the same time, the *Frontiers journal series* operates on a revolutionary invention, the tiered publishing system, initially addressing specific communities of scholars, and gradually climbing up to broader public understanding, thus serving the interests of the lay society, too.

Dedication to quality

Each Frontiers article is a landmark of the highest quality, thanks to genuinely collaborative interactions between authors and review editors, who include some of the world's best academicians. Research must be certified by peers before entering a stream of knowledge that may eventually reach the public - and shape society; therefore, Frontiers only applies the most rigorous and unbiased reviews. Frontiers revolutionizes research publishing by freely delivering the most outstanding research, evaluated with no bias from both the academic and social point of view. By applying the most advanced information technologies, Frontiers is catapulting scholarly publishing into a new generation.

What are Frontiers Research Topics?

Frontiers Research Topics are very popular trademarks of the *Frontiers journals series*: they are collections of at least ten articles, all centered on a particular subject. With their unique mix of varied contributions from Original Research to Review Articles, Frontiers Research Topics unify the most influential researchers, the latest key findings and historical advances in a hot research area.

Find out more on how to host your own Frontiers Research Topic or contribute to one as an author by contacting the Frontiers editorial office: frontiersin.org/about/contact

Advances in brain tumor therapy

Topic editors

Tanmay Abhay Kulkarni — Cancer Center, Mayo Clinic, United States

Ramcharan Singh Angom — Mayo Clinic Florida, United States

Joubert Banjop Kharlyngdoh — Tulane University, United States

Citation

Kulkarni, T. A., Angom, R. S., Kharlyngdoh, J. B., eds. (2025). *Advances in brain tumor therapy*. Lausanne: Frontiers Media SA. doi: 10.3389/978-2-8325-6603-9

Table of contents

frontiers | Frontiers in Neurology

TYPE Original Research
PUBLISHED 29 April 2024
DOI 10.3389/fneur.2024.1375723

OPEN ACCESS

EDITED BY
Tanmay Abhay Kulkarni,
Mayo Clinic, United States

REVIEWED BY
Huihui Chen,
Central South University, China
Kaijian Hou,
Shantou University, China

*CORRESPONDENCE
Yuan Cheng
✉ chengyuan@hospital.cqmu.edu.cn

RECEIVED 24 January 2024
ACCEPTED 15 April 2024
PUBLISHED 29 April 2024

CITATION
Huang M, Liu Y, Peng J and Cheng Y (2024) Causal effects of immune cells in glioblastoma: a Bayesian Mendelian Randomization study.
Front. Neurol. 15:1375723.
doi: 10.3389/fneur.2024.1375723

Causal effects of immune cells in glioblastoma: a Bayesian Mendelian Randomization study

Mingsheng Huang[1], Yiheng Liu[2], Jie Peng[1] and Yuan Cheng[1]*

[1]Department of Neurosurgery, Second Affiliated Hospital, Chongqing Medical University, Chongqing, China, [2]Department of Cardiology, Second Affiliated Hospital, Chongqing Medical University, Chongqing, China

Background: Glioblastoma (GBM) is a highly malignant brain tumor, and immune cells play a crucial role in its initiation and progression. The immune system's cellular components, including various types of lymphocytes, macrophages, and dendritic cells, among others, engage in intricate interactions with GBM. However, the precise nature of these interactions remains to be conclusively determined.

Method: In this study, a comprehensive two-sample Mendelian Randomization (MR) analysis was conducted to elucidate the causal relationship between immune cell features and the incidence of GBM. Utilizing publicly available genetic data, we investigated the causal associations between 731 immune cell signatures and the risk of GBM. Subsequently, we conducted a reverse Mendelian randomization analysis to rule out reverse causation. Finally, it was concluded that there is a unidirectional causal relationship between three subtypes of immune cells and GBM. Comprehensive sensitivity analyses were employed to validate the results robustness, heterogeneity, and presence of horizontal pleiotropy. To enhance the accuracy of our results, we concurrently subjected them to Bayesian analysis.

Results: After conducting MR analyses, we identified 10 immune phenotypes that counteract glioblastoma, with the most protective being FSC-A on Natural Killer T cells (OR = 0.688, CI = 0.515–0.918, $P = 0.011$). Additionally, we found 11 immune cell subtypes that promote GBM incidence, including CD62L– HLA DR++ monocyte % monocyte (OR = 1.522, CI = 1.004–2.307, $P = 0.048$), CD4+CD8+ T cell % leukocyte (OR = 1.387, CI = 1.031–1.866, $P = 0.031$). Following the implementation of reverse MR analysis, where glioblastoma served as the exposure variable and the outcomes included 21 target immune cell subtypes, we discerned that only three cell subtypes (CD45 on CD33+ HLA DR+ CD14dim, CD33+ HLA DR+ Absolute Count, and IgD+ CD24+ B cell Absolute Count) exhibited a unidirectional causal association with glioblastoma.

Conclusion: Our study has genetically demonstrated the close relationship between immune cells and GBM, guiding future clinical research.

KEYWORDS

glioblastoma, immunity, causal inference, MR analysis, Bayesian analysis

Introduction

Glioma is the most prevalent form of primary malignant tumor of the central nervous system with an incidence of 5.6/100,000 per year in adults (1). The most aggressive subtype of glioma is glioblastoma (GBM), currently classified as grade 4 astrocytoma with a mutation in the isocitrate dehydrogenase gene (IDH) according to The World

Health Organization (WHO) (2). Surgical resection of the tumor followed by radiotherapy and chemotherapy with temozolomide is a common GBM treatment method. Despite comprehensive treatment advances, GBM remains one of the deadliest human cancers due to its high recurrence rate and therapy resistance. Highly invasive nature, high heterogeneity, and immune evasion are regarded as pivotal determinants linked to treatment failure and disease relapse in GBM (3, 4). Overall, the prognosis of GBM is extremely poor, with a 5-year survival rate of <5%. It causes a heavy burden on families and society (5). Recently, immunotherapy has provided a new method to cure this disease. This primarily encompasses immune checkpoint inhibitors, personalized vaccines, Chimeric Antigen Receptor T (CAR-T) cell therapy, immune cell therapy, and other methodologies (6, 7). However, GBM is a highly immunosuppressive tumor with several immune escape mechanisms present (8, 9). Although immunotherapy has provided a new approach for treating glioblastoma, the lack of large-scale clinical randomized controlled trials to validate its efficacy and safety is attributed to ethical considerations and other factors. Moreover, the intricate relationship among immune cells, immunosuppressive cells, inflammatory responses, and the occurrence, development, and recurrence of glioblastoma is highly complex, making it challenging to arrive at a definitive conclusion regarding their interplay (10, 11). Microglia, as the indigenous macrophages of the central nervous system, are collectively known as tumor-associated macrophages (TAMs), forming the primary barrier of innate immunity within the central nervous system (12). TAMs adjust their phenotypes in response to the stimuli encountered within their microenvironment. Traditionally, two TAM phenotypes have been delineated: M1 macrophages, characterized by pro-inflammatory and anti-tumor properties, and M2 macrophages, which exhibit anti-inflammatory and pro-tumor characteristics (13). TAMs are a major type of immune cells in the tumor microenvironment. However, there is controversy surrounding the role of TAMs in glioblastoma. Some studies suggest that TAMs may promote the growth, invasion, and metastasis of glioblastoma, while others indicate that TAMs may counteract tumor growth (14–16). Furthermore, T cells constitute the principal lymphocytic constituent of the glioblastoma tumor microenvironment (TME), exerting both pro-tumor and anti-tumor functions. Various subsets of T cells can be discerned, including Cluster of Differentiation 4+ T (CD4+ T) helper cells, CD8+ cytotoxic T cells, and regulatory T cells (17). However, the role of T cells is also controversial. Some studies suggest that T cells can recognize and attack tumor cells, thereby combating tumor growth, while others have found that T cells may be suppressed by the tumor cells' immune evasion mechanisms in gliomas (18–20). Natural killer cells, originating from the bone marrow, possess effector functions mediated by cytokine production and cytotoxic activity. Their efficacy is often modulated by immunosuppressive factors released by tumor cells (21). Traditionally, microglial cells have been regarded as the immune cells of the central nervous system and may potentially counteract tumor growth. However, recent studies have suggested that in certain circumstances, microglial cells may promote the growth and metastasis of gliomas rather than inhibit them. This finding has sparked further debate regarding the functional role of microglial cells in gliomas (22, 23). While the roles of some immune cells in GBM have been elucidated, the diverse subtypes of immune cells contribute to ongoing research and controversies in the field. Therefore, further research is required to elucidate the roles of different subtypes of immune cells in glioblastoma.

Mendelian randomization (MR), a causal inference method, has been extensively applied in genetic epidemiology (24). In contrast to traditional observational studies, MR, utilizing genetic variation as instrumental variables (IVs), stands as a widely acknowledged approach to alleviate potential confounding factors (25). This method effectively navigates around issues related to reverse causation and confounding factors, enabling a more precise inference of the causal relationship between exposure and outcome. The rationality of the causal sequence in MR is of utmost importance. Previous observational studies have identified numerous associations between immune cell features and glioblastoma, validating the hypothesis of their correlation (26–28). In this study, a comprehensive two-sample MR analysis was conducted to ascertain the causal relationship between different immune cell subtypes and GBM.

Materials and methods

Study design

We performed a two-sample Mendelian Randomization (MR) analysis to evaluate the causal relationship between 731 immune cell features (categorized into seven groups) and glioblastoma. MR employs genetic variations as proxies for risk factors, and thus, valid instrumental variables in causal inference must meet three essential assumptions: (1) genetic variations are directly associated with the exposure; (2) genetic variations are not correlated with potential confounders between the exposure and outcome, and (3) genetic variations do not influence the outcome through pathways other than the exposure (Figure 1). The research investigations included in our analysis received approval from the respective institutional review boards, and participants provided informed consent.

Data sources

The GWAS summary statistics for glioblastoma (finngen_R10_C3_GBM_EXALLC) were sourced from FinnGen Database R10, including 253 cases of brain glioblastoma and

Abbreviations: WHO, World Health Organization; IDH, isocitrate dehydrogenase gene; GBM, glioblastoma; WM, weighted median; SD, standard deviation; AC, absolute cell; RC, relative cell; OR, odds ratio; CI, confidence interval; GWAS, genome-wide association study; HLA, human leukocyte antigen; IVs, instrumental variables; IVW, inverse variance weighting; LD, linkage disequilibrium; MFI, median fluorescence intensities; MP, morphological parameters; CDCs, conventional dendritic cells; MR, Mendelian Randomization; MR-PRESSO, MR pleiotropy residual sum and outlier; SNPs, single nucleotide polymorphisms; MHC, major histocompatibility complex; MDSCs, myeloid-derived suppressor cells; TANs, tumor-associated neutrophils; TADCs, tumor-associated dendritic cells; TCR, T-cell receptor; CD4+ T, cluster of differentiation 4+ T; CAR-T, Chimeric antigen receptor T; TBNK, T cells, B cells, natural killer cells; TAMs, tumor-associated macrophages; TME, tumor microenvironment.

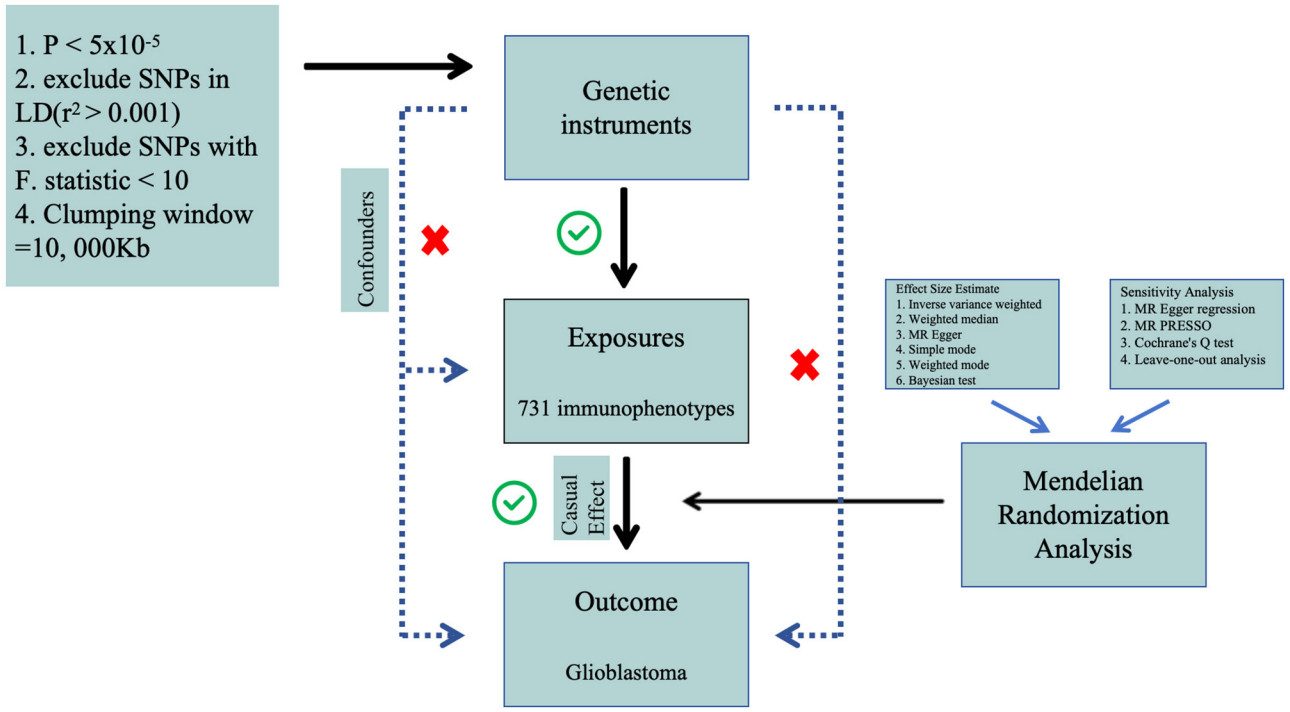

FIGURE 1
The flow diagram of Mendelian randomization analysis.

314,193 controls. The FinnGen project has amassed biological specimens and clinical data from more than 300,000 individuals in Finland. This dataset encompasses diverse data types, including genomic data, clinical diagnoses, biological sample sequencing, and medical records. Through the analysis of extensive genetic and clinical data, the project seeks to unveil associations between genes and various diseases, alongside the impact of environmental and lifestyle factors on these relationships. Its overarching goal is to elucidate the interplay between genes and health. As a publicly accessible resource, it can be accessed via the website (https://www.finngen.fi/en) (29).

GWAS summary statistics for each immune trait are publicly available from the GWAS Catalog (accession numbers within the range of GCST0001391 to GCST0002121) (30). The data contain 731 immunophenotypes, with categories such as absolute cell (AC) counts ($n = 118$), median fluorescence intensities (MFI) reflecting surface antigen levels ($n = 389$), morphological parameters [MP] ($n = 32$), and relative cell (RC) counts ($n = 192$). These features encapsulate various immune cell types, including B cells, conventional dendritic cells (CDCs), mature stages of T cells, monocytes, myeloid cells, TBNK (T cells, B cells, natural killer cells), and Treg panels. The initial GWAS analyses involved a cohort of 3,757 individuals of European descent, thereby ensuring a comprehensive and diverse representation of the datasets. Utilizing high-density arrays, genotyping was performed on an extensive set of around 22 million single nucleotide polymorphisms (SNPs). Subsequently, imputation was carried out employing the Sardinian sequence-based reference panel. Covariate adjustments, specifically accounting for sex, age, and age squared, were systematically incorporated into the association analyses (31). This rigorous methodology aimed to enhance the accuracy and reliability of the research findings while minimizing the risk of confounding factors.

Selection of instrumental variables (IVs)

In both forward MR studies (with immune cells as exposure and GBM as outcome) and reverse MR studies (with GBM as exposure and immune cells as outcome), we employed identical methodologies for experimentation. In the initial phase, single nucleotide polymorphisms associated with exposure were judiciously selected based on a genome-wide significance threshold ($P < 5 \times 10^{-5}$) in accordance with previous researches (30, 32). Subsequently, the independence of the chosen SNPs was assessed through pairwise linkage disequilibrium analysis, employing exclusion criteria for SNPs in linkage disequilibrium ($r^2 > 0.001$ and a clumping window <10,000 kb) (33). Thirdly, the F-statistic was computed to ascertain the robustness of each SNP, with the exclusion of SNPs possessing an F-statistic <10 (34). A rigorous data harmonization process was implemented to ensure concordance between SNP effects on exposure and outcome, aligning with the same allele. The F-statistic for each SNP was calculated using the formula $F = R^2/(1–R^2) \times (N – 2)$, where R^2 represents the variance of exposure explained by the instrumental variables (IVs), and N indicates sample size. The variance of exposure explained by the instrument variable was calculated with the formula $R^2 = \beta^2/(\beta^2 + se^2 \times N)$, in which β denotes the effect size for the genetic variant of interest, se represents the standard error for β, and N represents the sample size.

TABLE 1 Causal effects of immune cells on GBM by IVW.

Traits	Beta	OR	Low	Up	*P*-value
IgD+ CD24+ B cell absolute count	0.305	1.357	1.000	1.840	0.049
CD19 on IgD+ CD38dim B cell	0.127	1.136	1.015	1.270	0.025
CD19 on IgD+ CD24− B cell	0.116	1.122	1.003	1.256	0.043
CD20 on CD20− CD38− B cell	−0.327	0.721	0.542	0.960	0.025
CD38 on plasma blast-plasma cell	−0.336	0.715	0.532	0.959	0.025
CD62L− HLA DR++ monocyte %monocyte	0.420	1.522	1.004	2.307	0.048
CD86 on CD62L+ myeloid dendritic Cell	0.232	1.262	1.017	1.566	0.035
Myeloid dendritic cell absolute count	0.185	1.203	1.029	1.406	0.020
CD11c on monocyte	−0.203	0.816	0.667	1.000	0.049
CD3 on effector memory CD4+ T cell	−0.202	0.817	0.679	0.984	0.033
Effector memory CD4−CD8− T cell %CD4−CD8− T cell	−0.220	0.803	0.673	0.957	0.014
CD45 on CD33+ HLA DR+ CD14dim	0.268	1.307	1.072	1.595	0.008
CD33+ HLA DR+ absolute Count	−0.112	0.894	0.815	0.981	0.018
CD66b on CD66b++ myeloid cell	−0.213	0.808	0.685	0.952	0.011
CD4+CD8+ T cell %leukocyte	0.327	1.387	1.031	1.866	0.030
Lymphocyte absolute count	0.314	1.369	1.050	1.786	0.020
Granulocyte absolute count	0.310	1.363	1.044	1.780	0.023
CD8dim T cell %leukocyte	−0.230	0.795	0.633	0.997	0.047
FSC-A on natural killer T	−0.374	0.688	0.515	0.918	0.011
CD4 on activated & secreting CD4 regulatory T cell	0.141	1.152	1.007	1.317	0.039
CD3 on CD39+ resting CD4 regulatory T cell	−0.328	0.720	0.584	0.889	0.002

All $P < 0.05$.

Effect size estimate and sensitivity analysis

We employed the random-effect inverse variance-weighted (IVW) method as the primary analysis due to its robustness, providing a conservative estimate even in the presence of heterogeneity (35). Additionally, supplementary analyses were conducted employing the weighted median (WM) and MR-Egger methods to validate the robustness of the IVW estimates. MR-Egger regression served as a test for unbalanced pleiotropy and substantial heterogeneity (36). In the presence of pleiotropy, MR-Egger estimates were considered more persuasive than IVW estimates. Furthermore, when at least half of the weighted variance resulting from horizontal pleiotropy was valid, the WM estimates could provide robust effect estimates. In summary, a significant estimate consistently observed in the direction between IVW, WM, and MR-Egger was considered statistically significant.

We conducted a comprehensive set of sensitivity analyses, encompassing Cochran's *Q* tests, funnel plots, leave-one-out analyses, and MR-Egger intercept tests. Specifically, heterogeneity was assessed through Cochran's *Q* tests, and the intercept term derived from MR-Egger regression was employed to evaluate pleiotropy. Leave-one-out analyses were performed to determine whether the causal estimate was influenced by any single SNP. All analyses were executed using the "Two Sample MR" package (version 0.5.8) in R software (version 4.3.1). Statistical significance was defined at a two-sided *P*-value < 0.05. Effect estimates were reported as odds ratios (OR) per standard deviation (SD) increment of the corresponding exposure. To enhance the precision of our findings, we employed the coloc R package (https://chr1swallace.github.io/coloc/, version 5.1.0) for a Bayesian co-localization test on the MR results, enabling the estimation of the posterior probability associated with shared genetic variants (37).

Results

We conducted a comprehensive MR investigation to explore the causal impact of genetically predicted 731 immunophenotypes on the morbidity of glioblastoma. In summary, we selected SNPs to genetically predict the causal influence of 731 immune cell types on GBM. The number of SNPs utilized in each MR analysis varied between 11 and 32. Notably, the *F*-statistic values for each genetic instrument surpassed 10, indicative of their robust instrumental strength.

The causal effect between the immunophenotypes and glioblastoma

After conducting preliminary analyses on the associations between genetically instrumental immune cell features and the risk of glioblastoma mainly by IVW method, we identified causal

TABLE 2 Mendelian Randomization assessments regarding the connection between genetically instrumented immune cells and GBM.

Outcome	Exposure	Method	OR	95% CI	*P*-value
GBM	CD45 on CD33+ HLA DR+ CD14dim	MR Egger	1.263	(0.936–1.703)	0.150
		Weighted median	1.359	(1.013–1.823)	0.041
		IVW	1.307	(1.072–1.595)	0.008
		Simple mode	1.216	(0.767–1.927)	0.420
		Weighted mode	1.331	(0.977–1.812)	0.091
		BWMR	1.344	(1.073–1.683)	0.010
GBM	CD33+ HLA DR+ absolute count	MR Egger	0.852	(0.762–0.953)	0.009
		Weighted median	0.869	(0.751–1.006)	0.060
		IVW	0.894	(0.815–0.981)	0.018
		Simple mode	0.981	(0.785–1.227)	0.868
		Weighted mode	0.900	(0.794–1.019)	0.107
		BWMR	0.880	(0.784–0.989)	0.032
GBM	IgD+ CD24+ B cell absolute count	MR Egger	1.377	(0.775–2.445)	0.288
		Weighted median	1.495	(0.945–2.366)	0.086
		IVW	1.357	(1.000–1.840)	0.050
		Simple mode	2.043	(0.987–4.229)	0.067
		Weighted mode	1.555	(0.922–2.634)	0.112
		BWMR	1.375	(0.966–1.957)	0.077

associations for four groups of immune cells, comprising 21 distinct immune cell types including five were in the B cell panel, four in the CDC panel, two in the Maturation stages of T cell panel, three in the Myeloid cell panel, two in the Treg panel and five in the TBNK panel. We observed protective effects for 10 immunophenotypes against glioblastoma, while 11 immunological cell subtypes were found to promote its incidence. The most significant protective cell types are FSC-A on Natural Killer T cells (OR = 0.688, CI = 0.515–0.918, $P = 0.011$), CD38 on Plasma Blast-Plasma Cells (OR = 0.175, CI = 0.532–0.959, $P = 0.025$), CD3 on CD39+ resting CD4 regulatory T cells (OR = 0.720, CI = 0.584–0.889, $P = 0.002$), and CD20 on CD20-CD38- B cells (OR = 0.721, CI = 0.542–0.960, $P = 0.025$), respectively. While, the primary immune cell subtypes promoting the incidence of glioblastoma include CD62L–HLA DR++ monocyte % monocyte (OR = 1.522, CI = 1.004–2.307, $P = 0.048$), CD4+CD8+ T cell % leukocyte (OR = 1.387, CI = 1.031–1.866, $P = 0.031$), Lymphocyte Absolute Count (OR = 1.369, CI = 1.050–1.786, $P = 0.020$), Granulocyte Absolute Count (OR = 1.363, CI = 1.044–1.780, $P = 0.023$). The main results are presented in Table 1 and the detailed results are found in Supplementary Table S1.

Bi-directional causal inference between glioblastoma and 21 target immune cell subtypes

Given the observed statistically significant positive correlation, we deemed it essential to scrutinize the potential reverse association. The results of reverse Mendelian Randomization (MR) analysis indicate estimates of reverse causation effects. The reverse MR results reveal an inverse association between GBM and immune cells. The estimated effect of this reverse association is statistically significant (P-value < 0.05), suggesting a potential relationship between changes in GBM and variations in immune cells. To ensure accurate causal interpretation and enhance result reliability, our objective was to eliminate significant reverse associations during the analysis. Therefore, after conducting Mendelian Randomization analysis with glioblastoma as the exposure and the 21 target immune cell subtypes as outcomes, we identified only three cell subtypes with a unidirectional causal relationship with glioblastoma (CD45 on CD33+ HLA DR+ CD14dim, CD33+ HLA DR+ Absolute Count and IgD+ CD24+ B cell Absolute Count), and the OR measured by IVW method were OR = 1.307, CI = 1.072–1.595, $P = 0.008$ (Figures 3A, D), OR = 0.894, CI = 0.815–0.981, $P = 0.018$ (Figures 4A, D) and OR = 1.357, CI = 1.000–1.840, $P = 0.049$ (Figures 5A, D) respectively. The details of their effect estimates and confidence intervals, significance statements, and sensitivity analyses can be found in Table 2 and Figure 2. The complete dataset is available in the Supplementary Table S2.

SNP selection

Finally, 16, 30, and 23 SNPs were identified as IVs for CD45 on CD33+ HLA DR+ CD14dim, CD33+ HLA DR+ Absolute Count, and IgD+ CD24+ B cell Absolute Count, respectively.

10.3389/fneur.2024.1375723

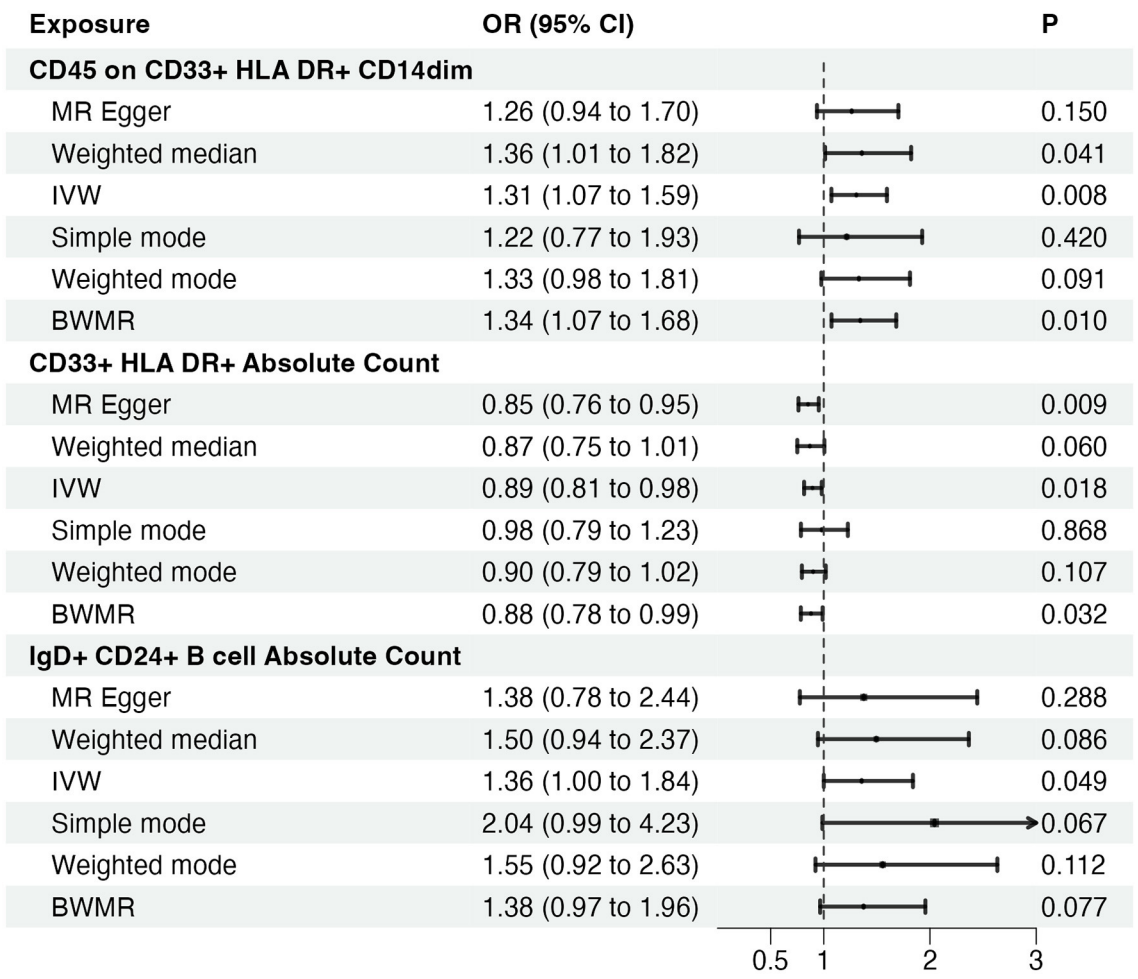

FIGURE 2
Causal effects of immune cells on glioblastoma. MR, Mendelian randomization; IVW, Inverse Variance Weighting; BWMR, Bayesian Mendelian Randomization.

TABLE 3 Assessment of diversity and directional pleiotropy employing various methodologies.

Immune cell	Heterogeneity	Horizontal pleiotropy	
	Cochran's *Q P*	MR-Egger intercept *P*	MR-PRESSO global test *P*
CD45 on CD33+ HLA DR+ CD14dim	0.591	0.766	0.641
CD33+ HLA DR+ absolute count	0.550	0.140	0.550
IgD+ CD24+ B cell absolute count	0.828	0.953	0.844

Moreover, the *F*-statistics for all IVs > 10, indicate no evidence of weak instrumental bias. The details of these IVs are shown in Supplementary Tables S4–S6. Similarly, in the reverse MR analysis, 30 SNPs were identified as instrumental variables for GBM. Importantly, all calculated *F*-values exceeded 10, ranging from 16.47260513 to 27.68019885. This observation indicates that the selected SNPs effectively represent the exposure variable, thereby enhancing the reliability and interpretability of the results. Consequently, these results ensure the credibility of the causal inferences derived from the Mendelian randomization approach (Supplementary Tables S7–S9).

Sensitivity analysis

Ultimately, sensitivity analyses were conducted for the results. No evidence of horizontal pleiotropy of exposure factors was detected when employing MR-Egger regression detection and the MR-PRESSO global test ($P > 0.05$; Figures 3B, 4B, 5B). Cochran's IVW *Q*-test results indicated no significant heterogeneity among IVs. For specific details refer to Table 3. Similarly, leave-one-out sensitivity analyses suggested that no individual SNP significantly influenced the causal association (Figures 3C, 4C, 5C).

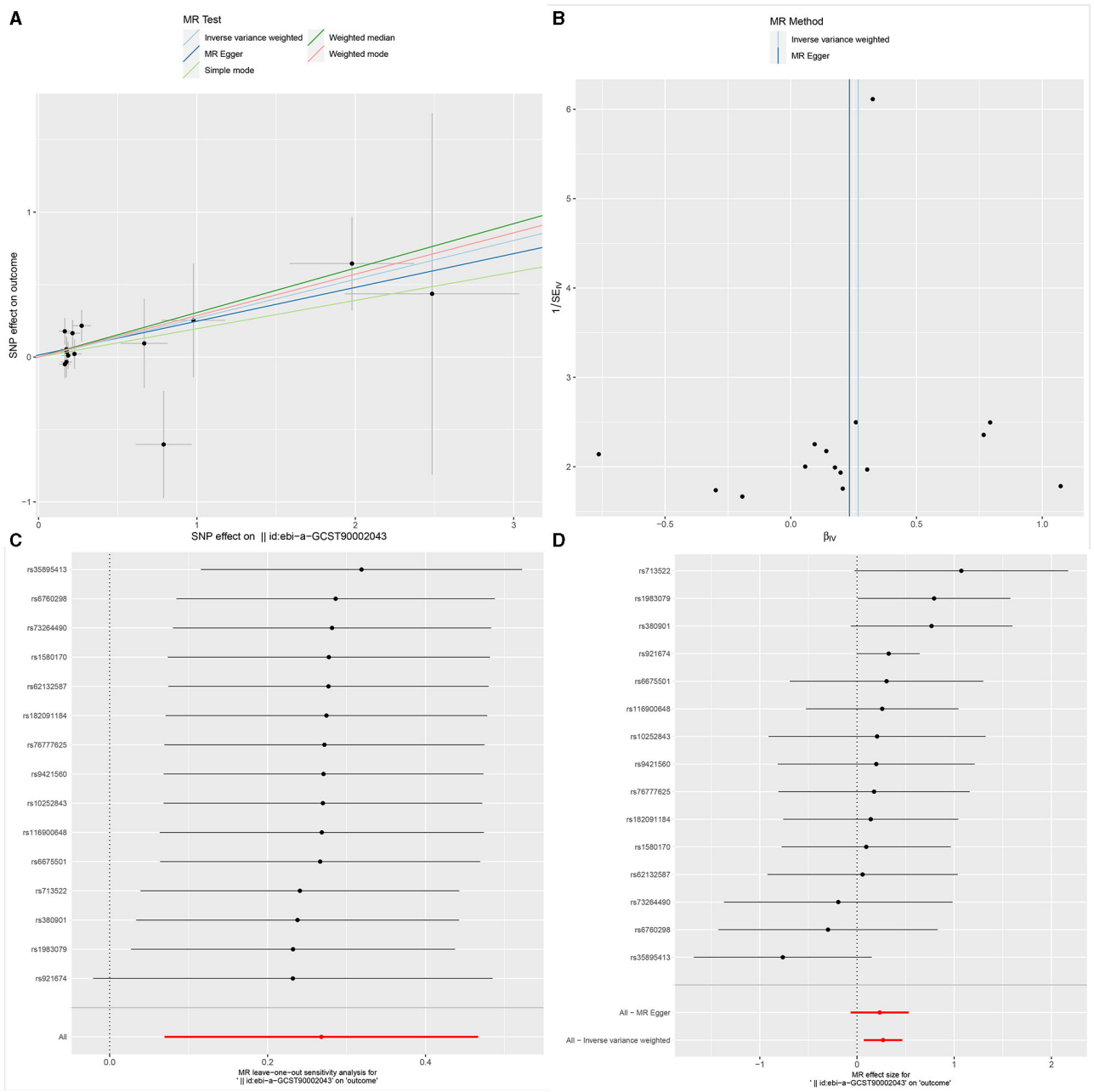

FIGURE 3
The Scatter plot, Funnel plot, leave-one-out sensitivity analysis, and Forest plot of CD45 on CD33+ HLA DR+ CD14dim.

Discussion

Through a two-sample MR analysis, we explored the causal relationships between different immune cell subtypes and the onset of GBM. The results indicated inhibitory effects on its occurrence for 10 immune cell subtypes exemplified by FSC-A on Natural Killer T cells (OR = 0.688, CI = 0.515–0.918, P = 0.011). Conversely, ten subtypes, including Lymphocyte Absolute Count (OR = 1.369, CI = 1.050–1.786, P = 0.020), exhibited a promoting effect on GBM incidence. Subsequently, through reverse MR analysis, we identified three distinct subtypes exhibiting singular causal relationships with GBM.

Our study revealed a decreased risk of GBM with an elevated mean fluorescence intensity of CD45 on CD33+ HLA DR+ CD14dim (Maturation stages of T cell panel). CD45 on CD33+ HLA DR+ CD14dim, where HLA DR is a component of the major histocompatibility complex (MHC) class II molecules encoded by the human leukocyte antigen complex on chromosome 6 region 6P21. CD45, a phosphatase typically expressed on the surface of leukocytes, especially immune system cells, plays a crucial role in regulating cell signaling and immune cell activity. CD33,

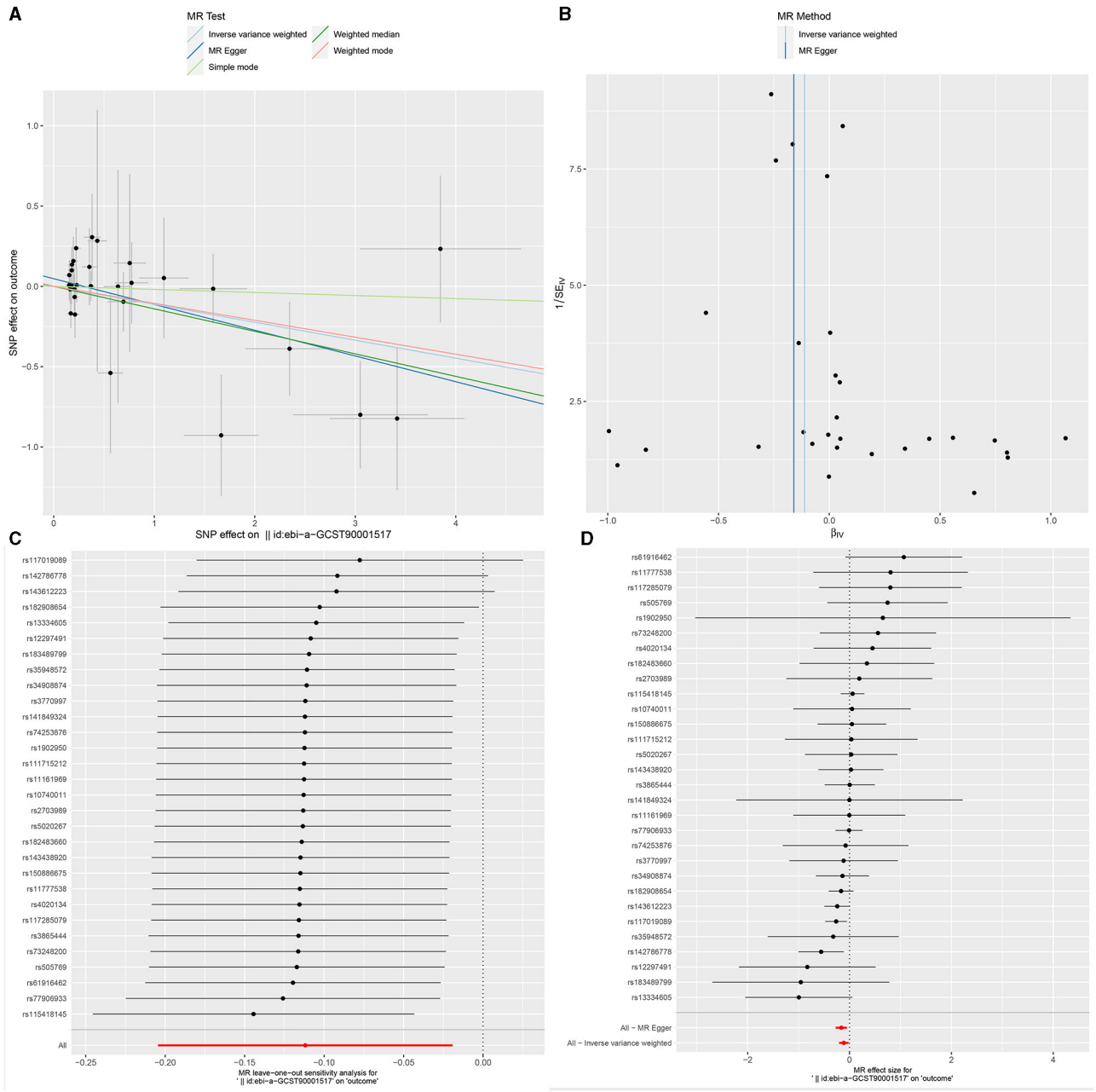

FIGURE 4
The Scatter plot, Funnel plot, leave-one-out sensitivity analysis, and Forest plot of CD33+ HLA DR+ Absolute Count.

a cell surface molecule commonly expressed in myeloid cells, particularly in the early stages of myeloid cell development, is involved in cell adhesion and immune regulation. CD14 is a surface marker typically found on monocytes and macrophages. In summary, CD45 on CD33+ HLA DR+ CD14dim describes a myeloid cell subtype characterized by surface markers CD45, CD33, HLA DR, and CD14dim. Through dephosphorylation and phosphorylation processes, CD45 plays a crucial role in regulating cell signaling, participating in cell activation and signal transduction. Its significance is particularly pronounced in the modulation of T-cell receptor (TCR) signal transduction. It aids in ensuring that T cells can undergo appropriate activation responses when stimulated by antigens.

The incidence of GBM correlates positively with the augmentation of CD33+ HLA DR+ Absolute Count (Myeloid cell panel). Previous research has indicated that myeloid cells are commonly observed within the tumor microenvironment (TME), undergoing polarization that includes myeloid-derived suppressor cells (MDSCs), tumor-associated macrophages, and microglia (TAMs), tumor-associated neutrophils (TANs), and tumor-associated dendritic cells (TADCs). This polarization serves to enhance both tumorigenesis and immune suppression (38, 39). CD33 is a cell surface molecule, characterized as a glycoprotein, and is involved in the development and regulation of immune cells. CD33 may play a role in immune modulation, with some studies suggesting its involvement in immunosuppression, including

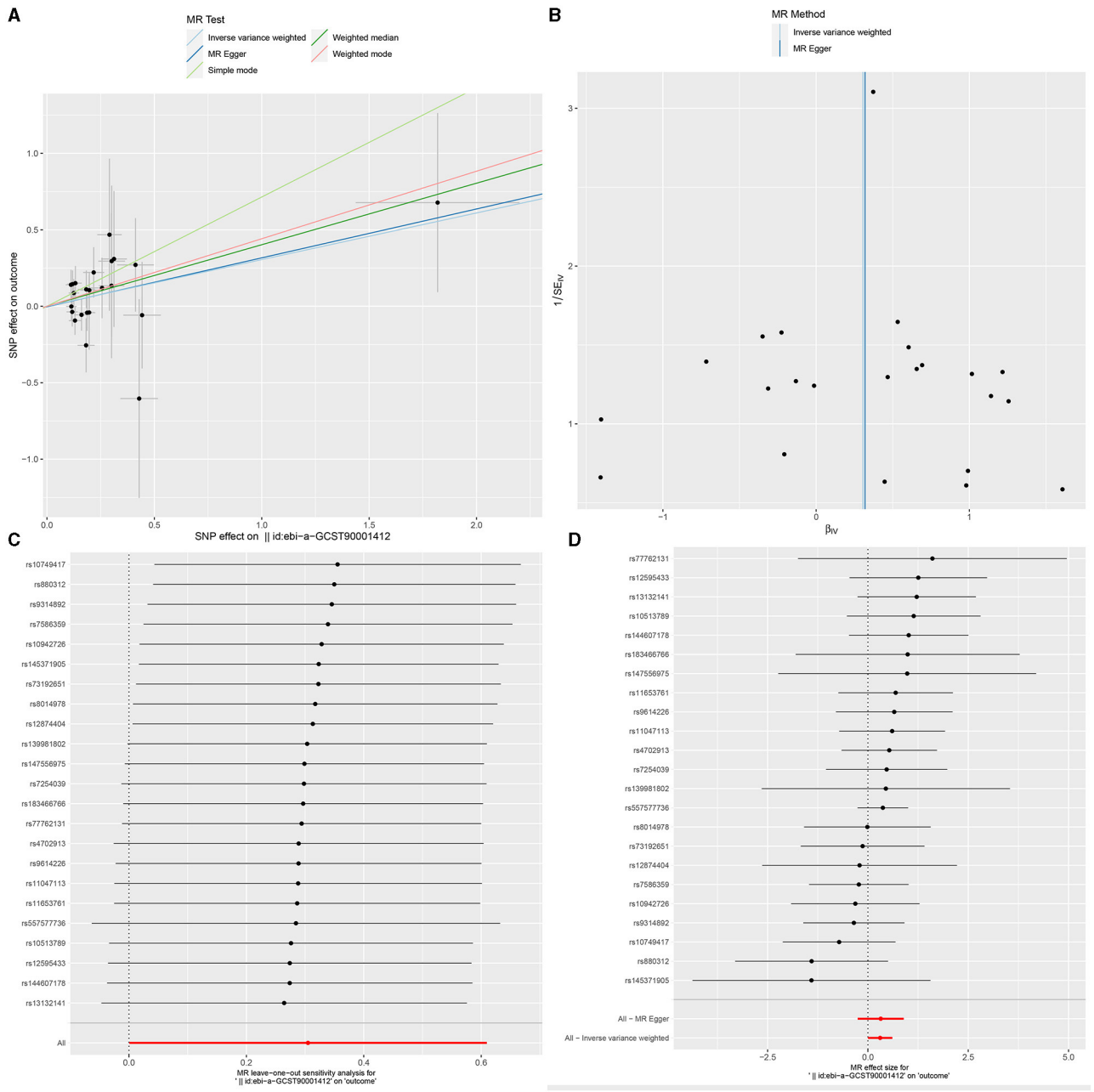

FIGURE 5
The Scatter plot, Funnel plot, leave-one-out sensitivity analysis, and Forest plot of IgD+ CD24+ B cell Absolute Count.

the inhibition of excessive immune activation. In the context of GBM, this regulatory function could impact the activity of immune cells, thereby influencing the immune response against the tumor. Additionally, there is evidence indicating that CD33 may contribute to anti-tumor immune responses. In certain scenarios, inhibiting CD33 has been proposed as a strategy to enhance the immune system's response to tumors. However, due to the highly heterogeneous nature of glioblastoma, characterized by variations in immune features and treatment responses among individuals, further in-depth experimental and clinical research is required to ascertain the precise role of CD33 in GBM.

A similar trend was observed in IgD+ CD24+ B cell Absolute Count (B cell panel), suggesting that an increase in the absolute count of these cells was associated with a higher risk of GBM. CD24 is a cell surface molecule involved in cell adhesion, signal transduction, and immune regulation. Within B cells, the expression of CD24 is likely associated with cellular differentiation and function. In the interaction between the immune system and the tumor microenvironment, these cells may play a distinct role. In certain instances, specific B cell subpopulations may participate in tumor immune evasion by modulating immune responses or promoting immune tolerance. This could contribute to the

tumor's ability to evade immune surveillance. Simultaneously, B cells may influence the immune characteristics of the tumor microenvironment through the secretion of cytokines, antibodies, or other molecules. This influence could impact the growth and development of the tumor. Furthermore, the interaction between B cells and T cells may play a crucial role in immune responses. In the field of tumor immunology, B cells may influence anti-tumor immune responses through their interactions with T cells (40, 41). Therefore, a comprehensive understanding of the role of IgD+ CD24+ B cells in GBM requires further experimental and clinical research.

Our study employed a MR design to investigate the causal effects of different immune cell subtypes on GBM. Because Mendelian Randomization utilizes natural genetic variation as a random allocation factor, based on the natural allocation of individual genetic variation, it reduces the influence of confounding factors and reverse causation. It has the advantage of simulating a randomized controlled trial, with lower costs and usually more ethically acceptable, as it does not require active intervention on participants and does not involve risks to individual health. However, it is important to acknowledge several limitations. Potential heterogeneity and horizontal pleiotropy were not comprehensively assessed, and the majority of GBM patients in our analysis were of European ancestry, thus limiting the generalizability of our findings and requiring validation across different populations. Furthermore, our GBM cases were sourced from public databases, with a relatively small sample size of only 253 cases, which may impact the robustness of our results. Additionally, we initially set the threshold for selecting single nucleotide polymorphisms associated with immune cells and GBM as exposures at $P < 5 \times 10^{-8}$. However, due to limited availability of such SNPs, we widened the threshold to $P < 5 \times 10^{-5}$, potentially introducing some instability into the results. Future research efforts could expand the sample range to encompass populations of various ethnic backgrounds and geographical regions to confirm the universality and reliability of the findings.

Conclusion

In summary, our comprehensive bidirectional Mendelian Randomization (MR) analysis has demonstrated the causal associations between multiple immunophenotypes and glioblastoma (GBM), highlighting the intricate pattern of interactions between the immune system and GBM. Moreover, our study significantly mitigated the impact of unavoidable confounding factors, reverse causality, and other influences. This may provide a novel avenue for researchers to explore immunotherapeutic interventions for glioblastoma, prompting discussions on early interventions and treatment strategies.

Perspectives

Based on the aforementioned discussions, our findings offer several avenues for future research. Firstly, it is imperative to incorporate a larger sample size to validate and replicate our results across diverse populations, ensuring their robustness and generalizability. Secondly, further investigations are warranted to elucidate the specific mechanisms and signaling pathways underlying the potential roles of different immune cell subtypes in glioblastoma pathogenesis. Thirdly, given the current focus on immunotherapy for glioblastoma, clinical trials assessing the therapeutic potential of immune modulation targeting newly identified immune cells may hold promise for improving patient outcomes. Lastly, embracing precision medicine approaches and integrating genetic, immunological, and clinical data into predictive models can optimize personalized treatment strategies for glioblastoma patients. These research directions are crucial for advancing our understanding of the intricate interplay between immune cell subtypes and glioblastoma, ultimately leading to enhanced diagnostic and therapeutic interventions for this devastating disease.

Data availability statement

The original contributions presented in the study are included in the article/Supplementary material, further inquiries can be directed to the corresponding author.

Ethics statement

Ethical review and approval was not required for the study on human participants in accordance with the local legislation and institutional requirements. Written informed consent from the patients/participants or patients/participants legal guardian/next of kin was not required to participate in this study in accordance with the national legislation and the institutional requirements.

Author contributions

MH: Writing – original draft, Writing – review & editing. YL: Conceptualization, Data curation, Formal analysis, Writing – review & editing. JP: Funding acquisition, Methodology, Writing – review & editing. YC: Writing – review & editing, Conceptualization, Methodology.

Funding

The author(s) declare that no financial support was received for the research, authorship, and/or publication of this article.

Acknowledgments

All data used in this study were obtained from openly available databases and consortiums. We express our sincere appreciation to them.

Conflict of interest

The authors declare that the research was conducted in the absence of any commercial or financial relationships that could be construed as a potential conflict of interest.

Publisher's note

All claims expressed in this article are solely those of the authors and do not necessarily represent those of their affiliated organizations, or those of the publisher, the editors and the reviewers. Any product that may be evaluated in this article, or claim that may be made by its manufacturer, is not guaranteed or endorsed by the publisher.

Supplementary material

The Supplementary Material for this article can be found online at: https://www.frontiersin.org/articles/10.3389/fneur.2024.1375723/full#supplementary-material

References

1. Li T, Li J, Chen Z, Zhang S, Li S, Wageh S, et al. Glioma diagnosis and therapy: current challenges and nanomaterial-based solutions. *J Control Release.* (2022) 352:338–70. doi: 10.1016/j.jconrel.2022.09.065

2. Louis DN, Perry A, Wesseling P, Brat DJ, Cree IA, Figarella-Branger D, et al. The 2021 WHO classification of tumors of the central nervous system: a summary. *Neuro Oncol.* (2021) 23:1231–51. doi: 10.1093/neuonc/noab106

3. Ostrom QT, Patil N, Cioffi G, Waite K, Kruchko C, Barnholtz-Sloan JS, et al. CBTRUS statistical report: primary brain and other central nervous system tumors diagnosed in the United States in 2013-2017. *Neuro Oncol.* (2020) 22:iv1–96. doi: 10.1093/neuonc/noaa200

4. Ou A, Yung WKA, Majd N. Molecular mechanisms of treatment resistance in glioblastoma. *Int J Mol Sci.* (2020) 22:351. doi: 10.3390/ijms22010351

5. Chen R, Smith-Cohn M, Cohen AL, Colman H. Glioma subclassifications and their clinical significance. *Neurotherapeutics.* (2017) 14:284–97. doi: 10.1007/s13311-017-0519-x

6. Sahm K, Weiss T. Immunotherapy against gliomas. *Nervenarzt.* (2024). 95:111–6. doi: 10.1007/s00115-023-01590-5

7. Tiwari S, Han Z. Immunotherapy: advancing glioblastoma treatment-a narrative review of scientific studies. *Cancer Rep.* (2023) 7:e1947. doi: 10.1002/cnr2.1947

8. Hernández A, Domènech M, Muñoz-Mármol AM, Carrato C, Balana C. Glioblastoma: relationship between metabolism and immunosuppressive microenvironment. *Cells.* (2021) 10:3529. doi: 10.3390/cells10123529

9. Yu C, Hsieh K, Cherry DR, Nehlsen AD, Resende Salgado L, Lazarev S, et al. Immune escape in glioblastoma: mechanisms of action and implications for immune checkpoint inhibitors and CAR T-cell therapy. *Biology.* (2023) 12:1528. doi: 10.3390/biology12121528

10. Genoud V, Kinnersley B, Brown NF, Ottaviani D, Mulholland P. Therapeutic targeting of glioblastoma and the interactions with its microenvironment. *Cancers.* (2023) 15:5790. doi: 10.3390/cancers15245790

11. Caverzán MD, Beaugé L, Oliveda PM, Cesca González B, Bühler EM, Ibarra LE, et al. Exploring monocytes-macrophages in immune microenvironment of glioblastoma for the design of novel therapeutic strategies. *Brain Sci.* (2023) 13:542. doi: 10.3390/brainsci13040542

12. Chen Z, Feng X, Herting CJ, Garcia VA, Nie K, Pong WW, et al. Cellular and molecular identity of tumor-associated macrophages in glioblastoma. *Cancer Res.* (2017) 77:2266–78. doi: 10.1158/0008-5472.CAN-16-2310

13. Murray PJ, Allen JE, Biswas SK, Fisher EA, Gilroy DW, Goerdt S, et al. Macrophage activation and polarization: nomenclature and experimental guidelines. *Immunity.* (2014) 41:14–20. doi: 10.1016/j.immuni.2014.06.008

14. Hambardzumyan D, Gutmann DH, Kettenmann H. The role of microglia and macrophages in glioma maintenance and progression. *Nat Neurosci.* (2016) 19:20–7. doi: 10.1038/nn.4185

15. Pyonteck SM, Akkari L, Schuhmacher AJ, Bowman RL, Sevenich L, Quail DF, et al. CSF-1R inhibition alters macrophage polarization and blocks glioma progression. *Nat Med.* (2013) 19:1264–72. doi: 10.1038/nm.3337

16. Noy R, Pollard JW. Tumor-associated macrophages: from mechanisms to therapy. *Immunity.* (2014) 41:49–61. doi: 10.1016/j.immuni.2014.06.010

17. Han S, Ma E, Wang X, Yu C, Dong T, Zhan W, et al. Rescuing defective tumor-infiltrating T-cell proliferation in glioblastoma patients. *Oncol Lett.* (2016) 12:2924–9. doi: 10.3892/ol.2016.4944

18. Woroniecka K, Chongsathidkiet P, Rhodin K, Kemeny H, Dechant C, Farber SH, et al. T-cell exhaustion signatures vary with tumor type and are severe in glioblastoma. *Clin Cancer Res.* (2018) 24:4175–86. doi: 10.1158/1078-0432.CCR-17-1846

19. Fecci PE, Mitchell DA, Whitesides JF, Xie W, Friedman AH, Archer GE, et al. Increased regulatory T-cell fraction amidst a diminished CD4 compartment explains cellular immune defects in patients with malignant glioma. *Cancer Res.* (2006) 66:3294–302. doi: 10.1158/0008-5472.CAN-05-3773

20. Woroniecka KI, Rhodin KE, Chongsathidkiet P, Keith KA, Fecci PE. T-cell dysfunction in glioblastoma: applying a new framework. *Clin Cancer Res.* (2018) 24:3792–802. doi: 10.1158/1078-0432.CCR-18-0047

21. Wiendl H, Mitsdoerffer M, Hofmeister V, Wischhusen J, Bornemann A, Meyermann R, et al. A functional role of HLA-G expression in human gliomas: an alternative strategy of immune escape. *J Immunol.* (2002) 168:4772–80. doi: 10.4049/jimmunol.168.9.4772

22. Platten M, Kretz A, Naumann U, Aulwurm S, Egashira K, Isenmann S, et al. Monocyte chemoattractant protein-1 increases microglial infiltration and aggressiveness of gliomas. *Ann Neurol.* (2003) 54:388–92. doi: 10.1002/ana.10679

23. Wei J, Gabrusiewicz K, Heimberger A. The controversial role of microglia in malignant gliomas. *Clin Dev Immunol.* (2013) 2013:285246. doi: 10.1155/2013/285246

24. Davey Smith G, Hemani G. Mendelian randomization: genetic anchors for causal inference in epidemiological studies. *Hum Mol Genet.* (2014) 23:R89–98. doi: 10.1093/hmg/ddu328

25. Sanderson E, Glymour MM, Holmes MV, Kang H, Morrison J, Munafò MR, et al. Mendelian randomization. *Nat Rev Methods Primers.* (2022) 2:26. doi: 10.1038/s43586-021-00092-5

26. Takenaka MC, Gabriely G, Rothhammer V, Mascanfroni ID, Wheeler MA, Chao CC, et al. Control of tumor-associated macrophages and T cells in glioblastoma via AHR and CD39. *Nat Neurosci.* (2019) 22:729–40. doi: 10.1038/s41593-019-0370-y

27. Liang J, Piao Y, Holmes L, Fuller GN, Henry V, Tiao N, et al. Neutrophils promote the malignant glioma phenotype through S100A4. *Clin Cancer Res.* (2014) 20:187–98. doi: 10.1158/1078-0432.CCR-13-1279

28. Curran CS, Bertics PJ. Eosinophils in glioblastoma biology. *J Neuroinflammation.* (2012) 9:11. doi: 10.1186/1742-2094-9-11

29. HedmKurki MI, Karjalainen J, Palta P, Sipilä TP, Kristiansson K, Donner KM, et al. FinnGen provides genetic insights from a well-phenotyped isolated population. *Nature.* (2023) 613:508–18. doi: 10.1038/s41586-022-05473-8

30. Orrù V, Steri M, Sidore C, Marongiu M, Serra V, Olla S, et al. Complex genetic signatures in immune cells underlie autoimmunity and inform therapy. *Nat Genet.* (2020) 52:1036–45. doi: 10.1038/s41588-020-0684-4

31. Sidore C, Busonero F, Maschio A, Porcu E, Naitza S, Zoledziewska M, et al. Genome sequencing elucidates Sardinian genetic architecture and augments association analyses for lipid and blood inflammatory markers. *Nat Genet.* (2015) 47:1272–81. doi: 10.1038/ng.3368

32. Bonder MJ, Kurilshikov A, Tigchelaar EF, Mujagic Z, Imhann F, Vila AV, et al. The effect of host genetics on the gut microbiome. *Nat Genet.* (2016) 48:1407–12. doi: 10.1038/ng.3663

33. Auton A, Brooks LD, Durbin RM, Garrison EP, Kang HM, Korbel JO, et al. A global reference for human genetic variation. *Nature.* (2015) 526:68–74. doi: 10.1038/nature15393

34. Burgess S, Thompson SG. Avoiding bias from weak instruments in Mendelian randomization studies. *Int J Epidemiol.* (2011) 40:755–64. doi: 10.1093/ije/dyr036

35. Burgess S, Small DS, Thompson SG. A review of instrumental variable estimators for Mendelian randomization. *Stat Methods Med Res.* (2017) 26:2333–55. doi: 10.1177/0962280215597579

36. Burgess S, Butterworth A, Thompson SG. Mendelian randomization analysis with multiple genetic variants using summarized data. *Genet Epidemiol.* (2013) 37:658–65. doi: 10.1002/gepi.21758

37. Zhao J, Ming J, Hu X, Chen G, Liu J, Yang C, et al. Bayesian weighted Mendelian randomization for causal inference based on summary statistics. *Bioinformatics.* (2020) 36:1501–8. doi: 10.1093/bioinformatics/btz749

38. Lin YJ, Wu CY, Wu JY, Lim M. The role of myeloid cells in GBM immunosuppression. *Front Immunol.* (2022) 13:887781. doi: 10.3389/fimmu.2022.887781

39. Gabrilovich DI, Ostrand-Rosenberg S, Bronte V. Coordinated regulation of myeloid cells by tumours. *Nat Rev Immunol.* (2012) 12:253–68. doi: 10.1038/nri3175

40. Helmink BA, Reddy SM, Gao J, Zhang S, Basar R, Thakur R, et al.. B cells and tertiary lymphoid structures promote immunotherapy response. *Nature.* (2020) 577:549–55. doi: 10.1038/s41586-019-1922-8

41. Tsou P, Katayama H, Ostrin EJ, Hanash SM. The emerging role of B cells in tumor immunity. *Cancer Res.* (2016) 76:5597–601. doi: 10.1158/0008-5472.CAN-16-0431

frontiers | Frontiers in Oncology

TYPE Review
PUBLISHED 28 May 2024
DOI 10.3389/fonc.2024.1388700

OPEN ACCESS

EDITED BY
Ramcharan Singh Angom,
Mayo Clinic Florida, United States

REVIEWED BY
Alak Manna,
Mayo Clinic Florida, United States
Anuradha Moirangthem,
Institute of Bio-Resources and Sustainable Development (IBSD), India
Hari Rachamala,
Mayo Clinic Florida, United States

*CORRESPONDENCE
Xiangrong Ni
nxr19930217@smu.edu.cn
Wubing Chen
13921101090@163.com
Ji Zhang
zhangji@sysucc.org.cn

RECEIVED 20 February 2024
ACCEPTED 10 May 2024
PUBLISHED 28 May 2024

CITATION
Xu J, Zhang J, Chen W and Ni X (2024) The tumor-associated fibrotic reactions in microenvironment aggravate glioma chemoresistance. *Front. Oncol.* 14:1388700. doi: 10.3389/fonc.2024.1388700

The tumor-associated fibrotic reactions in microenvironment aggravate glioma chemoresistance

Jiaqi Xu[1], Ji Zhang[2*], Wubing Chen[3] and Xiangrong Ni[1,4,5*]

[1]The Second Clinical Medical School, Zhujiang Hospital, Southern Medical University, Guangzhou, China, [2]Department of Neurosurgery, Sun Yat-sen University Cancer Center, Guangzhou, China, [3]Department of Radiology, Wuxi Fifth People's Hospital, Jiangnan University, Wuxi, China, [4]Translational Medicine Research Center, Zhujiang Hospital, Southern Medical University, Guangzhou, China, [5]Department of Plastic Surgery, Zhujiang Hospital, Southern Medical University, Guangzhou, China

Malignant gliomas are one of the most common and lethal brain tumors with poor prognosis. Most patients with glioblastoma (GBM) die within 2 years of diagnosis, even after receiving standard treatments including surgery combined with concomitant radiotherapy and chemotherapy. Temozolomide (TMZ) is the first-line chemotherapeutic agent for gliomas, but the frequent acquisition of chemoresistance generally leads to its treatment failure. Thus, it's urgent to investigate the strategies for overcoming glioma chemoresistance. Currently, many studies have elucidated that cancer chemoresistance is not only associated with the high expression of drug-resistance genes in glioma cells but also can be induced by the alterations of the tumor microenvironment (TME). Numerous studies have explored the use of antifibrosis drugs to sensitize chemotherapy in solid tumors, and surprisingly, these preclinical and clinical attempts have exhibited promising efficacy in treating certain types of cancer. However, it remains unclear how tumor-associated fibrotic alterations in the glioma microenvironment (GME) mediate chemoresistance. Furthermore, the possible mechanisms behind this phenomenon are yet to be determined. In this review, we have summarized the molecular mechanisms by which tumor-associated fibrotic reactions drive glioma transformation from a chemosensitive to a chemoresistant state. Additionally, we have outlined antitumor drugs with antifibrosis functions, suggesting that antifibrosis strategies may be effective in overcoming glioma chemoresistance through TME normalization.

KEYWORDS

chemoresistance, tumor-associated fibrotic reaction, glioma, antifibrosis therapy, tumor microenvironment (TME), cancer-associate fibroblasts

1 Introduction

Gliomas are stratified into grades 1 through 4 according to the World Health Organization's tiered grading system, and grade 4 is the most prevalent and virulent subtype, also known as glioblastoma. GBM, an unyielding primary cerebral malignancy, has a grim prognosis with a 5-year survival rate of less than 10% (1–3), despite standard therapies including the maximal tumor excision, combined with concomitant radiotherapy and temozolomide chemotherapy. So far, TMZ is the first-line chemotherapy drug for glioma. However, due to the frequent occurrence of TMZ resistance after chemotherapy, glioma is recalcitrant and refractory. To increase the prognosis of GBM patients, it's important to summarize the potential mechanisms of glioma chemoresistance and find useful strategies to overcome TMZ resistance.

Gliomas are characterized as easily chemoresistant intracranial malignancy through demethylation of O(6)-methylguanine-DNA methyltransferase (MGMT) promoter, overexpression of cell membrane glycoprotein, and the augmentation of stemness-associated molecules (4–7). Moreover, the chemoresistance could not only be developed by the cellular alterations in cancer cells but also, in part, be modulated by the specific TME (8). Many researchers recently have focused on the chemoresistance promoted by the GME and are increasingly aware of the significance of overcoming chemoresistance by normalizing GME. The nonneoplastic immune cells and stromal components foster an immunosuppressive GME under the interaction of glioma-secreted cytokines (9, 10). The prominent nonneoplastic stromal cells in gliomas consist of endothelial cells, microglia, and tumor-associated macrophages (TAMs), etc. (2, 11–13). In solid tumor stroma, cancer-associated fibroblasts (CAFs) secrete a lot of collagen after stimulation (14), and subsequently increase the stiffness of the tumor matrix which in turn enhances the proliferation, invasiveness, and stemness as well as chemoresistance of glioma cells. Different from others' attention on the glioma chemoresistance increased by the alterations of glioma cells themselves, in this review, we summarize the relationship between the chemoresistance and glioma-associated fibrotic reactions. Several investigators have attempted to enhance TMZ chemotherapy efficacy with reasonable combinations of some clinically approved conventional drugs (15), and among these drugs, the increased chemotherapy efficacy by some agents with antifibrosis function draws our attention. However, it is so little known why the antifibrosis medication is effective for solid tumors and how glioma-associated fibrotic reactions in GME specifically contribute to TMZ chemoresistance and poor prognosis for glioma patients. In this review, we thus explore the mechanism of the occurrence and development of tumor-associated fibrotic phenomena in GME and sum up the antifibrosis strategies for sensitizing chemotherapy, hoping to provide novel insights for glioma research and treatment.

2 The formation of tumor-associated fibrotic reactions in the tumor microenvironment

During the malignant progression of tumor cells, changes in the tumor stroma also take place including alterations of extracellular matrix (ECM) components, stroma stiffness, excessive vascularization, hypoxia, and paracrine cytokine secretion. As a principal non-cellular component, the ECM plays a crucial role in driving tumor malignancy by providing cells with architectural and mechanical supports, regulating nutrient supply, as well as engaging in multiple cellular processes as a reservoir of diverse cytokine regulators (16–19). The ECM components would transform into a specific status that can stimulate the growth of cancer cells and tumor-associated cells. As cancer occurs and develops, malignant and stromal cells can deposit, break down, and remodel the ECM through the production of multiple ECM proteins, including collagens, fibronectins, laminins, and proteolytic enzymes, which can stimulate the growth of cancer cells and tumor-associated cells (20). In addition, alterations in the biophysical properties of the ECM, such as stiffness, density, rigidity, tension, and protein deposition, are recognized as hallmarks of tumor stromal fibrosis (21, 22). In the TME, CAFs are one of the most critical stromal cell types functioning as the architects of matrix remodeling, which provides the "soil" for tumor survival (23). CAFs could be identified with molecular markers such as αSMA, FAP-1, desmin, podoplanin, NG2 (CSPG4), and PDGFR-α/β (24). These CAFs could secrete substantial quantities of ECM components after being activated and could mediate the malignant progression of tumors through the promotion of stromal inflammation and fibrosis (24, 25). Cancer cells exhibit multiple features of cancer progression, including the recruitment of various stromal cells to form the TME (26), which encompasses different functional subtypes of stromal cells and matrix polymers (27). Among these cells, CAFs promote the formation of a dense and rigid fibrotic microenvironment by large amounts of ECM proteins and cytokines secretions (28). In TME, tumor-associated fibrosis is the result of excessive accumulation of collagen, fibronectin, laminin, tendon protein, etc. (29, 30). Among these ECM components, the most abundant one is collagen protein which constitutes the main rigid structures of tumor stroma. There are more than 28 types of collagens which are categorized into four subtypes: fibril-forming collagens (I, II, III, V, XI, XXVI, XXVII), fibril-associated collagens with interrupted triple helices (FACITs: IX, XII, XIV, XVI, XIX, XX, XXI, XXII, XXIV), network-forming collagens (IV, VIII, X), and membrane-anchored collagens (MACITs: XIII, XVII, XXIII, XXV) (31). Among these collagens, types I, III, and V collagen are predominantly secreted by CAFs, while type IV collagen is mainly produced by epithelial and endothelial cells. It is worth noting that, under certain conditions, tumor cells and TAMs can also synthesize collagen (32). Collectively, tumor-associated fibrotic reactions are induced by the interactions between tumor cells and stromal cells.

In glioma, radiotherapy and cytotoxic chemotherapy can induce epithelial-mesenchymal transition (EMT) and upregulate the transforming growth factor-β (TGF-β) signal, which is the key signaling pathway to fibrosis initiation (33). EMT is associated with increased expression of TGF-β, collagen, fibronectin, α-SMA, and S100A4, suggesting that these molecular mechanisms could be involved in inducing stromal fibrotic reactions in glioma. Some researchers have proposed a "repurposing" strategy for treating GBM by using clinically approved conventional drugs to inhibit EMT. For instance, Kast et al. summarized six clinically approved drugs including fenofibrate, quetiapine, lithium, nifedipine, itraconazole, and metformin (33). These drugs are being explored as adjunctive agents to enhance chemosensitivity in tumor therapy. Given the heterogeneity of GBM, further research is needed to determine which molecular subtypes may benefit from these non-antitumor drugs.

3 Fibrotic components in extracellular matrix facilitate the malignant progression of glioma

The ECM in the normal brain tissues predominantly consists of hyaluronic acid, proteoglycans, and laminin, but very little collagen. However, in GBM, there is a substantial presence of collagen proteins, laminin, and fibronectin, primarily distributed in the vascular basement membrane in tumor tissue (34). Recent reports highlighted the role of collagen in enhancing GBM cell stemness and promoting EMT and invasion (35, 36). Some researchers found that type-I collagen, the main component of tumor-associated fibrosis, could be used to promote the formation of an invasive, tight GBM spheroid structure when the collagen concentrations increase to some extent (37). Huijbers et al. conducted histological analyses on 90 GBM cases, revealing a significant abundance of collagen proteins within the ECM of GBM (38). They also observed that the collagen receptors Endo180 are overexpressed on the surface of GBM cells. It is worth noting that Endo180 expression is particularly pronounced in stromal-rich high-grade gliomas (39), and its regulation is linked to the TGF-β signaling pathway (40). Additionally, the interactions between Endo180 and collagen significantly potentiates GBM invasion (38). In GBM, collagen XVI induces tumor invasion by modulating the activation pattern of integrin β1, possibly impacting the interactions between glioma cells and the stroma to further enhance the invasive phenotype (41). Furthermore, in order to confirm the association between tumor-associated fibrotic reactions and glioma prognosis, we analyzed the Chinese Glioma Genome Atlas (CGGA) (http://www.cgga.org.cn/) and Gene Expression Profiling Interactive Analysis (GEPIA) (http://gepia.cancer-pku.cn/index.html) databases. According to the CGGA dataset, fibrosis-related marker genes (*COL1A2*, *COL1A1*, *COL3A1*, *COL4A1*, *COL4A2*, *COL5A2*, *COL6A2*, *COL6A1*) are highly expressed in the mesenchymal (ME) and classical (CL) GBM subtypes, which are associated with shorter overall survival (Figures 1A, B). Meanwhile, analysis of the GEPIA dataset reveals that the high expressions of collagen-related genes (*COL1A1, COL3A1, COL4A1, COL5A2*, and *COL6A1*.) are associated with poor prognosis of glioma patients (Figures 1C–G). Collectively, it suggests that heavier fibrotic reactions play a critical role in glioma progression and predict a poor prognosis for glioma patients.

Knocking out the collagen XVI gene in GBM U87MG cells resulted in a significant decrease in invasive capabilities compared to the control group (42). Experimental evidence has also shown that the GBM cell compaction promotes the expression of more collagen proteins and vascular endothelial growth factors in GBM, notably elevating the mRNA and protein levels of collagen types VI and IV, as well as the collagen crosslinker named lysyl oxidase (LOX). Notably, β-aminopropionitrile (BAPN), a collagen inhibitor, significantly inhibits collagen crosslinking in the ECM components of GBM by specifically targeting and suppressing LOX. Studies concurrently demonstrated that LOX expression controls the malignant progression of GBM. In an *in situ* GBM mouse model, treatment with BAPN markedly inhibited intracranial tumor growth by suppressing LOX activities (34). In conclusion, these findings underscore the pivotal role of tumor-associated fibrotic components in fostering the malignant progression of glioma, shedding light on the potential therapeutic effect of antifibrosis medications for controlling this devastating disease.

4 The chemoresistance can be enhanced by glioma-associated fibrotic reactions

There are two aspects explaining the mechanism by which glioma-associated fibrotic reactions induce chemoresistance. Firstly, after treated with cytotoxic drugs in solid tumors, CAFs and mesenchymal stem cells (MSCs) are recruited and increased in ECM, along with the accumulation of cytokines and other secreting factors. This fortifies the tumor "stemness", thereby leading to chemoresistance (43). Secondly, the increased stiffness of tumor tissues with heavily fibrotic ECM components hinders the delivery of chemotherapeutic agents to tumor cells. This limits the penetration of drugs into tumor cells, thereby impairing chemotherapy efficacy (29).

4.1 Tumor-associated fibrotic reactions promote the stemness of glioma cells

The increased resistance of glioma stem cells (GSCs) to chemotherapeutic agents, which contribute to glioma refractoriness and recurrence, has been extensively documented (44, 45). GSCs are known to cause TMZ resistance through the upregulation of MGMT protein levels (46, 47). In TME, Oleynikova et al. found that the CAFs form the niche for tumor stem cells and these compartments surrounding tumor cells facilitated chemotherapy resistance. In agreement, CAFs may promote the stemness of cancer cells by establishing a survival niche to sustain cancer stem cells (CSCs) and protecting them from chemotherapy-induced cell death, hence, facilitating chemotherapy resistance (25, 28, 48). While it remains

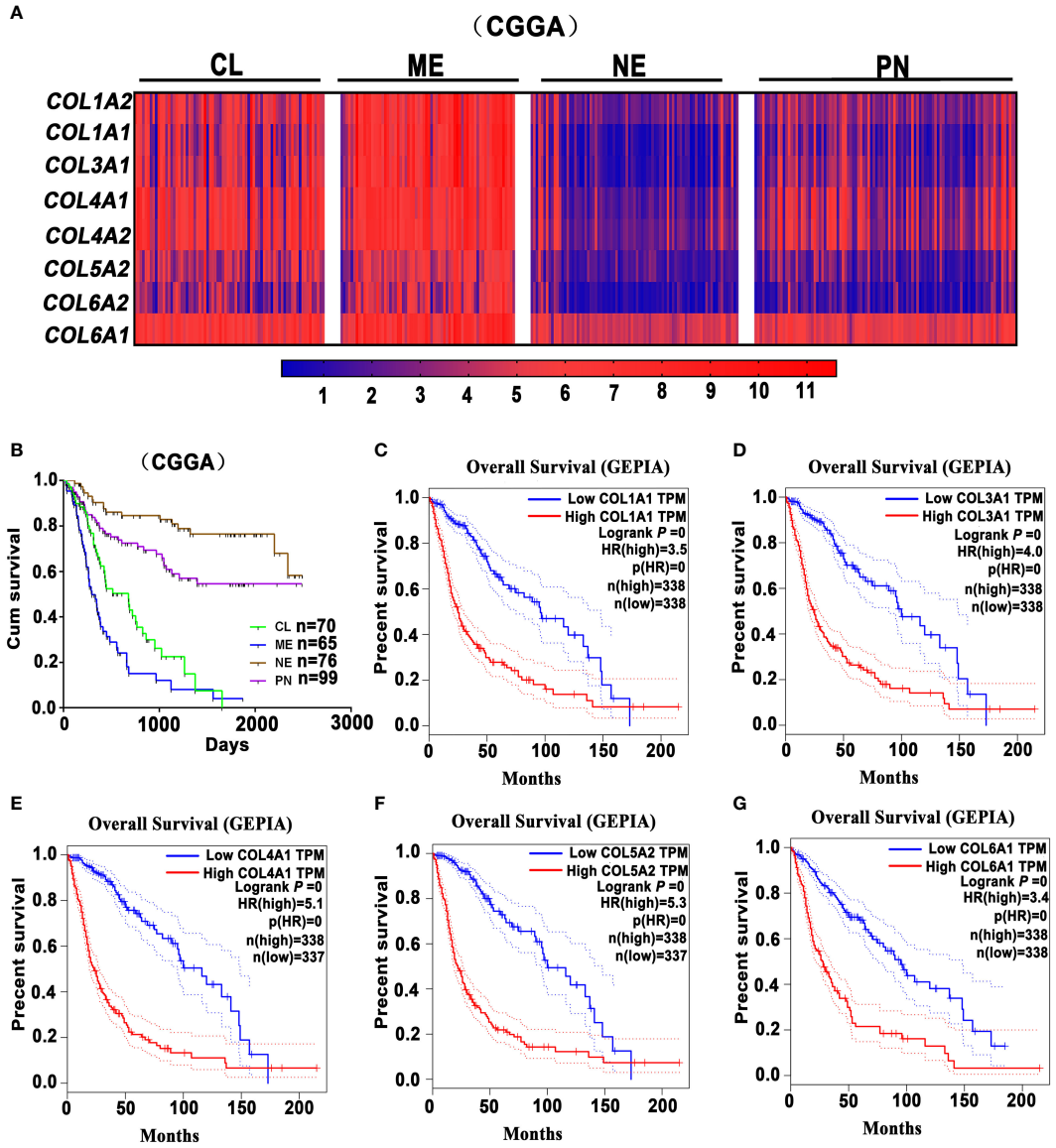

FIGURE 1
Glioma-associated fibrosis predicts poor prognosis of glioma patients. **(A)** The expression analysis of fibrosis-related marker genes *COL1A2*, *COL1A1*, *COL3A1*, *COL4A1*, *COL4A2*, *COL5A2*, *COL6A2*, *COL6A1* in the Proneural (PN), Classical (CL), Mesenchymal (ME), and Neural (NE) GBM subtypes in the CGGA dataset. **(B)** Kaplan-Meier survival curves indicate that ME and CL GBM subtypes predict a poor prognosis for glioma patients in the CGGA dataset. **(C–G)** Kaplan-Meier survival curves indicate that the high expression of collagen-related genes (*COL1A1*, *COL3A1*, *COL4A1*, *COL5A2*, and *COL6A1*) correlates with a poor prognosis for glioma patients in the GEPIA dataset. (GEPIA dataset includes TCGA LGG and GBM dataset.).

unclear how glioma-associated fibrotic reactions develop and which of the molecular characteristics of gliomas is more likely to form fibrosis. It has been widely reported that fibroblast activation protein-α (FAP-α) is involved in tumor-associated fibrosis. FAP-α, typically undetectable in normal tissues, however, exhibits overexpression within glioma cells and glioma stroma (49). Its selective localization in the tissue remodeling and repairing sites enhances the invasiveness and malignant progression of solid tumors including gliomas, implicating FAP-α as a potential target for addressing tumor-associated fibrosis dysregulation (12, 50). Currently, it has been reported that PT-100 significantly reduces CAF enrichment by targeting FAP-α in the tumor stroma, which enhances chemotherapeutic efficacy and reduces drug resistance when combined with oxaliplatin for colon cancer treatment (51). Also, the bone marrow derived MSCs have been demonstrated to enhance tumor stemness after being recruited to the tumor stroma, either through direct paracrine signaling or via its transformation into CAFs (43). Jia et al. compared the gene expression profiles of glioma cells between three-dimensional culture with collagen scaffolds and the conventional two-dimensional culture, and they found that collagen scaffolds could upregulate the expression of EMT-related molecules N-cadherin and vimentin, invasion-related matrix metalloproteinases

(MMPs) such as MMP1, MMP2, MMP3, and MMP7, as well as stemness-associated factors CD133, Nestin, Oct4, Sox2, c-Myc, Nanog, MSI1, MSI2 and BMI-1, etc. (35). The glioma stroma harbors a substantial population of TAMs and microglia, which secrete high levels of TGF-β. This cytokine in turn, promotes the invasiveness of CD133(+) GSCs. Moreover, the upregulated TGF-β1 levels are associated with the increased MMP9 production in GSCs (36). What's more, high serum levels of TGF-β positively correlate with poor prognosis in GBM, hinting at its pivotal role in the maintenance of glioma stemness and malignancy (52). Currently, the strategies targeting the TGF-β signaling have exhibited promising safety and efficacy profiles for gliomas. For instance, anti-TGF-β antibodies have significantly prolonged the survival of recurrent glioma patients (53). It has been proved that after TMZ treatment, the activation of the TGF-β signaling in GBM leads to connective tissue growth factor (CTGF) overexpression, which subsequently mediates TMZ resistance by enhancing the stemness of glioma cells (54). Therefore, these findings suggest that tumor-associated fibrotic reactions play a role in promoting chemoresistance by enhancing the stemness and EMT of glioma cells.

4.2 Glioma-associated fibrosis reduces drug delivery efficiency

The ECM consists of a variety of structural proteins that maintain tissue structure and regulate extracellular biochemical signals, thereby modulating cellular functions (18, 55). In the process of traveling from blood vessels to tumor cells, chemotherapeutic drugs must navigate through the ECM to reach their target cells. However, drug penetration can be hindered by low pH conditions that facilitate the binding of positively charged chemotherapy drugs to negatively charged ECM components, ultimately reducing the efficiency of drug delivery to cancer cells (29). What's more, positively charged drugs have more difficulty in crossing the hydrophobic plasma cell membranes (56, 57). As we know, only after the chemotherapeutic drugs penetrate cell membranes and reach the nucleus can they adequately exert their cytotoxic effects (29).

It is known that tissue stiffness varies across different diseases and organs; for instance, normal liver tissue exhibits a "stiffness" at 6 kPa, while the "stiffness" of fibrotic liver tissues can reach up to 12 kPa (58). As the tumor develops, the deposition of type I and IV collagen increases in the cross-linking and tumor-associated fibrosis process, leading to an increase in the "stiffness" of the ECM (59). The increased ECM stiffness corresponds to upregulated contractile and traction forces of the cell cytoskeleton as cells attempt to balance extracellular tension (29). Intercellular mechanotransduction is the process of converting external mechanical stimuli into intracellular biochemical signals. Changes in ECM stiffness are sensed by local junctions between cells, and these junctions are protein complexes containing mechanosensitive protein molecules such as talin and integrins (60). Due to the tension between intracellular contractile forces and extracellular stiffness, talin unfolds in response to the forces, resulting in the exposure of hidden intracellular binding sites that allow effector proteins to bind (61). What's more, focal adhesion kinase (FAK) is another element that can be activated by external rigidity, and this kinase activity can be utilized to initiate intracellular signaling pathways such as Yes-associated protein (YAP) nuclear localization (62). As mentioned before, the heightened tumor stiffness is closely associated with ECM compositions such as MMPs, hyaluronic acid, and abundant collagens and their cross-linking (18). During the progression of tumors, the accumulation of mechanical pressure can compress tumor blood vessels and lymphatic vessels, leading to reduced perfusion, hypoxia, and elevated interstitial pressure within tumor tissues, thus reducing chemotherapy efficacy (63, 64). Therefore, strategies aiming at reducing mechanical stress in glioma, such as tumor decompression therapy (65), can relieve vascular compression within tumors, enhance tissue perfusion, and improve the transport of chemotherapeutic drugs into tumor cells.

It is important to recognize that chemoresistance, in part, is modulated by collagen and hyaluronic acid in the TME (66) and the strategies specifically targeting these components may be useful tumor decompression therapies. Surprisingly, repurposing those conventionally approved drugs with antifibrosis function can indeed inhibit tumor growth by normalizing TME with the downregulated ECM synthesis. This, in turn, reduces tumor stiffness and mechanical stress, relieves vascular and lymphatic compression, and enhances drug permeability into tumor tissues (67–69). Currently, antifibrosis drugs such as tranilast, losartan, and pirfenidone, have been used to improve chemotherapy in solid tumors (63, 70, 71), while it warrants subsequent research to confirm their efficacy in glioma. As for stroma-rich tumors, researchers concentrate on developing nanomedicines targeting CAFs to reduce tumor matrix stiffness (72, 73). These nano-delivery systems have a double effect on enhancing chemotherapy. Firstly, they reverse tumor progression, immunosuppression, or drug-resistance phenotypes by inhibiting signaling between CAFs and tumor cells, thus increasing chemosensitivity. Secondly, by weakening CAFs function, nanomedicines reduce tumor solid-phase pressure, tumor tissue fluid pressure, and ECM density, leading to increased penetration depth of antitumor drugs and improved efficiency of chemotherapeutic drug delivery.

5 Molecular regulatory mechanisms of glioma-associated fibrosis

MMPs are a group of zinc-dependent endopeptidases involved in the dynamic remodeling of ECM, exhibiting proteolytic activities toward ECM components such as collagen (74). In normal circumstances, the synthesis and degradation of ECM is a homeostatic process regulated by the balanced activity of MMPs. However, in tumor tissues, this homeostasis is disrupted due to the overexpressed or hyperactivated of MMPs in gliomas, such as MMP2, MMP9 MMP3, MMP13, MMP14, MMP19, MMP26, and MMP28 (75–84). After effective treatment of U87 glioma xenografts with TMZ, MMP expression is downregulated, with the downregulation of MMP2 and MMP3 associated with the inhibitory effects of TMZ on gliomas (85). In addition, MMPs can promote tumor invasion by facilitating tumor cell degradation

of the surrounding matrix or by activating paracrine signaling factors through proteolytic cleavage. For instance, MMPs can lead to the secretion of large amounts of TGF-β, which subsequently promotes CAF activation, long-term fibrosis, and MMP expression and secretion (86).

TME contains numerous signaling molecules and growth factors that, upon binding to cell surface receptors, initiate intracellular signaling in cancer cells, ultimately leading to changes in gene expression. Signaling factors through this mechanism are significantly increased in tumors, for instance, growth factors such as epidermal growth factors (EGFs), fibroblast growth factors (FGFs), platelet-derived growth factors (PDGF), and hepatocyte growth factors (HGF) are abundant in TME (87). During ECM remodeling, the secretion of MMPs promotes the release of growth factors in ECM, such as TGF-β (18, 88). TGF-β exhibits a dual regulatory role in tumor cells, promoting both apoptosis and survival. It suggests that the switch from proapoptotic to prosurvival signaling in tumor cells is influenced by the TP53 gene mutation status (89) or the stiffness of the ECM (90). After the activation of CAFs by TGF-β, they play a crucial role in mediating the maintenance of the TME through paracrine signaling pathways (91). Both glioma cells and infiltrating immune cells in TME could secrete various cytokines, including TGF-β, CTGF, IL-6, and IL-10, contributing to the formation of an immunosuppressive GME (52), many of these cytokines promote chemoresistance in gliomas. Research has shown that in GBM, when treated with TMZ, the activation of the TGF-β signaling pathway leads to the overexpression of CTGF, and subsequently, CTGF increases the expression levels of glioma stem cell markers, including ALDH1, CD44, Nestin, and Nanog (54). In conclusion, the fibrotic alterations in GME are closely related to the maintenance of glioma cell stemness and the chemoresistance of glioma.

6 Tumor-associated fibrotic reactions contribute to immunotherapy resistance and TAMs-mediated chemoresistance in glioma

Nowadays, numerous glioma immunotherapies have been investigated in clinical and preclinical phases. These include immune checkpoint blockade targeting IDO, CTLA-4, and PD-L1 (92), as well as inhibitors of M2 macrophages such as CSF-1R (93, 94), PI3Kγ (8), and BAPN (11), and antibodies targeting cytokines like IL-6 (95), and CCL5 (96, 97), etc. However, the efficacy of many immunotherapy strategies for GBM remains very limited due to the absence of T lymphocytes, B lymphocytes, and NK cells, as well as the presence of the blood-brain barrier (BBB). Furthermore, during the process of tumor-associated fibrotic reactions, the stiff ECM, particularly the highly crosslinked collagen, creates hypoxic conditions in and around the TME (98) and hinders the infiltration of immune cells or immunotherapeutic agents into tumor tissues (99). Therefore, tumor-associated fibrotic reactions play a role in promoting an immunosuppressive TME, which mediates the immunotherapy resistance in solid tumors. As widely known, the mesenchymal subtype of GBM is characterized by abundant immune features (100), especially the M2 macrophages and microglias (101), suggesting that targeting macrophages could be a useful strategy for treating mesenchymal subtype GBM. Interactions between CAFs and M2 macrophages play a crucial role in the formation of tumor-associated fibrotic reactions (102). As is known, macrophages, contributing to glioma progression (11, 103), can also release significant amounts of TGF-β to initiate and accelerate fibrotic reactions. Furthermore, our investigation revealed that fibrosis-related collagens expression and M2 macrophage marker *CD163* expression may participate in glioma malignancy, and analysis from the GEPIA database shows that these collagens (*COL1A2*, *COL1A1*, *COL3A1*, *COL4A1*, *COL4A2*, *COL5A2*, *COL6A2*, *COL6A1*) and *CD163* expression are higher in GBM compared to low-grade glioma (LGG) (Figure 2A). The mesenchymal subtype of GBM exhibits severe glioma-associated fibrotic reactions, characterized by the most prominent collagen deposition and highest macrophage infiltration in the CGGA and GEPIA datasets (Figures 1A, 2B). It also suggests that the expression level of COL1A1 positively correlates with the expression level of CD163 (the M2 macrophage marker gene) (Figures 2C, D). TAMs-secreted IL-11 and LOX factors promote glioma chemoresistance and progression, while PI3Kγ inhibition (8) and LOX inhibitors (11) could significantly improve TMZ efficacy in orthotopic GBM mouse models. Furthermore, IL-11 (104) and LOX (105), two crucial determinants of tissue fibrosis, are therapeutic targets against organ fibrosis. This suggests that antifibrosis strategies may enhance chemosensitivity in glioma. Therefore, glioma progression and chemoresistance are not only directly promoted by M2 macrophage-secreted cytokines (IL-10, TGF-β, IL-6, etc.) but also modulated by M2 macrophage-mediated fibrotic reactions. Collectively, it suggests that fibrotic reactions partly contribute to macrophage-mediated chemoresistance.

7 Antifibrosis therapies explored and tested in glioma

Researchers have explored the antifibrosis therapies in solid tumors, showing definitive sensitization effects for chemotherapy. However, in the presence of the BBB, further research is warranted to determine the efficacy of antifibrosis drugs in sensitizing glioma chemotherapy. In this context, we have summarized the information concerning the utilization of antifibrotic therapies in glioma. According to the existing classifications of antifibrosis therapies by scholars (106), we conclude and discuss antifibrosis therapies in glioma as follows.

7.1 Targeting ECM and ECM modulators

As previously discussed, ECM components could be transformed into pro-tumor phenotypes during tumor progression. This transformation presents numerous viable antifibrosis targets for improving chemotherapy by reducing ECM

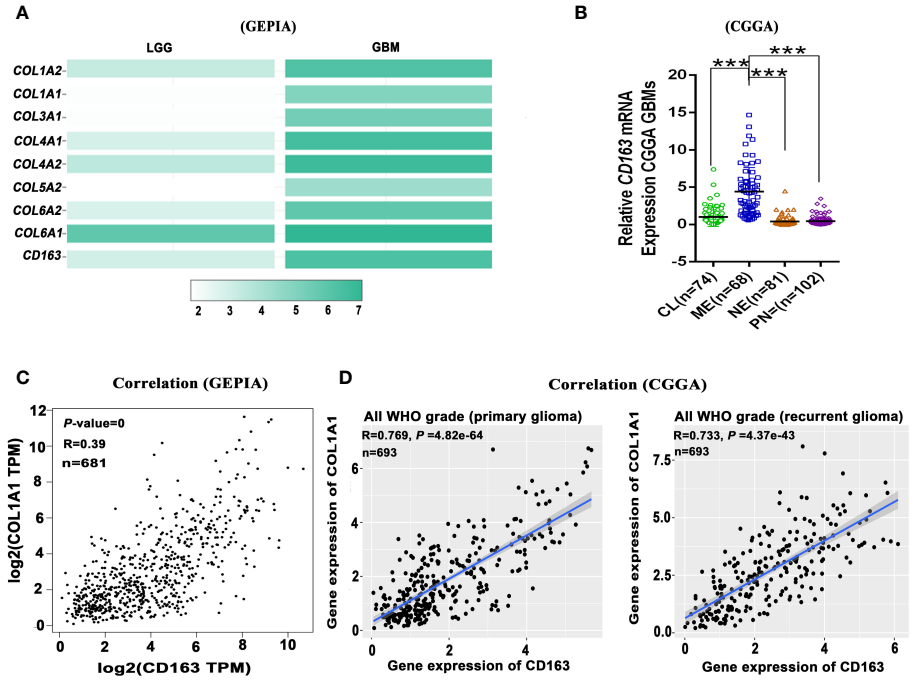

FIGURE 2
Glioma-associated fibrosis positively correlates with the expression of macrophage marker gene *CD163*. **(A)** The expression of fibrosis-related marker genes (*COL1A2, COL1A1, COL3A1, COL4A1, COL4A2, COL5A2, COL6A2, COL6A1*) and M2 macrophage marker gene (*CD163*) in low-grade glioma (LGG) and GBM in the GEPIA dataset. **(B)** Relative *CD163* mRNA expression levels of four GBM subtypes in the CGGA dataset. ***p < 0.001. **(C)** *CD163* expression positively correlates with *COL1A1* expression in all grade glioma (GEPIA). **(D)** *CD163* expression positively correlates with *COL1A1* expression in primary and recurrent glioma (CGGA). (GEPIA dataset includes TCGA LGG and GBM dataset.).

stiffness through downregulated ECM deposition and collagen-modifying enzymes.

Collagen is a prominent component of the ECM, and inhibiting collagen cross-linking has demonstrated significant efficacy in orthotopic GBM mouse models (34). LOX, a kind of collagen cross-linking enzyme, is significantly upregulated during glioma progression due to "cell compaction". Studies indicate that BAPN, a LOX inhibitor, can effectively inhibit the growth of intracranial *PTEN*-null GBM mouse models (34, 107). This suggests that BAPN can be a promising strategy for inhibiting glioma growth, possibly by negatively modulating tumor-associated fibrosis. Similarly, another enzyme involved in the process of collagen cross-linking, procollagen-lysine 2-oxoglutarate 5-dioxygenase 2 (PLOD2), has also been tested in GBM treatment. Elevated PLOD2 expression is significantly associated with GBM proliferation, invasion, metastasis, and poor overall survival (108–110). PLOD2 participates in the formation of tumor-associated fibrosis through promoting EMT transition (111), possibly via FAK (108), and PI3K-Akt (111) signaling pathways. Both *in vivo* and *in vitro* studies have demonstrated that PLOD2 knockdown inhibits the proliferation, invasion, and anchorage-independent growth of GBM (108, 110, 111). Minoxidil, a confirmed PLOD2 inhibitor (112), could suppress tumor metastasis, in part, by reversing collagen cross-linking in ECM (113, 114). Moreover, studies have found that minoxidil cloud increases the antitumor drug permeability of the blood-brain tumor barrier, resulting in improved and selective delivery to brain tumors, including GBM (115, 116). In conclusion, PLOD2 could serve as a viable target against glioma, possibly by normalizing GME with its antifibrosis function, and PLOD2 inhibitors like Minoxidil may offer potential benefits for glioma patients.

7.2 Targeting TGF-β signaling pathway

The TGF-β signaling pathway is recognized as the key signal that mediates tissue fibrosis processes and contributes to cancer progression (117, 118). It has been extensively explored whether repurposing antifibrosis drugs can increase chemotherapy sensitivity by targeting TGF-β signaling.

Antifibrosis drugs such as tranilast, pirfenidone, and losartan have shown encouraging efficacy in cancer treatment. Tranilast, for instance, has been demonstrated to reduce matrix mechanical pressure, lower tissue fluid hydrostatic pressure, and enhance tumor perfusion. And, it can enhance the efficacy of chemotherapy drugs with different molecular sizes, including doxorubicin, paclitaxel, and doxorubicin liposomes, by suppressing TGF-β signaling and expression of ECM components (63). Moreover, the combination of TMZ and tranilast significantly suppresses GBM patient-derived xenografts compared to TMZ

alone (119, 120). Collectively, repurposing tranilast can not only enhance the efficacy of conventional chemotherapy drugs but also improve the effectiveness of antitumor nanomedicines. Similarly, pirfenidone, another antifibrosis drug that has been clinically approved for the treatment of idiopathic pulmonary fibrosis, also exhibits the function of reducing collagen and hyaluronic acid synthesis (33). Pirfenidone is confirmed to inhibit TGF-β expression in malignant glioma cells, indicating its further application as an adjunctive drug to sensitize glioma TMZ chemotherapy (121). Losartan (LOS), an angiotensin receptor blocker, can reduce the production of collagen and hyaluronic acid by downregulating profibrotic signals such as TGF-β1, CCN2, and ET-1 (70). Therefore, LOS may enhance chemotherapy efficacy by upregulating vascular perfusion and reducing the solid-phase pressure in tumors, which improves the delivery of drugs and oxygen to tumors. Additionally, LOS could antagonize the neoangiogenetic, profibrotic, and immunosuppressive effects of angiotensin II and significantly inhibit its stimulatory effects on local estrogen production, suppressing glioma cell growth and alleviating cerebral edema (122, 123). As a cost-effective angiotensin receptor blocker with an established safety profile, LOS can be quickly repurposed as an adjuvant pharmacological tool prospectively for GBM.

Recent studies have indicated that histone deacetylase inhibitors (HDACi) exhibit antifibrotic effects in various experimental models by preventing histone deacetylation, inducing chromatin decondensation and antifibrotic genes upregulation (124, 125). Valproic acid (VPA), an HDACi agent, exerts its antifibrotic effects by upregulating Smad7 and inhibiting the TGF-β/Smad signaling pathway (126). VPA has been found to inhibit fibrosis in experimental models of various diseases, including liver (127), kidney (128), and heart diseases (129), by reducing macrophage infiltration and downregulating the TGF-β signaling pathway. Briefly, VPA exhibits a dual-purpose effect in glioma therapy, as it not only functions as antiepileptics but also sensitizes TMZ chemotherapy in brain tumor patients (130–132). Another HDACi, vorinostat, approved by the U.S. FDA for the treatment of T-cell lymphoma (133), reduces collagen formation and inhibits fibrosis (134). Studies have shown that the combination of vorinostat and TMZ significantly enhances TMZ efficacy for glioma (135, 136). However, it remains unclear whether the enhanced chemosensitivity induced by VPA and vorinostat is partly or mainly modulated by the inhibition of glioma-associated fibrosis.

Interestingly, Chinese traditional medicine with antifibrosis properties also demonstrates its antitumor efficacy. Berberine, an isoquinoline alkaloid present in many traditional Chinese medicines (137), is confirmed to reduce collagen accumulation in pulmonary fibrosis (138), diabetic nephropathy (138), and arthritis (139), the related mechanisms of which may involve inhibiting TGF-β signaling (140) and restraining EMT (141). Moreover, berberine could suppress glioma growth, migration, and invasion by inhibiting COL11A1 expression and also induce programmed cell death through ERK1/2-mediated mitochondrial damage in glioma cells (142). These studies suggest that berberine could inhibit glioma growth possibly through its antifibrosis properties. Therefore, these conventionally approved antifibrosis drugs could be used to sensitize chemotherapy in glioma through inhibition of TGF-β signaling.

7.3 Targeting CAFs

Various antitumor strategies have been developed by directly targeting CAFs (74) including the depletion (73) and normalization of CAFs (143). As for certain cancers, the population of CAFs consists of a collection of multiple subsets of cells with diverse and specific phenotypes at different developmental stages. FAP, a universally acknowledged marker of CAFs, serves as a potential target in both antitumor and antifibrosis therapies. In glioma, FAP expression is detected in glioma cells, mesenchymal cells, and pericytes, etc. (144). Studies have developed an oncolytic adenovirus targeting both GBM cells and GBM-associated stromal FAP^+ cells, highlighting its potential immunotherapy through depleting FAP^+ CAFs (145). Additionally, FAP-targeting CAR-T cells have demonstrated promising efficacy in a mouse xenograft model of GBM (146). Another new CAF phenotype in breast cancer, $CD10^+$ $GPR77^+$ CAFs, has been found to be associated with the acquisition of a chemoresistance phenotype. Targeting $CD10^+$ $GPR77^+$ CAFs has been demonstrated to retard tumor formation and reverse chemoresistance by destroying the survival niches for CSCs in both breast and lung cancers (25). However, apart from FAP^+ CAFs, further research is needed to explore specific CAF phenotypes associated with glioma chemoresistance.

Above all, we summarized the current glioma therapies with different antifibrosis targets (Figure 3, Table 1).

8 Conclusion and future perspective

Collectively, the mechanisms associated with glioma cells chemoresistance development can be attributed to two aspects: chemoresistance-related genetic alterations within glioma cells, and the GME changes contributing to drug resistance. The latter is, in part, induced and modulated by glioma-associated fibrosis, leading to increased tumor stiffness and decreased efficiency of chemotherapeutics delivery to the cancer cell nuclei. The features of the fibrotic GME include the abnormal vascular system, heightened ECM deposition, increased tumor stiffness, upregulated growth factors, etc. We further emphasize the crucial role of glioma-associated fibrotic reactions in glioma progression, prognosis, and chemoresistance. Intense glioma-associated fibrotic reactions positively correlate with poor outcomes in glioma patients, suggesting its clinical significance as both a prognostic indicator and a promising therapeutic target for overcoming glioma chemoresistance. Additionally, we propose a theory that chemotherapy-induced activation of TGF-β signaling could lead to tumor-associated fibrotic reactions in the GME, characterized by increased ECM stiffness. This, in turn, may hinder the penetration of chemotherapeutics into glioma cells. In this review, we emphasize that tumor-associated fibrotic reactions play a role in maintaining glioma stemness, leading to the acquisition of a chemoresistant phenotype (Figure 4). A comprehensive understanding of this mechanism promises new insights into

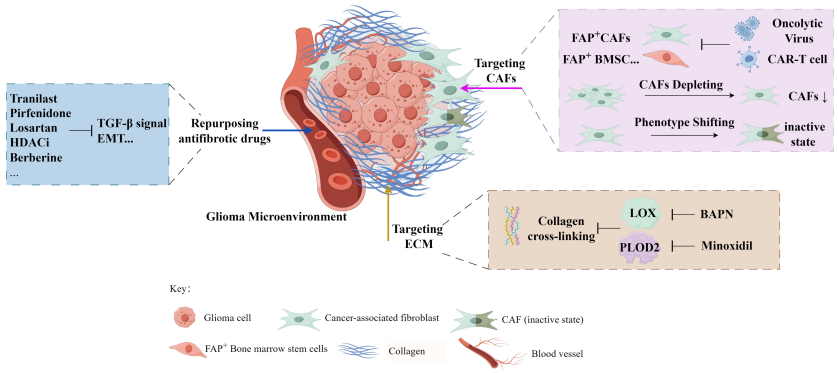

FIGURE 3
The exploration of antifibrosis-related strategies in glioma treatment (*by Figdraw*).

TABLE 1 Drugs with antifibrosis function are utilized and tested in the treatment of solid tumors including glioblastoma.

Drug Name	Conditions	Highest Status (phase)	NCT	Status	Sample size
Pirfenidone	**Non-small cell lung cancer**	**II**	**NCT04467723**	**Recruiting**	**25**
Tranilast	**Nasopharyngeal carcinoma**	**II**	**NCT05626829**	**Recruiting**	**18**
BAPN	**Glioblastoma**	**Preclinical**	-	-	-
Minoxidil	**Ovarian cancer**	**II**	**NCT05272462**	**Recruiting**	**34**
Losartan	**Glioblastoma**	**III**	**NCT01805453**	**Completed**	**80**
Valproic acid	**Glioblastoma**	**III**	**NCT03243461**	**Recruiting**	**167**
Vorinostat	**High-grade glioma**	**III**	**NCT01236560**	**Completed**	**101**
Berberine	**Non-small cell lung cancer**	**II**	**NCT03486496**	**Unknown**	**50**

effectively reversing chemoresistance. This review underscores the urgent need to decipher the complex relationship between glioma-associated fibrosis and chemotherapy sensitivity, providing a promising strategy to develop more effective interventions for glioma.

Despite our extensive summarization of numerous studies on how tumor-associated fibrosis facilitates chemoresistance, the exact molecular mechanisms still remain elusive in glioma. Therefore, in the future, it's warranted to explore which molecular characteristics of

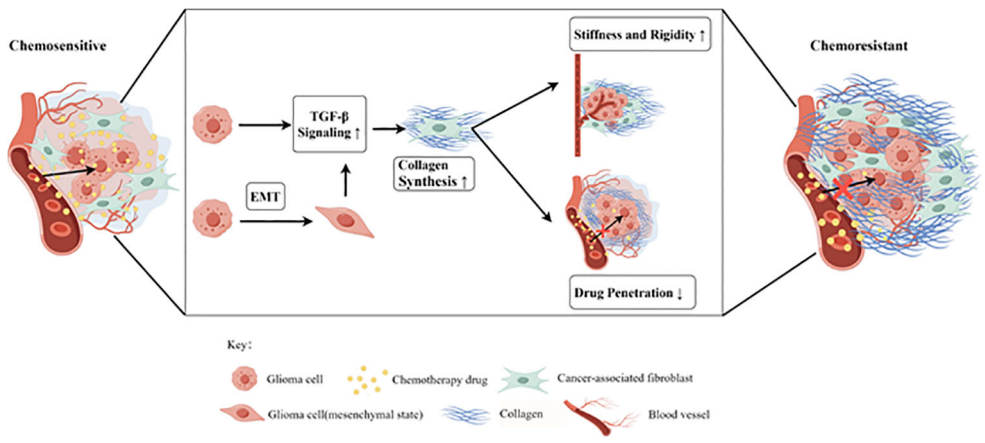

FIGURE 4
The tumor-associated fibrosis aggravates glioma chemoresistance by reducing the efficacy of drug delivery (*by Figdraw*). The TGF-β signaling pathway could be upregulated in glioma after chemotherapy and epithelial-mesenchymal transition (EMT), resulting in the increased collagen synthesis of cancer-associated fibroblasts (CAFs). In the tumor microenvironment (TME), the tumor-associated fibrosis increased the stiffness and rigidity of glioma tissues which in turn impairs the delivery of chemotherapeutic drugs to cancer cells, thus promoting chemoresistance.

glioma are more likely to develop fibrosis, and whether the ECM stiffness promotes the expression of chemoresistance-related proteins in glioma. Such insights would contribute to a deeper understanding of the interactions among these various chemoresistance mechanisms, potentially unveiling novel strategies to overcome chemoresistance. In addition to therapeutic agents directly targeting cancer cells, several innovative drugs are under investigation for their potential to overcome chemoresistance through modulating the TME. The antifibrosis therapy for solid tumors is one of the TME normalization strategies, with some showing significant tumor inhibition effects. Numerous studies have suggested that targeting CAFs and fibrosis with conventional clinically approved agents can enhance the chemosensitivity of solid tumors. However, further in-depth research is required to determine their efficacy specifically in the context of glioma treatment.

Author contributions

JX: Writing – review & editing, Writing – original draft. JZ: Writing – review & editing. WC: Visualization, Writing – review & editing. XN: Writing – review & editing.

Funding

The author(s) declare financial support was received for the research, authorship, and/or publication of this article. This study was funded by President Foundation of Zhujiang Hospital, Southern Medical University (yzjj2022qn06).

Conflict of interest

The authors declare that the research was conducted in the absence of any commercial or financial relationships that could be construed as a potential conflict of interest.

Publisher's note

References

1. Stupp R, Mason WP, van den Bent MJ, Weller M, Fisher B, Taphoorn MJ, et al. Radiotherapy plus concomitant and adjuvant temozolomide for glioblastoma. *N Engl J Med*. (2005) 352:987–96. doi: 10.1056/NEJMoa043330

2. Menna G, Mattogno PP, Donzelli CM, Lisi L, Olivi A, Della Pepa GM. Glioma-associated microglia characterization in the glioblastoma microenvironment through a 'Seed-and soil' Approach: a systematic review. *Brain Sci*. (2022) 12(6):718. doi: 10.3390/brainsci12060718

3. Stupp R, Hegi ME, Mason WP, van den Bent MJ, Taphoorn MJ, Janzer RC, et al. Effects of radiotherapy with concomitant and adjuvant temozolomide versus radiotherapy alone on survival in glioblastoma in a randomised phase III study: 5-year analysis of the EORTC-NCIC trial. *Lancet Oncol*. (2009) 10:459–66. doi: 10.1016/S1470-2045(09)70025-7

4. Ou A, Yung WKA, Majd N. Molecular mechanisms of treatment resistance in glioblastoma. *Int J Mol Sci*. (2020) 22(1):351. doi: 10.3390/ijms22010351

5. Zhang G, Tao X, Ji B, Gong J. Hypoxia-driven M2-polarized macrophages facilitate cancer aggressiveness and temozolomide resistance in glioblastoma. *Oxid Med Cell Longev*. (2022) 2022:1614336. doi: 10.1155/2022/1614336

6. Fidoamore A, Cristiano L, Antonosante A, d'Angelo M, Di Giacomo E, Astarita C, et al. Glioblastoma stem cells microenvironment: the paracrine roles of the niche in drug and radioresistance. *Stem Cells Int*. (2016) 2016:6809105. doi: 10.1155/2016/6809105

7. Kenig S, Faoro V, Bourkoula E, Podergajs N, Ius T, Vindigni M, et al. Topoisomerase IIβ mediates the resistance of glioblastoma stem cells to replication stress-inducing drugs. *Cancer Cell Int*. (2016) 16:58. doi: 10.1186/s12935-016-0339-9

8. Li J, Kaneda MM, Ma J, Li M, Shepard RM, Patel K, et al. PI3Kγ inhibition suppresses microglia/TAM accumulation in glioblastoma microenvironment to promote exceptional temozolomide response. *Proc Natl Acad Sci U.S.A*. (2021) 118 (16):e2009290118. doi: 10.1073/pnas.2009290118

9. Li I, Nabet BY. Exosomes in the tumor microenvironment as mediators of cancer therapy resistance. *Mol Cancer*. (2019) 18:32. doi: 10.1186/s12943-019-0975-5

10. Caponnetto F, Dalla E, Mangoni D, Piazza S, Radovic S, Ius T, et al. he miRNA content of exosomes released from the glioma microenvironment can affect Malignant progression. *Biomedicines*. (2020) 8(12):564. doi: 10.3390/biomedicines8120564

11. Chen P, Zhao D, Li J, Liang X, Li J, Chang A, et al. Symbiotic macrophage-glioma cell interactions reveal synthetic lethality in PTEN-null glioma. *Cancer Cell*. (2019) 35:868–84.e6. doi: 10.1016/j.ccell.2019.05.003

12. Mentlein R, Hattermann K, Hemion C, Jungbluth AA, Held-Feindt J. Expression and role of the cell surface protease seprase/fibroblast activation protein-α (FAP-α) in astroglial tumors. *Biol Chem*. (2011) 392:199–207. doi: 10.1515/bc.2010.119

13. Ye XZ, Xu SL, Xin YH, Yu SC, Ping YF, Chen L, et al. Tumor-associated microglia/macrophages enhance the invasion of glioma stem-like cells via TGF-β1 signaling pathway. *J Immunol*. (2012) 189:444–53. doi: 10.4049/jimmunol.1103248

14. Lakins MA, Ghorani E, Munir H, Martins CP, Shields JD. Cancer-associated fibroblasts induce antigen-specific deletion of CD8 (+) T Cells to protect tumour cells. *Nat Commun*. (2018) 9:948. doi: 10.1038/s41467-018-03347-0

15. Xu C, Zhao Y, Wu C, Li L. Repurposing drugs for the treatment of glioma. *Glioma*.(2019) 2:159–64. doi: 10.4103/glioma.glioma_26_19

16. Cox TR. The matrix in cancer. *Nat Rev Cancer*. (2021) 21:217–38. doi: 10.1038/s41568-020-00329-7

17. Yuan Z, Li Y, Zhang S, Wang X, Dou H, Yu X, et al. Extracellular matrix remodeling in tumor progression and immune escape: from mechanisms to treatments. *Mol Cancer*. (2023) 22:48. doi: 10.1186/s12943-023-01744-8

18. Bonnans C, Chou J, Werb Z. Remodelling the extracellular matrix in development and disease. *Nat Rev Mol Cell Biol*. (2014) 15:786–801. doi: 10.1038/nrm3904

19. Winkler J, Abisoye-Ogunniyan A, Metcalf KJ, Werb Z. Concepts of extracellular matrix remodelling in tumour progression and metastasis. *Nat Commun*. (2020) 11:5120. doi: 10.1038/s41467-020-18794-x

20. Mohan V, Das A, Sagi I. Emerging roles of ECM remodeling processes in cancer. *Semin Cancer Biol*. (2020) 62:192–200. doi: 10.1016/j.semcancer.2019.09.004

21. Wu JS, Sheng SR, Liang XH, Tang YL. The role of tumor microenvironment in collective tumor cell invasion. *Future Oncol*. (2017) 13:991–1002. doi: 10.2217/fon-2016-0501

22. Chen X, Song E. The theory of tumor ecosystem. *Cancer Commun (Lond)*. (2022) 42:587–608. doi: 10.1002/cac2.12316

23. Chen Z, Zhuo S, He G, Tang J, Hao W, Gao WQ, et al. Prognosis and immunotherapy significances of a cancer-associated fibroblasts-related gene signature in gliomas. *Front Cell Dev Biol*. (2021) 9:721897. doi: 10.3389/fcell.2021.721897

24. Oleynikova NA, Danilova NV, Mikhailov IA, Semina EV, Malkov PG. [Cancer-associated fibroblasts and their significance in tumor progression]. *Arkh Patol*. (2020) 82:68–77. doi: 10.17116/patol20208201168

25. Su S, Chen J, Yao H, Liu J, Yu S, Lao L, et al. CD10(+)GPR77(+) cancer-associated fibroblasts promote cancer formation and chemoresistance by sustaining cancer stemness. *Cell*.(2018) 172(4):841–56.e16. doi: 10.1016/j.cell.2018.01.009

26. Hanahan D, Weinberg RA. Hallmarks of cancer: the next generation. *Cell*.(2011) 144:646–74. doi: 10.1016/j.cell.2011.02.013

27. Lambrechts D, Wauters E, Boeckx B, Aibar S, Nittner D, Burton O, et al. Phenotype molding of stromal cells in the lung tumor microenvironment. *Nat Med*. (2018) 24:1277–89. doi: 10.1038/s41591-018-0096-5

28. Santi A, Kugeratski FG, Zanivan S. Cancer associated fibroblasts: the architects of stroma remodeling. *Proteomics*. (2018) 18:e1700167. doi: 10.1002/pmic.201700167

29. Yeldag G, Rice A, Del Río Hernández A. Chemoresistance and the self-maintaining tumor microenvironment. *Cancers (Basel)*. (2018) 10(12):471. doi: 10.3390/cancers10120471

30. Xu S, Xu H, Wang W, Li S, Li H, Li T, et al. The role of collagen in cancer: from bench to bedside. *J Transl Med*. (2019) 17:309. doi: 10.1186/s12967-019-2058-1

31. Ricard-Blum S. The collagen family. *Cold Spring Harb Perspect Biol*. (2011) 3: a004978. doi: 10.1101/cshperspect.a004978

32. Ohlund D, Lundin C, Ardnor B, Oman M, Naredi P, Sund M. Type IV collagen is a tumour stroma-derived biomarker for pancreas cancer. *Br J Cancer*. (2009) 101:91–7. doi: 10.1038/sj.bjc.6605107

33. Kast RE, Skuli N, Karpel-Massler G, Frosina G, Ryken T, Halatsch ME. Blocking epithelial-to-mesenchymal transition in glioblastoma with a sextet of repurposed drugs: the EIS regimen. *Oncotarget*.(2017) 8:60727–49. doi: 10.18632/oncotarget.v8i37

34. Mammoto T, Jiang A, Jiang E, Panigrahy D, Kieran MW, Mammoto A. Role of collagen matrix in tumor angiogenesis and glioblastoma multiforme progression. *Am J Pathol*. (2013) 183:1293–305. doi: 10.1016/j.ajpath.2013.06.026

35. Jia W, Jiang X, Liu W, Wang L, Zhu B, Zhu H, et al. Effects of three-dimensional collagen scaffolds on the expression profiles and biological functions of glioma cells. *Int J Oncol*. (2018) 52:1787–800doi: 10.3892/ijo

36. Qiu S, Deng L, Liao X, Nie L, Qi F, Jin K, et al. Tumor-associated macrophages promote bladder tumor growth through PI3K/AKT signal induced by collagen. *Cancer Sci*. (2019) 110:2110–8. doi: 10.1111/cas.14078

37. Calori IR, Alves SR, Bi H. Type-I collagen/collagenase modulates the 3D structure and behavior of glioblastoma spheroid. *Models*.(2022) 5:723–33. doi: 10.1021/acsabm.1c01138

38. Huijbers IJ, Iravani M, Popov S, Robertson D, Al-Sarraj S, Jones C, et al. A role for fibrillar collagen deposition and the collagen internalization receptor endo180 in glioma invasion. *PloS One*. (2010) 5:e9808. doi: 10.1371/journal.pone.0009808

39. Phillips HS, Kharbanda S, Chen R, Forrest WF, Soriano RH, Wu TD, et al. Molecular subclasses of high-grade glioma predict prognosis, delineate a pattern of disease progression, and resemble stages in neurogenesis. *Cancer Cell*. (2006) 9:157–73. doi: 10.1016/j.ccr.2006.02.019

40. Wienke D, Davies GC, Johnson DA, Sturge J, Lambros MB, Savage K, et al. The collagen receptor Endo180 (CD280) Is expressed on basal-like breast tumor cells and promotes tumor growth *in vivo*. *Cancer Res*. (2007) 67:10230–40. doi: 10.1158/0008-5472.CAN-06-3496

41. Grässel S, Bauer RJ. Collagen XVI in health and disease. *Matrix Biol*. (2013) 32:64–73. doi: 10.1016/j.matbio.2012.11.001

42. Bauer R, Ratzinger S, Wales L, Bosserhoff A, Senner V, Grifka J, et al. Inhibition of collagen XVI expression reduces glioma cell invasiveness. *Cell Physiol Biochem*. (2011) 27:217–26. doi: 10.1159/000327947

43. Chan TS, Shaked Y, Tsai KK. Targeting the interplay between cancer fibroblasts, mesenchymal stem cells, and cancer stem cells in desmoplastic cancers. *Front Oncol*. (2019) 9:688doi: 10.3389/fonc.2019.00688

44. Yu Q, Xue Y, Liu J, Xi Z, Li Z, Liu Y. Fibronectin promotes the Malignancy of glioma stem-like cells via modulation of cell adhesion, differentiation, proliferation and chemoresistance. *Front Mol Neurosci*. (2018) 11:130. doi: 10.3389/fnmol.2018.00130

45. Staberg M, Rasmussen RD, Michaelsen SR, Pedersen H, Jensen KE, Villingshøj M, et al. Targeting glioma stem-like cell survival and chemoresistance through inhibition of lysine-specific histone demethylase KDM2B. *Mol Oncol*. (2018) 12:406–20. doi: 10.1002/1878-0261.12174

46. Natsume A, Ishii D, Wakabayashi T, Tsuno T, Hatano H, Mizuno M, et al. IFN-beta down-regulates the expression of DNA repair gene MGMT and sensitizes resistant glioma cells to temozolomide. *Cancer Res*. (2005) 65:7573–9. doi: 10.1158/0008-5472.CAN-05-0036

47. Shen D, Guo CC, Wang J, Qiu ZK, Sai K, Yang QY, et al. Interferon-α/β enhances temozolomide activity against MGMT-positive glioma stem-like cells. *Oncol Rep*. (2015) 34:2715–21. doi: 10.3892/or.2015.4232

48. Schiffer D, Annovazzi L, Casalone C, Corona C. Glioblastoma: microenvironment and niche concept. *Cancers (Basel)*. (2018) 11(1):5. doi: 10.3390/cancers11010005

49. Scanlan MJ, Raj BK, Calvo B, Garin-Chesa P, Sanz-Moncasi MP, Healey JH, et al. Molecular cloning of fibroblast activation protein alpha, a member of the serine protease family selectively expressed in stromal fibroblasts of epithelial cancers. *Proc Natl Acad Sci U S A*. (1994) 91:5657–61. doi: 10.1073/pnas.91.12.5657

50. Juillerat-Jeanneret L, Tafelmeyer P, Golshayan D. Fibroblast activation protein-α in fibrogenic disorders and cancer: more than a prolyl-specific peptidase? *Expert Opin Ther Targets*. (2017) 21:977–91doi: 10.1080/14728222.2017.1370455

51. Li M, Li M, Yin T, Shi H, Wen Y, Zhang B, et al. Targeting of cancer–associated fibroblasts enhances the efficacy of cancer chemotherapy by regulating the tumor microenvironment. *Mol Med Rep*. (2016) 13:2476–84. doi: 10.3892/mmr.2016.4868

52. Ma Q, Long W, Xing C, Chu J, Luo M, Wang HY, et al. Cancer stem cells and immunosuppressive microenvironment in glioma. *Front Immunol*. (2018) 9:2924. doi: 10.3389/fimmu.2018.02924

53. Han J, Alvarez-Breckenridge CA, Wang QE, Yu J. TGF-β signaling and its targeting for glioma treatment. *Am J Cancer Res*. (2015) 5(3):945–55.

54. Zeng H, Yang Z, Xu N, Liu B, Fu Z, Lian C, et al. Connective tissue growth factor promotes temozolomide resistance in glioblastoma through TGF-β1-dependent activation of Smad/ERK signaling. *Cell Death Dis*. (2017) 8:e2885. doi: 10.1038/cddis.2017.248

55. Theocharis AD, Skandalis SS, Gialeli C, Karamanos NK. Extracellular matrix structure. *Adv Drug Delivery Rev*. (2016) 97:4–27. doi: 10.1016/j.addr.2015.11.001

56. Stylianopoulos T, Poh MZ, Insin N, Bawendi MG, Fukumura D, Munn LL, et al. Diffusion of particles in the extracellular matrix: the effect of repulsive electrostatic interactions. *Biophys J*. (2010) 99:1342–9. doi: 10.1016/j.bpj.2010.06.016

57. Tannock IF, Rotin D. Acid pH in tumors and its potential for therapeutic exploitation. *Cancer Res*. (1989) 49:4373–84.

58. Mueller S, Sandrin L. Liver stiffness: a novel parameter for the diagnosis of liver disease. *Hepat Med*. (2010) 2:49–67. doi: 10.2147/HMER

59. Levental KR, Yu H, Kass L, Lakins JN, Egeblad M, Erler JT, et al. Matrix crosslinking forces tumor progression by enhancing integrin signaling. *Cell*.(2009) 139:891–906. doi: 10.1016/j.cell.2009.10.027

60. Lu P, Weaver VM, Werb Z. The extracellular matrix: a dynamic niche in cancer progression. *J Cell Biol*. (2012) 196:395–406. doi: 10.1083/jcb.201102147

61. Haining AWM, Rahikainen R, Cortes E, Lachowski D, Rice A, von Essen M, et al. Mechanotransduction in talin through the interaction of the R8 domain with DLC1. *PloS Biol*. (2018) 16:e2005599. doi: 10.1371/journal.pbio.2005599

62. Lachowski D, Cortes E, Robinson B, Rice A, Rombouts K, Del Río Hernández AE. FAK controls the mechanical activation of YAP, a transcriptional regulator required for durotaxis. *FASEB J*. (2018) 32:1099–107. doi: 10.1096/fj.201700721R

63. Papageorgis P, Polydorou C, Mpekris F, Voutouri C, Agathokleous E, Kapnissi-Christodoulou CP, et al. Tranilast-induced stress alleviation in solid tumors improves the efficacy of chemo- and nanotherapeutics in a size-independent manner. *Sci Rep*. (2017) 7:46140. doi: 10.1038/srep46140

64. Naik A, Leask A. Tumor-associated fibrosis impairs the response to immunotherapy. *Matrix Biol*. (2023) 119:125–40doi: 10.1016/j.matbio.2023.04.002

65. Mascheroni P, López Alfonso JC, Kalli M, Stylianopoulos T, Meyer-Hermann M, Hatzikirou H. On the impact of chemo-mechanically induced phenotypic transitions in gliomas. *Cancers (Basel)*. (2019) 11(5):716. doi: 10.3390/cancers11050716

66. Stylianopoulos T, Martin JD, Chauhan VP, Jain SR, Diop-Frimpong B, Bardeesy N, et al. Causes, consequences, and remedies for growth-induced solid stress in murine and human tumors. *Proc Natl Acad Sci U S A*. (2012) 109:15101–8. doi: 10.1073/pnas.1213353109

67. Tajaldini M, Poorkhani A, Amiriani T, Amiriani A, Javid H, Aref P, et al. Strategy of targeting the tumor microenvironment via inhibition of fibroblast/fibrosis remodeling new era to cancer chemo-immunotherapy resistance. *Eur J Pharmacol*. (2023) 957:175991. doi: 10.1016/j.ejphar.2023.175991

68. Hauge A, Rofstad EK. Antifibrotic therapy to normalize the tumor microenvironment. *J Transl Med*. (2020) 18:207. doi: 10.1186/s12967-020-02376-y

69. Zhang B, Jiang T, Shen S, She X, Tuo Y, Hu Y, et al. Cyclopamine disrupts tumor extracellular matrix and improves the distribution and efficacy of nanotherapeutics in pancreatic cancer. *Biomaterials*.(2016) 103:12–21. doi: 10.1016/j.biomaterials.2016.06.048

70. Chauhan VP, Martin JD, Liu H, Lacorre DA, Jain SR, Kozin SV, et al. Angiotensin inhibition enhances drug delivery and potentiates chemotherapy by decompressing tumour blood vessels. *Nat Commun*. (2013) 4:2516. doi: 10.1038/ncomms3516

71. Polydorou C, Mpekris F, Papageorgis P, Voutouri C, Stylianopoulos T. Pirfenidone normalizes the tumor microenvironment to improve chemotherapy. *Oncotarget*.(2017) 8:24506–17. doi: 10.18632/oncotarget.v8i15

72. Guo J, Zeng H, Chen Y. Emerging nano drug delivery systems targeting cancer-associated fibroblasts for improved antitumor effect and tumor drug penetration. *Mol Pharm*. (2020) 17:1028–48. doi: 10.1021/acs.molpharmaceut.0c00014

73. Miao L, Liu Q, Lin CM, Luo C, Wang Y, Liu L, et al. Targeting tumor-associated fibroblasts for therapeutic delivery in desmoplastic tumors. *Cancer Res*. (2017) 77:719–31. doi: 10.1158/0008-5472.CAN-16-0866

74. Chen X, Song E. Turning foes to friends: targeting cancer-associated fibroblasts. *Nat Rev Drug Discovery*. (2019) 18:99–115. doi: 10.1038/s41573-018-0004-1

75. Moreira RK. Hepatic stellate cells and liver fibrosis. *Arch Pathol Lab Med*. (2007) 131:1728–34. doi: 10.5858/2007-131-1728-HSCALF

76. Zhou W, Yu X, Sun S, Zhang X, Yang W, Zhang J, et al. Increased expression of MMP-2 and MMP-9 indicates poor prognosis in glioma recurrence. *BioMed Pharmacother*. (2019) 118:109369. doi: 10.1016/j.biopha.2019.109369

77. Sun ZF, Wang L, Gu F, Fu L, Li WL, Ma YJ. [Expression of Notch1, MMP-2 and MMP-9 and their significance in glioma patients]. *Zhonghua Zhong Liu Za Zhi*. (2012) 34:26–30.

78. Sun C, Wang Q, Zhou H, Yu S, Simard AR, Kang C, et al. Antisense MMP-9 RNA inhibits Malignant glioma cell growth *in vitro* and *in vivo*. *Neurosci Bull*. (2013) 29:83–93. doi: 10.1007/s12264-012-1296-5

79. Lakka SS, Jasti SL, Gondi C, Boyd D, Chandrasekar N, Dinh DH, et al. Downregulation of MMP-9 in ERK-mutated stable transfectants inhibits glioma invasion *in vitro*. *Oncogene*. (2002) 21:5601–8. doi: 10.1038/sj.onc.1205646

80. Lee EJ, Kim SY, Hyun JW, Min SW, Kim DH, Kim HS. Glycitein inhibits glioma cell invasion through down-regulation of MMP-3 and MMP-9 gene expression. *Chem Biol Interact*. (2010) 185:18–24. doi: 10.1016/j.cbi.2010.02.037

81. Yeh WL, Lu DY, Lee MJ, Fu WM. Leptin induces migration and invasion of glioma cells through MMP-13 production. *Glia*. (2009) 57:454–64. doi: 10.1002/glia.20773

82. Wang L, Yuan J, Tu Y, Mao X, He S, Fu G, et al. Co-expression of MMP-14 and MMP-19 predicts poor survival in human glioma. *Clin Transl Oncol*. (2013) 15:139–45. doi: 10.1007/s12094-012-0900-5

83. Guo JG, Guo CC, He ZQ, Cai XY, Mou YG. High MMP-26 expression in glioma is correlated with poor clinical outcome of patients. *Oncol Lett*. (2018) 16:2237–42. doi: 10.3892/ol

84. Wang X, Chen X, Sun L, Bi X, He H, Chen L, et al. The function of MMP-28/TGF-β induced cell apoptosis in human glioma cells. *Exp Ther Med*. (2018) 16:2867–74. doi: 10.3892/etm

85. Li L, Du Y, Xiang D, Chen L, Shi Z, Tian J, et al. Prediction of the anti-glioma therapeutic effects of temozolomide through *in vivo* molecular imaging of MMP expression. *BioMed Opt Express*. (2018) 9:3193–207. doi: 10.1364/BOE.9.003193

86. Heerboth S, Housman G, Leary M, Longacre M, Byler S, Lapinska K, et al. EMT and tumor metastasis. *Clin Transl Med*. (2015) 4:6. doi: 10.1186/s40169-015-0048-3

87. Hanahan D, Coussens LM. Accessories to the crime: functions of cells recruited to the tumor microenvironment. *Cancer Cell*. (2012) 21:309–22. doi: 10.1016/j.ccr.2012.02.022

88. Costanza B, Umelo IA, Bellier J, Castronovo V, Turtoi A. Stromal modulators of TGF-β in cancer. *J Clin Med*. (2017) 6(1):7. doi: 10.3390/jcm6010007

89. Adorno M, Cordenonsi M, Montagner M, Dupont S, Wong C, Hann B, et al. A Mutant-p53/Smad complex opposes p63 to empower TGFbeta-induced metastasis. *Cell*.(2009) 137:87–98. doi: 10.1016/j.cell.2009.01.039

90. Leight JL, Wozniak MA, Chen S, Lynch ML, Chen CS. Matrix rigidity regulates a switch between TGF-β1-induced apoptosis and epithelial-mesenchymal transition. *Mol Biol Cell*. (2012) 23:781–91. doi: 10.1091/mbc.e11-06-0537

91. Erdogan B, Webb DJ. Cancer-associated fibroblasts modulate growth factor signaling and extracellular matrix remodeling to regulate tumor metastasis. *Biochem Soc Trans*. (2017) 45:229–36. doi: 10.1042/BST20160387

92. Wainwright DA, Chang AL, Dey M, Balyasnikova IV, Kim CK, Tobias A, et al. Durable therapeutic efficacy utilizing combinatorial blockade against IDO, CTLA-4, and PD-L1 in mice with brain tumors. *Clin Cancer Res*. (2014) 20:5290–301. doi: 10.1158/1078-0432.CCR-14-0514

93. Rao R, Han R, Ogurek S, Xue C, Wu LM, Zhang L, et al. Glioblastoma genetic drivers dictate the function of tumor-associated macrophages/microglia and responses to CSF1R inhibition. *Neuro Oncol*. (2022) 24:584–97. doi: 10.1093/neuonc/noab228

94. Quail DF, Bowman RL, Akkari L, Quick ML, Schuhmacher AJ, Huse JT, et al. The tumor microenvironment underlies acquired resistance to CSF-1R inhibition in gliomas. *Science*. (2016) 352:aad3018doi: 10.1126/science.aad3018

95. Yang F, He Z, Duan H, Zhang D, Li J, Yang H, et al. Synergistic immunotherapy of glioblastoma by dual targeting of IL-6 and CD40. *Nat Commun*. (2021) 12:3424. doi: 10.1038/s41467-021-23832-3

96. Pan Y, Smithson LJ, Ma Y, Hambardzumyan D, Gutmann DH. Ccl5 establishes an autocrine high-grade glioma growth regulatory circuit critical for mesenchymal glioblastoma survival. *Oncotarget*. (2017) 8:32977–89. doi: 10.18632/oncotarget.v8i20

97. Zhang XN, Yang KD, Chen C, He ZC, Wang QH, Feng H, et al. Pericytes augment glioblastoma cell resistance to temozolomide through CCL5-CCR5 paracrine signaling. *Cell Res*. (2021) 31(10):1072–87. doi: 10.1038/s41422-021-00528-3

98. Gilkes DM, Semenza GL, Wirtz D. Hypoxia and the extracellular matrix: drivers of tumour metastasis. *Nat Rev Cancer*. (2014) 14:430–9. doi: 10.1038/nrc3726

99. Grout JA, Sirven P, Leader AM, Maskey S, Hector E, Puisieux I, et al. Spatial positioning and matrix programs of cancer-associated fibroblasts promote T-cell exclusion in human lung tumors. *Cancer Discov*. (2022) 12(11):2606–25. doi: 10.1158/2159-8290.CD-21-1714

100. Verhaak RG, Hoadley KA, Purdom E, Wang V, Qi Y, Wilkerson MD, et al. Integrated genomic analysis identifies clinically relevant subtypes of glioblastoma characterized by abnormalities in PDGFRA, IDH1, EGFR, and NF1. *Cancer Cell*. (2010) 17:98–110. doi: 10.1016/j.ccr.2009.12.020

101. Jia D, Li S, Li D, Xue H, Yang D, Liu Y. Mining TCGA database for genes of prognostic value in glioblastoma microenvironment. *Aging (Albany NY)*. (2018) 10:592–605. doi: 10.18632/aging.v10i4

102. Buechler MB, Fu W, Turley SJ. Fibroblast-macrophage reciprocal interactions in health, fibrosis, and cancer. *Immunity*.(2021) 54:903–15. doi: 10.1016/j.immuni.2021.04.021

103. Ni X, Wu W, Sun X, Ma J, Yu J, He X, et al. Interrogating glioma-M2 macrophage interactions identifies Gal-9/Tim-3 as a viable target against PTEN-null glioblastoma. *Sci Adv*. (2022) 8(27):eabl5165. doi: 10.1126/sciadv.abl5165

104. Schafer S, Viswanathan S, Widjaja AA, Lim WW, Moreno-Moral A, DeLaughter DM, et al. IL-11 is a crucial determinant of cardiovascular fibrosis. *Nature*.(2017) 552:110–5. doi: 10.1038/nature24676

105. Tong X, Zhang S, Wang D, Zhang L, Huang J, Zhang T, et al. Azithromycin attenuates bleomycin-induced pulmonary fibrosis partly by inhibiting the expression of LOX and LOXL-2. *Front Pharmacol*. (2021) 12:709819. doi: 10.3389/fphar.2021.709819

106. Piersma B, Hayward MK, Weaver VM. Fibrosis and cancer: A strained relationship. *Biochim Biophys Acta Rev Cancer*. (2020) 1873:188356. doi: 10.1016/j.bbcan.2020.188356

107. Laczko R, Szauter KM, Jansen MK, Hollosi P, Muranyi M, Molnar J, et al. Active lysyl oxidase (LOX) correlates with focal adhesion kinase (FAK)/paxillin activation and migration in invasive astrocytes. *Neuropathol Appl Neurobiol*. (2007) 33:631–43. doi: 10.1111/j.1365-2990.2007.00858.x

108. Xu Y, Zhang L, Wei Y, Zhang X, Xu R, Han M, et al. Procollagen-lysine 2-oxoglutarate 5-dioxygenase 2 promotes hypoxia-induced glioma migration and invasion. *Oncotarget*. (2017) 8:23401–13. doi: 10.18632/oncotarget.v8i14

109. Dong S, Nutt CL, Betensky RA, Stemmer-Rachamimov AO, Denko NC, Ligon KL, et al. Histology-based expression profiling yields novel prognostic markers in human glioblastoma. *J Neuropathol Exp Neurol*. (2005) 64:948–55. doi: 10.1097/01.jnen.0000186940.14779.90

110. Kreße N, Schröder H, Stein KP, Wilkens L, Mawrin C, Sandalcioglu IE, et al. PLOD2 is a prognostic marker in glioblastoma that modulates the immune microenvironment and tumor progression. *Int J Mol Sci*. (2022) 23(11):6037. doi: 10.3390/ijms23116037

111. Song Y, Zheng S, Wang J, Long H, Fang L, Wang G, et al. Hypoxia-induced PLOD2 promotes proliferation, migration and invasion via PI3K/Akt signaling in glioma. *Oncotarget*. (2017) 8:41947–62. doi: 10.18632/oncotarget.v8i26

112. Lan J, Zhang S, Zheng L, Long X, Chen J, Liu X, et al. PLOD2 promotes colorectal cancer progression by stabilizing USP15 to activate the AKT/mTOR signaling pathway. *Cancer Sci*. (2023) 114(8):3190–202. doi: 10.1111/cas.15851

113. Eisinger-Mathason TS, Zhang M, Qiu Q, Skuli N, Nakazawa MS, Karakasheva T, et al. Hypoxia-dependent modification of collagen networks promotes sarcoma metastasis. *Cancer Discovery*. (2013) 3:1190–205. doi: 10.1158/2159-8290.CD-13-0118

114. Zuurmond AM, van der Slot-Verhoeven AJ, van Dura EA, De Groot J, Bank RA. Minoxidil exerts different inhibitory effects on gene expression of lysyl hydroxylase 1, 2, and 3: implications for collagen cross-linking and treatment of fibrosis. *Matrix Biol*. (2005) 24:261–70. doi: 10.1016/j.matbio.2005.04.002

115. Ningaraj NS, Sankpal UT, Khaitan D, Meister EA, Vats T. Activation of KATP channels increases anticancer drug delivery to brain tumors and survival. *Eur J Pharmacol*. (2009) 602:188–93. doi: 10.1016/j.ejphar.2008.10.056

116. Gu YT, Xue YX, Wang YF, Wang JH, Chen X, ShangGuan QR, et al. Minoxidil sulfate induced the increase in blood-brain tumor barrier permeability through ROS/RhoA/PI3K/PKB signaling pathway. *Neuropharmacology*.(2013) 75:407–15. doi: 10.1016/j.neuropharm.2013.08.004

117. Quante M, Tu SP, Tomita H, Gonda T, Wang SS, Takashi S, et al. Bone marrow-derived myofibroblasts contribute to the mesenchymal stem cell niche and promote tumor growth. *Cancer Cell*. (2011) 19:257–72. doi: 10.1016/j.ccr.2011.01.020

118. Shi X, Young CD, Zhou H, Wang X. Transforming growth factor-β Signaling in fibrotic diseases and cancer-associated fibroblasts. *Biomolecules*. (2020) 10(12):1666. doi: 10.3390/biom10121666

119. Gao L, Huang S, Zhang H, Hua W, Xin S, Cheng L, et al. Suppression of glioblastoma by a drug cocktail reprogramming tumor cells into neuronal like cells. *Sci Rep*. (2019) 9(1):3462. doi: 10.1038/s41598-019-39852-5

120. Khazaei M, Pazhouhi M, Khazaei S. Temozolomide and tranilast synergistic antiproliferative effect on human glioblastoma multiforme cell line (U87MG). *Med J Islam Repub Iran*. (2019) 33:39. doi: 10.47176/mjiri

121. Burghardt I, Tritschler F, Opitz CA, Frank B, Weller M, Wick W. Pirfenidone inhibits TGF-beta expression in Malignant glioma cells. *Biochem Biophys Res Commun*. (2007) 354:542–7. doi: 10.1016/j.bbrc.2007.01.012

122. Panza S, Malivindi R, Caruso A, Russo U, Giordano F, Győrffy B, et al. Novel Insights into the Antagonistic Effects of Losartan against Angiotensin II/AGTR1 Signaling in Glioblastoma Cells. *Cancers (Basel)*. (2021) 13(18):4555. doi: 10.3390/cancers13184555

123. Datta M, Chatterjee S, Perez EM, Gritsch S, Roberge S, Duquette M, et al. Losartan controls immune checkpoint blocker-induced edema and improves survival in glioblastoma mouse models. *Proc Natl Acad Sci USA*. (2023) 120(6):e2219199120. doi: 10.1073/pnas.2219199120

124. Reddy RG, Bhat UA, Chakravarty S, Kumar A. Advances in histone deacetylase inhibitors in targeting glioblastoma stem cells. *Cancer Chemother Pharmacol*. (2020) 86(2):165–79. doi: 10.1007/s00280-020-04109-w

125. Han W, Guan W. Valproic acid: A promising therapeutic agent in glioma treatment. *Front Oncol*. (2021) 11:687362. doi: 10.3389/fonc.2021.687362

126. Costalonga EC, de Freitas LJ, Aragone D, Silva FMO, Noronha IL. Anti-fibrotic effects of valproic acid in experimental peritoneal fibrosis. *PloS One*. (2017) 12:e0184302. doi: 10.1371/journal.pone.0184302

127. Aher JS, Khan S, Jain S, Tikoo K, Jena G. Valproate ameliorates thioacetamide-induced fibrosis by hepatic stellate cell inactivation. *Hum Exp Toxicol*. (2015) 34:44–55. doi: 10.1177/0960327114531992

128. Van Beneden K, Geers C, Pauwels M, Mannaerts I, Verbeelen D, van Grunsven LA, et al. Valproic acid attenuates proteinuria and kidney injury. *J Am Soc Nephrol*. (2011) 22:1863–75. doi: 10.1681/ASN.2010111196

129. Kee HJ, Sohn IS, Nam KI, Park JE, Qian YR, Yin Z, et al. Inhibition of histone deacetylation blocks cardiac hypertrophy induced by angiotensin II infusion and aortic banding. *Circulation*.(2006) 113:51–9. doi: 10.1161/CIRCULATIONAHA.105.559724

130. Nakada M, Furuta T, Hayashi Y, Minamoto T, Hamada J. The strategy for enhancing temozolomide against Malignant glioma. *Front Oncol*. (2012) 2:98. doi: 10.3389/fonc.2012.00098

131. Fu J, Shao CJ, Chen FR, Ng HK, Chen ZP. Autophagy induced by valproic acid is associated with oxidative stress in glioma cell lines. *Neuro Oncol*. (2010) 12:328–40. doi: 10.1093/neuonc/nop005

132. Kerkhof M, Dielemans JC, van Breemen MS, Zwinkels H, Walchenbach R, Taphoorn MJ, et al. Effect of valproic acid on seizure control and on survival in patients with glioblastoma multiforme. *Neuro Oncol*. (2013) 15:961–7. doi: 10.1093/neuonc/not057

133. Ververis K, Hiong A, Karagiannis TC, Licciardi PV. Histone deacetylase inhibitors (HDACIs): multitargeted anticancer agents. *Biologics*. (2013) 7:47–60. doi: 10.2147/BTT

134. Io K, Nishino T, Obata Y, Kitamura M, Koji T, Kohno S. SAHA suppresses peritoneal fibrosis in mice. *Perit Dial Int*. (2015) 35:246–58. doi: 10.3747/pdi.2013.00089

135. Hsu CC, Chang WC, Hsu TI, Liu JJ, Yeh SH, Wang JY, et al. Suberoylanilide hydroxamic acid represses glioma stem-like cells. *J BioMed Sci*. (2016) 23:81. doi: 10.1186/s12929-016-0296-6

136. Chen J, Luo B, Wen S, Pi R. Discovery of a novel rhein-SAHA hybrid as a multi-targeted anti-glioblastoma drug. *Invest New Drugs*. (2020) 38:755–64doi: 10.1007/s10637-019-00821-4

137. Kumar A, Ekavali, Chopra K, Mukherjee M, Pottabathini R, Dhull DK. Current knowledge and pharmacological profile of berberine: An update. *Eur J Pharmacol*. (2015) 761:288–97. doi: 10.1016/j.ejphar.2015.05.068

138. Ni WJ, Ding HH, Zhou H, Qiu YY, Tang LQ. Renoprotective effects of berberine through regulation of the MMPs/TIMPs system in streptozocin-induced diabetic nephropathy in rats. *Eur J Pharmacol*. (2015) 764:448–56. doi: 10.1016/j.ejphar.2015.07.040

139. Chitra P, Saiprasad G, Manikandan R, Sudhandiran G. Berberine inhibits Smad and non-Smad signaling cascades and enhances autophagy against pulmonary fibrosis. *J Mol Med (Berl)*. (2015) 93:1015–31doi: 10.1007/s00109-015-1283-1

140. Zhu L, Gu P, Shen H. Protective effects of berberine hydrochloride on DSS-induced ulcerative colitis in rats. *Int Immunopharmacol*. (2019) 68:242–51. doi: 10.1016/j.intimp.2018.12.036

141. Du H, Gu J, Peng Q, Wang X, Liu L, Shu X, et al. Berberine suppresses EMT in liver and gastric carcinoma cells through combination with TGFβR regulating TGF-β/smad pathway. *Oxid Med Cell Longev*. (2021) 2021:2337818. doi: 10.1155/2021/2337818

142. Sun Y, Huang H, Zhan Z, Gao H, Zhang C, Lai J, et al. Berberine inhibits glioma cell migration and invasion by suppressing TGF-β1/COL11A1 pathway. *Biochem Biophys Res Commun*. (2022) 625:38–45. doi: 10.1016/j.bbrc.2022.07.101

143. Nasiraee MR, Shahrivari S, Sayad S, Mahdavi H, Saraygord-Afshari N, Bagheri Z. An agarose-alginate microfluidic device for the study of spheroid invasion, ATRA inhibits CAFs-mediated matrix remodeling. *Cytotechnology*.(2023) 75:309–23. doi: 10.1007/s10616-023-00578-y

144. Shi Y, Kong Z, Liu P, Hou G, Wu J, Ma W, et al. Oncogenesis, microenvironment modulation and clinical potentiality of FAP in glioblastoma: lessons learned from other solid tumors. *Cells*. (2021) 10(5):1142. doi: 10.3390/cells10051142

145. Li M, Li G, Kiyokawa J, Tirmizi Z, Richardson LG, Ning J, et al. Characterization and oncolytic virus targeting of FAP-expressing tumor-associated pericytes in glioblastoma. *Acta Neuropathol Commun*. (2020) 8(1):221. doi: 10.1186/s40478-020-01096-0

146. Ebert LM, Yu W, Gargett T, Toubia J, Kollis PM, Tea MN, et al. Endothelial, pericyte and tumor cell expression in glioblastoma identifies fibroblast activation protein (FAP) as an excellent target for immunotherapy. *Clin Transl Immunol*. (2020) 9:e1191. doi: 10.1002/cti2.1191

frontiers | Frontiers in Oncology

TYPE Review
PUBLISHED 14 August 2024
DOI 10.3389/fonc.2024.1409519

OPEN ACCESS

EDITED BY
Tanmay Abhay Kulkarni,
Mayo Clinic, United States

REVIEWED BY
Vivekanand Yadav,
Children's Mercy Kansas City, United States
Ramcharan Singh Angom,
Mayo Clinic Florida, United States

*CORRESPONDENCE
Shenglan Huang
419182020@qq.com
Fang Xie
pennyxiefang@foxmail.com

†These authors have contributed equally to this work

RECEIVED 30 March 2024
ACCEPTED 29 July 2024
PUBLISHED 14 August 2024

CITATION
Du L, Zhang Q, Li Y, Li T, Deng Q, Jia Y, Lei K, Kan D, Xie F and Huang S (2024) Research progress on the role of PTEN deletion or mutation in the immune microenvironment of glioblastoma.
Front. Oncol. 14:1409519.
doi: 10.3389/fonc.2024.1409519

Research progress on the role of PTEN deletion or mutation in the immune microenvironment of glioblastoma

Leiya Du[1†], Qian Zhang[1†], Yi Li[1], Ting Li[1], Qingshan Deng[2], Yuming Jia[1], Kaijian Lei[1], Daohong Kan[3], Fang Xie[1*] and Shenglan Huang[1*]

[1]Department of Oncology, The Second People's Hospital of Yibin, Yibin, Sichuan, China, [2]Department of Neurosurgery, The Second People's Hospital of Yibin, Yibin, Sichuan, China, [3]Department of Burn and Plastic Surgery, The Second People's Hospital of Yibin, Yibin, Sichuan, China

Recent advances in immunotherapy represent a breakthrough in solid tumor treatment but the existing data indicate that immunotherapy is not effective in improving the survival time of patients with glioblastoma. The tumor microenvironment (TME) exerts a series of inhibitory effects on immune effector cells, which limits the clinical application of immunotherapy. Growing evidence shows that phosphate and tension homology deleted on chromosome ten (PTEN) plays an essential role in TME immunosuppression of glioblastoma. Emerging evidence also indicates that targeting PTEN can improve the anti-tumor immunity in TME and enhance the immunotherapy effect, highlighting the potential of PTEN as a promising therapeutic target. This review summarizes the function and specific upstream and downstream targets of PTEN-associated immune cells in glioblastoma TME, providing potential drug targets and therapeutic options for glioblastoma.

KEYWORDS

glioblastoma, PTEN, immunity, tumor microenvironment, immunosuppressive

1 Introduction

Glioma is the most common primary malignant tumor of the central nervous system (1). Its pathological types and molecular characteristics are varied, and about 80% of cases manifest as glioblastoma (GBM). Primary glioblastoma is the brain tumor with the highest degree of intracranial malignancy, characterized by strong invasion and poor prognosis; the average survival time of GBM patients is only 15 months (2, 3). Currently, postoperative adjuvant chemoradiotherapy is the standard treatment for glioblastoma (GBM) but only provides limited survival benefit. Immunotherapy, represented by immune checkpoint inhibitors, has revolutionized the treatment paradigm for many solid tumors, but only a

small percentage of GBM patients have shown objective efficacy (4). Compared with other tumors, GBM demonstrates stronger heterogeneity, lower tumor mutation load, and a highly immunosuppressive microenvironment. Due to the strong immunosuppressive tumor microenvironment (TME) of GBM, the application of immunotherapy in GBM remains suboptimal and requires further research (5). The most significant feature of the GBM tumor immune microenvironment is the absence of tumor-infiltrating lymphocytes (TILs) and natural killer cells (NK cells), as well as the elevated levels of tumor-associated macrophages (TAMs), myelogenic suppressor cells (MDSCs) and regulatory T cells (Tregs) (6). Enhancing the immune system's targeting effect on GBM has emerged as a promising approach to treating tumors.

Phosphate and tension homology deleted on chromosome ten (PTEN) is the first tumor suppressor gene with protein phosphatase activity and lipid phosphatase activity discovered so far. It is located on human chromosome 10q23.3 and regulates a variety of signaling pathways through its bispecific phosphatase activity, thereby regulating the life process of various cells (7). PTEN can be involved in cell cycle regulation, inhibition of tumor cell proliferation, adhesion, metastasis, angiogenesis, and promotion of cell apoptosis, differentiation, senescence, and other physiological and pathological activities. PTEN plays a crucial role in the occurrence and development of a variety of tumors (breast, melanoma, glioblastoma, prostate, liver, lung), and even a slight decrease in PTEN enzyme activity can affect cancer susceptibility (8). Mutations in IDH, PTEN, 1p/19g, TERT, ATRX, BRAF, and H3F3A in gliomas are of great significance for patient prediction and prognosis (Table 1) (9, 10). Overall, 40% of GBM cases exhibit PTEN mutation or deficiency, which is associated with a poorer prognosis than PTEN non-deletion GBM (11). Many recent studies have shown that PTEN mediates multiple mechanisms of immunosuppression in GBM immune regulation, and targeting PTEN can enhance the immune response of GBM (12, 13). This study summarizes the direct and indirect effects of PTEN on the various pathways of immune response in GBM, the mechanisms of mutual regulation between PTEN and immune cells in the immunosuppressive microenvironment, and the latest immunotherapy strategies for glioblastoma.

2 PTEN is involved in the GBM immunosuppressive pathway

In glioblastoma, PTEN deletion or mutation may affect the genomic stability, autophagy, and other aspects of the immune response, leading to immunotherapy failure (Figure 1). The P13K/Akt/mTOR signaling pathway mediates important physiological functions by regulating the cell cycle, protein synthesis, cell energy metabolism, and other pathways, and plays a central regulatory role in the process of cell proliferation, growth, and differentiation. Moreover, activation of this signal transduction pathway promotes cell survival and proliferation and participates in angiogenesis, thereby promoting tumor formation, tumor invasion, and metastasis (14). Studies (15) suggest that the P13K/Akt/mTOR signaling pathway also plays a key role in the occurrence and development of cerebral glioblastoma. The regulation of PTEN and mTOR plays an essential role in this transduction pathway. The protein encoded by the PTEN gene has phosphatase activity and can negatively regulate the P13K/Akt/mTOR signal transduction pathway by catalyzing the dephosphorylation of 3,4,5 phosphatidylinositol to 4,5 monophosphatidylinositol, thereby inducing cell apoptosis (16). As the upstream site of the P13K/Akt/mTOR signaling pathway, the PTEN gene inhibits tumor formation through negative regulation of this signaling pathway, whereas inactivating the PTEN gene reduces the negative regulation of this pathway and causes malignant changes in cells. Research (17) has shown that PTEN is involved in the tumor immune response, and PTEN deficiency activates the phosphatidylinositol 3-kinase (PI3K-AKT) pathway to form an immunosuppressive microenvironment. The combination of PI3K inhibitor and PD-1 blocker was found to have a synergistic effect in PTEN-deficient tumors and can improve patient prognosis. Furthermore, the PI3K-AKT-mTOR pathway

TABLE 1 The mutations genes in GBM patients.

Mutation genes	Location	Function	Clinical trial drugs
IDH	2q33;15q26	Mutated IDH has a gain of function to produce 2-hydroxyglutarate by NADPH-dependent reduction of alpha-ketoglutarate	Ivosidenib
PTEN	10q23.3	PTEN can be involved in cell cycle regulation, inhibition of tumor cell proliferation, adhesion, metastasis, angiogenesis, and promotion of cell apoptosis, differentiation, senescence, and other physiological and pathological activities	
1p/19q	1p/19q	Heterozygous deletions are important in determining the prognosis of glioma patients	
TERT	5p15.33	The TERT is an important component and functional unit of telomerase, which plays a key regulatory role in tumorigenesis and malignant proliferation, among others	
ATRX	Xq21.1	ATRX forms the ATRX-DAXX complex by binding to death structural domain-associated protein (DAXX), which accelerates the process of histone deposition and is involved in the regulation of remodeling chromatin, all of which are of considerable value for the maintenance of the stability of the human genome	
BRAF	7q34	BRAF is a serine/threonine kinase that functions in the MAPKs signaling pathway and is involved as a proto-oncogene in the development of many cancers, including gliomas	Vemurafenib; Dabrafenib

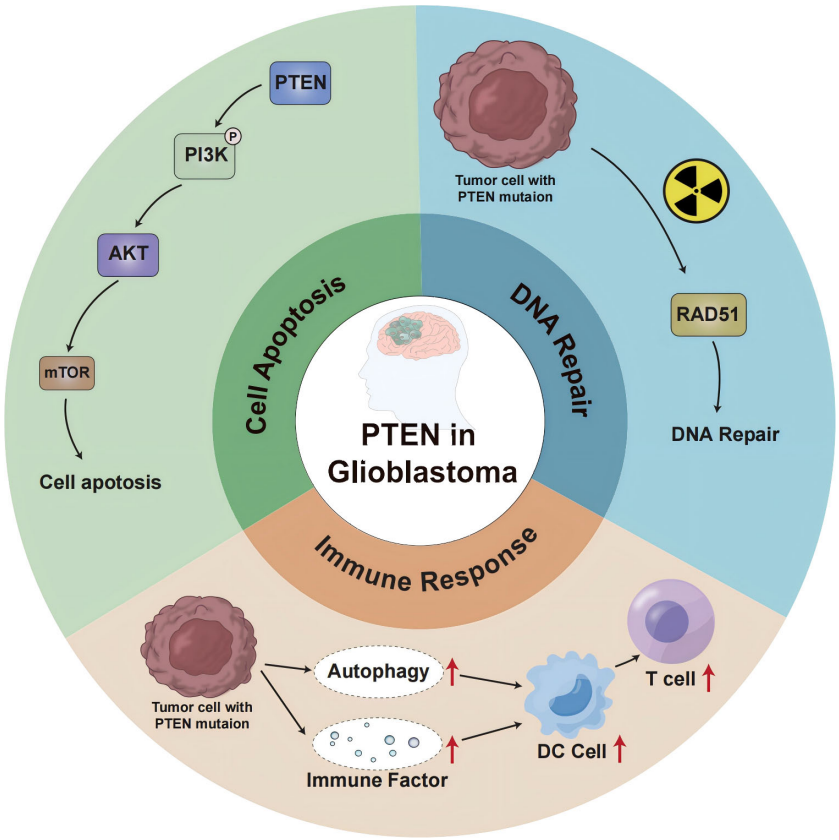

FIGURE 1
PTEN-mediated signaling pathway and molecular mechanism in GBM.

can directly affect the immune response in PTEN-deficient glioblastoma TME (18). Increased PD-L1 cell surface expression induced by PTEN loss led to decreased T-cell proliferation and increased apoptosis. Because PTEN loss is one mechanism regulating PD-L1 expression, agents targeting the PI3K pathway may increase the antitumor adaptive immune responses (19). PIK3CA-mutated PTEN-lost tumors showed a higher prevalence of CD274-positivity than PIK3CA-wild-type PTEN-lost tumors and PTEN-expressed tumors. These findings support the role of PI3K signaling in the CD274/PDCD1 pathway (20). AKT-mediated β-catenin S552 phosphorylation and nuclear β-catenin are positively correlated with PD-L1 expression and inversely correlated with the tumor infiltration of $CD8^+$ T cells in human glioblastoma specimens, highlighting the clinical significance of β-catenin activation in tumor immune evasion (21).

In addition to cytoplasmic functions that regulate cell growth and proliferation, PTEN also regulates genomic integrity and the stability of DNA repair in the nucleus. Studies (22) have shown that mice with PTEN deletion tumors exhibit increased genomic and chromosomal instability, resulting in centromeric breaks, chromosomal translocations, and spontaneous DNA double-strand breaks that occur independently of the PI3K-AKT-mTOR pathway. About 40% of GBM cases show a deficiency or mutation of the PTEN gene, which influences neurogenesis and gliogenesis, resulting in increased DNA damage repair and malignant progression of brain tumors (23). In glioblastoma (24), after cell exposure to ionizing radiation, DNA repair is weakened when nuclear PTEN is phosphorylated at position 240. Phosphorylated PTEN binds to chromatin and recruits RAD51 to facilitate DNA repair (25). Due to PTEN inactivation promoting higher genomic instability (26, 27), PTEN-deficient tumors are generally considered pro-inflammatory, exhibiting a greater mutation burden and higher immunogenicity in the TME. To counteract the effects of neoantigens, tumors with highly unstable genomes are likely to be able to suppress the host immune response against pro-inflammatory activity (28).

The expression of PTEN can induce autophagy, while the loss of PTEN function down-regulates autophagy, effectively supporting the development of tumors (29, 30). The etiology and pathogenesis of GBM remain incompletely understood, but growing evidence indicates the involvement of the ubiquitin-proteasome system (UPS) and autophagy-lysosome pathway (ALP) in the occurrence, development, and drug resistance of GBM. These effects are carried out by regulating the degradation of cancer-promoting/cancer-suppressing factors and mediating endoplasmic reticulum stress tolerance and misfolded protein reaction (31, 32). PTEN is frequently mutated in glioblastoma, and ectopic expression of functional PTEN in glioma cells induces autophagy flux and lysosomal mass. Furthermore, proteasome activity and protein ubiquitination are inhibited, restricting tumor development.

Interestingly, these effects were independent of PTEN lipid phosphatase activity and the PI3K/AKT/mTOR signaling pathway (33). These findings suggest a novel mTOR-independent signaling pathway through which PTEN can act on intracellular protein degradation, regulating autophagy. In addition, studies reported that the activation of the PI3K/Akt/mTOR-mediated signaling pathway can also inhibit autophagy (34–36). Therefore, the molecular components of the proteolytic system regulated by PTEN could represent an innovative therapeutic target for cancer treatment. Moreover, proteasome inhibitors were found to induce cell death in PTEN-deficient GBM organoids and inhibit tumor growth in mice (37). Proteasome inhibitors could be used as targeted therapies for GBM. Mechanistically, PTEN-deficient GBM cells secrete high levels of galectin-9 (Gal-9) via the AKT-GSK3β-IRF1 pathway. The secreted Gal-9 drives macrophage M2 polarization by activating its receptor Tim-3 and downstream pathways in macrophages. These macrophages, in turn, secrete VEGFA to stimulate angiogenesis and support glioma growth (38). Therefore, this study suggests that blockade of Gal-9/Tim-3 signaling is effective to impair glioma progression by inhibiting macrophage M2 polarization, specifically for PTEN-null GBM. PI3Kβ inactivation in the PTEN- null setting led to reduced STAT3 signaling and increased the expression of immune stimulatory molecules, thereby promoting anti-tumor immune responses (39). These findings demonstrate a molecular mechanism linking PTEN loss and STAT3 activation in cancer and suggest that PI3Kβ controls immune escape in PTEN-mutation tumors, providing a rationale for combining PI3Kβ inhibitors with immunotherapy. NF-κB activation was necessary and sufficient for inhibition of PTEN expression. The promoter, RNA, and protein levels of PTEN are down-regulated by NF-κB. The mechanism underlying suppression of PTEN expression by NF-κB was independent of p65 DNA binding or transcription function and involved sequestration of limiting pools of transcriptional coactivators CBP/p300 by p65. Restoration of PTEN expression inhibited NF-κB transcriptional activity and augmented TNF-induced apoptosis, indicating a negative regulatory loop involving PTEN and NF-κB. PTEN is, thus, a novel target whose suppression is critical for antiapoptosis by NF-κB (40).

In the context of tumor cell death, autophagy may lead to the secretion of damage-related molecular chaperones (41, 42). In addition, dead cancer cells may also release autophagosomes containing multiple tumor antigens, which subsequently induce the maturation of dendritic cells (DCS) and cross-present to T cells, promoting tumor immunity (43, 44). PTEN inhibits autophagy, which hinders an effective anti-tumor immune response. Research (45, 46) has revealed that the biology of the immune system determines the occurrence and progression of tumors through a balance between the effects of autophagy regulation and the tolerance response. Autophagy affects the biological functions of various cell types of the immune system, including natural killer cells, dendritic cells, macrophages, and T and B lymphocytes. Autophagy also regulates the secretion of cytokines and antibodies, which in turn impact the autophagy process itself. Transforming growth factor-β, interferon-gamma-γ, and several interleukins (IL) promote autophagy, whereas IL-4, IL-10, and IL-13 are inhibitors (47). Autophagy can be stimulated by innate immune receptors such as toll-like receptors (48); in adaptive immunity, it is a determinant of antigen presentation, lymphocyte differentiation, and cytokine secretion with tumor suppressor activity (49). Therefore, the ideal treatment combination could involve the combination of existing treatment strategies and autophagy-based inducers (PTEN inducers) to trigger cancer cell death and patient response.

3 PTEN affects the GBM immune microenvironment

The glioblastoma microenvironment (TME) is composed of tumor cells, extracellular matrix (ECM), blood vessels, innate immune cells (monocytes, macrophages, mast cells, microglia, and neutrophils), T cells and neurons, astrocytes, and oligodendrocytes (Figure 2). Infiltrating immune cells in GBM are mainly composed of tumor-associated macrophages (TAMs), myelo-derived suppressor cells (MDSC), and T lymphocytes (Table 2) (59). A growing number of studies have shown that the tumor immune microenvironment (TIME) plays a crucial role in regulating the growth and metastasis of GBM. Moreover, PTEN participates in the regulation of immune cell signaling; in contrast, PTEN deficiency can lead to an immunosuppressive tumor microenvironment (60) and hinder the anti-tumor immune response. For example, previous studies revealed that the loss of PTEN is significantly associated with reduced T-cell infiltration at the tumor site and resistance to PD-1 blocking therapy (61–64). The loss of PTEN also promotes the accumulation of inhibitory immune cells, such as MDSCs and Tregs, as well as the formation of an immunosuppressive microenvironment during tumorigenation and development (65–67).

3.1 Tumor-associated macrophages

In the glioblastoma microenvironment, tumor-associated macrophages are the most common infiltrating immune cells, accounting for 40% of the total tumor cells (68). Macrophages constitute the most prevalent non-tumor cells in GBM (23). GiomettoB also found that TAMs can be detected in 100% of GBM cases (69). Two different sources of tumor-associated macrophages have been reported in human glioma, namely from embryonic yolk sac monocytes (70) and from peripheral bone marrow-derived monocytes (50). The immunosuppressive anticancer microenvironment is maintained through the recruitment of monocytes, which are converted into macrophages in the glioma environment. TAMs can be divided into two types, M1 type and M2 type. M1-type TAMs typically express high levels of pro-inflammatory factors, promoting Th1 response and strong tumor-killing ability. In contrast, M2 TAMs promote tissue remodeling and tumor progression and secrete inhibitory inflammatory factors (51). Moreover, glioblastoma-associated macrophages have been reported to exert immunosuppressive effects (52). Previous studies have demonstrated that TAMs in the

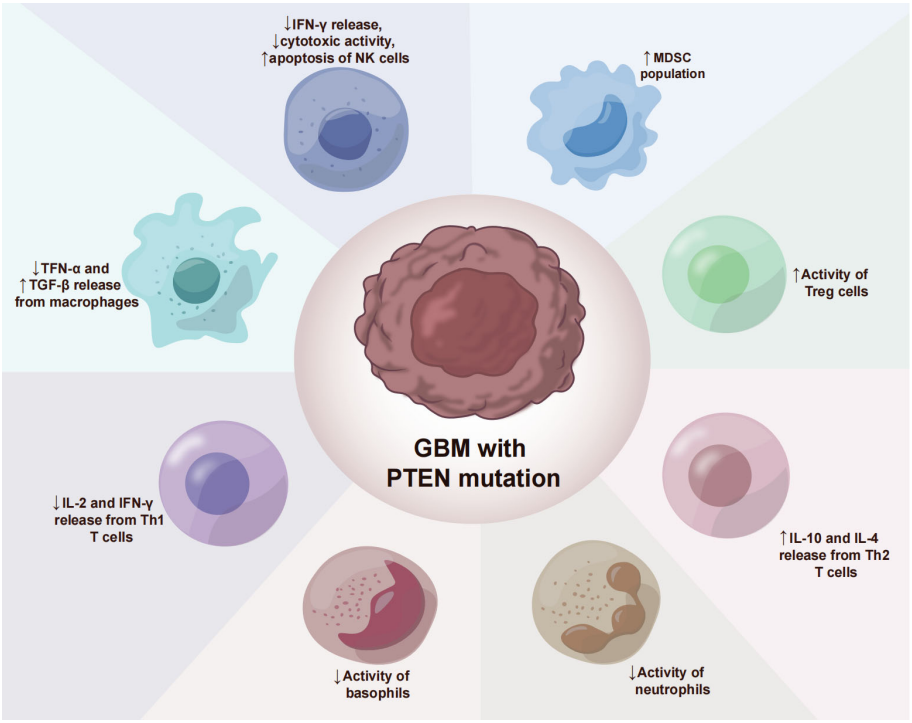

FIGURE 2
PTEN deficiency immunosuppressive mechanisms in GBM.

GBM microenvironment primarily adopt the M2-type polarization (53, 68), which fills the glioma microenvironment and controls tumor progression and immune escape mechanism. The M2 phenotype induces differential expression of receptors, cytokines, and chemokines, which produce IL-10, IL-1, and IL-6, thereby stimulating tumorigenesis and negatively affecting prognosis (54). M2 macrophages stimulate the proliferation and invasion of glioma cells and support the immune escape mechanism (71–73). Giotta's study confirmed (74) the prevalence of PTEN gene mutation in GBM, which is closely associated with poor prognosis and ultra-low survival rate. A recently published report on GBM showed (75, 76) that PTEN deficiency is associated with high macrophage density. Additionally, PTEN-deficient gliomas can recruit a large number of macrophages in the glioma microenvironment. Another study by Ni et al. (38) revealed that the ability of PTEN-deficient gliomas to induce M2 polarization in macrophages was significantly stronger than that of PTEN wild-type gliomas. In PTEN-deficient glioma cells, the activated AKT pathway inactivates GSK-3β by promoting Ser9 phosphorylation, thereby reducing GSK-3β-mediated degradation of IRF1, leading to the up-regulation of the transcription factor IRF1, which enters the nucleus to promote LGALS-9 gene transcription and Gal-9 expression. The activation of the Tim-3 receptor on macrophages by the Gal-9 ligand, in turn, activates transcription factors associated with M2-type polarization and induces macrophage migration, activation, and enrichment of macrophage-associated angiogenesis pathways in PTEN-null gliomas. Gal-9/Tim-3 is a promising target for the treatment of PTEN-deficient gliomas. Blocking Gal-9/Tim-3 can inhibit the malignant progression of gliomas by inhibiting the M2 polarization of macrophages. A new study on the effect of PTEN deletion on glioblastoma demonstrated (71) increased infiltration of macrophages via the YES-associated protein 1-Lysyl oxidase b1 (LOX-b1) -integrin-PYK2 axis. Furthermore, LOX expression was found to activate specific pathways in macrophages, facilitating the recruitment of macrophages to the TME. In the GBM model of PTEN deficiency (77), the loss of PTEN leads to the up-regulation of the macrophage chemotactic LOX in a YAP-1-dependent manner. In circulating monocytes, LOX-dependent up-regulation of β1 integrin receptor signaling drives its penetration into GBM tissues to obtain tumor-associated macrophage phenotype and promotes GBM survival and angiogenesis by secreting SPP1. Interfering with these interactions by inhibiting LOX signals can reduce TAM invasion and inhibit tumor growth. Other studies have found that PTEN regulates the activation of macrophages by activating the PI3K signaling pathway to increase the release of arginase I (78), resulting in a low-inflammation environment. Therefore, arginase I is also a potential therapeutic target.

3.2 T lymphocytes

GBM with PTEN mutation shows a reduced number of T cells (17). PTEN mutation can induce an immunosuppressive tumor microenvironment, which is not derived from traditional Treg cells but from tumor cells overexpressing CD44. Other studies have discovered (79) that PTEN regulates the type I interferon pathway in a PI3K-independent manner, inhibits the release of inflammatory factors, and reduces the number of CD8+T cells in GBM. Studies

TABLE 2 The role of PTEN in regulating signaling proteins in immune cells.

Immune cells	Proteins	Relationship with PTEN	References	Clinical trials
TAMs	IRF1	PTEN deficiency can activate the PI3K-AKT pathway, and IRF1 is up-regulated to promote the secretion of Gal-9, which in turn activates Tim-3 receptor on macrophages, resulting in macrophage enrichment.	(50)	Peng, Guang et al. Oncoimmunology vol. 12,1 2173422. 6 Feb. 2023
	LOX	The loss of PTEN causes the macrophage chemoattractant LOX to be upregulated in a YAP-1 dependent manner.	(51)	Gondek, Tomasz et al. BioMed research international vol. 2014 (2014): 102478.
	Arginase I	PTEN deficiency regulates macrophage activation by activating the PI3K signaling pathway to increase the release of arginase I	(52)	Lorentzen, Cathrine Lund et al. Frontiers in immunology vol. 13 1023023. 17 Oct. 2022,
T lymphocyte	CD44	PTEN mutation induces CD44 overexpression and decreases the number of T cells	(12)	Pazhohan, Azar et al. The Journal of steroid biochemistry and molecular biology vol. 178 (2018): 150-158.
CD8+T	IFN	PTEN regulated the type I interferon pathway via PI3K-independent way	(13, 53)	Boucher, Yves et al. Clinical cancer research: an official journal of the American Association for Cancer Research vol. 29,8 (2023): 1605-1619.
Tregs	Foxp3	PTEN directly regulated the expression of Foxp3, and promoted the Tregs generation and immunosuppressive abilities	(23)	Revenko, Alexey et al. Journal for immunotherapy of cancer vol. 10,4 (2022): e003892.
	mTORC2	PTEN deficiency modulates mTORC2-Akt activity and maintains Treg stability	(54)	Banerjee, Susana et al. JAMA oncology vol. 9,5 (2023): 675-682.
MDSCs	arginase	PTEN deficiency up-regulates arginase activity by activating PI3K signaling pathway, promotes the release of MDSCs, and inhibits T cell function.	(55)	Okła, Karolina et al. Frontiers in immunology vol. 10 691. 3 Apr. 2019
	GM-CSF	PTEN activates the STAT3 signaling pathway, which promotes GM-CSF to up-regulate IL-4Rα on MDSCs, and then mediates IL-13-induced arginase production, thereby inhibiting T cell function.	(56, 57)	Mody, Rajen et al. Journal of clinical oncology: vol. 38,19 (2020): 2160-2169.
	TGF-β1	PTEN activates the Akt pathway to regulate the expression of miR-494 in MDSCs induced by TGF-β1, which promotes the formation of bone marrow mesenchymal stem cells	(58)	Chen, Gang et al. Journal of experimental & clinical cancer research: CR vol. 40,1 218. 30 Jun. 2021,
	IL-6, VEGF, PGE-2	PTEN activates PI3K/AKT/mTOR or STAT3 signaling pathway, and increases the release of factors related to MDSCs proliferation (IL-6, VEGF, PGE-2)	(56, 57)	Bennouna, Jaafar et al. The Lancet. Oncology vol. 14,1 (2013): 29-37.

have shown (80) that PTEN lacks the upregulation of mTORC2-Akt activity, and loss of this activity can restore the function of Treg lacking in PTEN. From a mechanism perspective, PTEN can maintain the stability of Treg. Meanwhile, the phosphatase PTEN links Treg stability with inhibition of TH1 and follicular T-helper cell (TFH) responses. Further studies on glioblastoma (18) have revealed that anti-inflammatory cytokine release and T cell activity are significantly reduced in the absence of PTEN and dysregulation of PI3K signaling. Moreover, PTEN inducers or PI3K inhibitors may improve T cell function. Giotta's study (74) suggested that PTEN mutations were prevalent in GBM, regulating Foxp3 expression and promoting the production of Tregs. Tregs down-regulate T cell activity and regulate innate and adaptive responses to autoantigens, allergens, and infectious agents (81–84). PTEN-deficient tumors usually exhibit a high density of Treg cells in the TME, and Tregs inhibit the function of CD4+, CD8+, and NK cells, and exert immunosuppressive effects in the TME (55, 85, 86).

In addition, T lymphocytes are down-regulated and also exhibit impaired killing function, which is related to TAMs (56). Prostaglandin E2 was found to be produced in the GBM microenvironment, further inhibiting T-cell activity by TAMs and inducing apoptosis. In addition, glioma cells can down-regulate the expression of MHC Class II molecules in microglia and induce ineffective cloning of T cells (87). However, YangI et al. reported that GBM had higher CD8+T cell infiltration compared with pilocytic astrocytoma (57). This differential expression suggests that glioblastoma has a more obvious effect on the local immune microenvironment, but the number does not necessarily represent the potency of the killer cell function. Previous studies have shown that in addition to functional downregulation, CD8+T cells in the GBM microenvironment are involved in the immune escape mechanism.

3.3 Medullary inhibitory cells MDSC

Vidotto's study (81) reported that PTEN deficiency induces an increase in the density of tumor-infiltrating MDSC in TME. MDSCs

are a heterogeneous population composed of a large number of immature bone marrow precursor cells, which are activated under pathological conditions and show strong immunosuppressive activity (88). MDSCs protect tumor cells from host immune attack by negatively regulating immune response, including the depletion of amino acids required by T cells such as arginine and cysteine, the generation of reactive oxygen species nitric oxide and peroxynitrite, direct inhibition of macrophages and natural killer cells, and promotion of tumor angiogenesis (58).

In GBM, MDSCs account for a large proportion of tumor immune cells and play an essential role in promoting tumor growth, tumor cell survival, migration, and immune suppression (89). The glioma microenvironment contributes to the immunosuppressive function of MDSCs (90, 91). MDSCs promote glioma growth, invasion, and angiogenesis as well as the proliferation of Tregs cells (92). GIELEN et al. (93) confirmed that the increase of MDSCs in GBM is related to the increase of arginase activity and that the immunosuppressive function was mediated by inhibiting T cells. Studies have found that glioma cells express many factors related to the proliferation of MDSCs (IL-6, IL-10, VEGF, PGE-2, GM-CSF, and TGF-β2); however, blocking the chemokine CCL2 signaling pathway in glioma cells effectively reduces the recruitment of MDSCs (94). Relevant research data revealed a high proportion of microglial cells/macrophages (GAMs) and MDSCs in malignant GBM, with both GAMs and MDSCs having the ability to recruit Tregs to the tumor, further inhibiting the tumor immune response (59, 95). Studies have found that multiple miRNAs in the tumor microenvironment promote the expansion and immunosuppression of MDSCs by targeting inhibiting PTEN and activating the PI3K/AKT/mTOR or STAT3 signaling pathways (96, 97). In addition, GM-CSF up-regulates IL-4Rα on MDSCs via signal transduction and the transcriptional activator STAT3, thereby mediating IL-13-induced arginase production and inhibiting T cell function.

4 Glioma immunotherapy targeting PTEN

(1) Evidence suggests that PTEN deficiency plays a crucial role in the development of immunosuppressive cancer phenotypes in glioblastoma and is involved in tumor immune responses. Furthermore, PTEN deficiency activates the phosphatidylinositol 3-kinase (PI3K-Akt) pathway to form an immunosuppressive microenvironment. Since restoring PTEN's function is currently not feasible, suppressing PI3K signaling represents a potential approach to mitigate PTEN loss (98). Another study showed (17) that the combination of PI3K inhibitor and PD-1 blocker exerts a synergistic effect in PTEN-deficient tumors and can improve the prognosis of patients. In primary cultures of PTEN-deficient gliomas, inhibition of components of the PI3K-AKT-mTOR network resulted in reduced T cell death (99) and enhanced immune response.

(2) PTEN can regulate autophagy and affect GBM immune response through the PI3K/Akt/mTOR mediated signaling pathway and new mTOR independent signaling pathway. Therefore, the inducers of autophagy (PTEN inducers) and the molecular components of the proteolytic system associated with autophagy could be new therapeutic directions for GBM. In addition, some studies have found (37) that proteasome inhibitors specifically induce cell death in GBM organoids with PTEN defects and inhibit tumor growth in mice. Proteasome inhibitors can be used as targeted therapies for GBM.

(3) PTEN mediates immune responses independently of PI3K, so future therapies could also target other downstream pathways and signaling molecules that directly control the immune response in the microenvironment of glioblastoma. For example, PTEN-deficient glioblastomas overexpress CD44 cell-surface adhesion receptors and have a tighter tumor cell phenotype than wild-type glioblastomas (100), which can exclude angioforming and immune cells in TME, making them less responsive to immune checkpoint inhibitors (ICI) (17).

(4) From the above presentation of tumor-associated macrophages in glioblastoma with PTEN deletion or mutation, PTEN deletion or mutation was shown to lead to enhanced aggregation of macrophages into the tumor microenvironment (TME). These findings suggest that targeting M2-type TAMs may be particularly effective against gliomas with PTEN deletion. Inhibition of macrophage M2 polarization by targeting Gal-9/Tim-3 represents a potential target for precise immunotherapy for PTEN-deficient gliomas (38).

Immunotherapy is a therapeutic approach to achieve anti-tumor effects through the action of antibodies on the corresponding receptors. Currently, immunotherapy for gliomas includes vaccine therapy, immune checkpoint therapy, chimeric antigen receptor T-cell immunotherapy (CAR-T), natural killer (NK) cell therapy, and lysosomal viral therapy. However, some problems need to be solved. The main problem with immunotherapy is that normal tissues often have antigenic epitopes identical to those of tumor cells, and activation of the immune response can lead to cross-reactivity between the tumor and the body, resulting in toxicity and autoimmune disease (101). another key challenge is whether immunotherapeutic strategies can overcome the multiple mechanisms of immune evasion in gliomas and generate tumor-specific immune responses (102).In addition, the production of immunotherapeutic vaccines is often complex, with multiple methods of constructing the same vaccine, but the effects of the vaccine will vary (103), and the future of immunotherapy will not be limited to single-pharmacological treatments, but will require a combination of therapies to achieve a broad and long-lasting clinical benefit (101).

5 Conclusions and future prospects

A large number of studies have supported the role of PTEN in immune cells and illustrated the immunomodulatory effects of PTEN on glioblastoma TME. PTEN inhibits CD4+/CD8+T cells and dendritic cells while favoring M2 macrophages, Tregs, and MDSCs, participating in glioblastoma progression, metastasis, and

immunity. This study outlines the function of PTEN in glioblastoma TME immune cells, as well as their cascade gene activation and clinical outcomes. Increasing evidence demonstrates that targeting PTEN can not only improve the anti-tumor immune function of TME but also enhance the immunotherapy effect, highlighting PTEN as a promising therapeutic target. Nevertheless, whether the recovery of functional PTEN can regulate TME in tumors and improve the sensitivity of tumors to ICB therapy requires further research. Investigating the effectiveness of recovering functional PTEN as a means of cancer treatment holds important clinical significance.

Author contributions

LD: Conceptualization, Funding acquisition, Supervision, Writing – original draft, Writing – review & editing. QZ: Investigation, Supervision, Validation, Writing – original draft, Writing – review & editing. YL: Resources, Validation, Writing – review & editing. TL: Funding acquisition, Investigation, Resources, Writing – review & editing. QD: Investigation, Resources, Visualization, Writing – review & editing. YJ: Investigation, Resources, Writing – review & editing. KL: Investigation, Project administration, Resources, Writing – review & editing. DK: Investigation, Resources, Validation, Writing – review & editing. FX: Data curation, Writing – original draft, Writing – review & editing. SH: Funding acquisition, Investigation, Validation, Writing – original draft, Writing – review & editing.

Funding

The author(s) declare financial support was received for the research, authorship, and/or publication of this article. This study was supported by the 2021 hospital-level incubation Project of the Second People's Hospital of Yibin (Grant number: 2021FY05 and 2021FY16), the Yibin Health and Wellness Medical Research Project (2022YW011, 2023YW009), and the program of Southwest Medical University Higher Education Teaching Research and Reform (JG2022270). The authors declare no conflicts of interests.

Conflict of interest

The authors declare that the research was conducted in the absence of any commercial or financial relationships that could be construed as a potential conflict of interest.

Publisher's note

References

1. Ostrom QT, Gittleman H, Truitt G, Boscia A, Kruchko C, Barnholtz-Sloan JS. CBTRUS statistical report: Primary brain and other central nervous system tumors diagnosed in the United States in 2011-2015. *Neuro Oncol*. (2018) 20:iv1–iv86. doi: 10.1093/neuonc/noy131

2. Fakhoury KR, Ney DE, Ormond DR, Rusthoven CG. Immunotherapy and radiation for high-grade glioma: a narrative review. *Transl Cancer Res*. (2021) 10:2537–70. doi: 10.21037/tcr

3. Xu S, Tang L, Li X, Fan F, Liu Z. Immunotherapy for glioma: Current management and future application. *Cancer Lett*. (2020) 476:1–12. doi: 10.1016/j.canlet.2020.02.002

4. Jackson CM, Choi J, Lim M. Mechanisms of immunotherapy resistance: lessons from glioblastoma. *Nat Immunol*. (2019) 20:1100–9. doi: 10.1038/s41590-019-0433-y

5. Locarno CV, Simonelli M, Carenza C, Capucetti A, Stanzani E, Lorenzi E, et al. Role of myeloid cells in the immunosuppressive microenvironment in gliomas. *Immunobiology*. (2020) 225:151853. doi: 10.1016/j.imbio.2019.10.002

6. Majd N, De Groot J. Challenges and strategies for successful clinical development of immune checkpoint inhibitors in glioblastoma. *Expert Opin Pharmacother*. (2019) 20:1609–24. doi: 10.1080/14656566.2019.1621840

7. Yehia L, Keel E, Eng C. The clinical spectrum of PTEN mutations. *Annu Rev Med*. (2020) 71:103–16. doi: 10.1146/annurev-med-052218-125823

8. Milella M, Falcone I, Conciatori F, Cesta Incani U, Del Curatolo A, Inzerilli N, et al. PTEN: multiple functions in human Malignant tumors. *Front Oncol*. (2015) 5:24. doi: 10.3389/fonc.2015.00024

9. Arita H, Matsushita Y, Machida R, Yamasaki K, Hata N, Ohno M, et al. TERT promoter mutation confers favorable prognosis regardless of 1p/19q status in adult diffuse gliomas with IDH1/2 mutations. *Acta neuropathologica Commun*. (2020) 8:201. doi: 10.1186/s40478-020-01078-2

10. Wong QH, Li KK, Wang WW, Malta TM, Noushmehr H, Grabovska Y, et al. Molecular landscape of IDH-mutant primary astrocytoma Grade IV/glioblastomas. *Modern pathology: an Off J United States Can Acad Pathology Inc*. (2021) 34:1245–60. doi: 10.1038/s41379-021-00778-x

11. Verhaak RG, Hoadley KA, Purdom E, Wang V, Qi Y, Wilkerson MD, et al. Integrated genomic analysis identifies clinically relevant subtypes of glioblastoma characterized by abnormalities in PDGFRA, IDH1, EGFR, and NF1. *Cancer Cell*. (2010) 17:98–110. doi: 10.1016/j.ccr.2009.12.020

12. Yu J, Lai M, Zhou Z, Zhou J, Hu Q, Li J, et al. The PTEN-associated immune prognostic signature reveals the landscape of the tumor microenvironment in glioblastoma. *J neuroimmunology*. (2023) 376:578034. doi: 10.1016/j.jneuroim.2023.578034

13. Zhou S, Wang H, Huang Y, Wu Y, Lin Z. The global change of gene expression pattern caused by PTEN mutation affects the prognosis of glioblastoma. *Front Oncol*. (2022) 12:952521. doi: 10.3389/fonc.2022.952521

14. Chan SM, Weng AP, Tibshirani R, Aster JC, Utz PJ. Notch signals positively regulate activity of the mTOR pathway in T-cell acute lymphoblastic leukemia. *Blood*. (2007) 110:278–86. doi: 10.1182/blood-2006-08-039883

15. Chakravarti A, Zhai G, Suzuki Y, Sarkesh S, Black PM, Muzikansky A, et al. The prognostic significance of phosphatidylinositol 3-kinase pathway activation in human gliomas. *J Clin Oncol*. (2004) 22:1926–33. doi: 10.1200/JCO.2004.07.193

16. Davidson L, Maccario H, Perera NM, Yang X, Spinelli L, Tibarewal P, et al. Suppression of cellular proliferation and invasion by the concerted lipid and protein phosphatase activities of PTEN. *Oncogene*. (2010) 29:687–97. doi: 10.1038/onc.2009.384

17. Zhao J, Chen AX, Gartrell RD, Silverman AM, Aparicio L, Chu T, et al. Immune and genomic correlates of response to anti-PD-1 immunotherapy in glioblastoma. *Nat Med*. (2019) 25:462–9. doi: 10.1038/s41591-019-0349-y

18. Cretella D, Digiacomo G, Giovannetti E, Cavazzoni A. PTEN alterations as a potential mechanism for tumor cell escape from PD-1/PD-L1 inhibition. *Cancers*. (2019) 11(9):1318. doi: 10.3390/cancers11091318

19. Mittendorf EA, Philips AV, Meric-Bernstam F, Qiao N, Wu Y, Harrington S, et al. PD-L1 expression in triple-negative breast cancer. *Cancer Immunol Res*. (2014) 2:361–70. doi: 10.1158/2326-6066.CIR-13-0127

20. Ugai T, Zhao M, Shimizu T, Akimoto N, Shi S, Takashima Y, et al. Association of PIK3CA mutation and PTEN loss with expression of CD274 (PD-L1) in colorectal

carcinoma. *Oncoimmunology*. (2021) 10:1956173. doi: 10.1080/2162402X.2021.1956173

21. Du L, Lee JH, Jiang H, Wang C, Wang S, Zheng Z, et al. β-Catenin induces transcriptional expression of PD-L1 to promote glioblastoma immune evasion. *J Exp Med*. (2020) 217(11). doi: 10.1084/jem.20191115

22. Bassi C, Ho J, Srikumar T, Dowling RJ, Gorrini C, Miller SJ, et al. Nuclear PTEN controls DNA repair and sensitivity to genotoxic stress. *Sci (New York NY)*. (2013) 341:395–9. doi: 10.1126/science.1236188

23. Chen Z, Hambardzumyan D. Immune microenvironment in glioblastoma subtypes. *Front Immunol*. (2018) 9:1004. doi: 10.3389/fimmu.2018.01004

24. Shen WH, Balajee AS, Wang J, Wu H, Eng C, Pandolfi PP, et al. Essential role for nuclear PTEN in maintaining chromosomal integrity. *Cell*. (2007) 128:157–70. doi: 10.1016/j.cell.2006.11.042

25. Ma J, Benitez JA, Li J, Miki S, Ponte De Albuquerque C, Galatro T, et al. Inhibition of nuclear PTEN tyrosine phosphorylation enhances glioma radiation sensitivity through attenuated DNA repair. *Cancer Cell*. (2019) 35:816. doi: 10.1016/j.ccell.2019.04.011

26. Turajlic S, Litchfield K, Xu H, Rosenthal R, Mcgranahan N, Reading JL, et al. Insertion-and-deletion-derived tumour-specific neoantigens and the immunogenic phenotype: a pan-cancer analysis. *Lancet Oncol*. (2017) 18:1009–21. doi: 10.1016/S1470-2045(17)30516-8

27. Dudley JC, Lin MT, Le DT, Eshleman JR. Microsatellite instability as a biomarker for PD-1 blockade. *Clin Cancer research: an Off J Am Assoc Cancer Res*. (2016) 22:813–20. doi: 10.1158/1078-0432.CCR-15-1678

28. Vidotto T, Tiezzi DG, Squire JA. Distinct subtypes of genomic PTEN deletion size influence the landscape of aneuploidy and outcome in prostate cancer. *Mol cytogenetics*. (2018) 11:1. doi: 10.1186/s13039-017-0348-y

29. Arico S, Petiot A, Bauvy C, Dubbelhuis PF, Meijer AJ, Codogno P, et al. The tumor suppressor PTEN positively regulates macroautophagy by inhibiting the phosphatidylinositol 3-kinase/protein kinase B pathway. *J Biol Chem*. (2001) 276:35243–6. doi: 10.1074/jbc.C100319200

30. Gozuacik D, Kimchi A. Autophagy as a cell death and tumor suppressor mechanism. *Oncogene*. (2004) 23:2891–906. doi: 10.1038/sj.onc.1207521

31. Chen RH, Chen YH, Huang TY. Ubiquitin-mediated regulation of autophagy. *J Biomed science*. (2019) 26:80. doi: 10.1186/s12929-019-0569-y

32. Li ZY, Zhang C, Zhang Y, Chen L, Chen BD, Li QZ, et al. A novel HDAC6 inhibitor Tubastatin A: Controls HDAC6-p97/VCP-mediated ubiquitination-autophagy turnover and reverses Temozolomide-induced ER stress-tolerance in GBM cells. *Cancer Lett*. (2017) 391:89–99. doi: 10.1016/j.canlet.2017.01.025

33. Errafiy R, Aguado C, Ghislat G, Esteve JM, Gil A, Loutfi M, et al. PTEN increases autophagy and inhibits the ubiquitin-proteasome pathway in glioma cells independently of its lipid phosphatase activity. *PLoS One*. (2013) 8:e83318. doi: 10.1371/journal.pone.0083318

34. Jain MV, Paczulla AM, Klonisch T, Dimgba FN, Rao SB, Roberg K, et al. Interconnections between apoptotic, autophagic and necrotic pathways: implications for cancer therapy development. *J Cell Mol Med*. (2013) 17:12–29. doi: 10.1111/jcmm.12001

35. Czarny P, Pawlowska E, Bialkowska-Warzecha J, Kaarniranta K, Blasiak J. Autophagy in DNA damage response. *Int J Mol Sci*. (2015) 16:2641–62. doi: 10.3390/ijms16022641

36. Zhou ZW, Li XX, He ZX, Pan ST, Yang Y, Zhang X, et al. Induction of apoptosis and autophagy via sirtuin1- and PI3K/Akt/mTOR-mediated pathways by plumbagin in human prostate cancer cells. *Drug design Dev Ther*. (2015) 9:1511–54. doi: 10.2147/DDDT

37. Benitez JA, Finlay D, Castanza A, Parisian AD, Ma J, Longobardi C, et al. PTEN deficiency leads to proteasome addiction: a novel vulnerability in glioblastoma. *Neuro Oncol*. (2021) 23:1072–86. doi: 10.1093/neuonc/noab001

38. Ni X, Wu W, Sun X, Ma J, Yu Z, He X, et al. Interrogating glioma-M2 macrophage interactions identifies Gal-9/Tim-3 as a viable target against PTEN-null glioblastoma. *Sci Adv*. (2022) 8:eabl5165. doi: 10.14791/btrt.2022.10.Suppl

39. Bergholz JS, Wang Q, Wang Q, Ramseier M, Prakadan S, Wang W, et al. PI3Kβ controls immune evasion in PTEN-deficient breast tumours. *Nature*. (2023) 617:139–46. doi: 10.1038/s41586-023-05940-w

40. Vasudevan KM, Gurumurthy S, Rangnekar VM. Suppression of PTEN expression by NF-kappa B prevents apoptosis. *Mol Cell Biol*. (2004) 24:1007–21. doi: 10.1128/MCB.24.3.1007-1021.2004

41. Wang Y, Martins I, Ma Y, Kepp O, Galluzzi L, Kroemer G. Autophagy-dependent ATP release from dying cells via lysosomal exocytosis. *Autophagy*. (2013) 9:1624–5. doi: 10.4161/auto.25873

42. Michaud M, Martins I, Sukkurwala AQ, Adjemian S, Ma Y, Pellegatti P, et al. Autophagy-dependent anticancer immune responses induced by chemotherapeutic agents in mice. *Sci (New York NY)*. (2011) 334:1573–7. doi: 10.1126/science.1208347

43. Su H, Luo Q, Xie H, Huang X, Ni Y, Mou Y, et al. Therapeutic antitumor efficacy of tumor-derived autophagosome (DRibble) vaccine on head and neck cancer. *Int J nanomedicine*. (2015) 10:1921–30. doi: 10.1016/j.bcp.2014.07.006

44. Viry E, Paggetti J, Baginska J, Mgrditchian T, Berchem G, Moussay E, et al. Autophagy: an adaptive metabolic response to stress shaping the antitumor immunity. *Biochem Pharmacol*. (2014) 92:31–42. doi: 10.1016/j.bcp.2014.07.006

45. Jang YJ, Kim JH, Byun S. Modulation of autophagy for controlling immunity. *Cells*. (2019) 25(4):214–20. doi: 10.3390/cells8020138

46. Hagerling C, Casbon AJ, Werb Z. Balancing the innate immune system in tumor development. *Trends Cell Biol*. (2015) 25:214–20. doi: 10.1016/j.tcb.2014.11.001

47. Monkkonen T, Debnath J. Inflammatory signaling cascades and autophagy in cancer. *Autophagy*. (2018) 14:190–8. doi: 10.1080/15548627.2017.1345412

48. Pan H, Chen L, Xu Y, Han W, Lou F, Fei W, et al. Autophagy-associated immune responses and cancer immunotherapy. *Oncotarget*. (2016) 7:21235–46. doi: 10.18632/oncotarget.v7i16

49. Shibutani ST, Saitoh T, Nowag H, Münz C, Yoshimori T. Autophagy and autophagy-related proteins in the immune system. *Nat Immunol*. (2015) 16:1014–24. doi: 10.1038/ni.3273

50. Franco R, Fernández-Suárez D. Alternatively activated microglia and macrophages in the central nervous system. *Prog neurobiology*. (2015) 131:65–86. doi: 10.1016/j.pneurobio.2015.05.003

51. Martinez FO, Sica A, Mantovani A, Locati M. Macrophage activation and polarization. *Front bioscience: J virtual library*. (2008) 13:453–61. doi: 10.2741/2692

52. Grabowski MM, Sankey EW, Ryan KJ, Chongsathidkiet P, Lorrey SJ, Wilkinson DS, et al. Immune suppression in gliomas. *J neuro-oncology*. (2021) 151:3–12. doi: 10.1007/s11060-020-03483-y

53. Lisi L, Ciotti GM, Braun D, Kalinin S, Currò D, Dello Russo C, et al. Expression of iNOS, CD163 and ARG-1 taken as M1 and M2 markers of microglial polarization in human glioblastoma and the surrounding normal parenchyma. *Neurosci letters*. (2017) 645:106–12. doi: 10.1016/j.neulet.2017.02.076

54. Yunna C, Mengru H, Lei W, Weidong C. Macrophage M1/M2 polarization. *Eur J Pharmacol*. (2020) 877:173090. doi: 10.1016/j.ejphar.2020.173090

55. Kim JH, Kim BS, Lee SK. Regulatory T cells in tumor microenvironment and approach for anticancer immunotherapy. *Immune network*. (2020) 20:e4. doi: 10.4110/in.2020.20.e4

56. Khonina NA, Tsentner MI, Leplina O, Tikhonova MA, Stupak VV, Nikonov SD, et al. [Characteristics and immunologic changes in patients with Malignant brain tumors]. *Voprosy onkologii*. (2002) 48:196–201. doi: 10.1111/imm.12949

57. Yang I, Han SJ, Sughrue ME, Tihan T, Parsa AT. Immune cell infiltrate differences in pilocytic astrocytoma and glioblastoma: evidence of distinct immunological microenvironments that reflect tumor biology. *J neurosurgery*. (2011) 115:505–11. doi: 10.3171/2011.4.JNS101172

58. Vanhaver C, van der Bruggen P, Bruger AM. MDSC in mice and men: Mechanisms of immunosuppression in cancer. *J Clin Med*. (2021) 212(6):491–9. doi: 10.3390/jcm10132872

59. Gieryng A, Pszczolkowska D, Walentynowicz KA, Rajan WD, Kaminska B. Immune microenvironment of gliomas. *Lab investigation; J Tech Methods pathology*. (2017) 97:498–518. doi: 10.1038/labinvest.2017.19

60. Cao Y, Wang H, Yang L, Zhang Z, Li C, Yuan X, et al. PTEN-L promotes type I interferon responses and antiviral immunity. *Cell Mol Immunol*. (2018) 15:48–57. doi: 10.1038/cmi.2017.102

61. Peng W, Chen JQ, Liu C, Malu S, Creasy C, Tetzlaff MT, et al. Loss of PTEN promotes resistance to T cell-mediated immunotherapy. *Cancer discovery*. (2016) 6:202–16. doi: 10.1158/2159-8290.CD-15-0283

62. George S, Miao D, Demetri GD, Adeegbe D, Rodig SJ, Shukla S, et al. Loss of PTEN is associated with resistance to anti-PD-1 checkpoint blockade therapy in metastatic uterine leiomyosarcoma. *Immunity*. (2017) 46:197–204. doi: 10.1016/j.immuni.2017.02.001

63. Barroso-Sousa R, Keenan TE, Pernas S, Exman P, Jain E, Garrido-Castro AC, et al. Tumor mutational burden and PTEN alterations as molecular correlates of response to PD-1/L1 blockade in metastatic triple-negative breast cancer. *Clin Cancer research: an Off J Am Assoc Cancer Res*. (2020) 26:2565–72. doi: 10.1158/1078-0432.CCR-19-3507

64. Roh W, Chen PL, Reuben A, Spencer CN, Prieto PA, Miller JP, et al. Integrated molecular analysis of tumor biopsies on sequential CTLA-4 and PD-1 blockade reveals markers of response and resistance. *Sci Trans Med*. (2017) 151(1):3–12. doi: 10.1126/scitranslmed.aah3560

65. Feng S, Cheng X, Zhang L, Lu X, Chaudhary S, Teng R, et al. Myeloid-derived suppressor cells inhibit T cell activation through nitrating LCK in mouse cancers. *Proc Natl Acad Sci United States America*. (2018) 115:10094–9. doi: 10.1073/pnas.1800695115

66. Yang R, Cai TT, Wu XJ, Liu YN, He J, Zhang XS, et al. Tumour YAP1 and PTEN expression correlates with tumour-associated myeloid suppressor cell expansion and reduced survival in colorectal cancer. *Immunology*. (2018) 155:263–72. doi: 10.1111/imm.12949

67. Sharma MD, Shinde R, Mcgaha TL, Huang L, Holmgaard RB, Wolchok JD, et al. The PTEN pathway in Tregs is a critical driver of the suppressive tumor microenvironment. *Sci advances*. (2015) 1:e1500845. doi: 10.1186/s12929-019-0568-z

68. Mignogna C, Signorelli F, Vismara MF, Zeppa P, Camastra C, Barni T, et al. A reappraisal of macrophage polarization in glioblastoma: Histopathological and immunohistochemical findings and review of the literature. *Pathology Res practice*. (2016) 212:491–9. doi: 10.1016/j.prp.2016.02.020

69. Giometto B, Bozza F, Faresin F, Alessio L, Mingrino S, Tavolato B. Immune infiltrates and cytokines in gliomas. *Acta neurochirurgica*. (1996) 138:50–6. doi: 10.1007/BF01411724

70. Gomez Perdiguero E, Klapproth K, Schulz C, Busch K, Azzoni E, Crozet L, et al. Tissue-resident macrophages originate from yolk-sac-derived erythro-myeloid progenitors. *Nature*. (2015) 518:547–51. doi: 10.1038/nature13989

71. Chen Y, Song Y, Du W, Gong L, Chang H, Zou Z. Tumor-associated macrophages: an accomplice in solid tumor progression. *J Biomed science*. (2019) 26:78. doi: 10.1186/s12929-019-0568-z

72. Zhu C, Kros JM, Cheng C, Mustafa D. The contribution of tumor-associated macrophages in glioma neo-angiogenesis and implications for anti-angiogenic strategies. *Neuro Oncol*. (2017) 19:1435–46. doi: 10.1093/neuonc/nox081

73. Qian BZ, Pollard JW. Macrophage diversity enhances tumor progression and metastasis. *Cell*. (2010) 141:39–51. doi: 10.1016/j.cell.2010.03.014

74. Giotta Lucifero A, Luzzi S. Immune landscape in PTEN-related glioma microenvironment: A bioinformatic analysis. *Brain Sci*. (2022) 193(4):1717–27. doi: 10.4049/jimmunol.1302167

75. Fridman WH, Zitvogel L, Sautès-Fridman C, Kroemer G. The immune contexture in cancer prognosis and treatment. *Nat Rev Clin Oncol*. (2017) 14:717–34. doi: 10.1038/nrclinonc.2017.101

76. Chen P, Zhao D, Li J, Liang X, Li J, Chang A, et al. Symbiotic macrophage-glioma cell interactions reveal synthetic lethality in PTEN-null glioma. *Cancer Cell*. (2019) 35:868–84.e6. doi: 10.1016/j.ccell.2019.05.003

77. Chuntova P, Chow F, Watchmaker PB, Galvez M, Heimberger AB, Newell EW, et al. Unique challenges for glioblastoma immunotherapy-discussions across neuro-oncology and non-neuro-oncology experts in cancer immunology. Meeting Report from the 2019 SNO Immuno-Oncology Think Tank. *Neuro Oncol*. (2021) 23:356–75. doi: 10.1093/neuonc/noaa277

78. Sahin E, Haubenwallner S, Kuttke M, Kollmann I, Halfmann A, Dohnal AM, et al. Macrophage PTEN regulates expression and secretion of arginase I modulating innate and adaptive immune responses. *J Immunol (Baltimore Md: 1950)*. (2014) 193:1717–27. doi: 10.4049/jimmunol.1302167

79. Xing F, Xiao J, Wu J, Liang J, Lu X, Guo L, et al. Modulating the tumor microenvironment via oncolytic virus and PI3K inhibition synergistically restores immune checkpoint therapy response in PTEN-deficient glioblastoma. *Signal transduction targeted Ther*. (2021) 6:275. doi: 10.1038/s41392-021-00609-0

80. Shrestha S, Yang K, Guy C, Vogel P, Neale G, Chi H. Treg cells require the phosphatase PTEN to restrain TH1 and TFH cell responses. *Nat Immunol*. (2015) 16:178–87. doi: 10.1038/ni.3076

81. Vidotto T, Melo CM, Castelli E, Koti M, Dos Reis RB, Squire JA. Emerging role of PTEN loss in evasion of the immune response to tumours. *Br J cancer*. (2020) 122:1732–43. doi: 10.1038/s41416-020-0834-6

82. Grover P, Goel PN, Greene MI. Regulatory T cells: Regulation of identity and function. *Front Immunol*. (2021) 12:750542. doi: 10.3389/fimmu.2021.750542

83. Boer MC, Joosten SA, Ottenhoff TH. Regulatory T-cells at the interface between human host and pathogens in infectious diseases and vaccination. *Front Immunol*. (2015) 6:217. doi: 10.3389/fimmu.2015.00217

84. Scheinecker C, Göschl L, Bonelli M. Treg cells in health and autoimmune diseases: New insights from single cell analysis. *J autoimmunity*. (2020) 110:102376. doi: 10.1016/j.jaut.2019.102376

85. Togashi Y, Shitara K, Nishikawa H. Regulatory T cells in cancer immunosuppression - implications for anticancer therapy. *Nat Rev Clin Oncol*. (2019) 16:356–71. doi: 10.1038/s41571-019-0175-7

86. Okeke EB, Uzonna JE. The pivotal role of regulatory T cells in the regulation of innate immune cells. *Front Immunol*. (2019) 10:680. doi: 10.3389/fimmu.2019.00680

87. Tran CT, Wolz P, Egensperger R, Kösel S, Imai Y, Bise K, et al. Differential expression of MHC class II molecules by microglia and neoplastic astroglia: relevance for the escape of astrocytoma cells from immune surveillance. *Neuropathology Appl neurobiology*. (1998) 24:293–301. doi: 10.1046/j.1365-2990.1998.00120.x

88. Tcyganov E, Mastio J, Chen E, Gabrilovich DI. Plasticity of myeloid-derived suppressor cells in cancer. *Curr Opin Immunol*. (2018) 51:76–82. doi: 10.1016/j.coi.2018.03.009

89. Arcuri C, Fioretti B, Bianchi R, Mecca C, Tubaro C, Beccari T, et al. Microglia-glioma cross-talk: a two way approach to new strategies against glioma. *Front bioscience (Landmark edition)*. (2017) 22:268–309. doi: 10.2741/4486

90. Gielen PR, Schulte BM, Kers-Rebel ED, Verrijp K, Petersen-Baltussen HM, Ter Laan M, et al. Increase in both CD14-positive and CD15-positive myeloid-derived suppressor cell subpopulations in the blood of patients with glioma but predominance of CD15-positive myeloid-derived suppressor cells in glioma tissue. *J neuropathology Exp neurology*. (2015) 74:390–400. doi: 10.1097/NEN.0000000000000183

91. Parney IF. Basic concepts in glioma immunology. *Adv Exp Med Biol*. (2012) 746:42–52. doi: 10.1007/978-1-4614-3146-6_4

92. Wurdinger T, Deumelandt K, van der Vliet HJ, Wesseling P, De Gruijl TD. Mechanisms of intimate and long-distance cross-talk between glioma and myeloid cells: how to break a vicious cycle. *Biochim Biophys Acta*. (2014) 1846:560–75. doi: 10.1016/j.bbcan.2014.10.003

93. Gielen PR, Schulte BM, Kers-Rebel ED, Verrijp K, Bossman SA, Ter Laan M, et al. Elevated levels of polymorphonuclear myeloid-derived suppressor cells in patients with glioblastoma highly express S100A8/9 and arginase and suppress T cell function. *Neuro Oncol*. (2016) 18:1253–64. doi: 10.1093/neuonc/now034

94. Kohanbash G, Mckaveney K, Sakaki M, Ueda R, Mintz AH, Amankulor N, et al. GM-CSF promotes the immunosuppressive activity of glioma-infiltrating myeloid cells through interleukin-4 receptor-α. *Cancer Res*. (2013) 73:6413–23. doi: 10.1158/0008-5472.CAN-12-4124

95. Mei S, Xin J, Liu Y, Zhang Y, Liang X, Su X, et al. MicroRNA-200c promotes suppressive potential of myeloid-derived suppressor cells by modulating PTEN and FOG2 expression. *PLoS One*. (2015) 10:e0135867. doi: 10.1371/journal.pone.0135867

96. Li L, Zhang J, Diao W, Wang D, Wei Y, Zhang CY, et al. MicroRNA-155 and MicroRNA-21 promote the expansion of functional myeloid-derived suppressor cells. *J Immunol (Baltimore Md: 1950)*. (2014) 192:1034–43. doi: 10.4049/jimmunol.1301309

97. Liu Y, Lai L, Chen Q, Song Y, Xu S, Ma F, et al. MicroRNA-494 is required for the accumulation and functions of tumor-expanded myeloid-derived suppressor cells via targeting of PTEN. *J Immunol (Baltimore Md: 1950)*. (2012) 188:5500–10. doi: 10.4049/jimmunol.1103505

98. Mcloughlin NM, Mueller C, Grossmann TN. The therapeutic potential of PTEN modulation: Targeting strategies from gene to protein. *Cell Chem Biol*. (2018) 25:19–29. doi: 10.1016/j.chembiol.2017.10.009

99. Waldron JS, Yang I, Han S, Tihan T, Sughrue ME, Mills SA, et al. Implications for immunotherapy of tumor-mediated T-cell apoptosis associated with loss of the tumor suppressor PTEN in glioblastoma. *J Clin neuroscience: Off J Neurosurgical Soc Australasia*. (2010) 17:1543–7. doi: 10.1016/j.jocn.2010.04.021

100. Cheng F, Eng C. PTEN mutations trigger resistance to immunotherapy. *Trends Mol Med*. (2019) 25:461–3. doi: 10.1016/j.molmed.2019.03.003

101. Majc B, Novak M, Kopitar-Jerala N, Jewett A, Breznik B. Immunotherapy of glioblastoma: current strategies and challenges in tumor model development. *Cells*. (2021) 10(2). doi: 10.3390/cells10020265

102. Gilbert MR, Pugh SL, Aldape K, Sorensen AG, Mikkelsen T, Penas-Prado M, et al. NRG oncology RTOG 0625: a randomized phase II trial of bevacizumab with either irinotecan or dose-dense temozolomide in recurrent glioblastoma. *J neuro-oncology*. (2017) 131:193–9. doi: 10.1007/s11060-016-2288-5

103. Buchroithner J, Erhart F, Pichler J, Widhalm G, Preusser M, Stockhammer G, et al. Audencel immunotherapy based on dendritic cells has no effect on overall and progression-free survival in newly diagnosed glioblastoma: A phase II randomized trial. *Cancers*. (2018) 10(10). doi: 10.3390/cancers10100372

frontiers | Frontiers in Oncology

TYPE Original Research
PUBLISHED 04 September 2024
DOI 10.3389/fonc.2024.1443406

OPEN ACCESS

EDITED BY
Tanmay Abhay Kulkarni,
Mayo Clinic, United States

REVIEWED BY
Hari Rachamala,
Mayo Clinic Florida, United States
Michael Schulder,
Hofstra University, United States

*CORRESPONDENCE
Wei Gao
gaowei1977@tongji.edu.cn
Ping Dai
daiping@tongji.edu.cn

RECEIVED 04 June 2024
ACCEPTED 07 August 2024
PUBLISHED 04 September 2024

CITATION
Li X, Liu K, Fang H, Liu Z, Gao W and Dai P (2024) A theoretical study on evaluating brain tumor changes in tumor treating fields therapy by impedance detection. *Front. Oncol.* 14:1443406. doi: 10.3389/fonc.2024.1443406

A theoretical study on evaluating brain tumor changes in tumor treating fields therapy by impedance detection

Xing Li[1], Kaida Liu[1], Haohan Fang[1], Zirong Liu[1], Wei Gao[2*] and Ping Dai[2*]

[1]College of Automation Engineering, Nanjing University of Aeronautics and Astronautics, Nan Jing, Jiang Su, China, [2]Department of Radiotherapy, Shanghai Fourth People's Hospital, School of Medicine, Tongji University, Shanghai, China

TTFields is a novel FDA-approved technology utilized for treating glioblastoma multiforme (GBM) within the brain. Presently, the effectiveness of therapy is evaluated through MRI imaging at random two-month intervals. Electrical impedance is an important and effective parameter for reflecting changes in tissue properties. In TTFields treatment for brain tumors, electrodes attached to the scalp deliver electric field energy to the tumor region. We hypothesize that these electrodes can also serve as sensors to detect impedance changes caused by tumor alterations in real time, thus continuously assessing the effectiveness of the treatment. In this work, we propose and scrutinize this hypothesis by conducting an in silico study to confirm the potential feasibility of the proposed concept. Our results indicate that the impedance amplitude change measured between opposing TTFields electrode arrays utilizing voltage and frequency of 50 V and 200 kHz (typical TTFields treatment parameters), has enough resolution (> 1mm) and Signal-to-Noise Ratio (> 40 dB) to evaluate tumor size change in the head. The impedance detection technique may be a significant augmentation to TTFields cancer treatment, enabling the continuous evaluation of safety and efficacy throughout the procedure.

KEYWORDS

tumor treating fields, tumor changes, brain tumor, impedance detection, evaluating effectiveness

1 Introduction

Tumor Treating Fields (TTFields) constitute a safe and non-invasive technology for ablating malignant tissues. It relies on intermediate-frequency electric fields (100 kHz-500 kHz) of low intensity (< 3 V/cm) to impede the proliferation of cancer cells. This innovative technology was pioneered by Yoram Palti's team in the early 2000s (1). Clinical evidence demonstrating the effectiveness of TTFields in prolonging the survival of GBM patients,

importantly, without notable side effects. Consequently, the Food and Drug Administration (FDA) approved its use in GBM treatment (2, 3).

TTFields are delivered to the tumor by insulated electrode arrays that are directly applied to the patient's shaved scalp (4). In the GBM treatment, TTFields are activated by the patient through controlling the portable power generator in the backpack. To achieve maximum therapeutic effect, a primary magnetic resonance image (MRI) should be done to confirm the exact position of tumor in the brain, and then treatment electrodes will be personalized attached on each patient. For this purpose, the NovoTal System (NovoTal, USA) offers commercial software designed to optimize electrode placements. A comprehensive description of the methodology for optimizing electrode placements and selecting treatment parameters can be found in (4).

The TTFields treatment differs significantly from other clinical tissue ablation techniques based on biophysical phenomena. Most traditional ablation techniques, for instance, microwave ablation occurs during a brief, acute surgical procedure. Surgeons or radiologists administer the ablative energy, guided by real-time medical imaging, and the procedure's result can be evaluated shortly after its conclusion, typically through medical imaging assessments. In contrast, TTFields tissue ablation is an extended process that exclusively impacts replicating cells and involves the continuous delivery of electric fields over many months, and sometimes even years (5). As previously mentioned, the precise positioning of the electric field delivery electrodes is determined independently from the treatment itself. The electric fields are applied to the tumor typically for up to 18 hours each day (6). Due to the protracted nature of the TTFields ablation procedure, spanning months, it becomes challenging to continually assess its effectiveness throughout the treatment. Currently, the treatment's efficacy is assessed through follow-up MRI scans, typically conducted at intervals of every two months (4, 7). This lack of continuous monitoring, compounded by the extended treatment duration, represents a limitation in the GBM treatment by TTFields.

TTFields electrodes are strategically positioned at predetermined locations, carefully calculated to optimize the delivery of electric fields to the specific location and size of the tumor. As presented in Figure 1, the treatment system can be conceptualized as a complex electric circuit network, where the head within tumor is equivalent to a black box, and electrode arrays on the scalp serve as the accessible nodes.

This study introduces and delves into the concept that, owing to the contrasting electrical properties of normal and malignant brain tissue (8), any alterations in tumor size and composition result in modifications to the head's intricate black box circuit network. Real-time monitoring on the electrical impedance changes through TTFields electrodes can function as a method for detecting changes in the tumor undergoing TTFields treatment. According to the measurements, we can evaluate the effectiveness of the treatment. This approach replaces arbitrary timings for medical imaging follow-ups with follow-ups that hold clinical significance. If the impedance change abnormally, it could indicate that the treatment is ineffective, prompting a need for modification in the treatment parameters. The precise and rigid placement of electrodes, optimized for the targeted delivery of electric fields to the tumor, is likely to enhance the sensitivity of this monitoring technique to any changes in tumor dimensions, as the electrodes deliver the strongest electric fields to the tumor.

This monitoring technique has the potential to advance our fundamental understanding of the TTFields tissue ablation process and may evolve into a method for continuous assessment of treatment success throughout the procedure. It is worth noting that evaluate tissue composition change by measuring electrical impedance is not a novel concept. In fact, it forms the foundation for electrical impedance tomography (EIT) (9, 10) and magnetic induction tomography (11). Additionally, it is closely related to clinical applications, such as monitoring internal bleeding in the brain (12, 13).

In this paper, to investigate this concept, we have created an in silico finite element simulation model that simulates a TTFields treatment protocol within the brain. Through this model, we have calculated the alterations in impedance across the TTFields electrodes, considering variables such as tumor size, location, and frequency. We have then established a correlation between impedance changes and variations in the tumor's dimensions, assuming a known tumor location relative to the electrodes. These correlations serve as a means to evaluate how sensitive these measurements are to changes in the tumor's size. While we

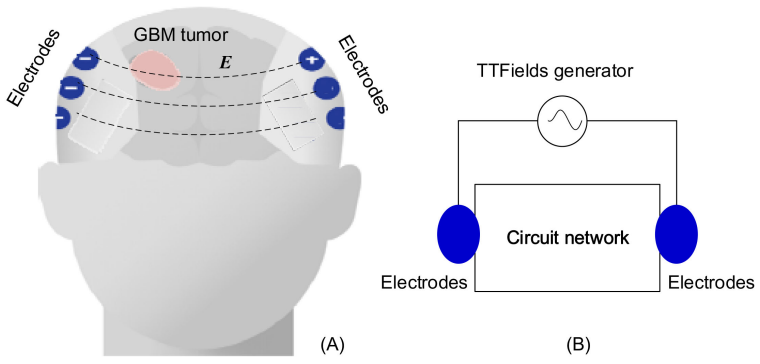

FIGURE 1
TTFields treatment on GBM: **(A)** configuration of electrode array, **(B)** equivalent lump model circuit.

should emphasize that this study represents an initial theoretical exploration, the results suggest that this approach may hold clinical significance and value.

2 Materials and methods

An in silico experimental configuration of a human head, with the brain, a tumor and the TTFields electrodes was developed in Multiphysics simulation COMSOL (version: 5.3), presented in Figure 2A (the front view) and Figure 2B (the top view). The brain was modeled by a half ellipsoid, with dimensions of 83 mm x 73 mm x 68 mm, relative to the ellipsoid centroid, in the x, y and z axis, respectively. The structure comprises five layers arranged from outer to inner layers, specifically the scalp, skull, cerebrospinal fluid (CSF), gray matter (GM), and white matter (WM). The first four layers, from the exterior to the interior are modeled as shells with a thickness of 8 mm, 6 mm, 0.75 mm, and 2 mm, in the respective order. The interior white matter fills the remainder of the half ellipsoid. These typical life-size dimensions of the head of an adult were drawn from existing publications and anatomical data (14–18). The TTFields treatment electrodes were simulated by four electrode arrays, attached to the scalp on the posterior, anterior, right and left sides of the head. Each electrode has a radius of 10 mm (19). An array six electrodes is constructed with a spacing of 5 mm between each electrode, as shown in Figure 2A. These TTFields treatment electrodes will serve as the sensors to detect the changes in impedance of the head, caused by changes in the tumor dimensions. The GBM tumor is shaped as a sphere and its size and location will be changed to simulate different tumor conditions. The mesh of the head model is composed of 590675 elements and 100038 nodes, as shown in Figure 2C.

We used the frequency domain AC/DC module in COMSOL to analyze the model. When the frequency is sub-MHz, the wavelength significantly exceeds the head's size, hence the quasi steady approximation of electromagnetic field is applicable. However, when the frequency is above about 200 MHz, the quasi steady approximation fails and the displacement current is considered in the mathematical model. The electrical characteristics of various head components are sourced from the ITIS tissue properties database (20). Previous studies show that the tumor has an electrical conductivity and relative permittivity significantly surpassing those of the surrounding healthy tissue, ranging from several times to ten times higher (21–23). As a conservative estimate, we set the electrical properties of the tumor to be double those of surrounding white matter. Through estimation, we set a contact impedance of 1kΩ to simulate the insulation impedance of the ceramic between the electrodes and shaved scalp skin. In the simulation, the voltage applied between two opposite arrays of six electrodes is taken to be 50 V. This is a typical amplitude used to generate the desired TTFields intensity (1-2 V/cm) in the brain, as recommended in (24). The theoretical study will employ various frequencies, ranging from 5 kHz to 500 MHz, to investigate the frequency characteristic and find an optimal detection frequency.

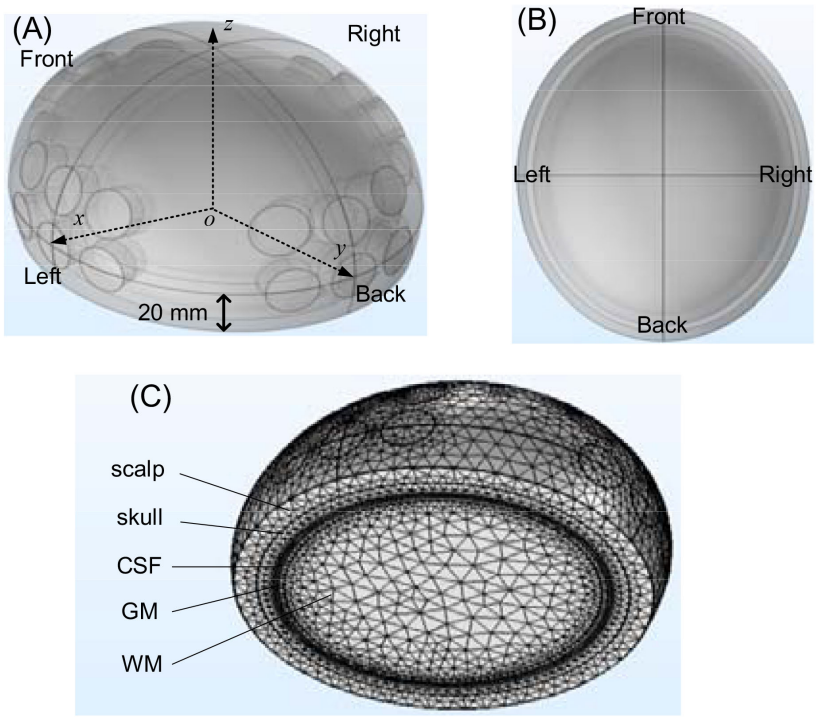

FIGURE 2
The head model built in COMSOL: **(A)** front view, **(B)** top view, **(C)** meshing result.

3 Results and discussions

The section initially investigates the variations in impedance affected by tumor size, considering different factors: A) Frequencies, B) Locations of electrode array pairs, C) Tumor locations. Subsequently, it presents the signal-to-noise effect of the voltage source in part D).

3.1 Effect of frequency

Due to the frequency-dependent character of tissues' electrical properties (20). In this part of the study, we have placed the tumor at a specific location and calculated the impedance between the TTFields electrodes for various size tumors over a frequency spectrum spanning from 5 kHz to 500 MHz. The electric properties of the tissues were set as functions of the scanning frequency according to the data in (20). Figure 3 was obtained for a spherical tumor located at, x = 20 mm, y = 0 mm, z = 0 mm relative to the centroid of the ellipsoid. The COMSOL simulation was performed for three radii of the tumor, r = 10 mm, 15 mm and 20 mm. The change in impedance between the left and right TTFields electrode arrays was calculated in comparison to a brain without a tumor. The change in amplitude and phase depended on the frequency, are illustrated in Figure 3. The curves exhibit a dispersion pattern, which is characteristic of the frequency-dependent properties inherent to biological matter (25). This is to be expected as the electrical properties of the tissues used in this model where taken from the literature. The change in amplitude due to the presence of a tumor increases with a decrease in frequency to 10^3 kHz, after which the disparity diminishes with an elevation in frequency. In contrast, the change in impedance phase shift is minimal at lower frequencies and only becomes noticeable at higher frequencies above 100 MHz, although it still remains relatively small.

Typical TTFields frequencies are ranging from 100 kHz to 300 kHz (26), as this range has been found to yield the most significant therapeutic benefits. Interestingly, changes in tumor size coincidentally result in substantial alterations in impedance amplitude within the identical frequency range employed for treatment administration. Recording these changes in amplitude at the specific frequency of 200 kHz presents a technologically straightforward approach to monitor variations in tumor size. Importantly, such a modification can be easily incorporated into existing clinical TTFields devices. Consequently, our subsequent numerical investigations will focus on assessing the impact of various parameters on the impedance amplitude change by setting the frequency as 200 kHz. This approach aligns directly with what we consider the preferred method for evaluating the therapeutic efficacy of TTFields in brain tumor treatment.

3.2 Effects of electrode array pairs location

TTFields electrode arrays are typically arranged in two opposing configurations, forming orthogonal pairs. Different impedance values can be measured by selecting opposite or adjacent electrode array pairs. For ease of reference, we assigned labels to the electrode arrays as depicted in the upper row of Figure 4. We defined the pairs of electrode arrays 1-3 and 2-4 as opposite detection pattern, and 3-4 as the adjacent detection pattern. In this section, our objective is to investigate the correlation between measurement sensitivity and the chosen detection pattern. In these investigations, the excitation voltage is 50 V, 200 kHz. We evaluate the impedance amplitude change between different TTFields electrode arrays pairs, as a function of tumor size at three typical locations of tumors. The tumors were placed at three different, x, y, z locations with values in mm, (20, 0, 0); (0, 0, 0) and (0, 20, 0). Figure 4 provides insights into the alteration in impedance amplitude concerning tumor size relative to the healthy brain without a tumor, considering various array pairs.

Figure 4 indeed illustrates that the opposite detection pattern exhibits the highest sensitivity to changes in tumor size. Given this observation, we will adopt the opposite detection pattern in the subsequent simulations. This choice aligns tentatively with the recommended detection pattern for clinical applications.

3.3 Effects of tumor location

In the preceding sections, we have established that the highest sensitivity for monitoring changes in tumor size during TTFields

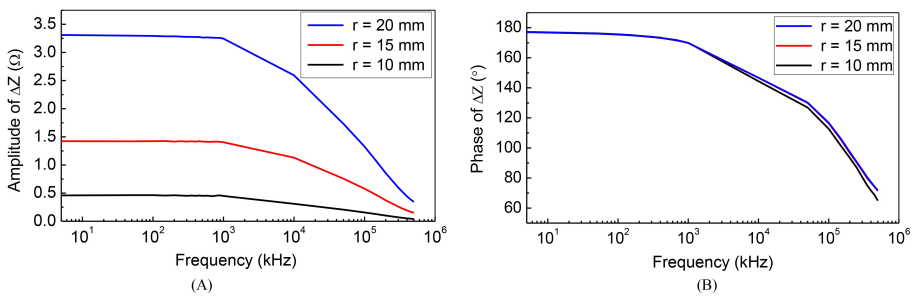

FIGURE 3
Frequency characteristic of impedance change: **(A)** amplitude-frequency **(B)** phase-frequency.

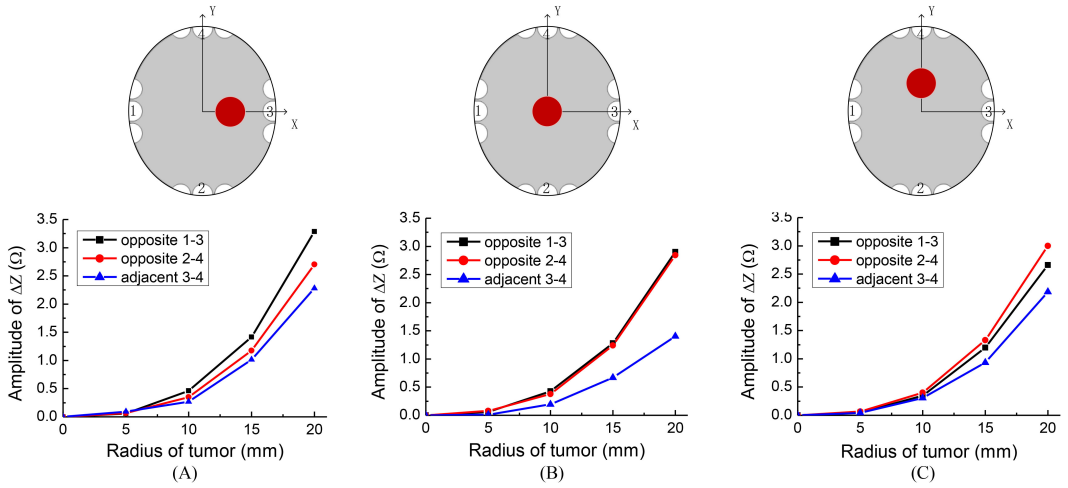

FIGURE 4
Sketches of different tumor locations and the impedance change results of different detection patterns, locations of tumor are: **(A)** (20, 0, 0), **(B)** (0, 0, 0), **(C)** (0, 20, 0).

treatment is achieved by measuring the amplitude change of impedance between opposite TTFields electrode arrays pairs at a standard treatment frequency. In this section, we will explore the sensitivity of these measurements concerning the tumor's position form the opposite detection electrode arrays.

To investigate the effect of tumor location along the x and y axes, we conducted the following simulations: For deviations along the x-axis, we positioned tumors at three different locations: x = 10 mm, 20 mm, 30 mm, with y = 0 mm and z = 0 mm. Similarly, for deviations along the y-axis, we placed tumors at four distinct locations: y = 10mm, 20 mm, 30 mm, 40 mm, with x = 0 mm and z = 0 mm. The detection electrode arrays are 1-3 for the tumor on the x-axis and 2-4 for the tumor on the y-axis. The results of the simulation are presented in Figure 5.

Interestingly, the findings indicate that the closer the tumor is to one of the orthogonal electrode arrays, the more substantial the change in amplitude, regardless of the tumor's radius. This is in agreement with findings made using conventional EIT (27). The results suggest that for optimal placement, the monitoring electrode arrays should be chosen in such a way that one of the orthogonal pairs is as close as possible to the location of the tumor.

3.4 Signal-to-noise ratio analysis

Based on the analysis in subsection C, it is evident that when the tumor is closer to the electrodes, the impedance change is more substantial, resulting in higher monitoring sensitivity or resolution. In this subsection, as a conservative approach, we will examine the extreme condition where the tumor is located at y = 10 mm, which corresponds to the lowest monitoring sensitivity. It is important to note that the same level of noise will have a smaller impact on cases with higher monitoring resolution.

To assess the monitoring resolution, we consider the first-order derivative of the impedance change concerning the tumor size. To calculate the resolution, we employed a cubic function to fit the curve for y = 10 in Figure 5B. The fitting function curve is depicted in Figure 6A, with a fitting error RMSE = 0.01452 and an Adjusted

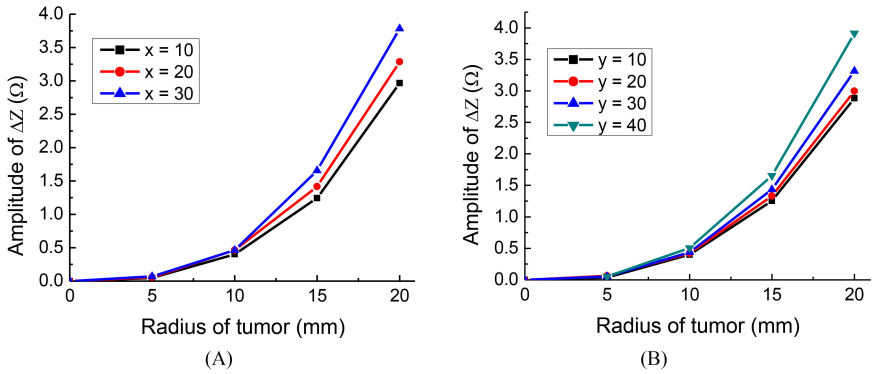

FIGURE 5
The impedance change of different tumor positions, tumor on: **(A)** x axis, **(B)** y axis.

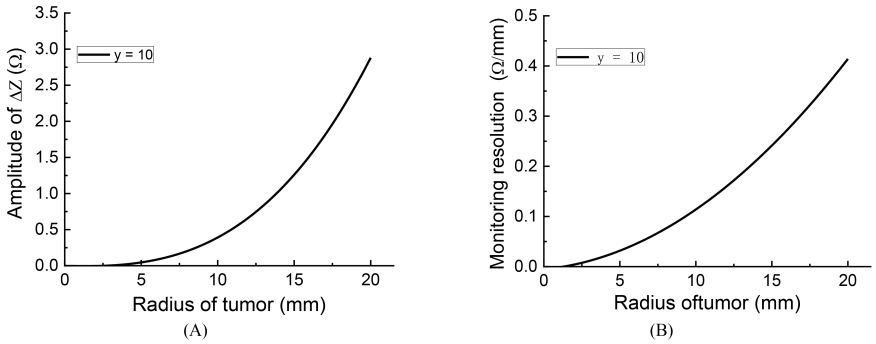

FIGURE 6
The fitting curve and monitoring resolution of impedance change curve y = 10: **(A)** fitting curve, **(B)** monitoring resolution.

R-square = 0.9999, indicating a good fit. Figure 6B illustrates the monitoring resolution derived from calculating the first derivative of the fitting function. The result indicates indicate that the larger the initial tumor size, the higher the monitoring resolution.

To assess the impact of voltage source noise on the results, we introduced varying levels of noise to the source and simulated the impedance change in relation to tumor size. According to the definition of Signal-to-Noise Ratio (SNR) (28):

$$\mathrm{SNR} = 20\lg\frac{V_s}{V_n} \tag{1}$$

In accordance with the formula provided, where Vs represents the accurate excitation voltage, and Vn stands for the voltage noise.

For simulating the voltage source noise, a Gaussian white noise generator was utilized in MATLAB, characterized as follows:

$$V = V_s + awgn(V_s, \frac{SNR}{2}) \tag{2}$$

In the Equation 2, V represents the actual voltage, and the term awgn(V_s, SNR/2) introduces Gaussian noise with a specific SNR to the accurate voltage V_s. It is important to note that the SNR definition used in the awgn function is based on power; hence, the division by 2 is necessary to convert from voltage SNR to power SNR.

After introducing noise to the voltage source, the impedance change curves for different SNR levels, along with the assessment of errors induced by the noise, are presented in Figure 7A.

Figure 7B illustrates that the presence of noise introduces errors in the measured impedance results, with smaller errors observed at higher SNR levels. Specifically, when the initial tumor size is smaller than 5 mm, noise can lead to significant errors in tumor size evaluations. However, for initial tumors larger than 10 mm, the high monitoring resolution within this range (r > 10 mm) allows for acceptable error levels, even with an SNR as low as 40 dB, resulting in a maximum tumor size evaluation error of approximately 1.0 mm. This level of error is generally considered acceptable and can be disregarded.

In practical applications, achieving an SNR of 40 dB is feasible and not particularly challenging in hardware systems. Therefore, the anti-noise capability is sufficiently robust for monitoring tumor size by measuring impedance changes across the treatment electrodes. It is important to emphasize that for tumors smaller than 5 mm, the monitoring resolution and anti-noise capacity are reduced, making it advisable to employ more precise monitoring techniques such as MRI or CT to evaluate changes in tumor size.

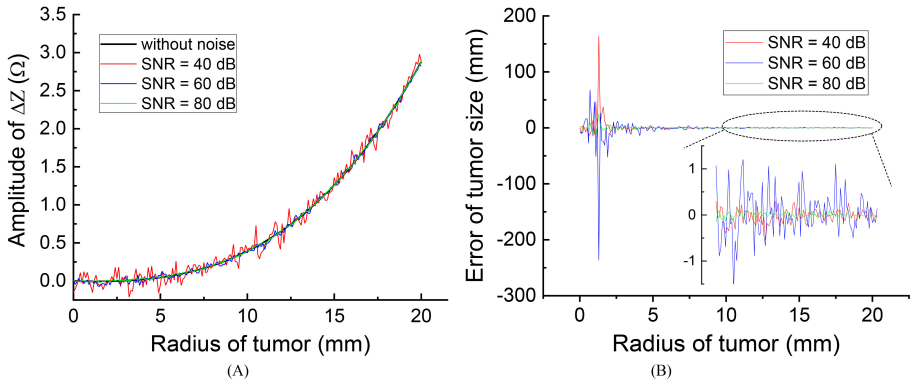

FIGURE 7
The effect of different source noise on the evaluation results: **(A)** effect on the impedance change curves **(B)** evaluation error of tumor size.

4 Conclusions

TTFields represent a relatively new cancer therapy technology designed to combat cancer by disrupting the mitosis of cancer cells. This treatment period typically lasts several months and even years, posing a challenge for monitoring its effectiveness over time. In this study, we explored the hypothesis that real-time monitoring of tumor condition change can be achieved by measuring the impedance change through TTFields treatment electrodes. An in silico study has provided initial evidence supporting the potential value of this proposed method. Preliminary findings suggest that it is feasible to detect tumor size change by measuring amplitude change of impedance across opposite TTFields electrode pairs, utilizing typical TTFields treatment excitation (50V, 200 kHz). Implementing this technique can be straightforward, involving enhancements to the impedance measurement functionality within the existing TTFields treatment hardware system. The scalp electrode arrays will serve dual functions, delivering TTFields and serving as impedance sensors. It is crucial to acknowledge that this study represents a preliminary feasibility investigation, and further validation through clinical studies is essential. If proven successful, this monitoring system could emerge as a valuable augmentation to TTFields cancer treatment technology, offering a means to monitor treatment effectiveness in real-time, potentially enhancing patient outcomes and care.

Data availability statement

The original contributions presented in the study are included in the article/supplementary material. Further inquiries can be directed to the corresponding authors.

Author contributions

XL: Conceptualization, Methodology, Writing – original draft, Funding acquisition. KL: Software, Writing – original draft. HF: Data curation, Writing – review & editing. ZL: Formal analysis, Writing – review & editing. WG: Writing – review & editing, Funding acquisition. PD: Writing – review & editing, Funding acquisition.

Funding

The author(s) declare financial support was received for the research, authorship, and/or publication of this article. Shanghai Fourth People's Hospital, School of Medicine, Tongji University, Talent Introduction and Scientific Research Startup Project, SYKYQD10101. The Natural Science Foundation of Jiangsu Province, BK20241417.

Conflict of interest

The authors declare that the research was conducted in the absence of any commercial or financial relationships that could be construed as a potential conflict of interest.

Publisher's note

All claims expressed in this article are solely those of the authors and do not necessarily represent those of their affiliated organizations, or those of the publisher, the editors and the reviewers. Any product that may be evaluated in this article, or claim that may be made by its manufacturer, is not guaranteed or endorsed by the publisher.

References

1. Kirson ED, Gurvich Z, Schneiderman R, Dekel E, Itzhaki A, Wasserman Y, et al. Disruption of cancer cell replication by alternating electric fields. *Cancer Res.* (2004) 64:3288–95. doi: 10.1158/0008-5472.CAN-04-0083

2. Rehman AA, Elmore KB, Mattei TA. The effects of alternating electric fields in glioblastoma: current evidence on therapeutic mechanisms and clinical outcomes. *Neurosurg Focus.* (2015) 38:E14. doi: 10.3171/2015.1.FOCUS14742

3. Mun EJ, Babiker HM, Weinberg U, Kirson ED, Von Hoff DD. Tumor-treating fields: a fourth modality in cancer treatment. *Clin Cancer Res.* (2018) 24:266–75. doi: 10.1158/1078-0432.CCR-17-1117

4. Trusheim J, Dunbar E, Battiste J, Iwamoto F, Mohile N, Damek D, et al. A state-of-the-art review and guidelines for tumor treating fields treatment planning and patient follow-up in glioblastoma. *CNS Oncol.* (2017) 6:29–43. doi: 10.2217/cns-2016-0032

5. Davies AM, Weinberg U, Palti Y. Tumor treating fields: a new frontier in cancer therapy. *Ann N Y Acad Sci.* (2013) 1291:86–95. doi: 10.1111/nyas.12112

6. Pohling C, Nguyen H, Chang E, Schubert KE, Nie Y, Bashkirov V, et al. Current status of the preclinical evaluation of alternating electric fields as a form of cancer therapy. *Bioelectrochemistry*. (2023) vol:108287. doi: 10.1016/j.bioelechem.2022.108287

7. Hottinger AF, Pacheco P, Stupp R. Tumor treating fields: a novel treatment modality and its use in brain tumors. *Neuro-oncology*. (2016) 18:1338–49. doi: 10.1093/neuonc/now182

8. Latikka J, Eskola H. The resistivity of human brain tumours. *Vivo" Ann Biomed Eng.* (2019) 47:706–13. doi: 10.1007/s10439-018-02189-7

9. Adler A, David H. *Electrical impedance tomography: methods, history and applications*. Boca Raton, FL, United States: CRC Press (2021).

10. Shi Y, Yang Z, Xie F, Ren S, Xu S. The research progress of electrical impedance tomography for lung monitoring. *Front Bioeng Biotech*. (2021) vol:726652. doi: 10.3389/fbioe.2021.726652

11. Griffiths H. Magnetic induction tomography. *Meas Sci Technol.* (2001) 12:1126. doi: 10.1088/0957-0233/12/8/319

12. Oziel M, Korenstein R, Rubinsky B. Non-Contact monitoring of temporal volume changes of a hematoma in the head by a single inductive coil: a numerical study. *IEEE Trans Biomed Eng.* (2018) 66:1328–36. doi: 10.1109/TBME.10

13. Boverman G, Kao TJ, Wang X, Ashe JM, Davenport DM, Amm BC. Detection of small bleeds in the brain with electrical impedance tomography. *Physiol Meas.* (2016) 37:727–50. doi: 10.1088/0967-3334/37/6/727

14. Madre M, Canales-Rodríguez EJ, Fuentes-Claramonte P, Alonso-Lana S, Salgado-Pineda P, Guerrero-Pedraza A, et al. Structural abnormality in schizophrenia versus bipolar disorder: a whole brain cortical thickness, surface area, volume and gyrification analyses. *NeuroImage: Clin.* (2020) 25:102131. doi: 10.1016/j.nicl.2019.102131

15. Demirci N, Holland MA. Cortical thickness systematically varies with curvature and depth in healthy human brains. *Hum Brain Mapp.* (2022) 43:2064–84. doi: 10.1002/hbm.25776

16. Karli R, Ammor H, Terhzaz J. Dosimetry in the human head for two types of mobile phone antennas at GSM frequencies. *Cent Eur J Eng.* (2014) 4:39–46. doi: 10.2478/s13531-013-0140-7

17. Lüders E, Steinmetz H, Jäncke L. Brain size and grey matter volume in the healthy human brain. *Neuroreport.* (2002) 13:2371–4. doi: 10.1097/00001756-200212030-00040

18. Haeussinger FB, Heinzel S, Hahn T, Scecklmann M, Ehlis A, Fallgatter AJ. Simulation of near-infrared light absorption considering individual head and prefrontal cortex anatomy: implications for optical neuroimaging. *PloS One*. (2011) 6:e26377. doi: 10.1371/journal.pone.0026377

19. Korshoej AR, Hansen FL, Thielscher A, OettingenJens GB, Sorensen JC, et al. Impact of tumor position, conductivity distribution and tissue homogeneity on the distribution of tumor treating fields in a human brain: A computer modeling study. *PloS One*. (2017) 12:e0179214. doi: 10.1371/journal.pone.0179214

20. IT'IS Foundation. Available online at: https://itis.swiss/virtual-population/tissue-properties/database/dielectric-properties/. (Accessed Sep. 16, 2020)

21. Fahmy H, Hamad AM, Sayed FA, Abdelaziz YS, Abu Serea ES, Mustafa AB, et al. Dielectric spectroscopy signature for cancer diagnosis: A review. *Microwave Opt Tech Let*. (2020) vol:3739–53. doi: 10.1002/mop.32517

22. Surowiec AJ, Stuchly SS, Barr JR, Swarup AA. Dielectric properties of breast carcinoma and the surrounding tissues. *IEEE Trans Biomed Eng*. (1988) 35:257–63. doi: 10.1109/10.1374

23. Wu Y, Hanzaee FF, Jiang D, Bayford RH, Demosthenous A. Electrical impedance tomography for biomedical applications: Circuits and systems review. *IEEE Open J Circuits Syst*. (2021) 2:380–97. doi: 10.1109/OJCAS.2021.3075302

24. Kirson ED, Dbaly V, Tovarys F, Palti Y. Alternating electric fields arrest cell proliferation in animal tumor models and human brain tumors. *Proc Natl Acad Sci USA*. (2007) 104:10152–7. doi: 10.1073/pnas.0702916104

25. Ponne CT, Bartels PV. Interaction of electromagnetic energy with biological material—relation to food processing. *Radiat Phys Chem*. (1995) 45:591–607. doi: 10.1016/0969-806X(94)00073-S

26. Salvador E, Köppl T, Hörmann J, Schönhärl S, Bugaeva P, Kessler AF, et al. Tumor treating fields (TTFields) induce cell junction alterations in a human 3D In vitro model of the blood-brain barrier. *Pharmaceutics*. (2023) 15:185. doi: 10.3390/pharmaceutics15010185

27. Li X, Yang F, Yu X, Tian H, Hu J, Qian Z. Study on the inverse problem of electrical impedance tomography based on self-diagnosis regularization. *Chin J Biomed Eng*. (2018) 35:460–7. doi: 10.7507/1001-5515.201708024

28. Mould M, Moore CJ, Gerosa D. Moore, Gerosa D. "Calibrating signal-to-noise ratio detection thresholds using gravitational-wave catalogs. *Phy Rev*. (2024) 109:063013. doi: 10.1103/PhysRevD.109.063013

frontiers | Frontiers in Oncology

TYPE Review
PUBLISHED 27 September 2024
DOI 10.3389/fonc.2024.1454370

OPEN ACCESS

EDITED BY
Joubert Banjop Kharlyngdoh,
Tulane University, United States

REVIEWED BY
Xiufeng Chu,
Houston Methodist Research Institute, United States
L. Nicolas Gonzalez Castro,
Harvard Medical School, United States

*CORRESPONDENCE
Steven Brem
Steven.Brem@pennmedicine.upenn.edu

RECEIVED 25 June 2024
ACCEPTED 09 September 2024
PUBLISHED 27 September 2024

CITATION
Tapescu I, Madsen PJ, Lowenstein PR, Castro MG, Bagley SJ, Fan Y and Brem S (2024) The transformative potential of mRNA vaccines for glioblastoma and human cancer: technological advances and translation to clinical trials.
Front. Oncol. 14:1454370.
doi: 10.3389/fonc.2024.1454370

The transformative potential of mRNA vaccines for glioblastoma and human cancer: technological advances and translation to clinical trials

Iulia Tapescu[1], Peter J. Madsen[1,2,3], Pedro R. Lowenstein[4,5,6], Maria G. Castro[4,5], Stephen J. Bagley[1,7,8], Yi Fan[8,9] and Steven Brem[1,3,8]*

[1]Perelman School of Medicine, University of Pennsylvania, Philadelphia, PA, United States, [2]Division of Neurosurgery, Children's Hospital of Philadelphia, Philadelphia, PA, United States, [3]Department of Neurosurgery, University of Pennsylvania, Philadelphia, PA, United States, [4]Department of Neurosurgery, The University of Michigan, Ann Arbor, MI, United States, [5]Department of Cell and Developmental Biology, The University of Michigan, Ann Arbor, MI, United States, [6]Department of Biomedical Engineering, The University of Michigan, Ann Arbor, MI, United States, [7]Division of Hematology/Oncology, Department of Medicine, University of Pennsylvania, Philadelphia, PA, United States, [8]Glioblastoma Translational Center of Excellence, Abramson Cancer Center, University of Pennsylvania, Philadelphia, PA, United States, [9]Department of Radiation Oncology, University of Pennsylvania, Philadelphia, PA, United States

Originally devised for cancer control, mRNA vaccines have risen to the forefront of medicine as effective instruments for control of infectious disease, notably their pivotal role in combating the COVID-19 pandemic. This review focuses on fundamental aspects of the development of mRNA vaccines, e.g., tumor antigens, vector design, and precise delivery methodologies, – highlighting key technological advances. The recent, promising success of personalized mRNA vaccines against pancreatic cancer and melanoma illustrates the potential value for other intractable, immunologically resistant, solid tumors, such as glioblastoma, as well as the potential for synergies with a combinatorial, immunotherapeutic approach. The impact and progress in human cancer, including pancreatic cancer, head and neck cancer, bladder cancer are reviewed, as are lessons learned from first-in-human CAR-T cell, DNA and dendritic cell vaccines targeting glioblastoma. Going forward, a roadmap is provided for the transformative potential of mRNA vaccines to advance cancer immunotherapy, with a particular focus on the opportunities and challenges of glioblastoma. The current landscape of glioblastoma immunotherapy and gene therapy is reviewed with an eye to combinatorial approaches harnessing RNA science. Preliminary preclinical and clinical data supports the concept that mRNA vaccines could be a viable, novel approach to prolong survival in patients with glioblastoma.

KEYWORDS

brain tumor, clinical trial, glioma, glioblastoma, immunotherapy, immuno-oncology, mRNA, vaccine

1 Introduction

In the realm of medical breakthroughs, few innovations have sparked as much excitement and promise as the advent of messenger ribonucleic acid (mRNA) vaccines (1–4), reflected in the award of the 2023 Nobel Prize in Physiology or Medicine to Katalin Karikó and Drew Weissman for their foundational discoveries of the mRNA vaccine platform (5). Importantly, the mRNA vaccine platform was originally adapted as a tool in the fight against cancer (6, 7). Sahin et al. noted a synergistic effect of mRNA vaccine with immune checkpoint blockade in patients with melanoma; antitumor responses were noted, paradoxically, in patients whose tumors had a low mutational burden, suggesting that mRNA vaccines could be effective in tumors (such as glioblastomas) with a low mutational burden (7).

The mRNA vaccine platform, however, emerged as a transformative force in the battle against infectious diseases, particularly its pivotal role to thwart COVID-19 (2–4, 8, 9). Recent research has shown that mRNA vaccines have therapeutic potential against solid cancers such as melanoma (10, 11), prostate (12), colorectal (13), pancreatic, head and neck cancers as well as non-small-cell lung cancer (14), and more recently, glioblastoma (15). In this review, we explore the basic components of mRNA vaccines (16), advances in mRNA vaccine design, and the potential of mRNA vaccines to treat glioblastomas, highlighting the progress made in personalized, precision mRNA medicine.

RNA technology is still in its infancy (17). Only a few years ago, almost all attention in immunotherapy was centered on the remarkable scientific and clinical advances in oncology resulting from the introduction of immune checkpoint blockade (18, 19). Although there is a distinct group of long-term survivors, including patients with metastatic cancer, most patients with cancer have recurrences and are resistant to immune checkpoint inhibitors (ICIs) when given as a single immunotherapy. Across the spectrum of human cancer, immune resistance results from an immunosuppressive, tumor microenvironment (TME) as well as insufficiency of numbers or functional, activated T cells (18). Therefore, ICIs are now being proposed to synergize within new "platforms" of cellular immunotherapy such as CAR T cells (20, 21) or dendritic cell (DC) vaccines (22).

Based on different preparation methods, platforms for cancer vaccines are divided into four categories (23): *i*) cell-based vaccines (CAR T cells, DC vaccines); *ii*) viruses-based, oncolytic vaccines (21, 24–26); *iii*) peptide-based vaccines; and *iv*) nucleic acids-based vaccines, which include DNA and RNA vaccines, composed of the encoding gene and carrier group of pathogen antigens (23). mRNA vaccines are synthesized *in vitro*, and then *in vivo* encode antigens and express proteins after internalization to stimulate an immune response (23), (Figure 1). In recent years, combining cancer vaccines with various immunotherapies or standard treatments has become a promising new avenue to overcome immune resistance and improve clinical outcomes (20–22).

A guide to the current concepts in the development of mRNA vaccines is featured in Table 1, including the comparative advantages and disadvantages of the four platforms for cancer vaccines, and their use as part of a combination regimen, as well as safety concerns (27–40). These topics will be discussed in greater detail, with an emphasis on applications to neuro-oncology (Section 4) based on the authors' translational studies and early-stage trials for glioblastoma and in a variety of human cancers (Table 2).

An important, but nuanced, biological advantage of mRNA vaccines is the recent discovery that in order for immunotherapy to eliminate solid tumors, there needs to be a functioning intratumoral "triad" of synergistic activity between *i*) antigen-presenting cells (APCs)/dendritic cells; *ii*) activated $CD4^+$ T cells and *iii*) activated $CD8^+$ T cells which licenses $CD8^+$ T cell cytotoxicity and elimination of cancer cells (41). mRNA vaccines are in a unique position to activate each of these three, critically important cell subpopulations by the method of uptake in the APC and the activation of both $CD8^+$ cells $CD4^+$ T cells through binding on the cell surface, respectively, to MHC (major histocompatibility class) I and II molecules (Figure 1). and then activation of the T cell receptor (28).

2 Mechanism of mRNA vaccine-mediated activation of anti-tumor immunity

Broadly speaking, mRNA cancer vaccines consist of mRNA molecules encoding specific tumor antigens. Upon administration, these mRNA molecules are subsequently internalized by APCs where they undergo translation, resulting in the production of protein antigens. These antigens are further processed into antigen peptides, which subsequently bind to MHC 1 molecules within the endoplasmic reticulum and are then presented or cross-presented on the surface of APCs (42, 43). This process activates $CD4^+$ and $CD8^+$ T cells, orchestrating a potent cell-mediated immune response (Figure 1). In parallel, protein antigens encoding mutated peptides are routed through the endosomal pathway. This alternative route enables the activation of $CD4^+$ and $CD8^+$ T cells through MHC Class I/II presentation (44). This dual activation of both $CD8^+$ and $CD4^+$ T cells amplify the breadth and potency of the immune response. Dual activation of both $CD8^+$ and $CD4^+$ T cells as well as APCs are required to successfully eliminate solid tumors, otherwise refractory to immunotherapy (41).

What are the specific steps by which targeted mRNA is internalized by the APC to trigger an immune response by releasing the translated antigen or presenting the epitopes onto the surface of cells? One model (28) describes a sequence of nine steps: *i)* the targeted mRNA-LNP binds to the cell surface receptor of the APC mediated by specific ligands; receptor activation can lead to interferons or other cytokine/chemokine production; *ii)* after endocytosis, mRNA in the endosome interacts with membrane-bound Toll-like receptors (TLRs); *iii)* triggering of TLR activates signal transduction pathways that selectively lead to production of Type 1 interferons (45) that upregulate the effector function of immune cells (e.g., DCs, T cells, and B cells) and/or pro-inflammatory cytokines; *iv)* entrapped mRNA then is released from the endosome into the cytosol where *v)* the mRNA is translated by ribosomes; *vi)* upon translation, the proteins are either a) secreted out

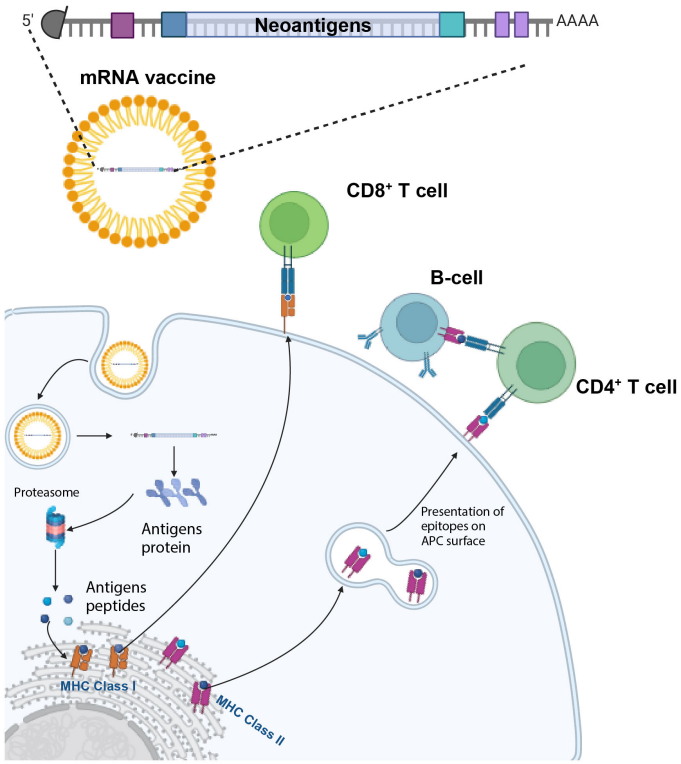

FIGURE 1
mRNA vaccines activate both humoral and cell-mediated immunity. The mRNA vaccine encoding several tumor neoantigens is injected and enters antigen-presenting cells (APCs). Here, the mRNA is endocytosed, and then translated, with the different antigens being processed by the proteasome and subsequently binds to MHC Class I molecules in the endoplasmic reticulum and are exported to the cell surface to activate $CD8^+$ T cells. In parallel, the processing of antigens through the endosomal pathway enables the activation of $CD4^+$ T-cells and B-cells. Created with BioRender.com.

of the host APC, or b) processed within the APC by the proteasome into smaller antigen peptides; *vii)* secreted extracellular mRNA is then taken up by another APC, degraded into peptides; these epitopes are subsequently presented on the cell surface by MHC class II molecules; *viii);*alternatively the intracellular peptides are processed within the endoplasmic reticulum and loaded onto MHC class I and/or class II molecules *ix)* the epitopes bound to MHC class I/II molecules migrate to the cell surface where they bind to the T cell receptor (TCR) of $CD8^+$ and/or $CD4^+$ T lymphocytes (28).

Furthermore, the secreted protein antigen, encoded by the mRNA vaccine, plays a critical role in stimulating B cells. This activation prompts the production of neutralizing antibodies, thereby bolstering the humoral arm of the immune response. In summation, mRNA vaccines exhibit remarkable potential in eliciting a comprehensive immune response against tumors by instigating both robust humoral and cell-mediated immunity (Figure 1). Four pivotal aspects come into play in the creation of an effective mRNA cancer vaccine: *i)* identification of tumor antigens; *ii*) vector design; *iii)* delivery; and *iv*) manufacturing.

2.1 Identification of tumor antigens

The accumulation of genetic mutations in cancer leads to the creation of unique tumor-specific antigens or neoantigens (46). These unique antigens can be displayed by the major histocompatibility molecules found on the surface of tumor cells. T-cells primed to identify these neoantigens launch targeted assaults on cancerous cells expressing these mutations (47). In the pursuit of neoantigens, most studies have concentrated on indels and non-synonymous single nucleotide variants (SNVs). Yet, numerous SNVs are unique to individual patients, and tumors with low mutational burden exhibit a small number of SNVs that is inadequate for vaccine design (48, 49). As a result, exploring supplementary reservoirs of cancer neoantigens, like gene fusions, alternative splicing variants, and post-translational modifications, holds promise in unearthing fresh targets for immunotherapeutic interventions (50).

2.2 mRNA vector design

In terms of mRNA vector design, several strategies are employed. The conventional mRNA encodes the vaccine immunogen, flanked by 5′ and 3′ UTRs, along with a 5' cap and polyA tail optimized for maximum stability and translational potential. In addition, many of the licensed SARS-CoV-2 vaccines contain nucleoside-modified mRNAs, using an N1-methylpseudouridine, which counters immune-related inhibition of translation and degradation (1, 51). This configuration allows for

TABLE 1 Current concepts in the development of mRNA vaccines for glioblastoma and other solid cancers: pearls and caveats in the selection, application, and combination of mRNA vaccines related to the landscape of cancer immunotherapy.

Current Concepts in the Development of mRNA Vaccines for Glioblastoma and Other Solid Cancers
1. ***Unmet Need***. Despite > 40 monoclonal antibodies and six CAR T cell therapies approved for a broad spectrum of malignancies, only a minority of cancer patients have a durable response to current immunotherapeutics (27). The only approved cancer vaccine, Sipuleucel-T (NCT00065442), an autologous dendritic cell therapy for prostate cancer, was approved in 2010, but never gained widespread use due to its high cost and underwhelming clinical efficacy (27). Currently the standard of care for glioblastoma includes surgery (maximal safe resection), chemotherapy (temozolomide) and radiation therapy with judicious use of tumor-treating fields, bevacizumab, and chemowafers. There is currently no FDA-approved immunotherapeutic regimen FDA-approved for glioblastoma. In the reignition of the Cancer Moonshot initiative by President Biden, two of the ten central research recommendations include translational immunotherapy and overcoming resistance (27).
2. ***Advantages of mRNA vaccines.*** The inherent *modularity* of mRNA-LNP vaccines enable the encapsulated mRNA to encode for *many proteins*, enables their formulation and clinical translation to be more *rapid* and *economical* than prior cell-based technologies (10, 27, 28). Specifically, manufacturing costs are low compared to other classes of vaccines (10), cost-effective and scalable – mainly due to high yields of *in vitro* transcription reactions (28). Also, there can be a "payload" targeting multiple proteins. Six of the first ten clinical trials using mRNA vaccines were individualized to a specific patient's specific neoantigens, thus offering a more *personalized approach* than other forms of immunotherapy (27). The ability to *develop patient-specific vaccines* has the potential to elicit therapeutic responses in those recalcitrant to existing treatments (27). mRNA vaccines can induce both *humoral* and *cellular* immune responses (10). Initially, for cancer immunotherapy, mRNA was used only as a template encoding tumor-associated antigens, but due to its versatility and design variability, the therapeutic potential of mRNA is now considered limitless (10). Because patient-derived mRNA can be amplified *in vitro*, a relatively small number of cells is needed to develop a mRNA vaccine, important for patients who only have a small, surgical biopsy (29).
3. ***mRNA Vaccines and Combination Therapies.*** Beyond personalizing vaccine antigens, mRNA provides a unique opportunity to develop combination therapies. Immune stimulating mRNA into vaccine formulations can combat the immunosuppressive TME, including boosting antigen presentation and DC activation. Although not validated through testing, the current concept is that immune stimulation with mRNA could be synergistic with other vaccine types (27). A vaccine format such as a mRNA vaccine (in combination with synthetic peptides, DNA vaccine, or viral vectors) allows for targeting of dozens of mutations per patients (30). This concept of "multiple warheads," can be used to combine complementary categories of neoepitopes such as MCH-1 and MHC-II, clonal and subclonal, undetected antigens, an approach that mitigates the risk of 'betting on a biological hypothesis that later is proved to be wrong' (30). Larger tumor loads, especially, might require combination immunotherapies (30). Neoepitope vaccines are safe and well-tolerated; combining them with drugs or ICIs could keep the repertoire of vaccine-induced T cell specificities functional (30). mRNA vaccines are capable of both priming and boosting immunological responses and can thus serve as an important backbone for any immunotherapeutic regimen (31)..
4. ***Safety of mRNA Vaccines.*** Vaccines that are centered on mRNA are generally considered safer than DNA and viral vectors as mRNA is the minimal genetic vector, containing only the elements directly required for the expression of the encoded protein (10). The risk of infection or insertional mutagenesis is minimal or negligible compared to viral or DNA vectors due to mRNA's non-infectious nature and non-integration with the genome (6, 16, 23, 28, 29, 32, 33).
5. ***Comparison of advantages of the four major cancer vaccine platforms***. The pros and cons of the four major platforms/categories of cancer vaccines (23) are summarized by Fan et al. (34): • **1) Nucleic Acid-based Vaccines**: **a) DNA Vaccines:** Advantages include stability (29), low cost (35); cell-independent production; durable immune response; and potential for targeting multiple neoantigens. Once plasmid DNA enters the nucleus, a single plasmid DNA can produce multiple mRNA copies, producing more antigens than a single mRNA molecule (23). Efforts to improve immunogenicity and clinical application of DNA vaccines include electroporation, codon optimization of plasmid constructs, or co-administration of adjuvants (35). An ideal technology for cancer vaccines should allow the codelivery of multiple $CD8^+$ and $CD4^+$ T cell epitopes from several cancer antigens (35). The concerns include low transfection efficiency; risk of autoimmune reactions; risk of integration into host genome. b) **mRNA Vaccines**: mRNA vaccines have rapidly emerged as agents that can induce robust antitumor activity against both shared ("off-the-shelf", mass produced, analogous to COVID-19 mRNA vaccine) and personalized antigens, with both approaches shown to be or likely to become commercially feasible in the near future (31).These are synthesized *in vitro*, encode antigens and express proteins after internalization to stimulate an immune response (23). mRNA is an ideal platform for personalized neoantigen vaccine preparation (23).Encoding full-field tumor antigens simultaneously and cross-presenting multiple epitopes of human leukocyte antigen (HLA) by APCs can induce a broader T cell response (23) Advantages, as noted, include: rapid development and easy modification; high immunogenicity; cell-independent production; able to enter non-dividing cells; intrinsic adjuvant effect; high efficiency into DCs (36). DNA molecules need to enter the cell nucleus to initiate transcription, while mRNA enters the cytoplasm to translate and express antigens directly. Therefore, mRNA antigen production is instantaneous and efficient. DNA vaccines need an extra step to go into the cell nucleus, leading to a lower immune response than mRNA vaccines (23). The concerns include fast degradation speed, especially linear mRNA (29), susceptibility to RNase degradation (37), potential for inflammatory reaction, and inefficiency of *in vivo* delivery (23) • **2) Peptide-based Vaccines**: Advantages include high specificity and safety; cell-independent production; low risk of autoimmunity; direct presentation on MHC in short peptides; proven clinical activity with synthetic long peptides. Disadvantages include high cost; complex manufacturing process; potential for HLA-restriction (32). • **3) Cell-based Vaccines:** The advantages are strong immune stimulation; multi-form antigen loading. Disadvantages include high cost; potential for undesirable immunogenicity of the cells (on target, off-tumor); and need for patient-specific customization (for autologous vaccines). • **4) Viral and Bacterial Vector Vaccines:** The benefits include high immunogenicity; long-term immune response; and self-adjuvanticity. The risks include potential for vector immunogenicity; and need for specialized storage conditions.
6. ***Comparison of mRNA vaccines with peptide vaccines.*** The early successes of mRNA vaccines could position this novel therapeutic class of vaccines as a superior "platform" compared to decades of testing with peptide vaccines that have been largely unsuccessful. mRNA vaccines provide greater flexibility, enabling the use of multiple permutations of targets, backbones, and combinations, with adaptability and encouraging progress to commercialize mRNA vaccines, making mRNA vaccines uniquely positioned to suppress malignant evolution (31), advancing the goal of "immuno-interception" (38). *Cancer is capable of progressing only when the normal function of the immune system is disrupted* (10).
7. ***Combination Therapies – Combining mRNA Vaccines with Other Vaccines and Immunomodulatory Approaches***. In recent years, combining cancer vaccines with various immunotherapies or standardized treatments has become an effective strategy for overcoming tumor resistance and improving clinical outcomes (23). Current protocols employ a multi-pronged approach that focus on three obstacles: a) T cell exhaustion with strategies to activate and refresh $CD4^+$ and $CD8^+$ T cells; b) the immunosuppressive TME, e.g., cytokine reprogramming using stereotactic radiation therapy, an inhibitor of IL-6 (tocilizumab) and an ICI (atezolizumab) (39); and iii) inhibition of immune checkpoint (PD-1/PD-L1) pathways using ICIs. A combination approach is also being applied to vaccine development (20, 21); For example, an mRNA vaccine, encoding a chimeric receptor directed towards CLDN6, was found to enhance the efficacy of claudin-CAR-T cells against solid tumors (40), use of a nanoparticulate RNA vaccine stimulated adoptively transferred CAR-T cells. Presentation of the CLDN6 antigen on resident APCs promoted cognate and selective

(Continued)

TABLE 1 Continued

Current Concepts in the Development of mRNA Vaccines for Glioblastoma and Other Solid Cancers
expansion of CAR-T cells; improved engraftment of CAR-T cells; regression of large tumors in difficult-to- treat mouse models was achieved at subtherapeutic CAR-T cell doses (40). In the field of cancer immunotherapy, we have entered into an era of combined treatments (18, 35), and the development of potent therapeutic anticancer vaccines may be the missing element for being able to efficiently treat more patients and a wider range of tumors. There is a strong rationale for combining cancer vaccines with other immunotherapy drugs, such as immune checkpoint inhibitors or oncolytic viruses. Combining cancer vaccine and tumor resection allowed the infiltration of activated T cells to the resection site with a strong impact on mouse survival in an aggressive GBM preclinical model (35). The positive experience of combinatorial strategies for CAR T cell therapy could be extended to the future use of mRNA vaccines. For example, the use of **oncolytic viruses** leads to M1 polarization, oncolysis, damage-associated molecular patterns (DAMP)s and release of tumor antigens, resulting in enhanced T cell activation (21). Combining mRNA vaccines with CAR T cells could activate APCs, attack tumor-associated antigens leading to T cell expansion, and ultimately, cancer cell death (21). Cytokines could be added to mRNA vaccine therapy, as suggested for CAR T cell therapy (21) to reverse the immunosuppressive TME.
8. *Combination with Immune Checkpoint Inhibitors.* The combination of mRNA vaccines with ICIs can enhance cell-mediated immunity (10). Combined with CAR T cell therapies, ICIs enhance the function of tumor infiltrating lymphocytes (TILs), restoring their ability to attack cancer cells (21).
9. *Results of Early Clinical Trials using mRNA Vaccines.* Although there are no FDA-approved mRNA vaccines, the results of early clinical trials are promising (Table 2)**, including encouraging phase II studies across various platforms, an ongoing phase III trial and auspicious data from patients with poorly immunogenic tumors** (15, 31).

the translation of the antigen from the nonreplicating transcript (52). One drawback of conventional mRNA vaccines is the limited antigen expression, which is proportional to the number of mRNA transcripts that are delivered, thus necessitating larger doses of vaccine or repeat administrations. One way to overcome this limitation is the use of self-amplifying mRNAs. This alternative strategy employing self-amplifying mRNA has additional elements such as 5′ and 3′ conserved sequence elements (CSE), the nsP1-4 genes, and a subgenomic promoter of an alphavirus, and the vaccine immunogen (52, 53). Post-*in situ* translation, both the antigen and RNA-dependent RNA polymerase are generated (Figure 2). The latter identifies the CSEs, subsequently amplifying the vaccine-encoding transcripts, resulting in an augmented accumulation of tumor antigens within the cell (Figure 2). Trans-amplifying mRNAs introduce two distinct transcripts into the equation. One encodes for the RNA-dependent RNA polymerase (nsp1-4), while the other encodes the CSE and the viral antigen. This dual-transcript configuration achieves an even stronger self-amplifying effect (52) (Figure 2).

3 Delivery systems for mRNA vaccines

Various delivery systems facilitate the deployment of mRNA vaccines. These encompass lipid-based, polymer-based, and emulsion-based delivery systems, all utilizing cationic molecules to transport the anionic mRNA across the cell membrane (53). Critical elements of the mRNA delivery system include achieving optimal intracellular and targeted delivery, ensuring stability to facilitate antigen translation, and triggering appropriate immune activation (54).

To this end, the lipid nanoparticle (LNP) system has been recognized as a powerful and versatile delivery platform (55). These LNPs have an ionizable lipid, a helper lipid, cholesterol, and a PEG-conjugated lipid (54). A crucial aspect of the LNP system lies in its utilization of pH-sensitive cationic lipids, which facilitate cellular internalization via receptor-mediated endocytosis. The low pH within the endosome causes the ionization of cationic lipids, which interact with anionic lipids on the endosomal membrane, leading to the disruption of the endosomal membrane and release of the mRNA into the cytoplasm (53). The helper lipid, usually a phospholipid, helps stabilize the LNP structure, the cholesterol promotes membrane fusion and prolongs the half-life, while the PEG-conjugated lipid increases particle stability (56). Advances in high throughput screens and rational design approaches have yielded specific ionizable lipids tailored for diverse applications, such as systemic delivery for the SARS-CoV-2 vaccine (57) and targeted delivery to the lung epithelium (58) or placenta (59) for CRISPR-editing purposes. To identify mRNA delivery vehicles that facilitate mRNA delivery *in vivo* and provide potent, specific immune activation, a heterocyclic lipid formulation was found to demonstrate robust immune responses and tumor growth inhibition in melanoma and human papillomavirus E7 tumor models via the STING pathway, with minimized systemic cytokine expression (60).

Additional novel mRNA-LNP delivery approaches include devising targeting approaches to specifically deliver the mRNA payload into cell types once deemed inaccessible (61). Passive targeting approaches require intratumoral administration, however, the injected particles are heterogeneously distributed throughout the tumor and often accumulate in the liver and lymphatic organs (62). Additional active strategies require modifying the surface of mRNA-LNPs to allow for delivery to specific cells, for example by functionalizing antibodies on LNPs or including tRNAs with cell-type expression patterns in the cargo (61). Recently, a novel platform of activated LNPs with surface-conjugated human CD3 and CD28 antibody fragments has been introduced as a rapid, one-step method to enhance mRNA CAR T cell therapy to decrease tumor burden, and the potential to reduce the complexity, cost and time of mRNA CAR T cell production as well as to support other immunotherapy applications (63). Targeting brain cancers represents a particular challenge because of the blood-brain barrier; recently, a specific class of LNPs with structurally diverse ionizable lipids shows promise to traverse the blood-brain barrier (64).

Advances continue to be made to all individual elements of mRNA vaccine from novel types of tumor antigens and self-

TABLE 2 Active clinical trials for mRNA cancer vaccines registered on clinicaltrials.gov.

NCT Number	Study Status	Phase	Target Malignancy	Treatment- Specifics	Sponsor
NCT05192460	Recruiting	NA	Gastric Cancer, Esophageal Cancer, Liver Cancer	Neoantigen tumor vaccine +/-PD-1/L1	NeoCura
NCT05359354	Recruiting	NA	Solid Tumor	Personalized neoantigen tumor vaccine	NeoCura
NCT05981066	Recruiting	NA	Advanced Hepatocellular Carcinoma	ABOR2014/IPM511 vaccine	Peking Union Medical College Hospital
NCT03908671	Recruiting	NA	Esophageal Cancer, Non-Small Cell Lung Cancer	Personalized mRNA tumor vaccine	Stemirna Therapeutics, The First Affiliated Hospital of Zhengzhou University
NCT05940181	Recruiting	NA	Solid Tumor	Sintilimab	NeoCura
NCT05949775	Not yet recruiting	NA	Advanced Malignant Solid Tumors	Neoantigen personalized vaccine	Stemirna Therapeutics
NCT06353646	Not yet recruiting	NA	Pancreatic cancer	XH001 mRNA vaccine + Ipilimumab + Chemotherapy	NeoCura
NCT05761717	Not yet recruiting	NA	Postoperative Hepatocellular Carcinoma	Neoantigen mRNA Personalized Cancer vaccine + Sintilimab	Shanghai Zhongshan Hospital
NCT06141369	Recruiting	NA	Adrenal Cortical, Carcinoma Medullary, Thyroid Cancer, Thymic Neuroendocrine Carcinoma, Pancreatic Neuroendocrine Tumor	Individualized mRNA neoantigen vaccine (mRNA-0523-L001)	Shanghai Jiao Tong University School of Medicine
NCT06326736	Recruiting	Early phase I	Resectable Pancreatic Cancer	Personalized vaccine SJ-Neo006 + Gemcitabine + Abraxane + Camrelizumab	Jinling Hospital, China
NCT02872025	Recruiting	Early phase I	Carcinoma, Intraductal, Noninfiltrating	Intralesional mRNA 2752 + Pembrolizumab	Merck Sharp & Dohme LLC, ModernaTX, Inc.
NCT06156267	Not yet recruiting	Early phase I	Pancreatic Cancer	mRNA tumor vaccine + Adebrelimab	Fudan University, Shanghai Regenelead Therapies Co., Ltd.
NCT05579275	Recruiting	I	Advanced Malignant Solid Tumors	Self-replicating JCXH-212 mRNA vaccine	Peking University Cancer Hospital & Institute
NCT05738447	Recruiting	I	Liver Cancer, Hepatocellular Carcinoma	HBV mRNA vaccine	West China Hospital
NCT06019702	Recruiting	I	Digestive System Neoplasms	Ineo-Vac-R01	Sir Run Run Shaw Hospital, Hangzhou Neoantigen Therapeutics Co., Ltd.
NCT05198752	Recruiting	I	Solid Tumor	Personalized neoantigen mRNA cancer vaccine	Stemirna Therapeutics
NCT06026800	Recruiting	I	Digestive System Neoplasms	Ineo-Vac-R01 + standard first line treatment	Sir Run Run Shaw Hospital, Hangzhou Neoantigen Therapeutics Co., Ltd.
NCT04745403	Recruiting	I	Hepatocellular Carcinoma	MRNA HBV/TCR T-cells	Lion TCR Pte. Ltd.
NCT05938387	Active Not Recruiting	I	Glioblastoma	CV09050101 mRNA vaccine	CureVac
NCT05714748	Recruiting	I	Malignant Tumors	EBV mRNA vaccine	West China Hospital
NCT06026774	Recruiting	I	Digestive System Neoplasms	Ineo-Vac-R01 + standard adjuvant therapy	Sir Run Run Shaw Hospital, Hangzhou Neoantigen Therapeutics Co., Ltd.
NCT05264974	Recruiting	I	Melanoma	Autologous total tumor mRNA loaded DOTAP liposome vaccine	University of Florida

(Continued)

TABLE 2 Continued

NCT Number	Study Status	Phase	Target Malignancy	Treatment- Specifics	Sponsor
NCT04573140	Recruiting	I	Adult Glioblastoma	Autologous total tumor mRNA and pp65 LAMP mRNA loaded DOTAP liposome vaccine, RNA-LPs	University of Florida, Pacific Pediatric Neuro-Oncology Consortium, University of California, San Francisco, CureSearch, Team Jack Foundation, Florida Department of Health
NCT05942378	Not yet recruiting	I	Advanced Solid Tumor	HRXG-K-1939 mRNA vaccine + Adebrelimab	Fudan University
NCT06195384	Not yet recruiting	I	Solid Tumor, Adult	Neoantigen mRNA Vaccine	Second Affiliated Hospital of Guangzhou Medical University
NCT05978102	Recruiting	I|II	Advanced Solid Tumor	STI-7349 mRNA + Pembrolizumab	The Fourth Affiliated Hospital of Zhejiang University School of Medicine
NCT06273553	Not yet recruiting	I|II	HPV- Associated Intraepithelial Neoplasia	RG002 mRNA vaccine	RinuaGene Biotechnology Co., Ltd.
NCT06249048	Not yet recruiting	I|II	Advanced Solid Tumor	STX-001 mRNA vaccine+ pembrolizumab	Strand Therapeutics Inc.
NCT04534205	Recruiting	II	Unresectable, Metastatic or Recurrent Head and Neck Squamous Cell Carcinoma	Bnt113+ pembrolizumab	BioNTech SE
NCT03688178	Active Not Recruiting	II	Glioblastoma	Human CMV pp65-LAMP mRNA-pulsed autologous DCs + Temozolomide; Varlilumab, Unpulsed DCs	Celldex Therapeutics
NCT03897881	Recruiting	II	Melanoma	MRNA-4157+Pembrolizumab	ModernaTX, Inc.
NCT03815058	Active Not Recruiting	II	Untreated Melanoma	Autogene cevumeran+ Pembrolizumab	Genentech, Inc.

NA, not applicable.

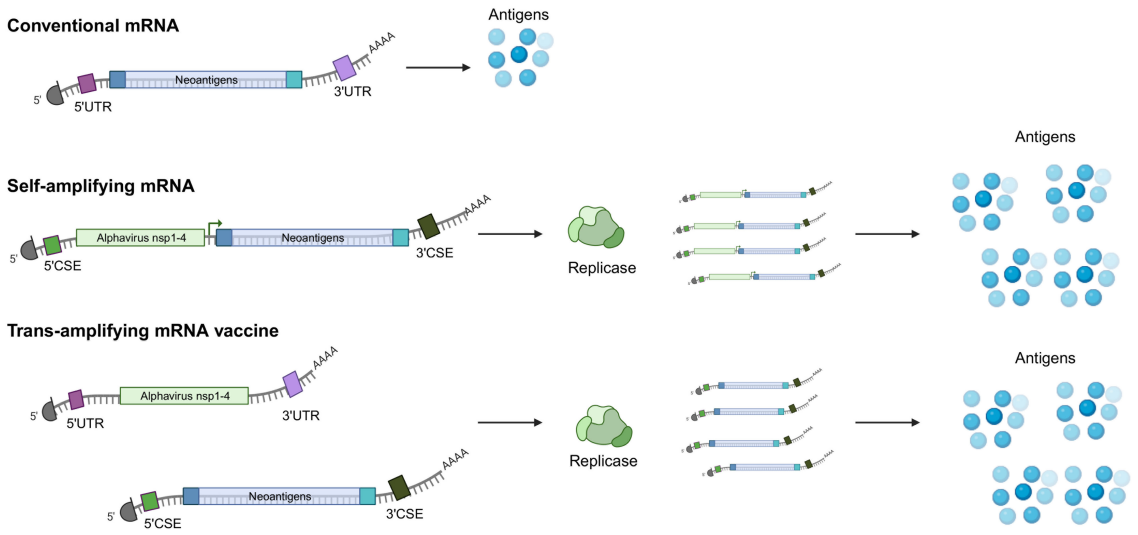

FIGURE 2
Conventional and self-amplifying mRNAs. (top) Conventional mRNAs contain the nucleoside-modified coding elements targeting tumor antigens, 5′ and 3′ untranslated regions, a polyA tail as well and a 5′ cap analog, which have all been designed to improve stability and translational potential. (middle) Self-amplifying mRNAs also encode an RNA polymerase, usually derived from alphaviruses as well as a 5′ and a 3′ conserved sequence element (CSE). The viral RNA replicase recognizes the structural CSE elements and directs the synthesis of negative-sense RNA intermediates, which are transcribed into many copies of the coding mRNA template and amplified antigen expression. (bottom) Another strategy of self-applying mRNA vaccine involves using two distinct mRNAs, one encoding for the replicase and one for the tumor antigens. Both types of self-amplifying strategies result in enhanced expression and prolonged expression of the encoded tumor antigen. Created with BioRender.com.

amplifying mRNA vectors to targetable LNPs. Focusing on several difficult-to-treat cancers, this review describes recent advances in mRNA vaccines for solid tumors outside of the CNS, such as pancreatic cancer, head and neck cancers, melanoma, and then focuses on the challenge of glioblastoma.

4 mRNA vaccines in human cancer

4.1 Pancreatic cancer

The transformative potential of mRNA vaccines is best demonstrated by recent breakthroughs in one of the most formidable cancers, pancreatic carcinoma (65, 66). Pancreatic cancer has one of the highest death rates of any solid organ malignancy, with an overall 5-year survival of less than 10%; it is currently the third most common and on a projected course to become the second most common cause of cancer-related deaths in the United States by 2030 (67–69). Surgery currently is the only modality that offers a chance of a cure (67), but 5-year survival rates after surgical resection alone are low, approximately 10% (67, 70), and up to 30% with resection and adjuvant chemotherapy (68, 70). Unfortunately, only 10-20% of patients are diagnosed with localized, surgically resectable disease (68), and over 90% relapse 7-9 months after resection (70). Pancreatic cancers have historically shown resistance to immunotherapy, partly attributed to a complex immunosuppressive microenvironment, poor T cell infiltration, and reduced mutational burden leading to reduced activation of antitumor T cells (71, 72). In addition, pancreatic cancer is thought to harbor very few neoantigens (an average of 35 compared to hundreds in melanoma), thus having weak antigenicity (71, 73, 74). Multiple pancreatic cancer immune subtypes have been identified. For example, pancreatic tumors categorized as immunologically "cold" typically exhibit low immunogenicity and/or a high presence of reactive stroma (75). Pancreatic adenocarcinoma, akin to glioblastoma, has proven almost entirely insensitive to immune checkpoint inhibition with a response rate < 5% (70); this insensitivity can be partially ascribed to the low mutation rate, and the consequent scarcity of neoantigens (70) as well as intratumoral and inter-tumoral heterogeneity (76). Thus, a combination of a personalized mRNA vaccine with immunogenic chemotherapy, stromal modulation, and ICI may be needed for an effective therapy (76).

Despite these challenges, Rojas and colleagues conducted a phase I clinical trial that implemented a personalized mRNA vaccine strategy, wherein at least five, and up to 20 neoantigens specific to each patient's tumor, were identified and integrated into the vaccine (65). The vaccine was delivered using lipoplex nanoparticles via intravenous injection after surgical resection and in combination with the standard mFOLFIRINOX chemotherapy. Notably, all participants also received a single dose of an ICI before receiving their personalized mRNA vaccine. Encouragingly, T cells recognizing specific neoantigens were detected in half of the trial participants, categorized as immune responders. Strikingly, immune responders showed no signs of cancer recurrence at a median follow-up of 18 months, compared to a median time to recurrence of 13.4 months in non-responders (65). Nevertheless, treating pancreatic cancer remains challenging as half of the participants did not respond to the vaccine and most patients were not eligible for surgery and thus ineligible for the vaccine. Strategies to boost the response to the vaccine and predict responsiveness will be an advance to enrich the percentage of responders. One possibility, going forward, would be to treat patients harboring unresectable cancers with FOLFIRINOX neoadjuvant chemotherapy who then might qualify for the surgery and enable them to get the personalized mRNA vaccine (77, 78).

4.2 Head and neck cancers

Head and neck squamous cell carcinomas (HNSCCs), arising from the mucosal epithelium, represent the most prevalent histological type of head and neck malignancy (79). These cancers are characterized by their multifactorial etiology, stemming from infections with high-risk human papillomaviruses (HPVs) (80–82) or Epstein–Barr virus (83, 84) and lifestyle-related risk factors including alcohol consumption and smoking (85, 86). Despite significant advancements in treatment modalities for HNSCCs, encompassing surgical interventions, radiotherapy, and chemotherapy, the 5-year overall survival rate remains in the range of 40–50%; however, the use of ICIs (e.g., pembrolizumab or nivolumab) has led to superior outcomes, leading to the integration of immunotherapy for this challenging disease (87). However, based on clinical trials (88–90), less than a third of patients respond to immunotherapy (91); therefore, additional therapies such as mRNA vaccines are needed. Given the diverse etiologies of HNSCC, the HNSCC-associated neoantigens can broadly be divided into either virus-derived tumor antigens or non-virus-derived. HNSCC arising due to persistent infection with high-risk human papillomavirus 16 (HPV-16) is associated with improved survival (92, 93), likely due to the enhanced immunogenicity of HPV-derived neoantigens.

The potential of mRNA vaccines for HPV-specific-HNSCC has also been recently shown in murine models. The most common HPV subtype found in HPV-positive HNSCC is HPV-16, which accounts for over 90% of HPV-positive HNSCC (94). While the majority of HPV infections are cleared, infections in the epithelium of palatine and lingual tonsil can persist (95), leading to constitutive expression of E6 and E7 oncoproteins (96). Mouse model experiments with mRNA vaccines against E7 promoted tumor regression, prevented relapse, and re-sensitized mice to PD-L1 immunotherapy, rendering anti-PD-L1 refractory tumors responsive (96). Similarly, mouse model experiments using three different mRNA platforms, an unaltered non-replicating mRNA vaccine, a modified non-replicating mRNA vaccine with modified nucleosides, and a self-amplifying mRNA vaccine, showed that a single injection led to significant control of tumor growth in two murine models of HPV-16 tumors (97). From the foundation provided by these studies, current clinical trials are underway. For example, a phase II clinical trial (AHEAD-MERIT) using the BNT113 mRNA, encoding HPV16-derived neoantigens E6/7 is administered with and without pembrolizumab to treat HPV16-positive HNSCC expressing the PD-L1 protein (NCT04534205) (Table 2).

Several studies are also emerging to assess the potential of mRNA vaccines against non-viral HNSCC neoantigens. Chen et al.

used The Cancer Genome Atlas (TCGA) and the Gene Expression Omnibus databases to analyze alternative splicing and mutations of genes with HNSCC (98). Seven potential tumor antigens, [SREBF1, LUC7L3, LAMA5, PCGF3, HNRNPH1, KLC4, and OFD1], which were associated with nonsense-mediated mRNA decay factor expression, overall survival, and infiltration of APCs and would thus induce a potent anti-tumor T-cell response. Furthermore, the authors used clustering analysis to select suitable patients whose immune subtypes made them likely to respond to vaccination. Potential biomarkers included several genes that were identified to serve as potential prognostic biomarkers for mRNA vaccines: IGKC, IGHV3-15, IGLV1-40, IGLV1-51, IGLC3, IGLC2, and CD79A (98). To further distinguish the immune subtypes of HNSCCC to select suitable patients for vaccination, another group identified three genes as targets for developing mRNA vaccines: CCR4, TMCO1, and SPACA4 that were upregulated, and correlated with survival and tumor infiltration by both B and T cells, inducing a potent immune response (99). Paradoxically, patients with immune subtype C3, or the immune "cold" subtype – tumors with a lower IFN-γ and TGF-β response, fewer macrophages, T cells, and CD4 memory responses–were most likely to respond to mRNA vaccines against HNSCC (99). The authors speculate that mRNA vaccines would be most effective in transforming tumors that have a "cold" (immunoresistant) TME (100). Recognizing that histologically distinct tumors have unique immune landscapes, if these results apply to glioblastomas, it would further support the use of mRNA vaccines for human glioblastoma, a tumor known to be characterized by a "cold" TME.

4.3 mRNA vaccines in other non-CNS human cancers

Two clinical trials with personalized mRNA vaccine encoding neoantigens are underway in China, for patients with advanced esophageal cancer and non-small cell lung cancer (NCT03908671), and advanced gastrointestinal cancer (esophageal, liver, and advanced gastric cancer (NCT05192460). Additional trials are underway and include mRNA vaccines designed for patients with liver cancer (NCT05761717), and endocrine cancer (NCT06141369). Trials are also underway for bladder cancer (100), melanoma, prostate cancer, breast cancer, and other solid tumors as detailed in Table 1. In patients with stage IIB to stage IV resected melanoma, ICIs are standard therapy, but many patients recur; when a mRNA-vaccine, individualized therapy (mRNA-4157) is added to ICI (pembrolizumab),18-month recurrence-free survival was increased in the combination group (79%) compared to ICI alone (62%) with a hazard ratio for recurrence or death of 0.53, p=0.05 (NCT03897881, KEYNOTE-942) (11). Importantly, there was a lower recurrence or death rate (22%) in the combination group compared to 40% in the group treated with ICI alone (11). A phase I trial of intratumoral STX-001, a novel LNP, self-replicating mRNA expressing the cytokine IL-12 for an extended duration, is being evaluated in advanced, treatment-refractory solid tumors (NCT06249048) (101).

5 Brain tumors: pediatric and adult gliomas

Novel approaches to glioblastoma are urgently needed because standard therapy is associated with a median survival of eight months, and a five-year survival of 6.9% (102). Numerous biological barriers to immunotherapy include cellular heterogeneity, plasticity, and an immunosuppressive TME (103, 104). Immune cells constitute an important component of the glioma microenvironment, constituting as much as 50% of the tumor mass (103). Glioblastoma is immunologically "cold" with a TME resistant to T-cell and DC infiltration (105). Furthermore, there is *i*) a scarcity of circulating T cells with sequestration of T cells in the bone marrow; *ii*) a localized immunosuppression due to secretion of immunosuppressive cytokines, such as TGF-β, IL-6, PGE_2 and *iii*) an upregulation of PD-1 and PD-L1 (106, 107). Compared to tumors such as melanoma with a high mutation burden, glioblastoma has a reduced array of immunogenic neoantigens (107). Despite these challenges, several recent studies have sought to broaden the pool of targetable neoantigens in glioblastoma, offering potential avenues for mRNA vaccines (108–110). Given the substantial challenges, there is recent, encouraging data showing biological and clinical evidence of converting the glioblastoma TME into an immune responsive environment (15, 24, 111–117). It appears that a multimodal approach using an mRNA vaccine in combination with other strategies to boost the immune system could ultimately extend survival and change the outlook for patients. Recent advances in six pillars of immunotherapy are summarized:

a) mRNA vaccine. In a first-in-human clinical trial (NCT04573140, Table 2), Mendez-Gomez et al. recently reported a striking expansion of the immune response to tumor-associated antigens in patients with glioblastoma, using a novel RNA lipid particle aggregate (LPA), associated with a clinical increase in overall survival (15). The LPA differs from the commonly used LNPs (Figure 1) that are size-limited to permit endocytosis; by contrast, the LPA-based mRNA vaccine does not rely on TLR for engagement, enabling the delivery of multiple mRNA payloads to the same cancer cell, as shown in a canine model of glioma using the LPAs to elicit a potent RIG-I (retinoic acid-inducible gene I protein)-mediated stimulation of the immune system (15). Additional candidate genes are being identified by mining databases, including the TCGA and the Chinese Glioma Gene Atlas to identify multiple genes suitable for mRNA vaccine development (108, 110, 118).

b) DNA vaccine. Advantages of DNA vaccines include stability, relatively low-cost, cell-independent production, a durable immune response, and potential for targeting multiple neoantigens (Table 1). *hTERT* (human telomerase reverse transcriptase), regarded as the first truly universal tumor antigen (119), a surprisingly immunogenic target that is fundamental to oncogenesis (20). Vaccination with *hTERT* DNA is being used for "immuno-interception" in individuals with *BRCA1* or *BRCA2* mutations and therefore at high risk of breast, ovarian, pancreas, prostate, and other cancers (NCT04367675) (120). Using a similar DNA vaccine (NCT03491683), given by electroporation, targeting *hTERT*

(INO-5401) combined with an IL-12 DNA plasmid (INO-9012) and a PD-1 inhibitor (cemiplimab), Reardon et al. reported promising survival results for patients with glioblastoma with activated $CD4^+$ and $CD8^+$ T cells (121). The tumor tissue, post-treatment, showed genomic alterations linked to activation of the immune system, and evidence of T cell infiltration and cytolysis (121). A new generation of DNA vaccines with plasmids encoding T cell tumor epitopes (pTOP) significantly increased survival in preclinical models (GL261) of glioblastoma (35). Interestingly, vaccine monotherapy by itself was ineffective, but surgical resection of glioblastoma, followed by the vaccine, resulted in a dramatic increase in survival and delayed recurrence, associated with infiltration of activated T cells to the resection site (35).

c) Dendritic cell vaccine. Because APCs, such as dendritic cells, are key to initiating antigen-specific immune responses (41), early work to develop immunotherapy for cancer involved DC-mRNA vaccines (16, 122). A review of 33 early clinical trials revealed the potential of DC vaccines for glioblastoma, "*we can expect immune modulation to make its way into standard therapeutic protocols in neuro-oncology … in the near future, surgery, cytotoxic therapies (i.e., radio-chemotherapy), and immunotherapy will form a three-pronged therapeutic approach that will enhance clinical outcomes* (123). Indeed, a significant survival benefit was reported for patients with newly diagnosed (112) and recurrent glioblastoma (112, 124), with meaningful "tails" in the Kaplan-Meier survival curves, reflecting long-term survivorship. Furthermore, adding additional agents such as pembrolizumab (125) or poly-ICLC (111) can further activate the immune system, detected by a polarized interferon response in circulating monocytes and $CD8^+$ T cells, translating to prolonged survival and delayed disease progression in the responders (111). RNA-pulsed DCs, using nanoparticles, are safe and under evaluation (NCT04573140) (32).

d) CAR T cell therapy. mRNA vaccines show potential in combination with CAR T cell approaches to treat intractable pediatric brain tumors (126). The mRNA vector is expressed only transiently, which minimizes off-target toxicity, especially in the brain (127). The use of mRNA-CAR constructs prolonged survivals in preclinical models of diffuse midline glioma and medulloblastoma targeting GPC2 (127). Clinical trials are underway to target GPC2 in patients with neuroblastoma (NCT05650749). CAR T cell therapy is also being evaluated in pediatric high-grade gliomas targeting B7-H3 HER-2 (NCT03500991), and GD2.C7R (NCT04099797) (128). For adult human glioblastoma, clinical studies have shown that CAR-T cells can feasibly traffic to active regions of glioblastoma with on-target, biological activity (129, 130). Recent advances in patients with recurrent glioblastoma show that intrathecal delivery of CAR T cells targeting IL13α2 (NCT002208362) (116), or bivalent CAR T cells targeting two antigens, EGFR and IL13α2, (NCT05168423) (113), and EGFR/EGFRvIII with a T-cell engaging antibody, TEAM, (NCT05660369) (115), leads to compelling results (117) assessed by CAR T cell proliferation, rapid reduction in tumor size, bioactivity and safety signals. The next challenge is to transform the transient responses into long-term outcomes, converting an otherwise fatal glioblastoma into a chronic, treatable disease (117). The use of mRNA-targeted CAR T cells (131, 132) or the use of CAR natural killer cells instead of T cells (128), could be additional steps to provide durable responses. The fourth generation of CAR *T cells redirected for universal cytokine-mediated killing* (TRUCKs) results in simultaneous CAR T-Cell mediated killing and immune modulation of the TME via secretion of cytokines that has the dual effect of enhancing the survival of CAR T cells and modulating the TME by repolarizing tumor-associated macrophages or activating natural killer cells (133). Multiple phase 1 trials (NCT03542799, NCT03932565) use TRUCKS for systemic cancer (133), opening the potential combination of TRUCKs with a personalized mRNA vaccine.

e) Viral oncolytic therapy. One of the main immunotherapeutic platforms consists of viral oncolytic therapy (23–26), which has the dual effect of *i*) direct killing of tumor (glioblastoma) cells and ii) the dying cells release neoantigens that can attract APCs and, in turn, activate $CD4^+$ and $CD8^+$ T cells. Many viruses have been re-engineered as vectors for gene therapy of glioblastoma, e.g., retroviruses, adenoviruses, or herpes-simplex type 1 viruses (134). Other viruses have been engineered to replicate within brain tumors in a limited manner without causing encephalitis. To increase the effectiveness of oncolytic herpes virus, Todo et al. injected active virus into the surgical resection cavity, or unresectable tumor, up to six times (135). An alternative, novel, minimally invasive approach to treat glioblastoma is to develop viral vectors using variants of the capsid of adenovirus, AAV9, that bind to the transferrin receptor BI-hTFR1, allowing efficient transfer of genes across the blood-brain barrier, and delivered via the systemic circulation rather than direct injection (136).

The use of mRNA vaccines that leverage the genome of oncolytic viruses holds great promise to treat glioblastoma (137). Studies aimed at identifying potential antigens in glioblastoma (GBM) for the development of advanced mRNA-based therapies identified numerous distinct antigen sets, thereby meeting the challenge of comprehensive, multimodal treatment (137, 138). Initial results of ABTC 1603 (NCT00589875), using an adenovirus-tk (CAN-2409) in combination with an ICI (nivolumab), are promising, suggesting a survival advantage (139). A first-in-human trial of CAN-31100, an engineered herpes simplex 1 virus, shows safety signals and may extend survival by immune stimulation-especially in patients with antibodies to HSV1 (26). As proof of concept that oncolytic viruses can overcome the immunosuppressive TME, a combination of reovirus and CAR T-cells caused the expansion of T cells and cured > 80% of mice with intracranial EGFRvIII tumors (140). In a phase I-II trial, the use of intratumoral, oncolytic DNX-2401 virotherapy, followed by pembrolizumab, was well-tolerated in patients with recurrent glioblastoma, with notable survival benefit in select patients (141). Specifically, objective responses led to longer survival; 56.2% of patients had a clinical benefit, defined as stable disease or objective response (141). In a separate study, patients with recurrent glioblastoma, injected with an oncolytic herpes virus showed improved survival in individuals seropositive for HSV1, associated with immunoactivation – changes in the tumor/PBMC T cell counts, peripheral expansion of specific T cell clonotypes, and tumor transcriptomic signatures of immune activation (26). These results provide validation in patients that intralesional oncolytic

HSV treatment enhances anticancer immune responses, even in the immunosuppressive TME, especially in individuals with cognate serology to the injected virus (26).

f) Cytokine reprogramming of the glioblastoma microenvironment. In preclinical models, targeting IL-6 leads to a remarkable change in the TME, with a "switch" from the M2 immunosuppressive, (pro-tumorigenic) macrophage phenotype to an immunostimulatory (M1) phenotype, resulting in a significant increase in survival (142). Adding CD40 agonist enhanced the activity of infiltrated T cells, and an almost complete cure in glioblastoma models (143). Adding immune checkpoint inhibitors further improves survival (143, 144). Taken together, these findings led to an ongoing multicenter trial, NRG-BN-010 (NCT047299959), combining inhibition of IL-6R (tocilizumab), PD-L1 (atezolizumab) and stereotactic radiosurgery to treat recurrent glioblastoma (39). Recently, IL-6 blockade was found to promote tumor immunity through activation of the immunostimulatory IL-12 pathway, while abrogating the toxicity of checkpoint blockade, thus decoupling tumor immunity from autoimmune toxicity (145). Taken together, combining anti-IL6 blockade with a mRNA vaccine would be an attractive approach. One caveat, however, is the LNPs that coat the mRNA are by themselves immunostimulatory, acting as an adjuvant component, fostering T-follicular helper cells (Tfh cells) and humoral responses that are abrogated if Il-6 induction by the LNP is blocked using an antibody or using Il-6 deficient mice (55); the implications for cancer therapy in humans are unknown. Another approach to cytokine reprogramming is the use of convection-enhanced delivery and targeting of the IL-4 signaling pathway (NCT02858895), producing a dose-dependent, survival benefit with a high-dose immunotoxin (bizaxofusp) that targets the interleukin-4 receptor, IL4R (146). Single treatment with bizaxofusp increased median overall survival by up to 50% and 12-month progression-free survival by almost 100% when compared to FDA-approved therapies (146). A novel method to convert the immunosuppressive TME of glioblastoma is to arm CAR T cells with a dominant-negative TGF-β receptor II which in a rodent model of glioblastoma lowers the levels of the immunosuppressive cytokine TGF-β in the TME, enhances T cell proliferation, eradicates intracranial tumors, and significantly improves survival (114).

g) Immune checkpoint inhibitors in combination with mRNA vaccine. A synergistic effect of mRNA vaccines with ICIs is reported in glioma models, with a favorable shift in the TME from an immunologically "cold" resistant environment to one that is "hot," associated with improved survival (110, 147). Multimodal immunotherapy with ICIs for glioblastoma is under active investigation (39, 148, 149) and has been effective in preclinical models (143). Ultimately, there is a large body of evidence that a mRNA vaccine for human glioblastoma would benefit from the use of concomitant ICIs.

6 Challenges and caveats

In addition to the identification of the optimal tumor antigens to target in glioblastoma, key issues include delivery systems that can traverse the blood-brain barrier as well as boosting antigen production. An entirely novel method to meet this challenge is to harness the power of machine learning to reprogram glioblastoma cells into APCs that function like dendritic cells in terms of phagocytosis, direct presentation of endogenous antigens, cross presentation of exogenous antigens, and priming of naïve $CD8^+$ cytotoxic lymphocytes (CTLs). The result is reduction of glioblastoma growth, associated with extensive infiltration of $CD4^+$ cells and activated $CD8^+$ CTLs in the TME (150). These induced cells act synergistically with PD-decoy immunotherapy and a CD-based glioblastoma vaccine with robust killing of highly resistant glioblastoma cells by tumor-specific $CD8^+$ CTLs with significant improval in survival in immunocompetent animals (150). This novel approach could be used synergistically with mRNA vaccines.

Furthermore, the brain is one of the organs with the highest expression of RNA-binding proteins (RBPs); targeting the RBP complex, LOC-DHX15, with blood-brain barrier-penetrant small molecules improves treatment efficacy, impedes stem-like properties of glioblastoma cells, increases survival and offers a novel therapeutic approach to harness RNA science (151), and potentially enhance the efficacy of mRNA vaccines.

The challenges of RNA vaccines include optimization of delivery and the innate instability and immunogenicity of mRNA (152). These challenges have been largely overcome by *i*) designing modifications of the mRNA structure to avoid degradation by RNases; *ii*) optimizing purification methods to protect mRNA from contamination by double-stranded RNA to reduce nonspecific activation of the innate immune system; and *iii*) mRNA can be formulated into various nano delivery systems to deliver mRNA stably and efficiently, such as LNPs, polymers, or peptides (152). Identifying highly immunogenic, tumor-associated antigens is an inherent challenge because of individual variability; many aspects of neoepitope prediction remain to be standardized (152, 153). The large-scale production, transportation, and storage are also challenges for future applications of mRNA cancer vaccines. The speed of screening and identification of neoantigens directly affects the clinical efficacy of mRNA vaccines (153). Exploring more combinations of mRNA cancer vaccine with other therapeutic modalities is also a promising strategy (152). In view of the heterogeneity of the TME, the development of immune-based combination therapies has been a key trend in the development of cancer vaccines and in clinical trials (20–22, 153). Combinations have included the use of checkpoint inhibitors, co-stimulatory molecules (e.g., CD40), or vaccine combinations such as adoptive T cell transfer using CAR T cells (22). As a single approach, a monotherapy, is unlikely to be totally effective to eradicate a heterogeneous malignancy, especially aggressive gliomas (104), so that mRNA vaccination can be increasingly used as a "platform", similar to the proposed use of DC vaccines (22). Additional hurdles to develop effective immunotherapies for glioblastoma center on the immunosuppressive TME, systemic immunosuppression, and immune escape mechanisms (107). These same factors pose significant challenges for the use of cellular immunotherapy for glioblastoma (129, 154) and recent advances in combination therapy for CAR T cell therapy (21) could accelerate the

development of mRNA vaccines for glioblastoma and other human cancers.

Cancer cells, for example, can evolve to lose targeted antigens, thus evading the engineered CAR T cells, a phenomenon known as antigen-loss relapse (21). Efficacy can be increased by combining CAR T cell therapy with other vaccines, ICIs, oncolytic viruses, or small molecules such as ibrutinib or lenalidomide (21) that are brain penetrant (155, 156). Furthermore, ibrutinib increases survival in rodent glioma models (156); lenalidomide may help prevent T cell exhaustion (21). Within the targeted tumor, diverse cell populations add to the complexity of immunotherapeutic approaches, but recent data indicates that immune triads- a close interaction between DCs, $CD4^+$ T cells, and $CD8^+$ T cells, working synergistically, can dramatically eliminate solid tumors by reprogramming the $CD8^+$ T cell to become functional and tumor cytolytic for a range of cancers (41). Importantly, activated T cells are uniquely able to attack dormant, disseminated cancer cells, which escape the normal immune system, standard therapy, and lead to cancer persistence, recurrence, and progression (157). If mRNA vaccines could indeed eradicate the disseminated, microscopic, minimally residual disease in glioblastoma, associated with genetic and epigenetic instability, neoplastic infiltration, oncoplasticity (104), located beyond the surgical or radiation field, it could transform the clinical outcome for patients. It appears that we have entered a new era of combined treatments (20, 21, 35). The sequencing, dosing, and timing of these multiple combinations will require well-designed clinical trials. In experimental models, combining cancer vaccines and tumor resection enables the effective infiltration of activated T cell to the resection site, with a strong impact on mouse survival (35) in an otherwise aggressive glioblastoma.

What about safety? Preliminary experience suggests that a mRNA vaccine will be relatively nontoxic (152, 153, Table 1). In preclinical models, a mRNA vaccine was well-tolerated: detailed toxicology in forty organs at three time points revealed no gross or microscopic findings (15). In patients with glioblastoma, a mRNA vaccine produces rapid and transient increases in pro-inflammatory cytokines, a lymphocyte nadir and neutrophilia six hours after infusion, with immune-related adverse events (e.g., low-grade fever, nausea, chills, rigors), which defervesced within 24 to 48 hours (15). These findings indicated an immunological reset with expansion and polarization of adaptive T cell responses (15). Given the early and limited experience with mRNA vaccines for human cancer, it is too early whether patients will develop cytokine release syndrome (CRS), immune effector cell-associated neurotoxicity (ICANS) or macrophage activation syndrome (MAS) which are caused by high levels of proinflammatory cytokines secreted by activated T cell and myeloid cells (21); clinical trials are exploring therapeutic interventions using antibodies such as tocilizumab for CRS and anakinra for ICANS (21). These agents, in addition to corticosteroids, would be applicable to mRNA vaccines in the event that immune-related toxicities become severe.

It is assumed that mRNA vaccines will be relatively safe because there is no integration into the DNA so the vaccine itself should not cause genomic alterations (152), as could potentially occur with plasmid-based DNA vaccines (158, 159). Furthermore, the widespread use of nucleoside-modified synthetic mRNA (*nms*-mRNA) to immunize against COVID-19 resulted in more than 782 million doses distributed to an estimated 462 million individuals by September 2022, per WHO data, and so an ongoing search for delayed safety signals remains a priority (159). There is a widespread consensus that as exogenous *"mRNA is a non-integrating platform, there is no potential risk of … insertional mutagenesis."* (16, 159). However, a study showed that vaccine *nms*-mRNA can activate the expression of endogenous transposable elements (TEs), undergo reverse transcription and enter the cell nucleus (160), while another study showed that reverse-transcribed SARS-CoV-2 viral RNA can integrate into the genome of cultured human cell and be expressed in patient-derived tissues (161). Taken together, Acevedo-Whitehouse and Bruno hypothesized an intricate mechanism whereby the vaccine nms-mRNA, release from the LPNs into the cytosol could unsilence TE expression, enhance the expression of proinflammatory cytokines, lead to DNA damage via insertional mutagenesis and genomic instability, resulting in expression of proinflammatory cytokines (159). With the introduction of any new class of agents targeting cancer, great enthusiasm must be matched with due caution since novel interventions are frequently double-edged swords (159, 162, 163). To date, the safety signals for mRNA vaccines in clinical trials are reassuring.

7 Future directions

The route of delivery of mRNA, whether through an intravenous route or direct injection into tumor stands to make a difference, with some data suggesting that direct intratumor injection, "taking the fight to the tumor" (24, 26, 137, 164), could be advantageous. Local delivery of cytokine-based mRNAs can lead to a robust antitumor immune response and tumor regression in multiple tumor models (164). The cytokine-mRNA combination resulted in a ~ 50% cure rate in preclinical models of melanoma, increasing to a ~80% cure rate with the addition of ICIs, blocking metastases (164). The antitumor activity extended beyond the treated lesions and inhibited the growth of distant and disseminated tumors (164); combining mRNAs with immunomodulatory antibodies enhanced tumor regression and improved survival, leading to clinical trials of the cytokine-encoding mRNA combination (164).

As an alternative to the intratumoral release of mRNA, non-transformed cells in the liver can be exogenously transduced with mRNA in lipid formulations, thereby activating systemic biodistribution of the encoded immunostimulating factors (165). Because MHC-1 antigen presentation deficiency is a common cancer immune escape mechanism, combining tumor-targeting antibodies with IL-2 mRNA restored CD8+ T cell neoantigen immunity in MHC class I-deficient tumors that were otherwise resistant to immune-, chemo-, and radiotherapy (166). Another approach to potentiate the efficacy of mRNA vaccines would be to encode the costimulator Oxford 40 ligand, OX40L, which significantly reduces tumor growth and increases survival in preclinical models (167).

The use of small extracellular vesicles (sEVs) is a novel approach to target glioblastoma cells and generate potent

antitumor activity *in vivo* (168). Using a microfluidic electroporation, which combines nano- and milli-second pulses, producing large amounts of IFN-γ mRNA-loaded sEVs with CD64 overexpressed on the surface of cells; the CD64 molecule serves as an adaptor to dock targeting ligands, such as anti-CD71 and anti-PD-L1 antibodies (168). Encapsulation of IL-12 mRNA in extracellular vesicles enables targeted delivery to treat lung cancer while promoting a systemic immune response, measured by immune memory, tumor-specific T cell priming, and expansion of tumor cytotoxic immune effector cells; IL-12 exosome-based systems could potentially be applied to other tumor types (169). RNA-loaded hydrogels have been shown to be effective *in vitro* against triple-negative breast cancer (170) and are in development for glioblastoma (32).

The use of CRISPR-Cas9 gene editing has the potential to permanently disrupt tumor survival genes, which could overcome the repeated dosing limitations of cancer therapy and improve efficacy. As proof of concept, CRISPR-Cas9 technology was applied to lipid nanoparticles containing Cas9mRNA and single-guided (sg) RNA into orthotopic glioblastoma, resulting in ~70% gene editing *in vivo*, tumor cell apoptosis, and reduction of tumor growth by 50% with improved survival by 30% (171). An elegant model of spatial manipulation of CRISPR-Cas13a activity was developed with customized RNA nanococoons featuring tumor-specific recognition and spatial-controlled activation of Cas13a and applied to suppress EGFRvIII mRNA for synergistic therapy of glioblastoma *in vitro* and *in vivo* (29).

Progress in neural networks and deep learning could be of great value to predict design of optimal antigens; high - quality, cancer neoantigen datasets could meaningfully harness the data generated by these informatic tools (172). Vaccine manufacturing will benefit from emerging solutions for the mass production of individualized vaccines, including digitization of production processes and autonomous cloud-controlled production plants fostered by advances in computational power, connectivity, human–machine interactions, robotics and innovative 3D technology enabling the building at scale of parallel, miniaturized production lines (172).

The next wave of cellular immunotherapy, including CAR T cells and dendritic cells, can take advantage of mRNA-LNP as a platform to target DCs or $CD8^+$ T cells using personalized formulations incorporating neoantigens arising from genomic alterations using next-generation sequencing, immune peptidomics, and bioinformatics (173). Immune-monitoring at the single-cell or population level can be performed using peptide/MHC multimers, RNA sequencing (RNA-seq), and T cell receptor sequencing (TCR-seq) (173).

Initially, nine biotechnology startups began developing next-generation RNA drugs (174). The next wave of RNA-based drugs is using more sophisticated approaches, including tRNA to correct for errors in the genetic code that would otherwise impair protein production (174). Self-replicating RNAs, as noted (52, 53, 97) are also attractive because of their self-perpetuating, durable nature (174). Furthermore, circular RNA is more stable than its mRNA counterpart (174, 175), and there are multiple methods to produce circular RNA designed to treat glioblastoma (29). A dozen or more biotechnology firms are now pursuing therapeutics based on engineered circular RNA (circRNA), raising over US$1billion in venture capital during the past three years, betting that circRNA will emerge as the preferred RNA platform, leading to next-generation vaccines (175).

Significant challenges, however, include immunosuppressive TME, optimal candidate identification, immune response evaluation, and the need for biomarkers, as well as vaccine manufacturing acceleration (29). Undesired immunostimulation and potential impurities of the LNPs also pose a significant challenge (176). Nevertheless, the field is poised to overcome hurdles and improve patient outcomes in the future by acknowledging these clinical complexities and persistently striving to surmount inherent constraints (29). Not surprisingly, the first ARPA-H grant is centered on a mRNA platform targeting melanoma (177), hailed by President Joe Biden, urging Americans to come together for a new 'national purpose' (178).

8 Conclusion

Given the feasibility of production, the personalized approach, the minimal toxicity, and the explosion in RNA science following the success of the COVID vaccines, it is easy to predict that mRNA vaccines will be an important therapeutic option as a strategy to harness the immune system to prolong survival in patients with glioblastoma and other solid tumors. Initial results in humans using mRNA vaccines for glioblastoma are promising and support further development of mRNA vaccines as a novel approach to brain tumor therapy.

Author contributions

IT: Conceptualization, Writing – original draft, Writing – review & editing, Investigation. PM: Conceptualization, Writing – original draft, Writing – review & editing. PL: Writing – original draft, Writing – review & editing. MC: Writing – original draft, Writing – review & editing. SJB: Conceptualization, Writing – review & editing. YF: Writing – review & editing. SB: Conceptualization, Investigation, Methodology, Visualization, Writing – original draft, Writing – review & editing.

Funding

The author(s) declare that no financial support was received for the research, authorship, and/or publication of this article.

Acknowledgments

We acknowledge the assistance of Dr. Katalin Karikó and Dr. Drew Weissman who each reviewed the manuscript and provided invaluable insights and advice.

Conflict of interest

The authors declare that the research was conducted in the absence of any commercial or financial relationships that could be construed as a potential conflict of interest.

The author(s) declared that they were an editorial board member of Frontiers, at the time of submission. This had no impact on the peer review process and the final decision.

Publisher's note

References

1. Karikó K, Buckstein M, Ni H, Weissman D. Suppression of RNA recognition by Toll-like receptors: the impact of nucleoside modification and the evolutionary origin of RNA. *Immunity*. (2005) 23:165–75. doi: 10.1016/j.immuni.2005.06.008

2. Karikó K, Weissman D. RNA containing modified nucleosides and methods of use thereof. US Patent #9,750,824 B2 (9/5/2017) . Available online at: https://patents.google.com/patent/US9750824B2/ (Accessed September 4, 2024).

3. Laczkó D, Hogan MJ, Toulmin SA, Hicks P, Lederer K, Gaudette BT, et al. A single immunization with nucleoside-modified mRNA vaccines elicits strong cellular and humoral immune responses against SARS-CoV-2 in mice. *Immunity*. (2020) 53:724–32.e7. doi: 10.1016/j.immuni.2020.07.019

4. Polack FP, Thomas SJ, Kitchin N, Absalon J, Gurtman A, Lockhart S, et al. Safety and efficacy of the BNT162b2 mRNA Covid-19 vaccine. *N Engl J Med*. (2020) 383:2603–15. doi: 10.1056/NEJMoa2034577

5. Buggert M, Höglund P. The prize of prizes: mRNA research paving the way for COVID-19 vaccine success wins the Nobel Prize in Physiology or Medicine 2023. *Scand J Immunol*. (2023) 98:e13340. doi: 10.1111/sji.13340

6. Sahin U, Karikó K, Türeci Ö. mRNA-based therapeutics – developing a new class of drugs. *Nat Rev Drug Discovery*. (2014) 13:759–80. doi: 10.1038/nrd4278

7. Sahin U, Oehm P, Derhovanessian E, Jabulowsky RA, Vormehr M, Gold M, et al. An RNA vaccine drives immunity in checkpoint-inhibitor-treated melanoma. *Nature*. (2020) 585:107–12. doi: 10.1038/s41586-020-2537-9

8. Baden LR, El Sahly HM, Essink B, Kotloff K, Frey S, Novak R, et al. Efficacy and safety of the mRNA-1273 SARS-CoV-2 vaccine. *N Engl J Med*. (2021) 384:403–16. doi: 10.1056/NEJMoa2035389

9. Sahin U, Muik A, Derhovanessian E, Vogler I, Kranz LM, Vormehr M, et al. COVID-19 vaccine BNT162b1 elicits human antibody and T_H1 T cell responses. *Nature*. (2020) 586:594–99. doi: 10.1038/s41586-020-2814-7

10. Bidram M, Zhao Y, Shebardina NG, Baldin AV, Bazhin AV, Ganjalikhany MR, et al. mRNA-based cancer vaccines: A therapeutic strategy for the treatment of melanoma patients. *Vaccines*. (2021) 9:1060. doi: 10.3390/vaccines9101060

11. Weber J, Carlino MS, Khattak A, Meniawy T, Ansstas G, Taylor MH, et al. Individualized therapy mRNA-4157 (V940) plus pembrolizumab versus pembrolizumab monotherapy in resected melanoma (KEYNOTE-942): a randomized, phase 2b study. *Lancet*. (2024) 403:632–44. doi: 10.1016/S0140-6736(23)02268-7

12. Kübler H, Scheel B, Gnad-Vogt U, Miller K, Schultze-Seemann W, Vom Dorp F, et al. Self-adjuvanted mRNA vaccination in advanced prostate cancer patients: a first-in-man phase I/IIa study. *J Immunother Cancer*. (2015) 3:26. doi: 10.1186/s40425-015-0068-y

13. Shahnazari M, Samadi P, Pourjafar M, Jalali A. Therapeutic vaccines for colorectal cancer: The progress and future prospect. *Int Immunopharmacol*. (2020) 88:106944. doi: 10.1016/j.intimp.2020.106944

14. Fiedler K, Lazzaro S, Lutz J, Rauch S, Heidenreich R. mRNA cancer vaccines. *Recent Results Cancer Res*. (2016) 209:61–85. doi: 10.1007/978-3-319-42934-2_5

15. Mendez-Gomez HR, DeVries A, Castillo P, von Roemeling C, Qdaisat S, Stover BD, et al. RNA aggregates harness the danger response for potent cancer immunotherapy. *Cell*. (2024) 187:2521–35. doi: 10.1016/j.cell.2024.04.003

16. Pardi N, Hogan MJ, Porter FW, Weissman D. mRNA vaccines—a new era in vaccinology. *Nat Rev Drug Discovery*. (2018) . 17:261–79. doi: 10.1038/nrd.2017.243

17. Yu D, Petsch B. Preface to mRNA vaccines. *Curr Top Microbiol Immunol*. (2022) 440:viii. doi: 10.1007/978-3-031-18070-5

18. Fares CM, Van Allen EM, Drake CG, Allison JP, Hu-Lieskovan S. Mechanisms of resistance to immune checkpoint blockade: why does checkpoint inhibitor immunotherapy not work for all patients? *Am Soc Clin Oncol Educ Book*. (2019) 39:147–64. doi: 10.1200/EDBK_240837

19. Schuchter LM. Adjuvant melanoma therapy – Head-spinning progress. *N Engl J Med*. (2017) 377:1888–90. doi: 10.1056/NEJMe1711199

20. Wu A, Lim M. Advancing combination therapy for recurrent glioblastoma. *Nat Med*. (2023) 29:1318–9. doi: 10.1038/s41591-023-02350-3

21. Uslu U, Castelli S, June CH. CAR T cell combination therapies to treat cancer. *Cancer Cell*. (2024) 42:1319–25. doi: 10.1016/j.ccell.2024.07.002

22. Datsi A, Sorg RV. Dendritic cell vaccination of glioblastoma: Road to success or dead end. *Front Immunol*. (2021) 12:770390. doi: 10.3389/fimmu.2021.770390

23. Liu J, Fu M, Wang M, Wan D, Wei Y, Wei X. Cancer vaccines as promising immuno-therapeutics: platforms and current progress. *J Hematol Oncol*. (2022) 15:28. doi: 10.1186/s13045-022-01247-x

24. van Solinge TS, Nieland L, Chiocca EA, Broekman MLD. Advances in local therapy for glioblastoma—taking the fight to the tumour. *Nat Rev Neurol*. (2022) 18:221–36. doi: 10.1038/s41582-022-00621-0

25. Forsyth PA, Abate-Daga D. Oncolytic virotherapy for Malignant glioma. *J Clin Oncol*. (2018) 36:1440–2. doi: 10.1200/JCO.2017.77.3192

26. Ling AL, Solomon IH, Landivar AM, Nakashima H, Woods JK, Santos A, et al. Clinical trial links oncolytic immunoactivation to survival in glioblastoma. *Nature*. (2023) 623:157–66. doi: 10.1038/s41586-023-06623-2

27. Raimondo TM, Reed K, Shi D, Langer R, Anderson DG. Delivering the next generation of cancer immunotherapies with RNA. *Cell*. (2023) 186:1535–40. doi: 10.1016/j.cell.2023.02.031

28. Clemente B, Denis M, Silveira CP, Schiavetti F, Brazzoli M, Stranges D. Straight to the point: targeted mRNA-delivery to immune cells for improved vaccine design. *Front Immunol*. (2023) 14:1294929. doi: 10.3389/fimmu.2023.1294929

29. Dain L, Zhu G. Nucleic acid immunotherapeutics and vaccines: A promising approach to glioblastoma multiforme treatment. *Int J Pharm*. (2023) 638:11294. doi: 10.1016/j.ijpharm.2023.122924

30. Lang F, Schrörs B, Löwer M, Türeci O, Sahin U. Identification of neoantigens for individualized therapeutic cancer vaccines. *Nat Rev Drug Discovery*. (2022) 21:261–82. doi: 10.1038/s41573-021-00387-y

31. Sayour EJ, Boczkowski D, Mitchell DA, Nair SK. Cancer mRNA vaccines: clinical advances and future opportunities. *Nat Rev Clin Oncol*. (2024) 21:489–500. doi: 10.1038/s41571-024-00902-1

32. Melnick K, Dastmalchi F, Mitchell D, Rahman M, Sayour EJ. Contemporary RNA therapeutics for glioblastoma. *Neuromol Med*. (2022) 24:8–12. doi: 10.1007/s12017-021-08669-9

33. Rahman MM, Zhou N, Huang J. An overview on the development of mRNA-based vaccines and their formulation strategies for improved antigen expression in *vivo*. *Vaccines*. (2021) 9:244. doi: 10.3390/vaccines9030244

34. Fan T, Zhang M, Yang J, Zhu Z, Cao W, Dong C. Therapeutic cancer vaccines: advancements, challenges, and prospects. *Signal Transduct Target Ther*. (2023) 8:450. doi: 10.1038/s41392-023-01674-3

35. Lopes A, Bastiancich C, Bausart M, Ligot S, Lambricht L, Vanvarenberg K, et al. New generation of DNA-based immunotherapy induces a potent immune response and increases the survival in different tumor models. *J Immunother Cancer*. (2021) 9:e001243. doi: 10.1136/jitc-2020-001243

36. Naik R, Peden K. Regulatory consideration on the development of mRNA vaccines. *Curr Top Microbiol Immunol*. (2022) 440:187–205. doi: 10.1007/82_2020_220

37. Wei J, Hui AM. The paradigm shift in treatment from Covid-19 to oncology with mRNA vaccines. *Cancer Treat Rev*. (2022) 107:102405. doi: 10.1016/j.ctrv.2022.102405

38. Domchek SM, Vonderheide RH. Advancing cancer interception. *Cancer Discovery*. (2024) 14:600–4. doi: 10.1158/2159-8290.CD-24-0015

39. Bagley S, Polley M-Y, Kotecha R, Brem S, Tolakanahalli R, Iwamoto F, et al. A safety run-in and phase II study evaluating the combination of tocilizumab, atezolizumab, and fractionated stereotactic radiotherapy in recurrent glioblastoma – trial in progress. *Neuro-Oncol*. (2022) 24:vii64. doi: 10.1093/neuonc/noac209.253

40. Reinhard K, Rengstl B, Oehm P, Michel K, Billmeier A, Hayduk N, et al. An RNA vaccine drives expansion and efficacy of claudin-CAR-T cells against solid tumors. *Science*. (2020) 367:446–53. doi: 10.1126/science.aay5967

41. Espinosa-Carrasco G, Chiu E, Scrivo A, Zumbo P, Dave A, Betel D, et al. Intratumoral immune triads are required for immunotherapy-mediated elimination of solid tumors. *Cancer Cell*. (2024) 42:1202–16. doi: 10.1016/j.ccell.2024.05.025

42. Xu S, Yang K, Li R, Zhang L. mRNA vaccine era—mechanisms, drug platform and clinical prospection. *Int J Mol Sci*. (2020) 21:6582. doi: 10.3390/ijms21186582

43. Gu Y, Duan J, Yang N, Yang Y, Zhao X. mRNA vaccines in the prevention and treatment of diseases. *Med Comm*. (2022) 3:e167. doi: 10.1002/mco2.167

44. Rijkers GT, Weterings N, Obregon-Henao A, Lepolder M, Dutt TS, van Overveld FJ, et al. Antigen presentation of mRNA-based and virus-vectored SARS-CoV-2 vaccines. *Vaccines*. (2021) 9:848. doi: 10.3390/vaccines9080848

45. Murira A, Lamarre A. Type-I interferon responses: From friend to foe in the battle against viral infection. *Front Immunol*. (2016) 7:609. doi: 10.3389/fimmu.2016.00609

46. Zhang Z, Lu M, Qin Y, Gao W, Tao L, Su W, et al. Neoantigen: A new breakthrough in tumor immunotherapy. *Front Immunol*. (2021) 12:672356. doi: 10.3389/fimmu.2021.672356

47. Esprit A, de Mey W, Bahadur Shahi R, Thielemans K, Franceschini L, Breckpot K. Neo-antigen mRNA vaccines. *Vaccines*. (2020) 8:776. doi: 10.3390/vaccines8040776

48. Bjerregaard A-M, Nielsen M, Jurtz V, Barra CM, Hadrup SR, Szallasi Z, et al. An analysis of natural T cell responses to predicted tumor neoepitopes. *Front Immunol*. (2017) 8:1566. doi: 10.3389/fimmu.2017.01566

49. Warminski M, Mamot A, Depaix A, Kowalska J, Jemielity J. Chemical modifications of mRNA ends for therapeutic applications. *Acc Chem Res*. (2023) 56:2814–26. doi: 10.1021/acs.accounts.3c00442

50. Capietto A-H, Hoshyar R, Delamarre L. Sources of cancer neoantigens beyond single-nucleotide variants. *Int J Mol Sci*. (2022) 23:10131. doi: 10.3390/ijms231710131

51. Schoenmaker L, Witzigmann D, Kulkarni JA, Verbeke R, Kersten G, Jiskoot W, et al. mRNA-lipid nanoparticle COVID-19 vaccines: Structure and stability. *Int J Pharm*. (2021) 601:120586. doi: 10.1016/j.ijpharm.2021.120586

52. Bloom K, van den Berg F, Arbuthnot P. Self-amplifying RNA vaccines for infectious diseases. *Gene Ther*. (2021) 28:117–29. doi: 10.1038/s41434-020-00204-y

53. Blakney AK, Ip S, Geall AJ. An update on self-amplifying mRNA vaccine development. *Vaccines*. (2021) 9:97. doi: 10.3390/vaccines9020097

54. Witten J, Hu Y, Langer R, Anderson DG. Recent advances in nanoparticulate RNA delivery systems. *Proc Natl Acad Sci*. (2024) 121:e2307798120. doi: 10.1073/pnas.2307798120

55. Alameh M-G, Tombácz I, Bettini E, Lederer K, Ndeupen S, Sittplangkoon C, et al. Lipid nanoparticles enhance the efficacy of mRNA and protein subunit vaccines by inducing robust T follicular helper cell and humoral responses. *Immunity*. (2021) 54:2877–92. e2877. doi: 10.1016/j.immuni.2021.11.001

56. Hou X, Zaks T, Langer R, Dong Y. Lipid nanoparticles for mRNA delivery. *Nat Rev Mater*. (2021) 6:1078–94. doi: 10.1038/s41578-021-00358-0

57. Reichmuth AM, Oberli MA, Jaklenec A, Langer R, Blankschtein D. mRNA vaccine delivery using lipid nanoparticles. *Ther Delivery*. (2016) 7:319–34. doi: 10.4155/tde-2016-0006

58. Qiu M, Tang Y, Chen J, Muriph R, Ye Z, Huang C, et al. Lung-selective mRNA delivery of synthetic lipid nanoparticles for the treatment of pulmonary lymphangioleiomyomatosis. *Proc Natl Acad Sci USA*. (2022) 119:e2116271119. doi: 10.1073/pnas.2116271119

59. Swingle KL, Safford HC, Geisler HC, Hamilton AG, Thatte AS, Billingsley MM, et al. Ionizable lipid nanoparticles for in *vivo* mRNA delivery to the placenta during pregnancy. *J Am Chem Soc*. (2023) 145:4691–706. doi: 10.1021/jacs.2c12893

60. Miao L, Li L, Huang Y, Delcassian D, Chahal J, Han J, et al. Delivery of mRNA vaccines with heterocyclic lipids increases anti-tumor efficacy by STING-mediated immune cell activation. *Nat Biotechnol*. (2019) 37:1174–85. doi: 10.1038/s41587-019-0247-3

61. Kon E, Ad-El N, Hazan-Halevy I, Stotsky-Oterin L, Peer D. Targeting cancer with mRNA–lipid nanoparticles: key considerations and future prospects. *Nat Rev Clin Oncol*. (2023) 20:739–54. doi: 10.1038/s41571-023-00811-9

62. Huang A, Pressnall MM, Lu R, Huayamares SG, Griffin JD, Groer C, et al. Human intratumoral therapy: Linking drug properties and tumor transport of drugs in clinical trials. *J Control Release*. (2020) 326:203–21. doi: 10.1016/j.jconrel.2020.06.029

63. Metzloff AE, Padilla MS, Gong N, Billingsley MM, Han X, Merolle M, et al. Antigen presenting cell mimetic lipid nanoparticles for rapid mRNA CAR T cell cancer immunotherapy. *Adv Mater*. (2024) 36(26):e2313226. doi: 10.1002/adma.202313226

64. Han EL, Padilla MS, Palanki R, Kim D, Mrksich K, Li JJ, et al. Predictive high-throughput platform for dual screening of mRNA lipid nanoparticle blood-brain barrier transfection and crossing. *Nano Lett*. (2024) 24:1477–86. doi: 10.1021/acs.nanolett.3c03509

65. Rojas LA, Sethna Z, Soares KC, Olcese C, Pang N, Patterson E, et al. Personalized RNA neoantigen vaccines stimulate T cells in pancreatic cancer. *Nature*. (2023) 618:144–50. doi: 10.1038/s41586-023-06063-y

66. Vonderheide R. Q&A: Personalized mRNA vaccine immunogenic against PDAC. *Cancer Discovery*. (2023) 13:1504. doi: 10.1158/2159-8290.CD-ND2023-0002

67. Conroy T, Hammel P, Hebbar M, Ben Abdelghani M, Wei AC, Raoul J-L, et al. FOLFIRINOX or gemcitabine as adjuvant therapy for pancreatic cancer. *N Engl J Med*. (2018) 379:2395–406. doi: 10.1056/NEJMoa1809775

68. Strobel O, Neoptolemos J, Jäger D, Büchler MW. Optimizing the outcomes of pancreatic cancer surgery. *Nat Rev Clin Oncol*. (2019) 16:11–26. doi: 10.1038/s41571-018-0112-1

69. Connor AA. Gallinger S.Pancreatic cancer evolution and heterogeneity: integrating omics and clinical data. *Nat Rev Cancer*. (2022) 22:131–42. doi: 10.1038/s41568-021-00418-1

70. Kang N, Zhang S, Wang Y. A personalized mRNA vaccine has exhibited potential in the treatment of pancreatic cancer. *Holist Integr Oncol*. (2023) 2:18. doi: 10.1007/s44178-023-00042-z

71. Balachandran VP, Beatty GL, Dougan SK. Broadening the impact of immunotherapy to pancreatic cancer: challenges and opportunities. *Gastroenterology*. (2019) 156:2056–72. doi: 10.1053/j.gastro.2018.12.038

72. Bear AS, Vonderheide RH, O'Hara MH. Challenges and opportunities for pancreatic cancer immunotherapy. *Cancer Cell*. (2020) 38:788–802. doi: 10.1016/j.ccell.2020.08

73. Van Allen EM, Miao D, Schilling B, Shukla SA, Blank C, Zimmer L, et al. Genomic correlates of response to CTLA-4 blockade in metastatic melanoma. *Science*. (2015) 350:207–11. doi: 10.1126/science.aad0095

74. Balli D, Rech AJ, Stanger BZ, Vonderheide RH. Immune cytolytic activity stratifies molecular subsets of human pancreatic cancer. *Clin Cancer Res*. (2017) 23:3129–38. doi: 10.1158/1078-0432.CCR-16-2128

75. Wartenberg M, Cibin S, Zlobec I, Vassella E, Eppenberger-Castori S, Terracciano L, et al. Integrated genomic and immunophenotypic classification of pancreatic cancer reveals three distinct subtypes with prognostic/predictive significance. *Clin Cancer Res*. (2018) 24:4444–54. doi: 10.1158/1078-0432.CCR-17-3401

76. Huang X, Zhang G, Tang T-Y, Gao X, Liang T-B. Personalized pancreatic cancer therapy: from the perspective of mRNA vaccine. *Mil Med Res*. (2022) 9:53. doi: 10.1186/s40779-022-00416-w

77. Hackert T, Sachsenmaier M, Hinz U, Schneider L, Michalski CW, Springfeld C, et al. Locally advanced pancreatic cancer: neoadjuvant therapy with Folfirinox results in resectability in 60% of the patients. *Ann Surg*. (2016) 264:457–63. doi: 10.1097/SLA.0000000000001850

78. Murphy JE, Wo JY, Ryan DP, Clark JW, Jiang W, Yeap BY, et al. Total neoadjuvant therapy with FOLFIRINOX in combination with losartan followed by chemoradiotherapy for locally advanced pancreatic cancer: a phase 2 clinical trial. *JAMA Oncol*. (2019) 5:1020–7. doi: 10.1001/jamaoncol.2019.0892

79. Aupérin A. Epidemiology of head and neck cancers: an update. *Curr Opin Oncol*. (2020) 32:178–86. doi: 10.1097/CCO.000000000000629

80. Syrjänen S. Human papillomavirus (HPV) in head and neck cancer. *J Clin Virol*. (2005) 32:59–66. doi: 10.1016/j.jcv.2004.04.11.017

81. D'Souza G, Kreimer AR, Viscidi R, Pawlita M, Fakhry C, Koch WM, et al. Case–control study of human papillomavirus and oropharyngeal cancer. *New Engl J Med*. (2007) 356:1944–56. doi: 10.1056/NEJMoa065497

82. Syrjänen S, Waterboer T, Kero K, Rautava J, Syrjänen K, Grenman S, et al. Oral human papillomavirus infection in men might contribute to HPV serology. *Eur J Clin Microbiol Infect Dis*. (2015) 34:237–45. doi: 10.1007/s10096-014-2223-7

83. Pathmanathan R, Prasad U, Chandrika G, Sadler R, Flynn K, Raab-Traub N. Undifferentiated, nonkeratinizing, and squamous cell carcinoma of the nasopharynx. Variants of Epstein-Barr virus-infected neoplasia. *Am J Pathol*. (1995) 146:1355–67.

84. Tsao SW, Tsang CM, Lo KW. Epstein–Barr virus infection and nasopharyngeal carcinoma. *Philos Trans R Soc Lond B Biol Sci*. (2017) 372:20160270. doi: 10.1098/rstb.2016.0270

85. Andre K, Schraub S, Mercier M, Bontemps P. Role of alcohol and tobacco in the aetiology of head and neck cancer: a case-control study in the Doubs region of France. *Eur J Cancer B Oral Oncol*. (1995) 31:301–9. doi: 10.1016./0964-1955(95)0041-0

86. Sinha P, Logan HL, Mendenhall WM. Human papillomavirus, smoking, and head and neck cancer. *Am J Otolaryngol*. (2012) 33:130–6. doi: 10.1016/j.amjoto.2011.02.001

87. Rao YJ, Goodman JF, Haroun F, Bauman JE. Integrating immunotherapy into multimodal treatment of head and neck cancer. *Cancers*. (2023) 15:672. doi: 10.3390/cancers15030672

88. Harrington KJ, Burtness, Greil R, Soulières D, Tahara M, de Castro G, et al. Pembrolizumab with or without chemotherapy in recurrent or metastatic head and neck squamous cell carcinoma: Updated results of the phase III KEYNOTE-048 study. *J Clin Oncol*. (2023) 41:790–802. doi: 10.1200/JCO.21.02508

89. Machiels J-P, Tao Y, Licitra L, Burtness B, Tahara M, Rischin D, et al. Pembrolizumab plus concurrent chemoradiotherapy versus placebo plus concurrent chemoradiotherapy in patients with locally advanced squamous cell carcinoma of the head and neck (KEYNOTE-412): a randomized, double-blind, phase 3 trial. *Lancet Oncol*. (2024) 25:572–5887. doi: 10.1016/S1470-2045(24)00100-1-

90. Mehra R, Seiwert TY, Gupta S, Weiss J, Gluck I, Eder JP, et al. Efficacy and safety of pembrolizumab in recurrent/metastatic head and neck squamous cell carcinoma: pooled analyses after long-term follow-up in KEYNOTE-012. *Br J Cancer*. (2018) 119:153–9. doi: 10.1038/s41416-018-01131-9

91. Ritter A, Koirala N, Wieland A, Kaumaya PT, Mitchell DL. Therapeutic cancer vaccines for the management of recurrent and metastatic head and neck cancer: A review. *JAMA Otolaryngol Head Neck Surg*. (2023) 149:168–76. doi: 10.1001/jamaoto.2022.4264

92. Lassen P, Eriksen JG, Hamilton-Dutoit S, Tramm T, Alsner J, Overgaard J. Effect of HPV-associated p16INK4A expression on response to radiotherapy and survival in squamous cell carcinoma of the head and neck. *J Clin Oncol*. (2009) . 27:1992–98. doi: 10.1200/JCO.2008.20.2853

93. Caudell JJ, Gillison ML, Maghami E, Spencer S, Pfister DG, Adkins D, et al. NCCN guidelines® Insights: head and neck cancer, version 1. *J Natl Compr Canc Netw*. (2022) 20:224–34. doi: 10.6004/jnccn.2022.0016

94. Kreimer AR, Clifford GM, Boyle P, Franceschi S. Human papillomavirus types in head and neck squamous cell carcinomas worldwide: a systematic review. *Cancer Epidemiol Biomarkers Prev*. (2005) 14:467–75. doi: 10.1158/1055-9965.EPI-04-0551

95. Alizon S, Murall CL, Bravo IG. Why human papillomavirus acute infections matter. *Viruses*. (2017) 9:293. doi: 10.3390/v9100293

96. Grunwitz C, Salomon N, Vascotto F, Selmi A, Bukur T, Diken M, et al. HPV16 RNA-LPX vaccine mediates complete regression of aggressively growing HPV-positive mouse tumors and establishes protective T cell memory. *Oncoimmunology*. (2019) . 8: e1629259. doi: 10.1080/2162402X.2019.1629259

97. Ramos da Silva J, Bitencourt Rodrigues K, Formoso Pelegrin G, Silva Sales N, Muramatsu H, de Oliveira Silva M, et al. Single immunizations of self-amplifying or non-replicating mRNA-LNP vaccines control HPV-associated tumors in mice. *Sci Transl Med*. (2023) 15:eabn3464. doi: 10.1126/scitranslmed.abn3464

98. Chen Y, Jiang N, Chen M, Sui B, Liu X. Identification of tumor antigens and immune subtypes in head and neck squamous cell carcinoma for mRNA vaccine development. *Front Cell Dev Biol*. (2022) 10:1064754. doi: 10.3389/fcell.2022.1064754

99. Li H-X, Liu T-R, Tu Z-X, Xie C-B, Wen W-P, Sun W. Screening of tumor antigens and construction of immune subtypes for mRNA vaccine development in head and neck squamous cell carcinoma. *Biomolecules*. (2022) 13:90. doi: 10.3390/biom13010090

100. Bogen JP, Grzeschik J, Jakobsen J, Bähre A, Hock B, Holmar H. Treating bladder cancer: engineering of current and next generation antibody-, fusion protein-, mRNA-, cell- and viral-based therapeutics. *Front Oncol*. (2021) 11:672262. doi: 10.3389/fonc.2021.672262

101. Luke JJ, Kennedy LC, Sankar N, Menzies AM, van Akkooi ACJ, Gonzalez M, et al. A phase I trial of intratumoral STX-001: A novel self-replicating mRNA expressing IL-12 alone or with pembrolizumab in advanced solid tumors. *J Clin Oncol*. (2024) 42:16 suppl, TPS2696-TPS2696.

102. Ostrom QT, Price M, Neff C, Cioffi G, Waite KA, Kruchko C, et al. CBTRUS statistical report: primary brain and other central nervous system tumors diagnosed in the United States in 2015–2019. *Neuro-oncol*. (2022) 24:v1–v95. doi: 10.1093/neuonc/noac202

103. Gargini R, Segura-Collar B, Sánchez-Gómez P. Cellular plasticity and tumor microenvironment in gliomas: the struggle to hit a moving target. *Cancers*. (2020) 12:1622. doi: 10.3390/cancers12061622

104. Richardson TE, Walker JM, Hambardzumyan D, Brem S, Hatanpaa KJ, Viapiano MS, et al. Genetic and epigenetic instability as an underlying driver of progression and aggressive behavior in IDH-mutant astrocytoma. *Acta Neuropathol*. (2024) 148:5. doi: 10.1007/s00401-024-02761-7

105. Tomaszewski W, Sanchez-Perez L, Gajewski TF, Sampson JH. Brain tumor microenvironment and host state: implications for immunotherapy. *Clin Cancer Res*. (2019) 25:4202–10. doi: 10.1158/1078-0432.CCR-18-1627

106. Nduom EK, Wei J, Yaghi NK, Huang N, Kong L-Y, Gabrusiewicz K, et al. PD-L1 expression and prognostic impact in glioblastoma. *Neuro-oncology*. (2015) 18:195–205. doi: 10.1093/neuonc/nov172

107. Himes BT, Geiger PA, Ayasoufi K, Bhargav AG, Brown DA, Parney IF. Immunosuppression in glioblastoma: current understanding and therapeutic implications. *Front Oncol*. (2021) 11:770561. doi: 10.3389/fonc.2021.770561

108. Chen Z, Wang X, Yan Z, Zhang M. Identification of tumor antigens and immune subtypes of glioma for mRNA vaccine development. *Cancer Med*. (2022) 11:2711–26. doi: 10.1002/cam4.46334

109. Lin H, Wang K, Xiong Y, Zhou L, Yang Y, Chen S, et al. Identification of tumor antigens and immune subtypes of glioblastoma for mRNA vaccine development. *Front Immunol*. (2022) 13:773264. doi: 10.3389/fimmu.2022.773264

110. Wu C, Qin C, Long W, Wang X, Xiao K, Liu Q. Tumor antigens and immune subtypes of glioblastoma: the fundamentals of mRNA vaccine and individualized immunotherapy development. *J Big Data*. (2022) 9:1–25. doi: 10.1186/s40537-022-00643-x

111. Everson RG, Hugo W, Sun L, Antonios J, Lee A, Ding L, et al. TLR agonists polarize interferon responses in conjunction with dendritic cell vaccination in Malignant glioma: a randomized phase II trial. *Nat Commun*. (2024) 15:3882. doi: 10.1038/s41467-024-48073-y

112. Liau LM, Ashkan K, Brem S, Campian JL, Trusheim JE, Iwamoto FM, et al. Association of autologous tumor lysate-loaded dendritic cell vaccination with extension of survival among patients with newly diagnosed and recurrent glioblastoma: A phase 3 prospective externally controlled cohort trial. *JAMA Oncol*. (2023) 9:112–21. doi: 10.1001/jamaoncol.2022.5370

113. Bagley SJ, Logun M, Fraietta JA, Wang X, Desai AS, Bagley LJ, et al. Intrathecal bivalent CAR T cells targeting EGFR and IL13α2 in recurrent glioblastoma: phase 1 trial interim results. *Nat Med*. (2024) 30:1320–9. doi: 10.1038/s41591-024-02893-z

114. Li N, Rodriguez JL, Yin Y, Logun MT, Zhang L, Yu S, et al. Armored bicistronic CAR T cells with dominant-negative TGF-β receptor II to overcome resistance in glioblastoma. *Mol Ther*. (2024) 31. doi: 10.1016/j.ymthe.2024.07.020

115. Choi BD, Gerstner ER, Frigault MJ, Leick MB, Mount CW, Balaj L, et al. Intraventricular CARv3-TEAM-E T cells in recurrent glioblastoma. *N Engl J Med*. (2024) 390:1290–98. doi: 10.1056/NEJMoa2314390

116. Brown CE, Hibbard JC, Alizadeh D, Blanchard MS, Natri HM, Wang D, et al. Locoregional delivery of IL-13Rα2-targeting CAR-T cells in recurrent high-grade glioma: a phase 1 trial. *Nat Med*. (2024) 30:1001–12. doi: 10.1038/s41591-024-02875-1

117. Lowenstein PR, Varela ML, Castro MG. Three recent breakthroughs in CAR T cells for the treatment of glioblastoma: Is it the light at the end of the tunnel? *Mol Ther*. (2024) 32(5):1187–9. doi: 10.1016/j.ymthe.2024.04.018

118. Ma S, Ba Y, Ji H, Wang F, Du J, Hu S. Recognition of tumor-associated antigens and immune subtypes in glioma for mRNA vaccine development. *Front Immunol*. (2021) 12:738435. doi: 10.3389/fimmu.2021.738435

119. Vonderheide RH, Kraynyak KA, Shields AF, McRee AJ, Johnson JM, Sun W, et al. Phase 1 study of safety, tolerability and immunogenicity of the human telomerase (hTERT)-encoded DNA plasmids INO-1400 and INO-1401 with or without IL-12 DNA plasmid INO-9012 in adult patients with solid tumors. *J Immunother Cancer*. (2021) 9:e003019. doi: 10.1136/jitc-2021-003019

120. Schiller JT, Lowy DR, Frazer IH, Finn OJ, Vilar E, Lyerly HK, et al. Cancer vaccines. *Cancer Cell*. (2022) 40:559–64. doi: 10.1016/j.ccell.2022.05.015

121. Reardon DA, Brem S, Desai AS, Bagley SJ, Kurz SC, de la Fuente MI, et al. Intramuscular (IM) INO-5401 + INO-9012 with electroporation (EP) in combination with cemiplimab (REGN2810) in newly diagnosed glioblastoma. *J Clin Oncol*. (2022) 40:2004. doi: 10.1200/JCO.2022.40.16_suppl.2004

122. Boczkowski D, Nair SK, Snyder D, Gilboa E. Dendritic cells pulsed with RNA are potent antigen-presenting cells. *Vitro vivo. J Exp Med*. (1996) 184:465–72. doi: 10.1084/jem.184.2.465

123. Eagles ME, Nassiri F, Badhiwala JH, Suppiah S, Almenawer SA, Zadeh G, et al. Dendritic cell vaccines for high-grade gliomas. *Ther Clin Risk Manag*. (2018) 14:1299–313. doi: 10.2147/TCRM.S135865

124. de Godoy LL, Chawla S, Brem S, Wang S, O'Rourke DM, Nasrallah MP, et al. Assessment of treatment response to dendritic cell vaccine in patients with glioblastoma using a multiparametric MRI-based prediction model. *J Neurooncol*. (2023) 163:173–83. doi: 10.1007/s11060-023-04324-4

125. Liau LM, Ashkan K, Brem S, Campian J, Trusheim J, Iwamoto F, et al. Autologous tumor lysate-loaded dendritic cell vaccination improves survival in patients with newly diagnosed and recurrent glioblastoma: Survival results from a phase 3 trial. Unpublished data. *Neuro-Oncol*. (2022) 24:vii66. doi: 10.1093/neuonc/noac209.259

126. Foster JB, Griffin C, Rokita JL, Stern A, Brimley C, Rathi K, et al. Development of GPC2-directed chimeric antigen receptors using mRNA for pediatric brain tumors. *J Immunother Cancer*. (2022) 10:e004450. doi: 10.1136/jitc-2021-004450

127. Foster MC, Savoldo B, Lau W, Rubinos C, Grover N, Armistead P, et al. Utility of a safety switch to abrogate CD19 CAR T-cell–associated neurotoxicity. *Blood*. (2021) 137:3306–09. doi: 10.1182/blood.2021010784

128. Kowalczyk A, Zarychta J, Marsolek A, Zawitkowska J, Lejman M. Chimeric antigen receptor T cell and chimeric antigen receptor NK cell therapy in pediatric and adult high-grade glioma—Recent advances. *Cancers*. (2024) 16:623. doi: 10.3390/cancers16030623

129. O'Rourke DM, Nasrallah MP, Desai A, Melenhorst JJ, Mansfield K, Morrissette JJD, et al. A single dose of peripherally infused EGFRvIII-directed CAR T cells mediates antigen loss and induces adaptive resistance in patients with recurrent gliobalstoma. *Sci Transl Med*. (2017) 9:eaaa0984. doi: 10.1126/scitranslmed.aaa0984

130. Chen X, Cui Y, Zou L. Treatment advances in high-grade gliomas. *Front Oncol*. (2024) 14:1287725. doi: 10.3389/fonc.2024.1287725

131. Beatty GL, Haas AR, Maus MV, Torigian DA, Soulen MC, Plesa G, et al. Mesothelin-specific chimeric antigen receptor mRNA-engineered T cells induce anti-tumor activity in solid Malignancies. *Cancer Immunol Res*. (2014) 2:112–20. doi: 10.1158/2326-6066.CIR-13-0170

132. Shah PD, Huang AC, Xu X, Orlowski, Amaravadi RK, Schuchter LM, et al. Phase I trial of autologous RNA-electroporated cMET-directed CAR T cells administered intravenously in patients with melanoma and breast carcinoma. *Cancer Res Commun*. (2023) 3:821–9. doi: 10.1158/2767-9764.CRC-22-0486

133. Montoya M, Gallus M, Phyu S, Haegelin J, de Groot J, Okada H. A roadmap of CAR-T-cell therapy in glioblastoma: challenges and future perspectives. *Cells*. (2024) 13:726. doi: 10.3390/cells13090726

134. Varela ML, Comba A, Faisal SM, Argento A, Franson A, Barissi MN, et al. Gene therapy for high grade glioma: The clinical experience. *Expert Opin Biol Ther*. (2023) 23:145–61. doi: 10.1080/14712598.2022.2157718

135. Todo T, Ito H, Ino Y, Ohtsu H, Ota Y, Shibahara J, et al. Intratumoral oncolytic herpes virus G47Δ for residual or recurrent glioblastoma: a phase 2 trial. *Nat Med*. (2022) 28:1630–9. doi: 10.1038/s41591-022-01897-x

136. Huang Q, Chan KY. An AAV capsid reprogrammed to bind human transferring receptor mediates brain-wide gene delivery. *Science*. (2024) 384:1220–7. doi: 10.1126/science.adm8386

137. Guterres A, Filho PNS, Moura-Neta V. Breaking barriers: A future perspective on glioblastoma therapy with mRNA-based immunotherapies and oncolytic viruses. *Vaccines*. (2024) 12:61. doi: 10.3390/vaccines12010061

138. Guterres A, Abrahim M, da Costa Neves PC. The role of immune subtyping in glioma mRNA vaccine development. *Immunotherapy*. (2023) 15:1057–72. doi: 10.2217/imt-2023-0027

139. Wen P, Aguilar L, Ye X, Reardon D, Bi WL, Peruzzi P, et al. Phase 1 trial of oncolytic viral immunotherapy with CAN-2409 + valacylovir in combination with nivolumab and standard of care (SOC) in newly diagnosed high-grade glioma (HGG). *Neuro-Oncol*. (2021) 23:vi52. doi: 10.1093/neuonc/noab196.205

140. Evgin L, Kottke T, Tonne J, Thompson J, Huff AL, van Floten J, et al. Oncolytic virus-mediated expansion of dual-specific CAR T cells improves efficacy against solid tumors in mice. *Sci Transl Med*. (2022) 14:eabn2231. doi: 10.1126/scitranslmed.abn2231

141. Nassiri F, Patil V, Yefet LS, Singh O, Liu J, Dang RMA, et al. Oncolytic DNX-2401 virotherapy plus pembrolizumab in recurrent glioblastoma: a phase 1/2 trial. *Nat Med*. (2023) 29:1370–78. doi: 10.1038/s41591-023-02347-y

142. Wang Q, He Z, Huang M, Liu T, Wang Y, Xu H, et al. Vascular niche IL-6 induces alternative macrophage activation in glioblastom through HIF-2α. *Nat Commun*. (2018) 9:559. doi: 10.1038/s41467-018-03050-0

143. Yang F, He Z, Duan H, Zhang D, Li J, Yang H, et al. Synergistic immunotherapy of glioblastoma by dual targeting of IL-6 and CD40. *Nat Commun*. (2021) 12:4324. doi: 10.1038/s41467-021-23832-3

144. Lamano JB, Lamano JB, Li YD, DiDomenico JD, Choy W, Veliceasa D, et al. Glioblastoma-derived IL6 induces immunosuppressive peripheral myeloid cell PD-L1 and promotes tumor growth. *Clin Cancer Res*. (2019) 25:3543–657. doi: 10.1158/1078-0432.CCR-18-2402

145. Hailemichael Y, Johnson DH, Abdel-Wahab N, Foo WC, Bentebiel S-E, Daher M, et al. Interleukin-6 blockade abrogates immunotherapy toxicity and promotes tumor immunity. *Cancer Cell*. (2022) 40:509–23. doi: 10.1016/j.ccell.2022.04.004

146. Sampson JH, Singh Achrol A, Aghi MK, Bankiewicz, Bexon M, Brem S, et al. Targeting the IL4 receptor with MDNA55 in patients with recurrent glioblastoma: Results of a phase IIb trial. *Neuro-Oncol*. (2023) 25:1085–97. doi: 10.1093/neuonc/noac285

147. Trivedi V, Yang C, Klippel K, Yegorov O, von Roemeling C, Hoang-Minh L, et al. mRNA-based precision targeting of neoantigens and tumor-associated antigens in malignant brain tumors. *Genome Med*. (2024) 16:17. doi: 10.1186/s13073-024-01281-z

148. Akintola OO, Reardon DA. The current landscape of immune checkpoint blockade in glioblastoma. *Neurosurg Clin N Am*. (2021) 32:2018235–48. doi: 10.1016/j.nec.2020.12.003

149. Goutnik M, Iakovidis A, Still ME, Moor RS, Melnick K, Yan S, et al. Advancements in chimeric antigen receptor-expressing T-cell therapy for glioblastoma multiforme: Literature review and future directions. *Neurooncol Adv*. (2024) 6:1–10. doi: 10.1093/noajnl/vdae025

150. Liu T, Jin D, Le SB, Chen D, Sebastian M, Riva A, et al. Machine learning-directed conversion of glioblastoma cells to dendritic cell-like antigen-presenting cells as cancer immunotherapy. *Cancer Immunol Res*. (2024). doi: 10.1158/2326-6066.CIR-23-0721

151. Wu L, Zhao Z, Shin YJ, Yin Y, Raju A, Selvan Vaiyapuri T, et al. Tumour microenvironment programming by an RNA-RNA binding protein complex creates a druggable vulnerability in IDH-wild-type glioblastoma. *Nat Cell Biol*. (2024) 26:1003–18. doi: 10.1038/s41556-024-01428-5

152. Liu X, Huang P, Yang R, Deng H. mRNA cancer vaccines: Construction and boosting strategies. *ACS Nano*. (2023) 17:19550–80. doi: 10.1021/acsnano.3c05635

153. He Q, Gao H, Tan D, Zhang H, Wang JZ. mRNA cancer vaccines: Advances, trends, and challenges. *Acta Pharm Sin B*. (2022) 12:2969–89. doi: 10.1016/j.apsb.2022.03.011

154. Bagley SJ, Binder ZA, Lamrani L, Marinari E, Desai AS, MacLean P, et al. Repeated peripheral infusions of anti-EGFRvIII CAR T cells in combination with pembrolizumab show no efficacy in glioblastoma: a phase I trial. *Nat Cancer*. (2024) 5:517–31. doi: 10.1038/s43018-023-00709-6

155. Calimeri T, Marcucci F, Corti A. Overcoming the blood-brain barrier in primary central nervous system lymphoma: a review on new strategies to solve an old problem. *Ann Lymph*. (2021) 5:20. doi: 10.21037/aol-20-54

156. Lim S, Kwak M, Kang J, Cesaire M, Tang K, Robey RW, et al. Ibrutinib disrupts blood-tumor barrier integrity and prolongs survival in rodent glioma model. *Acta Neuropathol Commun*. (2024) 12:9987. doi: 10.1186/s40478-024-01763-6

157. Goddard ET, Linde MH, Srivastava S, Klug G, Shabaneh TB, Klug G, et al. Immune evasion of dormant disseminated tumor cells is due to their scarcity and can be overcome by T cell immunotherapies. *Cancer Cell*. (2024) 42:119–34. doi: 10.1016/j.ccell.2023.12.011

158. Wang Z, Troilo PJ, Wang X, Griffiths TG, Pacchione SJ, Barnum AB, et al. Detection of integration of plasmid DNA into host genomic DNA following intramuscular injection and electroporation. *Gene Ther*. (2004) 11:711–21. doi: 10.1038/sj.gt.3302213

159. Acevedo-Whitehouse K, Bruno R. Potential health risks of mRNA-based vaccine therapy: A hypothesis. *Med Hypotheses*. (2023) 171:111015. doi: 10.1016/j.mehy.2023.111015

160. Aldén M, Olofsson Falla F, Yang D, Barghouth M, Luan C, Rasmussen M, et al. Intracellular reverse transcription of Pfizer BioNTech COVID-19 mRNA vaccine BNT162b2 in *vitro* in human liver cell line. *Curr Issues Mol Biol*. (2022) 44:1115–26. doi: 10.3390/cimb44030073

161. Zhang L, Richards A, Barrasa MI, Hughes SH, Young RA, Jaenisch R. Reverse-transcribed SARS-CoV-2RNA can integrate into the genome of cultured human cells and can be expressed in patient-derived tissues. *Proc Natl Acad Sci USA*. (2021) 118: e2105968118. doi: 10.1073/pnas.2105968118

162. Wong ET, Brem S. Taming glioblastoma: targeting angiogenesis. *J Clin Oncol*. (2007) 25:4705–6. doi: 10.1200/JCO.2007.13.1037

163. Wong ET, Brem S. Taming glioblastoma by targeting angiogenesis: 3 years later. *J Clin Oncol*. (2011) 29:124–6. doi: 10.1200/JCO.2007.13.1037

164. Hotz C, Wagenaar TR, Gieseke F, Bangari DS, Callahan M, Cao H, et al. Local delivery of mRNA-encoded cytokines promotes antitumor immunity and tumor eradication across multiple preclinical tumor models. *Sci Transl Med*. (2021) 13: eabc7804. doi: 10.1126/scitranslmed.abc7804

165. Berraondo P, Gomis G, Melero I. The liver as a cytokine factory working on mRNA blueprints for cancer immunotherapy. *Cancer Cell*. (2024) 42:502–4. doi: 10.1016/j.ccell.2024.02.015

166. Beck JD, Diken M, Suchan M, Streuber M, Diken E, Kolb L, et al. Long-lasting mRNA-encoded interleukin-2 restores $CD8^+$ T cell neoantigen immunity in MHC class 1-deficient cancers. *Cancer Cell*. (2024) 42:1–15. doi: 10.1016/j.ccell.2024.02.013

167. Deng Z, Yang H, TGian Y, Liu Z, Sun F, Yang P. An OX40L mRNA vaccine inhibits the growth of hepatocellular carcinoma. *Front Oncol*. (2022) 12:975408. doi: 10.3389/fonc.2022.975408

168. Dong S, Liu X, Bi Y, Wang Y, Antony A, Lee D, et al. Adaptive design of mRNA-loaded extracellular vesicles for targeted immunotherapy of cancer. *Nat Commun*. (2023) 14:6610. doi: 10.1038/s41467-023-42365-5

169. Liu M, Hu S, Yan N, Popowski KD, Cheng K. Inhalable extracellular vesicle delivery of IL-12mRNA to treat lung cancer and promote systemic immunity. *Nat Nanotechnol*. (2024) 19:565–75. doi: 10.1038/s41565-023-01580-3

170. Ding L, Li J, Wu C, Yan F, Li X, Zhang S. A self-assembled RNA-triple helix hydrogel drug delivery system targeting triple-negative breast cancer. *J Mater Chem B*. (2020) 8:3527–33. doi: 10.1039/c9tb01610d

171. Rosenblum D, Gutkin A, Kedmi R, Ramishetti S, Veiga N, Jacobi AM, et al. CRISPR-Cas9 genome editing using targeted lipid nanoparticles for cancer therapy. *Sci Adv*. (2020) 6:eabc9450. doi: 10.1126/sciadv.abc9450

172. Lang F, Schrörs B, Löwer M, Tureci Ö, Sahin U. Identification of neoantigens for individualized therapeutic cancer vaccines. *Nat Rev Drug Discovery*. (2022) 21:261–82. doi: 10.1038/s41573-021-00387-y

173. Linette GP, Carreno BM. On the twentieth anniversary of dendritic cell vaccines – Riding the next wave. *Cancer Res*. (2022) 82:966–8. doi: 10.1158/0008-5472.CAN-21-4440

174. Bell J. *Next-generation RNA technologies: making longer-lasting drugs with a broader reach* (2023). BioPharma Dive (Accessed September 4, 2024).

175. Dolgin E. Why rings of RNA could be the next blockbuster drug. *Nature*. (2023) 622:22–4. doi: 10.1038/d41586-023-03058-7

176. Sharma P, Hoorn D, Aitha A, Breier D, Peer D. The immunostimulatory nature of mRNA lipid nanoparticles. *Adv Drug Delivery Rev*. (2024) 205:115175. doi: 10.1016/j.addr.2023.115175

177. Tallent A. ARPA-H funds two cancer "Manhattan Projects". *Cancer Discovery*. (2024) 14:11–2. doi: 10.1158/2159-8290.CD-NB2023-0085

178. Weintraub K. *mRNA, made famous by COVID vaccine, now enlisted for cancer treatment (usatoday.com)* (2023). USA Today (Accessed 04 September 2024).

Glossary

APC	Antigen presenting cell
circRNA	circular RNA
CNS	central nervous system
CRS	cytokine release syndrome
CSE	conserved sequence element
CTL	cytotoxic T lymphocyte
DAMP	damage-associated molecular patterns
DC	dendritic cell
GBM	glioblastoma
HNSCC	head and neck squamous cell carcinoma
HLA	human leukocyte antigen
HPV	human papilloma virus
HSV1	herpes simplex virus 1
hTERT	human telomerase reverse transcriptase
ICANS	immune effector cell-associated neurotoxicity
ICI	immune checkpoint inhibition/inhibitor
LNP	lipid nanoparticle
LPA	lipid particle aggregate
MAS	macrophage activation syndrome
MHC	major histocompatibility class
mRNA	messenger ribonucleic acid
nms-mRNA	nucleoside-modified synthetic mRNA
RBP	RNA-binding protein
RIG-I	retinoic acid-inducible gene I protein
SNV	single nucleotide variant
TCGA	The Cancer Genome Atlas
sEV	small Extracellular vesicle
TCR	T cell receptor
TE	transposable elements
TIL	tumor infiltrating lymphocyte
TLR	Toll-like receptor
TME	tumor microenvironment
TRUCK	T cells redirected for universal cytokine-mediating killing

frontiers | Frontiers in Neurology

TYPE Original Research
PUBLISHED 17 October 2024
DOI 10.3389/fneur.2024.1413236

OPEN ACCESS

EDITED BY
Ramcharan Singh Angom,
Mayo Clinic Florida, United States

REVIEWED BY
Hari Rachamala,
Mayo Clinic Florida, United States
Mateusz Edward Bilski,
Medical University of Lublin, Poland
Esteban Quiceno,
University at Buffalo, United States

*CORRESPONDENCE
Wenbin Li
✉ liwenbin@ccmu.edu.cn
Zhige Zou
✉ zouzhige@hust.edu.cn

†These authors have contributed equally to this work and share first authorship

RECEIVED 06 April 2024
ACCEPTED 10 September 2024
PUBLISHED 17 October 2024

CITATION
Cai Z, Yang Z, Wang Y, Li Y, Zhao H, Zhao H, Yang X, Wang C, Meng T, Tong X, Zheng H, He Z, Niu C, Yang J, Chen F, Yang Z, Zou Z and Li W (2024) Tumor treating induced fields: a new treatment option for patients with glioblastoma.
Front. Neurol. 15:1413236.
doi: 10.3389/fneur.2024.1413236

Tumor treating induced fields: a new treatment option for patients with glioblastoma

Zehao Cai[1†], Zukai Yang[2†], Ying Wang[2], Ye Li[3], Hong Zhao[3], Hanwen Zhao[4], Xue Yang[1], Can Wang[1], Tengteng Meng[3], Xiao Tong[2], Hao Zheng[2], Zhaoyong He[2], Chunli Niu[3], Junzhi Yang[3], Feng Chen[1], Zhi Yang[5], Zhige Zou[4*] and Wenbin Li[1*]

[1]Department of Neuro-oncology Cancer Center, Beijing Tiantan Hospital, Capital Medical University, Beijing, China, [2]School of Basic Medical Science, Capital Medical University, Beijing, China, [3]Kunlun Tripot (Beijing) Medical Technology Co., Ltd., Beijing, China, [4]School of Integrated Circuits, Huazhong University of Science and Technology, Wuhan, Hubei, China, [5]School of Biomedical Engineering, Capital Medical University, Beijing, China

Purpose: Currently, a range of electromagnetic therapies, including magnetic field therapy, micro-currents therapy, and tumor treating fields, are under investigation for their potential in central nervous system tumor research. Each of these electromagnetic therapies possesses distinct effects and limitations. Our focus is on overcoming these limitations by developing a novel electric field generator. This generator operates by producing alternating induced currents within the tumor area through electromagnetic induction.

Methods: Finite element analysis was employed to calculate the distribution of electric fields. Cell viability was assessed using the CCK-8 assay. Tumor volumes and weights served as indicators to evaluate the effectiveness of TTIF. The *in-vivo* imaging system was utilized to confirm tumor growth in the brains of mice.

Results: TTIF significantly inhibited the proliferation of U87 cells both *in vitro* and *in vivo*.

Conclusion: TTIF significantly inhibited the proliferation of U87 cells both *in vitro* and *in vivo*. Consequently, TTIF emerges as a potential treatment option for patients with progressive or metastatic GBM.

KEYWORDS

electromagnetic therapy, glioblastoma, central nervous system, electromagnetic induction, transformer

Introduction

The dysregulation of biological characteristics in tumors arises from changes occurring at both the cellular and tissue levels. One mechanism of dysregulation is through bioelectrical changes (1). Tumor cells exhibit a resting membrane potential of approximately −25 mV, significantly lower than that of normal cells (2). Moreover, multiple ion channels are found to be overexpressed in various types of tumor cells (3–6). Consequently, tumor cells disrupt local ionic environments, resulting in the generation of distinct local electric fields (EFs) (7). These EFs are present within the tumor interior and

on its surface, leading to outward electric currents at tumor sites (8). The differences in metabolism, structure, and electrical properties between tumors and normal tissues provide the mechanistic basis for electromagnetic therapy to selectively kill tumor cells through non-thermal effects, while minimally impacting normal cells.

Low-frequency (<100 Hz) alternating magnetic fields (MFs) and pulsed magnetic fields generated by the coil exhibit anti-tumor effects by inducing cell apoptosis, oxidative stress, increasing intracellular calcium levels, and reducing angiogenesis (9–15). One direct effect of magnetic field therapy is the disruption of ion movement by the Lorentz force. Another hypothesis suggests that alternating magnetic fields induce currents within tumors. Research on central nervous system (CNS) tumors has indicated that MFs enhance the apoptotic effects of temozolomide (TMZ) through redox regulation in U87 cells (16, 17). However, there is a lack of relevant clinical-level studies.

Common current therapies include direct current therapy (DCT) and alternating current therapy. DCT involves inserting electrodes into tumors and delivering stable direct current (40–80 mA) at low voltage (6–8 V). Direct current exerts its anti-tumor effects through electrochemical reactions, anti-angiogenesis, and altering the pH of the surrounding environment (18–20). One study demonstrated that sustained exposure to low-frequency (50 Hz), low-intensity (7.5 μA) alternating current can impact the proliferation of rat glioma C6 cells, and increasing the frequency and intensity can enhance its cytotoxic effect (21). Additionally, alternating current with a frequency of 100–200 kHz, intensity of 10–50 mA, and intermittent exposure (30 min/day) significantly inhibits the proliferation of breast cancer cells and glioma cells (22). However, due to the requirement of surgical implantation, there is currently a lack of clinical research on CNS tumors.

Tumor treating fields (TTFields) delivered by a pair of insulated electrodes are an intermediate-frequency (100–300 kHz), low-intensity(1–3 V/cm), alternating electric fields (23, 24). The early proposed TTFields' anti-tumor mechanism of action involved polymerization-depolymerization process of microtubules and mitotic disruption interfered by electrical forces on cell structure proteins (25). Recent research showed that TTFields can exert anti-tumor effects through multiple mechanisms, including disrupting cell membrane potential, increasing cell membrane permeability, affecting calcium ion channels, damaging DNA and inhibiting DNA repair (26–29). Currently, multiple clinical trial results demonstrated that TTFields have excellent anti-tumor effects in various types of cancers, including glioblastoma (GBM), malignant pleural mesothelioma (MPM), non-small cell lung cancer (NSCLC), and pancreatic carcinoma (PAC) (30–38). The median overall survival (OS) time of patients with newly diagnosed glioblastoma received temozolomide-only is 16.0 months. When TTFields are administrated, the median OS time is 20.9 months. Due to the unique treatment form of TTFields, it can not only treat tumors alone but is also particularly suitable for combination with other treatment methods, such as radiotherapy (RT), chemotherapy, targeted therapy, and immunotherapy (39). TTFields therapy has demonstrated promising results in the treatment of GBM when combined with targeted therapies such as bevacizumab. And one case report described a patient with thalamic glioblastoma who achieved a complete radiological response following treatment with proton therapy, temozolomide (TMZ), and TTFields (40). Multiple combination therapies incorporating TTFields are currently in Phase 2 clinical trials.

Over the past 20 years, numerous preclinical studies on electromagnetic therapy for CNS tumors have shown promising results, but clinical studies have been very limited. The unique tissue structure and biological functions of the CNS have posed barriers to the translation of devices into clinical practice. The application of invasive electromagnetic devices has been approached with caution. Even the TTFields device, which is a capacitor-like device delivering electric fields, has limitations. Insulated electrodes are placed on the shaved scalp when patients receive TTFields therapy. While the existing TTFields device has demonstrated efficacy against supratentorial GBM, its efficacy against infratentorial and spinal cord GBM has not been confirmed (41). It is challenging to arrange two opposite arrays on the face and the skin adjacent to the spinal cord to ensure that the threshold of electric field intensity is sufficient to arrest cellular proliferation (42).

We are committed to addressing these limitations by developing a new electric field generator. We have found that a transformer-like electric fields device offers several advantages, including the feasibility of vertical electric fields covering the infratentorial and spinal cord areas, wearability, and non-disposable packaging. The device generates alternating induced currents in the tumor area based on electromagnetic induction. In the present study, we propose and validate, for the first time to our knowledge, the feasibility of Tumor-treating Induced Fields (TTIF) therapy delivered by a transformer-like electric fields device.

Methods

TTIF device

The TTIF device mainly consists of one motor, wires, one capacitor, and one magnetic ring (Figure 1A). The electric coil wound around the magnetic core, together with the capacitor, forms an LC resonance circuit. The switch on the LC resonance circuit is turned off after the motor is powered once, and energy is continuously transferred in the inductor and capacitor. Based on electromagnetic induction, alternating current in the inductor coil generates an alternating magnetic field within the magnetic ring. Then, the alternating magnetic field within the magnetic ring generates an alternating electric field radiating outward. Consequently, the tumor microenvironment exhibits micro-alternating induced currents. The function of the switch and the LC resonance circuit is to convert the low voltage direct current in the wire into high voltage, medium-frequency alternating current in the inductor coil. In cellular experiments, the current density in the tumor cell region reached 1,000 mA/m^2. This result was obtained through finite element analysis.

Finite element analysis

The electric field distribution around the device was calculated using the finite element method to solve the quasi-static approximation of the Maxwell's equations, which is valid for this model. For the model we utilized the Comsol Multiphysics, version 6.2. The following boundary conditions were imposed: continuity of the normal component of the current density at all interior

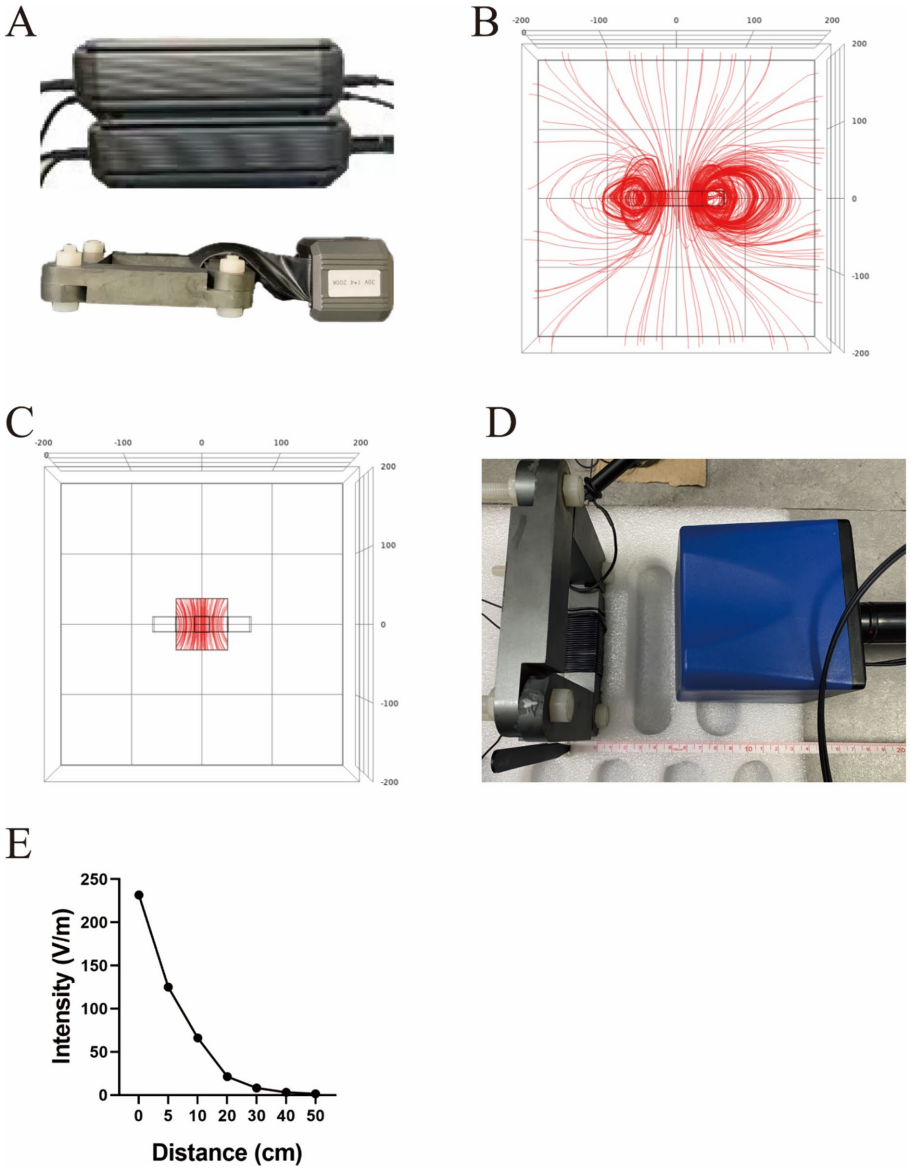

FIGURE 1
Structure diagram of the TTIF device **(A)**. Distribution of electric field lines generated by TTIF **(B)**. Vertical electric field lines at the center of the magnetic ring **(C)**. Detection of electric field intensity **(D)**. Relationship between electric field intensity and distance **(E)**.

boundaries and electric insulation at the external boundaries. The frequency was set to 200 kHz.

Cell viability

In this study, TTIF was applied to glioblastoma cells at 200 kHz, based on previous research. The cell dish was positioned at the center of the magnetic ring, perpendicular to its plane. Cell viability was assessed using the Cell Counting Kit-8 (CCK-8). A total of $1 \times 10\text{^}5$ cells were seeded into a 35 mm culture dish and incubated overnight. At each time point, the medium was replaced with 1 mL of media containing 10% CCK-8 reagent and incubated for 1–2 h at 37°C with 5% CO_2. Subsequently, the media from each 35 mm culture dish were transferred into 96-well plates (100 µL/well). The absorbance of each well was measured at 450 nm using a microplate reader.

Animal models

Both subcutaneous and intracranial xenograft tumor models were utilized to evaluate the effect of TTIF on GBM *in vivo*.

The subcutaneous tumor models

Female BALB/c-nu mice aged 6 weeks were obtained from Beijing Si Bei Fu Experimental Animal Technology Co., Ltd. Subcutaneous injections of U87 GBM tissue (8mm^3) with 200 µL phosphate-buffered

saline (PBS) were administered in the right groin of the mice. Successful inductions of 75 mm^3 subcutaneous tumors were observed within 10 days. The mice were randomly divided into different groups: Control or Tumor-Treating Induced Fields (TTIF) groups. The maximum allowable tumor size in the mice before euthanasia was 2,000 mm^3. Tumors were isolated and measured at the end of the experiment. Tumor volumes were calculated using the following formula: width^2 × length × 0.52.

The brain tumor models

A total of 0.32 μL of the G261-luc cell suspension was injected into the brains of C57BL/6 mice, approximately 1.8 mm lateral and 1 mm posterior to the bregma in the right brain hemisphere, over 4 min using a stereotactic rodent brain injection system. In total, either 1 × 10^4 or 1 × 10^5 G261-luc glioma cells were injected. Mice underwent bioluminescence imaging with an *in-vivo* imaging system (IVIS) before and after treatment to confirm tumor growth. Total flux (p/s) was calculated from the Region of Interest (ROI) in Living Image Software to quantitatively assess treatment efficacy.

Statistical analysis

Statistical analyses were conducted using GraphPad Prism 8.0.1. One-way ANOVA tests were utilized to compare tumor volumes and total flux between treatment groups. The normality of data was assessed using the Shapiro–Wilk test. Unpaired *t*-tests were employed to compare tumor weight and cell viability. Log-rank tests were conducted to compare overall survival (OS) between two groups. A *p*-value of <0.05 was considered statistically significant. Numerical values were reported as mean ± standard error of mean (SEM). When P is greater than or equal to 0.05, the figure is labeled with "ns." When P is less than 0.05 but greater than or equal to 0.01, the figure is labeled with "*." When P is less than 0.01, the figure is labeled with "**."

Results

The TTIF device generated a vertical electric field at the center of the magnetic ring

Initially, a quadrilateral magnetic ring was utilized as the electric field generator, and FEA was conducted to analyze the electric field distribution. The results indicated that the TTIF device produced circular, closed electric fields surrounding the magnetic ring (Figure 1B). As proximity to the center of the magnetic ring increased, the curvature of the electric field lines decreased, tending towards perpendicularity to the plane of the magnetic ring (Figure 1C). Electric field intensity in the air surrounding the magnetic ring was measured (Figure 1D), showing values exceeding 50 V/m within a 10 cm range (Figure 1E).

TTIF inhibited the proliferation of U87 cells *in vitro*

Following 72 h of TTIF treatment with a current density exceeding 1,000 mA/m^2, U87 cell density markedly decreased, accompanied by noticeable alterations in cell morphology (Figures 2A,B). Circular cell proportion increased, while cytoplasmic vacuoles emerged (Figures 2C,D). The inhibitory effect of TTIF was found to be dependent on exposure time, with efficacy increasing with prolonged treatment durations (Figure 2E).

TTIF inhibited the growth of GBMs in the subcutaneous murine model

To investigate the anti-tumor effects of TTIF *in vivo*, we initially transplanted U87 tissue subcutaneously into BALB/c-nu mice ($n = 4$ for each group). The tumor-bearing mice in the TTIF group were housed at the center of the magnetic ring and received continuous TTIF treatment for 21 days. Tumor volume was assessed every 7 days using a caliper (Figure 3A). The time-tumor volume curve indicated that TTIF significantly suppressed the growth of subcutaneous glioma volumes in mice ($p = 0.007$, Figure 3B). Following 21 days of TTIF treatment, the tumor volume of the experimental group mice was notably smaller than that of the control group mice (Figure 3C). Supporting this observation, the data on tumor weight also demonstrated a significant difference ($p = 0.010$, Figure 3D). Additionally, we assessed the weight of various organs in mice, with results showing no statistically significant difference between the two groups (Figure 3E).

TTIF prolonged the OS of intracranial tumor-bearing mice

1×10^4 G261 glioma cells were injected into the brains of C57 mice ($n = 10$), and IVIS was used on days 7, 14, 21, and 28 (Figure 4A). On day 7, after confirming successful induction of brain tumors using IVIS, mice were randomly divided into control and TTIF groups. Although the difference was not statistically significant, we observed a trend of decreasing luciferase intensity in mice receiving TTIF treatment compared to the control group ($p = 0.0826$, Figures 4B,C).

To further investigate TTIF's ability to inhibit tumor growth in the *in situ* brain tumor murine model, the number of cells injected was increased to 1×10^5. On day 3, mice were randomly divided into control and TTIF groups. Subsequently, we recorded the OS of each mouse. TTIF-treated mice showed prolonged survival, with a median survival of 47 days compared to 37 days in the control group ($p = 0.0274$, Figure 4D).

The characteristics of the small magnetic ring

In previous research, we thoroughly examined the characteristics and verified the therapeutic efficacy of a large magnetic ring. Subsequently, we pursued the development of a smaller magnetic ring, measuring 4 cm in external diameter and 1.6 cm in internal diameter (Figure 5A). However, we encountered challenges stemming from inadequate miniaturization and insufficient reduction in weight of the smaller ring, impeding its applicability in animal experiments involving tumor-bearing mice. To overcome this hurdle, we devised a simplified cubic model of human head tissue for finite element analysis, aimed at

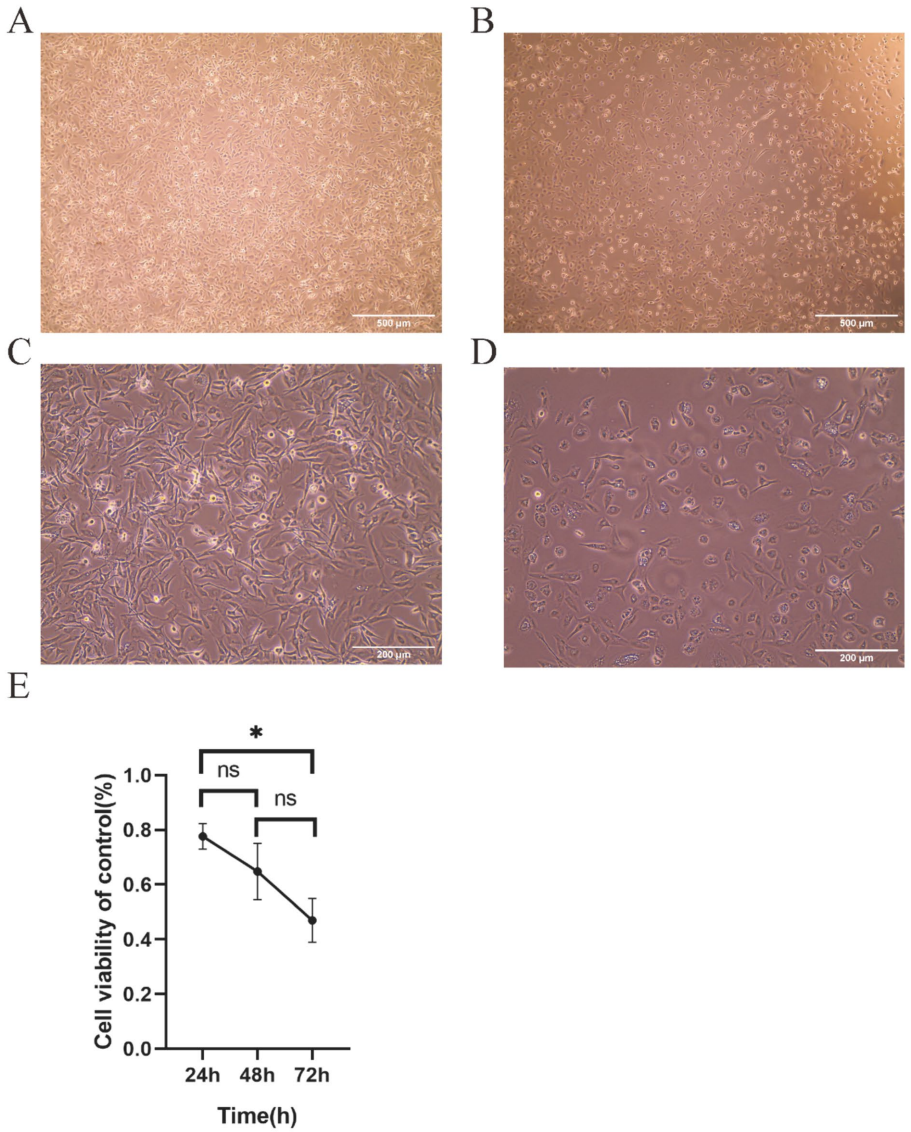

FIGURE 2
The 30 V TTIF device can inhibit the proliferation of U87 cells, achieving a current density of up to 1,000 mA/m^2 in the cell area. Comparison of cell images between the control group **(A)** and the electric field group **(B)** under a 4x phase-contrast microscope. Cell images of the control group **(C)** and the electric field group **(D)** under a 10x phase-contrast microscope. Relationship between cell viability and TTIF exposure time **(E)**.

investigating the behavior of small magnetic coils. This model comprehensively incorporates the scalp, skull, cerebrospinal fluid, gray matter, and white matter, each with distinct thicknesses of 5 mm, 6 mm, 3 mm, and 4 mm, respectively. Upon situating the small magnetic ring on the surface of the head tissue, a radial fountain-like distribution of electric field lines manifests within the head (Figure 5B). Upon reaching voltage levels comparable to those of clinical TTFields equipment, we observed the emergence of a specific intensity of electric field and longitudinal induced conduction current in the vicinity of the brain, adjacent to the ring (Figures 5C,D).

Discussion

GBM stands as the most aggressive primary tumor affecting the central nervous system (43). The standard treatment protocol for newly diagnosed GBM involves surgery followed by radiotherapy (RT) concurrently with TMZ, along with adjuvant TMZ, optionally supplemented with TTFields (44). Advanced stages of glioblastoma exhibit notably aggressive characteristics (45). Approximately 4.5% of patients diagnosed with supratentorial glioblastoma experience infratentorial metastases, while 3–5% present with metastatic spinal dissemination (MSD) (46, 47). Autopsy findings have revealed frequent incidental spread from supratentorial regions to the brain stem and spine, in contrast to relatively infrequent clinical incidences (48, 49). Complications such as infratentorial recurrence (ITR) and MSD may occur more frequently. Presently, there exists no standardized treatment approach for managing ITR and MSD. Although these patients may undergo additional radiotherapy and chemotherapy, their median OS, which are 5.5 months for ITR and 4 months for MSD, significantly lag behind those of the general GBM patient population (9.1 months).

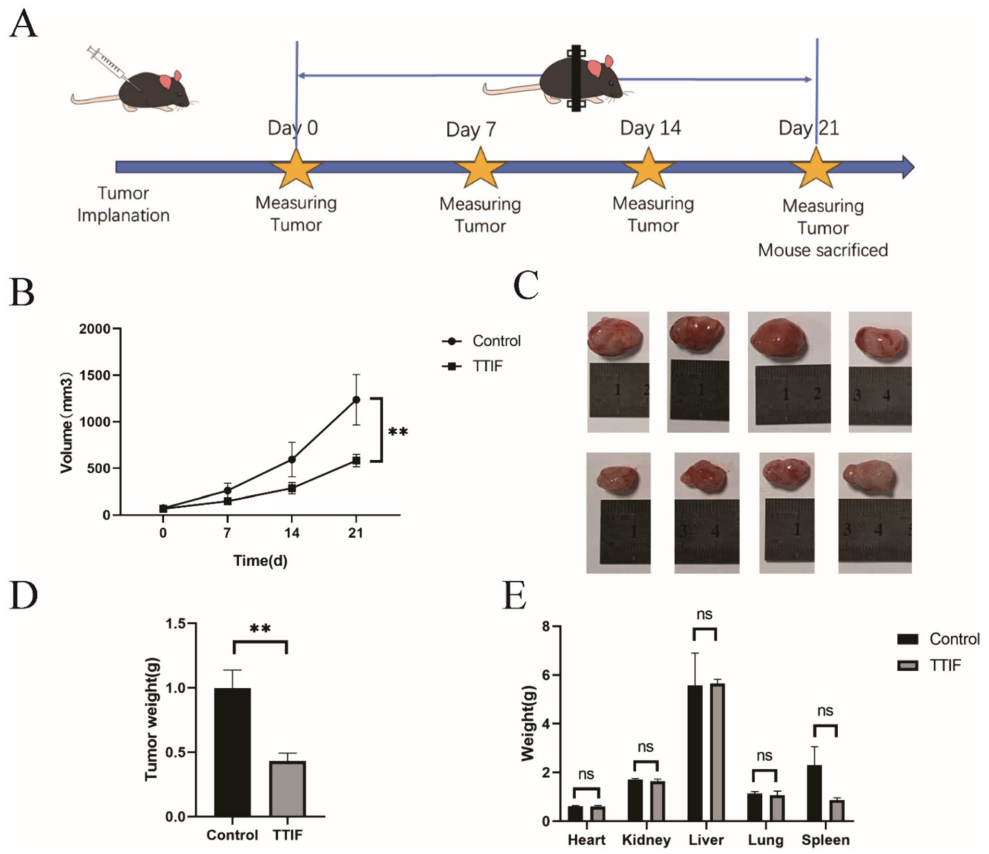

FIGURE 3
BALB/c-nu mice were chosen for the experiment involving subcutaneous tumor formation, and the voltage of the TTIF device was set to 30 V. Schedule of TTIF treatment for subcutaneous tumor-bearing mice **(A)**. Relationship between tumor volume and TTIF treatment duration **(B)**. Comparison of tumor sizes between the control group mice and the TTIF group mice **(C)**. Comparison of tumor weights between the control group mice and the TTIF group mice **(D)**. Comparison of organ weights between the control group mice and the TTIF group mice **(E)**.

The grim prognosis observed in GBM patients is partly attributed to the challenges associated with successful drug delivery across the blood–brain barrier (BBB) (50). The presence of the BBB limits the availability of traditional chemotherapy and targeted drugs for GBM. Since 2005, only a few new drugs—namely, Temozolomide, bevacizumab, and regorafenib—have been included in the NCCN guidelines as first- and second-line treatments for glioblastoma GBM (51, 52). However, research into new treatments for GBM is advancing rapidly (53). One promising option is vemurafenib, a highly selective BRAF V600 inhibitor that has demonstrated long-term antitumor effects in some patients with BRAF V600 mutant gliomas (54). Additionally, combination therapy targeting both BRAF and MEK has shown advantages over monotherapy with BRAF inhibitors. In a study involving the combination of dabrafenib and trametinib for recurrent or refractory high-grade gliomas (HGG) with the BRAF V600E mutation, an objective response was observed in 32% of GBM patients, with a complete response in 6.5% of cases (55). Furthermore, paxalisib, a small molecule capable of penetrating the blood–brain barrier and inhibiting the PI3K/AKT/mTOR pathway, has demonstrated clinical activity in newly diagnosed GBM patients with unmethylated MGMT promoters (56).

During radiation therapy, particularly reirradiation, the tolerance of normal brain tissue to radiation doses emerges as a significant limiting factor (54). Another important factor in qualifying patients for re-radiation is the increased risk of radionecrosis. The two primary directions in the development of radiotherapy for central nervous system tumors are: (1) modifying the radiotherapy regimen, including approaches such as preoperative radiotherapy and phased radiotherapy; and (2) enhancing the capabilities of radiotherapy equipment, exemplified by advancements in gamma knife and proton therapy technologies (57).

Electromagnetic therapy presents itself as a potentially viable option for treating CNS tumors. However, when utilizing TTFields, the range of EFs remains highly restricted. While TTFields delivered through capacitor-like devices demonstrate effectiveness primarily for supratentorial GBM, their application may not extend to infratentorial and spinal cord GBM. Consequently, patients with GBM face a dearth of sufficient treatment options when tumors progress or metastasize.

TTIF emerges as a potential treatment option for these patients. The TTIF device generates an alternating electric field at the center and on both sides of the magnetic ring through a circular alternating magnetic field. When tissues or tumors are in proximity to the TTIF device, alternating currents are induced. The device is non-invasive and easy to wear. The small magnetic ring is positioned on the skin surface corresponding to the tumor's location. Compared to TTFields electrodes, the advantage of TTIF's small magnetic ring is that it can be used individually, allowing placement on the skin atop the head or

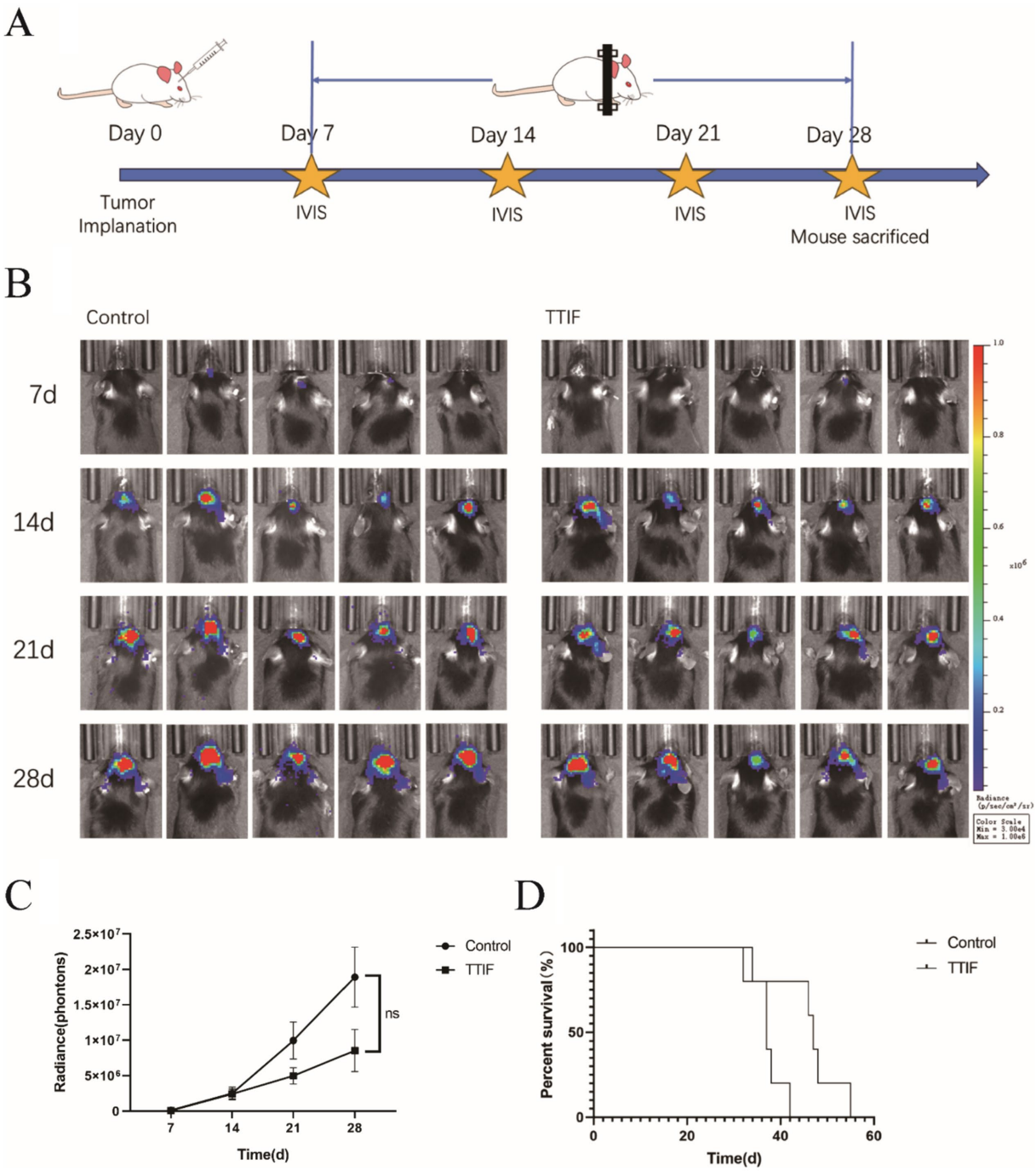

FIGURE 4
BALB/c-nu mice were chosen for the experiment involving intracranial tumor formation, and the voltage of the TTIF device was set to 45 V. Schedule of TTIF treatment for intracranial tumor mice **(A)**. Bioluminescence imaging's of tumors at various time points **(B)**. Relationship between tumor fluorescence intensity and time **(C)**. Comparison of OS between the TTIF group mice and the control group mice **(D)**.

over the cerebellum. With a larger magnetic ring, tumors experience vertical induced currents at the center of the magnetic ring.

TTIF can be utilized clinically in various forms. When used alone as an alternative to TTFields, TTIF effectively treats tumors located within a large magnetic ring placed over the body, such as the head, as well as those within a specific range above and below the plane of the ring. Additionally, a small magnetic ring can be worn similarly to a transcranial magnetic stimulation (TNS) therapy device, generating a radial TTIF to treat tumors throughout the body. TTIF offers comparable and enhanced benefits when combined with other treatments. There is ongoing debate regarding the potential impact of wearing a TTFields device on the efficacy of radiation therapy. The necessity to remove TTFields can also lead to increased treatment costs due to the disposable nature of the electrodes. In contrast, TTIF equipment is designed for easy wear and removal, providing added convenience. Furthermore, TTIF can complement the effects of

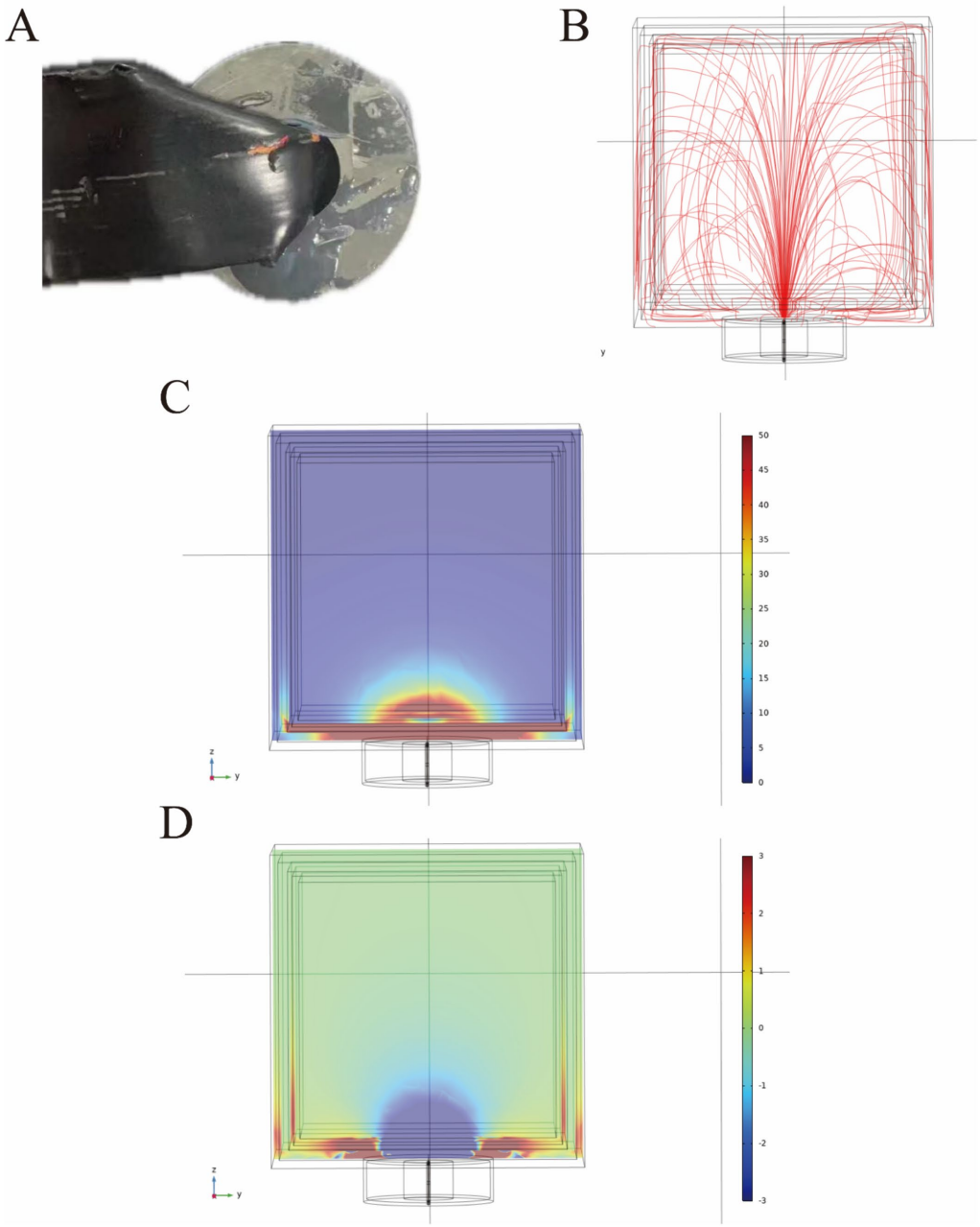

FIGURE 5
The appearance of the small magnetic ring **(A)**. The small magnetic ring generates a radial, geyser-like distribution of electric field lines in the head **(B)**. The distribution of the electric field in human head tissue under a voltage of 120 V is expressed in volts per meter (V/m) **(C)**. Additionally, the distribution of induced longitudinal conduction current in the human head is presented, with current density expressed in amperes per square meter (A/m^2) **(D)**.

TTFields therapy. When TTFields are employed to treat supratentorial tumors, TTIF can be utilized as an adjunct therapy to prevent supratentorial metastases or to address spinal-disseminated tumors. Further FEA is required to determine specific treatment options for both scenarios.

Our study is subject to several limitations. The frequency and induced current density utilized in cellular experiments with the TTIF device were derived from various prior studies. In our initial study, we focused exclusively on 200 kHz, which is recognized as the most sensitive frequency for TTFields treatment of GBM cells. However, it is important to note that the electric field characteristics of TTIF may differ from those of TTFields. These differences could include variations such as non-conserved electric fields and conservative electric fields, potentially resulting in distinct efficacy and frequency sensitivity between the two treatments. However, due to the design of the LC resonance circuit, which causes these two physical parameters to vary together, the relationship between frequency and current density and their effective threshold was not established in this study. Furthermore, the efficacy of the small magnetic ring has not been validated in animal experiments, primarily because the ring has not been adequately miniaturized to reduce weight. Additionally, further research is warranted to elucidate additional mechanisms of action.

Conclusion

We introduced the transformer-like induced fields/currents device for the first time in the field of electromagnetic therapy, outlining its feasible device structure and testing its functionality. Our findings indicate that TTIF significantly inhibited the proliferation of U87 cells both *in vitro* and *in vivo*. Consequently, TTIF emerges as a potential treatment option for patients with progressive or metastatic GBM.

Data availability statement

The raw data supporting the conclusions of this article will be made available by the authors, without undue reservation.

Ethics statement

The animal study was approved by Medical Ethics Committee, Beijing Tiantan Hospital, Capital Medical University. The study was conducted in accordance with the local legislation and institutional requirements.

Author contributions

ZC: Writing – review & editing, Writing – original draft, Validation, Software, Methodology, Investigation, Data curation. ZuY: Writing – original draft. YW: Writing – review & editing, Methodology, Investigation. YL: Writing – review & editing, Validation. HonZ: Writing – review & editing, Validation. HanZ: Writing – review & editing, Software, Formal analysis. XY: Writing – review & editing, Validation, Data curation. CW: Writing – review & editing, Methodology. TM: Writing – review & editing, Data curation. XT: Writing – review & editing, Validation. HaoZ: Writing – review & editing, Validation. ZH: Writing – review & editing, Validation. CN: Writing – review & editing, Methodology, Investigation. JY: Writing – review & editing, Methodology, Investigation. FC: Writing – review & editing, Methodology. ZhY: Writing – review & editing, Methodology. ZZ: Writing – review & editing, Methodology. WL: Writing – review & editing, Methodology.

Funding

The author(s) declare that financial support was received for the research, authorship, and/or publication of this article. This study received support from the Beijing Tiantan Hospital contract project titled "Effectiveness, Safety, and Mechanism of Action of Pulsed Electromagnetic Field Therapy for Malignant Tumors." Additionally, funding was provided through the Beijing Tiantan Hospital Talent Introduction Program under grant number RCYJ-2020-2025-LWB.

Conflict of interest

YL, HonZ, TM, CN, and JY were employed by Kunlun Tripot (Beijing) Medical Technology Co., Ltd.

The remaining authors declare that the research was conducted in the absence of any commercial or financial relationships that could be construed as a potential conflict of interest.

Publisher's note

References

1. Sheth M, Esfandiari L. Bioelectric dysregulation in Cancer initiation, promotion, and progression. *Front Oncol*. (2022) 12:846917. doi: 10.3389/fonc.2022.846917

2. Persinger M, Lafrenie R. The Cancer cell plasma membrane potentials as energetic equivalents to astrophysical properties. *Int Lett Chem Phys Astron*. (2014) 36:67–77. doi: 10.18052/www.scipress.com/ILCPA.36.67

3. Lastraioli E, Iorio J, Arcangeli A. Ion channel expression as promising cancer biomarker. *Biochim Biophys Acta*. (2015) 1848:2685–702. doi: 10.1016/j.bbamem.2014.12.016

4. Tsavaler L, Shapero MH, Morkowski S, Laus R. Trp-p8, a novel prostate-specific gene, is up-regulated in prostate cancer and other malignancies and shares high homology with transient receptor potential calcium channel proteins. *Cancer Res*. (2001) 61:3760–9.

5. Girault A, Privé A, Trinh NT, Bardou O, Ferraro P, Joubert P, et al. Identification of KvLQT1 K+ channels as new regulators of non-small cell lung cancer cell proliferation and migration. *Int J Oncol*. (2014) 44:838–48. doi: 10.3892/ijo.2013.2228

6. Ma PF, Chen JQ, Wang Z, Liu JL, Li BP. Function of chloride intracellular channel 1 in gastric cancer cells. *World J Gastroenterol*. (2012) 18:3070–80. doi: 10.3748/wjg.v18.i24.3070

7. Zhu K, Hum NR, Reid B, Sun Q, Loots GG, Zhao M. Electric fields at breast Cancer and Cancer cell collective Galvanotaxis. *Sci Rep*. (2020) 10:8712. doi: 10.1038/s41598-020-65566-0

8. Li L, Zhang K, Lu C, Sun Q, Zhao S, Jiao L, et al. Caveolin-1-mediated STAT3 activation determines electrotaxis of human lung cancer cells. *Oncotarget*. (2017) 8:95741–54. doi: 10.18632/oncotarget.21306

9. Xu A, Wang Q, Lv X, Lin T. Progressive study on the non-thermal effects of magnetic field therapy in oncology. *Front Oncol*. (2021) 11:638146. doi: 10.3389/fonc.2021.638146

10. Sadeghipour R, Ahmadian S, Bolouri B, Pazhang Y, Shafiezadeh M. Effects of extremely low-frequency pulsed electromagnetic fields on morphological and biochemical properties of human breast carcinoma cells (T47D). *Electromagn Biol Med*. (2012) 31:425–35. doi: 10.3109/15368378.2012.683844

11. Loja T, Stehlikova O, Palko L, Vrba K, Rampl I, Klabusay M. Influence of pulsed electromagnetic and pulsed vector magnetic potential field on the growth of tumor cells. *Electromagn Biol Med*. (2014) 33:190–7. doi: 10.3109/15368378.2013.800104

12. Harris PA, Lamb J, Heaton B, Wheatley DN. Possible attenuation of the G2 DNA damage cell cycle checkpoint in HeLa cells by extremely low frequency (ELF) electromagnetic fields. *Cancer Cell Int*. (2002) 2:3. doi: 10.1186/1475-2867-2-3

13. Costa FP, de Oliveira AC, Meirelles R, Machado MC, Zanesco T, Surjan R, et al. Treatment of advanced hepatocellular carcinoma with very low levels of amplitude-modulated electromagnetic fields. *Br J Cancer*. (2011) 105:640–8. doi: 10.1038/bjc.2011.292

14. Grassi C, D'Ascenzo M, Torsello A, Martinotti G, Wolf F, Cittadini A, et al. Effects of 50 Hz electromagnetic fields on voltage-gated Ca2+ channels and their role in modulation of neuroendocrine cell proliferation and death. *Cell Calcium*. (2004) 35:307–15. doi: 10.1016/j.ceca.2003.09.001

15. Tatarov I, Panda A, Petkov D, Kolappaswamy K, Thompson K, Kavirayani A, et al. Effect of magnetic fields on tumor growth and viability. *Comp Med*. (2011) 61:339–45.

16. Akbarnejad Z, Eskandary H, Dini L, Vergallo C, Nematollahi-Mahani SN, Farsinejad A, et al. Cytotoxicity of temozolomide on human glioblastoma cells is enhanced by the concomitant exposure to an extremely low-frequency electromagnetic field (100Hz, 100G). *Biomed Pharmacother*. (2017) 92:254–64. doi: 10.1016/j.biopha.2017.05.050

17. Ahmadi-Zeidabadi M, Akbarnejad Z, Esmaeeli M, Masoumi-Ardakani Y, Mohammadipoor-Ghasemabad L, Eskandary H. Impact of extremely low-frequency electromagnetic field (100 Hz, 100 G) exposure on human glioblastoma U87 cells during temozolomide administration. *Electromagn Biol Med*. (2019) 38:198–209. doi: 10.1080/15368378.2019.1625784

18. Holandino C, Veiga VF, Rodrigues ML, Morales MM, Capella MA, Alviano CS. Direct current decreases cell viability but not P-glycoprotein expression and function in human multidrug resistant leukemic cells. *Bioelectromagnetics*. (2001) 22:470–8. doi: 10.1002/bem.75

19. Nilsson E, von Euler H, Berendson J, Thorne A, Wersall P, Naslund I, et al. Electrochemical treatment of tumours. *Bioelectrochemistry*. (2000) 51:1–11. doi: 10.1016/S0302-4598(99)00073-2

20. Nordenstrom BE. Electrostatic field interference with cellular and tissue function,leading to dissolution of metastases that enhances the effect of chemotherapy. *Eur J Surg Suppl*. (1994) 574:121–35.

21. Cucullo L, Dini G, Hallene KL, Fazio V, Ilkanich EV, Igboechi C, et al. Very low intensity alternating current decreases cell proliferation. *Glia*. (2005) 51:65–72. doi: 10.1002/glia.20188

22. Tong JQ, Liu RT, Zhao LY, Kong WC, Tang JT. Inhibiting human breast Cancer cells (MCF-7) with alternating Micro-current at intermediate frequency (ACIF) in vitro and in vivo. *IFMBE Proc*. (2013) 39:1596–9. doi: 10.1007/978-3-642-29305-4_419

23. Kirson ED, Gurvich Z, Schneiderman R, Dekel E, Itzhaki A, Wasserman Y, et al. Disruption of cancer cell replication by alternating electric fields. *Cancer Res*. (2004) 64:3288–95. doi: 10.1158/0008-5472.CAN-04-0083

24. Zhu P, Zhu J-J. Tumor treating fields: a novel and effective therapy for glioblastoma: mechanism, efficacy, safety and future perspectives. *Chin Clin Oncol*. (2017) 6:41. doi: 10.21037/cco.2017.06.29

25. Gera N, Yang A, Holtzman TS, Lee SX, Wong ET, Swanson KD. Tumor treating fields perturb the localization of septins and cause aberrant mitotic exit. *PLoS One*. (2015) 10:e0125269. doi: 10.1371/journal.pone.0125269

26. Li X, Yang F, Rubinsky B. A theoretical study on the biophysical mechanisms by which tumor treating fields affect tumor cells during mitosis. *IEEE Trans Biomed Eng*. (2020) 67:2594–602. doi: 10.1109/TBME.2020.2965883

27. Chang E, Patel CB, Pohling C, Young C, Song J, Flores TA, et al. Tumor treating fields increases membrane permeability in glioblastoma cells. *Cell Death Discov*. (2018) 4:113. doi: 10.1038/s41420-018-0130-x

28. Karanam NK, Srinivasan K, Ding L, Sishc B, Saha D, Story MD. Tumor-treating fields elicit a conditional vulnerability to ionizing radiation via the downregulation of BRCA1 signaling and reduced DNA double-strand break repair capacity in non-small cell lung cancer cell lines. *Cell Death Dis*. (2017) 8:e2711. doi: 10.1038/cddis.2017.136

29. Voloshin T, Schneiderman RS, Volodin A, Shamir RR, Kaynan N, Zeevi E, et al. Tumor treating fields (TTFields) hinder cancer cell motility through regulation of microtubule and acting dynamics. *Cancers*. (2020) 12:3016. doi: 10.3390/cancers12103016

30. Stupp R, Wong ET, Kanner AA, Steinberg D, Engelhard H, Heidecke V, et al. NovoTTF-100A versus physician's choice chemotherapy in recurrent glioblastoma: a randomised phase III trial of a novel treatment modality. *Eur J Cancer*. (2012) 48:2192–202. doi: 10.1016/j.ejca.2012.04.011

31. Stupp R, Taillibert S, Kanner AA, Kesari S, Steinberg DM, Toms SA, et al. Maintenance therapy with tumor-treating fields plus temozolomide vs temozolomide alone for glioblastoma: a randomized clinical trial. *JAMA*. (2015) 314:2535–43. doi: 10.1001/jama.2015.16669

32. Grosso F, Mądrzak J, Crinò L, Chella A, Weinberg U, Ceresoli GL. STELLAR – a phase II trial of TTFields with chemotherapy for first line treatment of malignant mesothelioma. *J Thorac Oncol*. (2016) 11:S150–0. doi: 10.1016/S1556-0864(16)30322-7

33. Pless M, Droege C, von Moos R, Salzberg M, Betticher D. A phase I/II trial of tumor treating fields (TTFields) therapy in combination with pemetrexed for advanced non-small cell lung cancer. *Lung Cancer*. (2013) 81:445–50. doi: 10.1016/j.lungcan.2013.06.025

34. Weinberg U, Farber O, Giladi M, Bomzon Z, Kirson ED. Tumor treating field concurrent with standard of care for stage 4 non-small cell lung cancer (NSCLC) following platinum failure: phase III LUNAR study. *Ann Oncol*. (2018) 29:viii543. doi: 10.1093/annonc/mdy292.120

35. Vergote I, VonMoos R, Manso L, Van Nieuwenhuysen E, Concin N, Sessa C. Tumor treating fields in combination with paclitaxel in recurrent ovarian carcinoma: results of the INNOVATE pilot study. *Gynecol Oncol*. (2018) 150:471–7. doi: 10.1016/j.ygyno.2018.07.018

36. Vergote IB, Copeland L, Monk BJ, Coleman RL, Cibula D, Sehouli J, et al. Tumour treating fields (200 kHz) concomitant with weekly paclitaxel for platinum-resistant ovarian cancer: phase III INNOVATE-3/ENGOT-ov50 study. *Ann Oncol*. (2019) 30:v431.

37. Rivera F, Benavides M, Gallego J, Guillen-Ponce C, Lopz-Martin J, Kung M. Tumor treating fields in combination with gemcitabine or gemcitabine plus nab-paclitaxel in pancreatic cancer: results of the PANOVA phase 2 study. *Pancreatology*. (2019) 19:64–72. doi: 10.1016/j.pan.2018.10.004

38. Jones TH, Song JW, Abushahin L. Tumor treating fields: an emerging treatment modality for thoracic and abdominal cavity cancers. *Transl Oncol*. (2022) 15:101296. doi: 10.1016/j.tranon.2021.101296

39. Szklener K, Bilski M, Nieoczym K, Mańdziuk D, Mańdziuk S. Enhancing glioblastoma treatment through the integration of tumor-treating fields. *Front Oncol*. (2023) 13:1274587. doi: 10.3389/fonc.2023.1274587

40. Gürten B, Yenigül E, Sezer AD, Altan C, Malta S. Targeting of temozolomide using mag-netic nanobeads: an in vitro study. *Braz J Pharm Sci*. (2020) 56:56. doi: 10.1590/s2175-97902019000418579

41. Makimoto A, Nishikawa R, Terashima K, Kurihara J, Fujisaki H, Ihara S, et al. Tumor-treating fields therapy for pediatric brain tumors. *Neurol Int*. (2021) 13:151–65. doi: 10.3390/neurolint13020015

42. Chaudhry A, Benson L, Varshaver M, Farber O, Weinberg U, Kirson E, et al. NovoTTF™-100A system (tumor treating fields) transducer array layout planning for glioblastoma: a NovoTAL™ system user study. *World J Surg Oncol*. (2015) 13:316. doi: 10.1186/s12957-015-0722-3

43. Lukas RV, Wainwright DA, Ladomersky E, Sachdev S, Sonabend AM, Stupp R. Newly diagnosed glioblastoma: a review on clinical management. *Oncology (Williston Park)*. (2019) 33:91–100.

44. Wen PY, Weller M, Lee EQ, Alexander BM, Barnholtz-Sloan JS, Barthel FP, et al. Glioblastoma in adults: a Society for Neuro-Oncology (SNO) and European Society of Neuro-Oncology (EANO) consensus review on current management and future directions. *Neuro-Oncology*. (2020) 22:1073–113. doi: 10.1093/neuonc/noaa106

45. Tong H, Xinguang Y, Xuechun L, Wang P. Downregulation of solute carriers of glutamate in gliosomes and synaptosomes may explain local brain metastasis in anaplastic glioblastoma. *IUBMB Life*. (2015) 67:306–11. doi: 10.1002/iub.1372

46. Kawauchi D, Ohno M, Honda-Kitahara M, Miyakita Y, Takahashi M, Yanagisawa S, et al. Clinical characteristics and prognosis of glioblastoma patients with infratentorial recurrence. *BMC Neurol*. (2023) 23:9. doi: 10.1186/s12883-022-03047-9

47. Chen J, Shi Q, Li S, Zhao Y, Huang H. Clinical characteristics of glioblastoma with metastatic spinal dissemination. *Ann Palliat Med*. (2022) 11:506–12. doi: 10.21037/apm-21-3387

48. Drumm MR, Dixit KS, Grimm S, Kumthekar P, Lukas RV, Raizer JJ, et al. Extensive brainstem infiltration, not mass effect, is a common feature of end-stage cerebral glioblastomas. *Neuro-Oncology*. (2020) 22:470–9. doi: 10.1093/neuonc/noz216

49. Vertosick FT Jr, Selker RG. Brain stem and spinal metastases of supratentorial glioblastoma multiforme: a clinical series. *Neurosurgery*. (1990) 27:516–22. doi: 10.1227/00006123-199010000-00002

50. Van Tellingen O, Yetkin-Arik B, de Gooijer MC, Wesseling P, Wurdinger T, de Vries HE. Overcoming the blood-brain tumor barrier for effective glioblastoma treatment. *Drug Resist Updat*. (2015) 19:1–12. doi: 10.1016/j.drup.2015.02.002

51. Lombardi G, De Salvo GL, Brandes AA, Eoli M, Rudà R, Faedi M, et al. Regorafenib compared with lomustine in patients with relapsed glioblastoma (REGOMA): a multicentre, open-label, randomised, controlled, phase 2 trial. *Lancet Oncol*. (2019) 20:110–9. doi: 10.1016/S1470-2045(18)30675-2

52. Kim MM, Umemura Y, Leung D. Bevacizumab and glioblastoma: past, present, and future directions. *Cancer J*. (2018) 24:180–6. doi: 10.1097/PPO.0000000000000326

53. Kaley T, Touat M, Subbiah V, Hollebecque A, Rodon J, Lockhart AC, et al. BRAF inhibition in BRAFV600-mutant gliomas: results from the VE-BASKET study. *J Clin Oncol*. (2018) 36:3477–84. doi: 10.1200/JCO.2018.78.9990

54. Wen PY, Stein A, van den Bent M, De Greve J, Wick A, de Vos F, et al. Dabrafenib plus trametinib in patients with BRAF(V600E)-mutant low-grade and high-grade glioma (ROAR): a multicentre, open-label, single-arm, phase 2, basket trial. *Lancet Oncol*. (2022) 23:53–64. doi: 10.1016/S1470-2045(21)00578-7

55. Wen PY, de Groot JF, Battiste J, Goldlust SA, Garner JS, Friend J, et al. Paxalisib in patients with newly diagnosed glioblastoma with unmethylated MGMT promoter status: final phase 2 study results. *J Clin Oncol*. (2022) 40:2047. doi: 10.1200/JCO.2022.40.16_suppl.2047

56. Szklener K, Mazurek M, Wieteska M, Wacławska M, Bilski M, Mańdziuk S. New directions in the therapy of glioblastoma. *Cancers (Basel)*. (2022) 14:5377. doi: 10.3390/cancers14215377

57. Minniti G, Niyazi M, Alongi F, Navarria P, Belka C. Current status and recent advances in reirradiation of glioblastoma. *Radiat Oncol*. (2021) 16:36. doi: 10.1186/s13014-021-01767-9

frontiers | Frontiers in Oncology

TYPE Original Research
PUBLISHED 25 October 2024
DOI 10.3389/fonc.2024.1333798

OPEN ACCESS

EDITED BY
Joubert Banjop Kharlyngdoh,
Tulane University, United States

REVIEWED BY
Jianping Chu,
The First Affiliated Hospital of Sun Yat-sen University, China
Nghi C. D. Truong,
University of Texas Southwestern Medical Center, United States

*CORRESPONDENCE
Xiaoyue Ma
maxiaoyue0822@163.com
Jingliang Cheng
fccchengjl@zzu.edu.cn
Zujun Hou
houzj@sibet.ac.cn

†These authors share first authorship

RECEIVED 08 January 2024
ACCEPTED 30 September 2024
PUBLISHED 25 October 2024

CITATION
Zhao K, Huang H, Gao E, Qi J, Chen T, Zhao G, Zhao G, Zhang Y, Wang P, Bai J, Zhang Y, Hou Z, Cheng J and Ma X (2024) Distributed parameter model of dynamic contrast-enhanced MRI in the identification of IDH mutation, 1p19q codeletion, and tumor cell proliferation in glioma patients. *Front. Oncol.* 14:1333798.
doi: 10.3389/fonc.2024.1333798

Distributed parameter model of dynamic contrast-enhanced MRI in the identification of IDH mutation, 1p19q codeletion, and tumor cell proliferation in glioma patients

Kai Zhao[1†], Huiyu Huang[1†], Eryuan Gao[1], Jinbo Qi[1], Ting Chen[1], Gaoyang Zhao[1], Guohua Zhao[1], Yu Zhang[1], Peipei Wang[1], Jie Bai[1], Yong Zhang[1], Zujun Hou[2*], Jingliang Cheng[1*] and Xiaoyue Ma[1*]

[1]Department of Magnetic Resonance Imaging, the First Affiliated Hospital of Zhengzhou University, Zhengzhou, China, [2]Jiangsu Key Laboratory of Medical Optics, Suzhou Institute of Biomedical Engineering and Technology, Chinese Academy of Sciences, Suzhou, China

Objectives: To investigate the clinical value of hemodynamic parameters derived from dynamic contrast-enhanced MRI (DCE-MRI) in predicting glioma genotypes including isocitrate dehydrogenase (*IDH*) mutation, *1p/19q* codeletion status and the tumor proliferation index (*Ki-67*) noninvasively. And to compare the diagnostic performance of parameters of distributed parameter (DP)model and extended Tofts (Ex-Tofts) model.

Materials and methods: Dynamic contrast-enhanced MRI (DCE-MRI) data of patients with glioma were prospectively enrolled from April 2021 to May 2023. The imaging data were analyzed using DP and Ex-Tofts model for evaluating the perfusion and permeability characteristics of glioma. Comparisons were performed according to *IDH* genotype in all glioma patients and *1p/19q* codeletion in *IDH* mutation glioma patients. Receiver operating characteristic (ROC) curves were generated for DCE-MRI parameters. The Spearman rank correlation coefficients were calculated between DCE MRI parameters and *Ki-67* index.

Results: In *IDH*-mutation gliomas, a higher blood flow (F) was found in *1p/19q* codeletion gliomas than in *1p/19q* intact gliomas. No parameter derived from Ex-Tofts model showed significant differences in predicting *1p/19q* status. Fractional volume of interstitial space (V_e) derived from both the DP and Ex-Tofts models exhibited optimal performance in predicting IDH genotype (AUC = 0.818, 0.828, respectively). V_e also showed the highest correlations with *Ki-67* LI within their

respective models in all gliomas (ρ = 0.62, 0.61), indicating comparable moderate positive associations. *Ki-67*

Conclusion: DP model showed a clear advantage in predicting *1p/19q* status compared to Ex-Tofts model. The DP and Ex-Tofts models performed similarly in predicting *IDH* mutation and *Ki-67* index.

KEYWORDS

glioma, dynamic contrast-enhanced MRI, distributed parameter model, IDH mutation, *1p/19q* codeletion, Ki-67

1 Introduction

Gliomas, being the most commonly occurring primary malignant brain tumors in adults (1), are classified by the 2021 version of the World Health Organization (WHO) into three groups based on two critical molecular markers: the isocitrate dehydrogenase (*IDH*) genotype and *1p/19q* codeletion status. The groups include *IDH* wild-type, *IDH* mutation with *1p/19q* intact, and *IDH* mutation with *1p/19q* codeletion (2). This new classification system applies to the glioma subtype, thus establishing a link between the grade of glioma and not just its natural disease progression but also the impact of clinical treatment on the course and prognosis of the disease. *Ki-67*, a nuclear antigen involved in cellular proliferation, represents a valuable biomarker for the evaluation of cell proliferation. An elevation in *Ki-67* labeling index (LI) indicates augmented tumor proliferation, which in turn correlates with inferior prognosis among glioma patients (3). Studies have demonstrated that certain genetic factors, including *IDH* mutation, *1p/19q* codeletion, and o6-methylguanine-DNA-methyltransferase (*MGMT*) promoter methylation, can predict treatment response, particularly in the context of chemotherapy (4, 5). Moreover, in recent years, additional treatment modalities, such as targeted therapy and radioimmunotherapy, have emerged and are currently under investigation in clinical trials (6, 7). These innovative approaches rely on the identification of specific molecular targets within glioma cells, highlighting the significance of genetic molecular diagnosis in guiding treatment decisions and identifying suitable targets for these therapies.

Therefore, the histological diagnosis and gene molecular diagnosis of glioma play a pivotal role in developing personalized preoperative treatment strategies, and have substantial implications in improving patients' quality of life and prognosis. Currently, histopathological analysis based on resection or biopsy is considered the most reliable means for molecular diagnosis of glioma genes (8). However, it is characterized by its high cost, demanding expertise, and the risk of sampling errors (9). Particularly in patients unsuitable for surgery, obtaining necessary pathological information without increasing patient burden and risk can maximize their benefits. Against this backdrop, many radiologists are actively exploring the relationship between imaging techniques and molecular biomarkers, aiming to predict molecular information non-invasively (10).

Dynamic contrast-enhanced magnetic resonance imaging (DCE-MRI) is a technique employed to assess blood-brain barrier (BBB) disruption and neovascularization in gliomas. These characteristics offer essential insights into the tumor microenvironment and metabolic properties of various glioma subtypes (11). Several recent reviews (12–14) have collectively concluded that while DCE imaging exhibits promising clinical application prospects in predicting *IDH* status, it lacks satisfactory performance in identifying *1p/19q* codeletion, and further research is still needed to investigate the use of DCE imaging in predicting *1p/19q* status. In DCE-MRI, mathematical models are employed to estimate pharmacokinetic parameters that provide insights into the perfusion and permeability of lesions. The accurate characterization of these parameters relies on an appropriate mathematical model. Presently, the extended Tofts (Ex-Tofts) model is widely used in DCE-MRI due to its relatively relaxed requirements for equipment and scan duration (15). However, the main parameter, transfer constant (K^{trans}), in Ex-Tofts model does not accurately reflect vascular permeability since it does not differentiate between the intravascular transport of tracer molecules and the exchange process of tracer molecules between the intravascular and interstitial spaces (16). As technology and equipment continue to advance, the distributed parameter (DP) model was proposed to addresses such limitation by separately considering the intravascular transport and the exchange between the intravascular and interstitial compartments (17). DP model incorporates two key parameters: blood flow (F), which characterizes intravascular transport, and the permeability-surface area product (PS), which describes the exchange process.

In this study, our objective was to evaluate the potential of DCE-MRI using the DP model in predicting the *IDH* genotype, chromosome *1p/19q* codeletion status, and *Ki-67* LI in adult diffuse gliomas, and to assess whether the DP model offers advantages in the molecular diagnosis of glioma, which may enhance their clinical management.

2 Materials and methods

This retrospective study was approved by our hospital's institutional review board, and informed consent was waived.

2.1 Study participants

Patients with glioma who underwent DCE examination between April 2021 and May 2023 were retrospectively collected. The inclusion criteria were as follows: DCE-MRI performed within two weeks prior to surgery and before the initiation of antitumor therapy, and a diagnosis of gliomas of grade 2-4 based on the 2021 WHO guideline on brain tumor classification following tumor resection and pathology examination. The exclusion criteria were: a diagnosis of WHO grade 1 glioma; inadequate MRI quality. The *IDH*1/2 mutations in the hotspot codons R132 and R172 on the excised surgical specimens were determined by Sanger sequencing or immunohistochemical staining. A mutation in any one of them was diagnosed as an *IDH* mutation. The *1p/19q* deletions were detected through fluorescence *in situ* hybridization analysis. The *Ki-67* labeling index was determined by using immunohistochemistry.

2.2 MR imaging acquisition

All scans were conducted using a 3.0 T MRI scanner from Siemens Healthcare (Magnetom Prisma). The DCE scan employed an axial fast-spoiled gradient (SPGR) echo sequence. This sequence included a pre-contrast and a post-contrast phase with the following parameters: TR/TE (3.03 ms/1.06 ms), FOV (230 × 230mm^2), matrix (192×134.4), slice thickness (5 mm), flip angles for the pre-contrast scan (3°, 6°, and 9°), and for the post-contrast scan (9°). For each flip angle, ten dynamic pre-contrast scans were acquired, while the post-contrast sequence consisted of 180 dynamic scans, with a temporal resolution of 2 seconds. The contrast agent used was Gadovist (Magnevist; Bayer Schering Pharma AG), administered at an injection rate of 3.5 mL/sec (followed by a 20 mL normal saline flush), with a dose of 0.1 mmol/kg body weight.

2.3 Image processing

DCE images were processed using a commercially software (MItalytics, FITPU Healthcare, Singapore). Two experienced neuroradiologists (K.Z. and X.M., with 3 and 11 years of experience, respectively) manually delineated the tumor region of interest (ROI) in reference to the late-phase dynamic T1-enhanced image (with obvious enhanced lesions) or the T2-FLAIR sequence images (without obvious enhanced lesions). The delineation includes the solid components of the tumor and avoids areas of necrosis, hemorrhage, calcification, large vessels, and cystic regions. Voxels in ROI were aggregated, and the median values of following kinetic parameters were calculated for each patient: Ex-Tofts model derived transfer constant K^{trans} (min^{-1}), fractional volume of extravascular extracellular space V_e (mL/100 mL), plasma fractional volume V_p (mL/100 mL), efflux rate constant K_{ep} (min^{-1}). DP model derived blood flow F (mL/min/100 mL), permeability-surface area product PS (mL/min/100 mL), extraction ratio of first pass E (%), V_e and V_p (same as in the Ex-Tofts model). To ensure completeness, the operational equations of these models, which specify the relationship between tissue tracer concentration $C_{tiss}(t)$ (as a function of time t) and AIF as well as relevant physiological parameters, are presented below:

Ex-Tofts model:

$$C_{tiss}(t) = AIF_{vp} + AIF \otimes K^{trans} \exp\left(-\frac{K^{trans}}{V_e} t\right) \quad (1)$$

DP model:

$$C_{tiss}(t) = AIF \otimes \left\{ F_p \left\{ \begin{array}{l} u(t) - u\left(t - \frac{v_p}{F_p}\right) + \\ u\left(t - \frac{v_p}{F_p}\right)\left\{1 - \exp\left(-\frac{PS}{F_p}\right)\left[1 + \int_0^{t-\frac{v_p}{F_p}} \exp\left(-\frac{PS}{v_e}\tau\right)\sqrt{\frac{PS}{v_e}\frac{1}{F_p}\tau}\, I_1\left(2\sqrt{\frac{PS}{v_e}\frac{PS}{F_p}\tau}\right) d\tau\right]\right\} \end{array} \right\} \right\} \quad (2)$$

2.4 Statistical analysis

Statistical analysis was performed using R software (version 4.3.1; https://www.R-project.org/). Normality of data and homogeneity of variance were assessed using Shapiro-Wilk and Levene's tests, respectively. Differences in parameters and mean age were evaluated between *IDH*-mutation and *IDH*-wild-type gliomas, as well as *IDH* mutation&*1p/19q* intact and *IDH* mutation&*1p/19q* codeletion gliomas using independent t-test or Mann–Whitney U test according to the results of test for normality and homoscedasticity. Benjamini-Hochberg correction was applied to adjust the *P* values of DCE parameters for multiple comparisons. The receiver operating characteristic (ROC) curves were utilized for assessing the performance of kinetic parameters in predicting *IDH* mutation and *1p/19q* status. The diagnostic performance was quantified using the area under the ROC curve (AUC). The DeLong test was conducted to compare the diagnostic performance of the Ex-Tofts model and the DP model by comparing their respective parameters with the largest AUC values in each model. The method of Youden index was utilized to determine the optimal threshold for classification and compute the corresponding sensitivity, specificity, and accuracy. Relationship between Ex-Tofts parameters, DP parameters and *Ki-67* LI was assessed using the Spearman correlation test. Statistical significance was set at $P< 0.05$.

3 Results

3.1 Patient characteristics

48 glioma patients were finally included in the study. Table 1 summarizes the clinical, demographic, and pathological characteristics of the patients. Based on the 2021 WHO classification of CNS tumors, the tumors were classified into *IDH*-mutation and *1p/19q* intact glioma (WHO grade 2 astrocytoma, n=3; WHO grade 3 astrocytoma, n=3;

TABLE 1 Clinical and demographic data of the study cohort.

	Male	Female	Age (years)	P Value of Sex	P Value of Age
IDH mutation	17	7	44 ± 9	0.079	0.004
IDH wild-type	11	13	53 ± 12		
IDH mutation&*1p/19q* intact	7	2	42 ± 10	0.144	0.346
IDH mutation&*1p/19q* codeleted	10	5	46 ± 9		

WHO grade 4 astrocytoma, n=3), *IDH*-mutation and *1p/19q* codeletion glioma (WHO grade 2 oligodendroglioma, n=7; WHO grade 3 oligodendroglioma, n=8), and *IDH*-wild-type glioma (WHO grade 4 glioblastoma, n=24). Patients with *IDH* wild-type glioma were found to be older than those with *IDH*-mutation glioma. There was no significant difference between glioma subtypes in terms of sex distribution.

3.2 Kinetic parameters in identification of molecular subtypes

As the distribution of all data did not meet the criteria for normality according to the Shapiro-Wilk test at a significance level of 5%, the Mann-Whitney U test was used to assess the differences between parameters. K_{ep} derived from Ex-Tofts model was found significantly higher in *IDH* mutation gliomas than in *IDH* wild-type gliomas. V_e, V_p derived from Ex-Tofts model and V_e, V_p, PS, E derived from DP model were found significantly lower in *IDH* mutation gliomas compared to *IDH* wild-type gliomas (Table 2). Only the F derived from DP model exhibited a significant difference between *1p/19q* codeleted glioma and *1p/19q* intact glioma, and the *1p/19q* codeleted glioma had a higher F value compared to the *1p/19q* intact glioma. No parameters in Ex-Tofts showed significant differences in predicting *1p/19q* status (Table 3). Representative cases of three different subtypes glioma are shown in Figure 1. Figure 2 shows the boxplots of Ex-Tofts and DP parameters,

TABLE 2 Results of kinetic parameters in predicting *IDH* genotype.

	IDH Mutation	*IDH* Wild-type	U	P
Ex-Tofts_ K^{trans}	0.014 (0.008,0.024)	0.022 (0.017,0.032)	201	0.149
Ex-Tofts_ V_e	0.633 (0.214,5.370)	6.825 (4.712,12.221)	99	< 0.001*
Ex-Tofts_ V_p	0.078 (0.026,0.473)	0.544 (0.444,0.831)	149	0.011*
Ex-Tofts_ K_{ep}	0.926 (0.466,5.069)	0.31 (0.254,0.446)	452	0.003*
DP_F	8.532 (6.569,10.002)	7.454 (6.308,13.777)	272	0.866
DP_ V_p	0.345 (0.206,0.590)	0.897 (0.600,1.508)	158	0.017*
DP_ V_e	0.415 (0.235,4.625)	6.739 (3.558,11.505)	105	< 0.001*
DP_PS	0.896 (0.356,2.241)	2.445 (1.769,3.527)	143	0.009*
DP_E	9.400 (3.092,20.535)	22.696 (12.670,30.283)	144	0.009*

*P< 0.05.

TABLE 3 Results of kinetic parameters in predicting *1p/19q* status.

	1p/19q intact	*1p/19q* codeleted	U	P
Ex-Tofts_ K^{trans}	0.014 (0.008,0.026)	0.014 (0.010,0.021)	68	> 0.99
Ex-Tofts_ V_e	0.217 (0.076,5.887)	0.643 (0.249,4.365)	83	0.669
Ex-Tofts_ V_p	0.053 (0.012,0.435)	0.093 (0.036,0.600)	81	0.669
Ex-Tofts_ K_{ep}	1.427 (0.503,5.400)	0.798 (0.397,4.298)	54	0.669
DP_F	6.607 (5.196,6.997)	8.963 (8.32,12.418)	107	0.040*
DP_ V_p	0.380 (0.149,0.542)	0.283 (0.215,0.679)	73	0.866
DP_ V_e	0.276 (0.182,4.969)	0.415 (0.247,3.201)	76	0.823
DP_PS	1.437 (0.281,2.257)	0.872 (0.457,1.245)	67	> 0.99
DP_E	20.057 (2.636,26.107)	8.728 (3.394,15.575)	59	0.823

*P< 0.05.

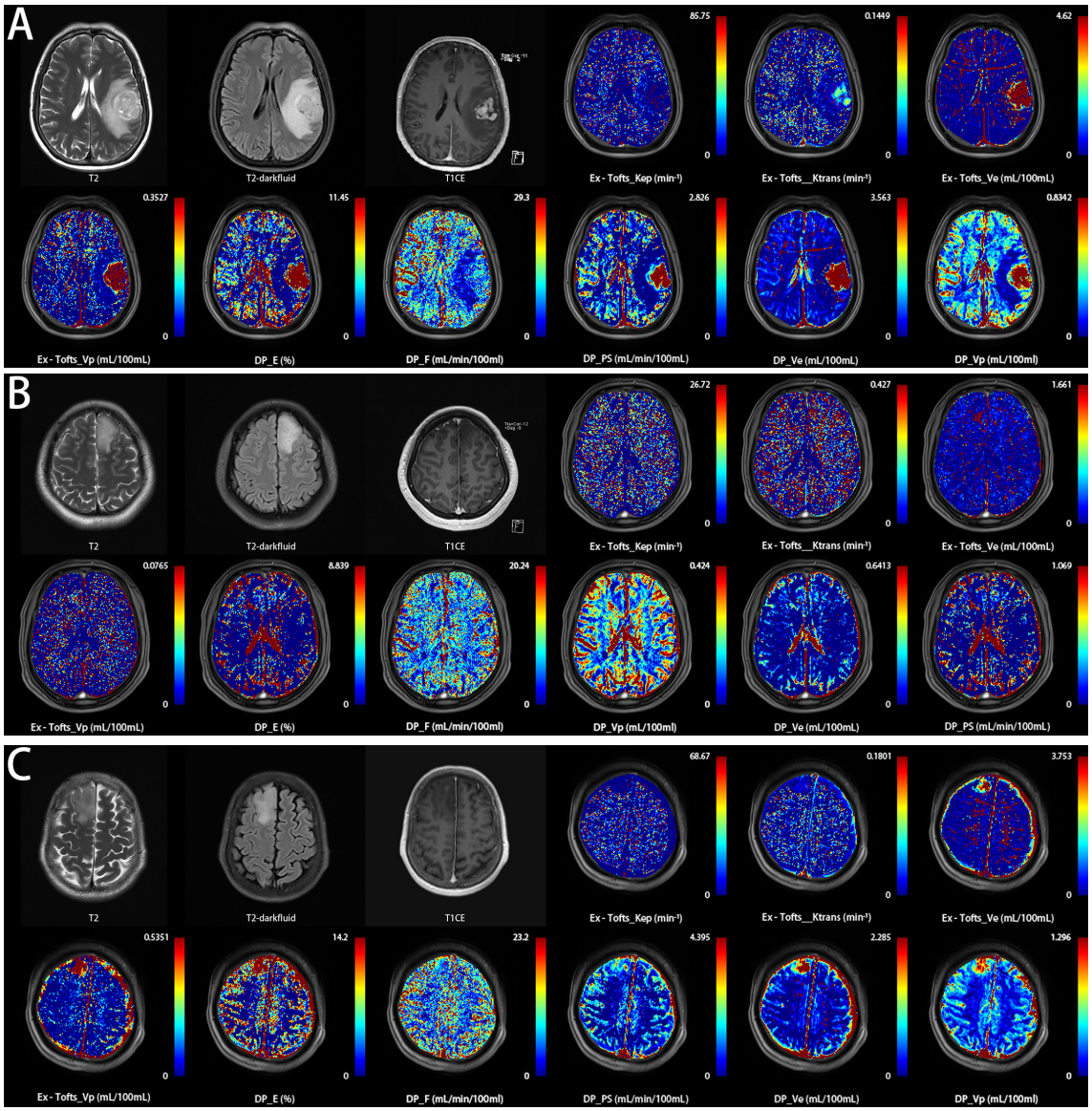

FIGURE 1
Three representative patients with glioma were correctly classified into their respective subtypes based on the threshold values of DCE parameters in this study, using pathological examination results as the gold standard. **(A)** a 59-year-old female with histologically proven glioblastoma IDH wild-type (Ex-Tofts_V_e = 16.08; DP_F = 9.21). **(B)** a 46-year-old male with histologically proven astrocytoma IDH mutation&*1p/19q* intact (Ex-Tofts_V_e = 0.08; DP_F = 7.00). **(C)** a 47-year-old female with histologically proven oligodendroglioma IDH mutation&*1p/19q* codeleted (Ex-Tofts_V_e = 1.34; DP_F = 8.82).

illustrating the intergroup differences in the distribution of kinetic parameters.

3.3 ROC curve analysis

Tables 4 and 5 respectively summarizes the results of ROC curve analysis in differentiating *IDH* mutation (mutation vs. wild-type) and *1p/19q* codeletion status in *IDH* mutation glioma (intact vs. codeleted). V_e attained the best performance in discriminating *IDH*-mutation from *IDH*-wild-type gliomas in both Ex-Tofts and DP model (AUC = 0.828 and 0.818, respectively). Delong test showed no significant difference between the AUCs of above two parameters (z = 0.509, P = 0.611). Among DP-derived parameters, F showed a good performance in predicting *1p/19q* status with AUC = 0.793. The plots of ROC curves are shown in Figure 3.

3.4 Correlation of kinetic parameters with the Ki–67 LI

The correlation results between the DCE parameters and *Ki-67* LI are shown in Figure 4. The corresponding P values are shown in the supplementary materials. V_e derived from DP model and the

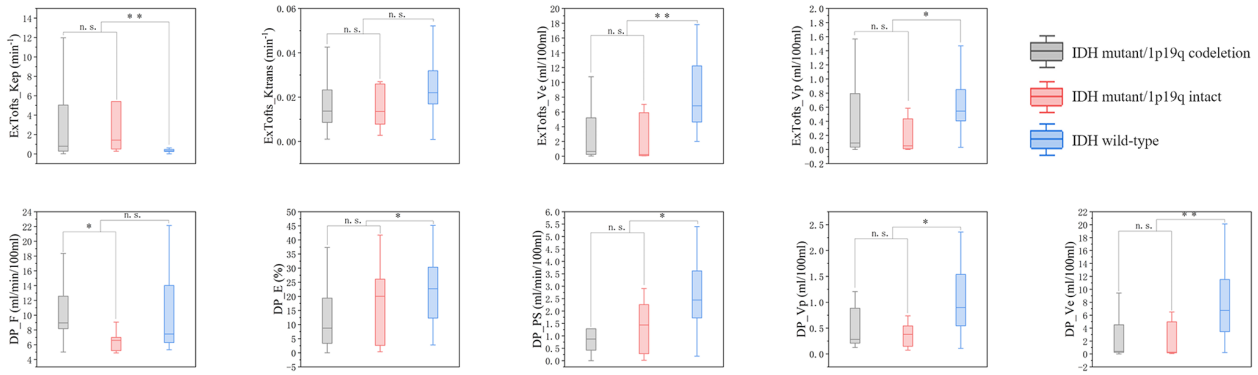

FIGURE 2
Boxplots of kinetic parameters in differentiating three types of gliomas, n.s. stands for not significant, *P< 0.05, **P< 0.01, ***P< 0.001.

Ex-Tofts model was correlated best with *Ki-67* LI within their respective models in all gliomas with similar moderate positive correlations (ρ = 0.62, 0.61).

4 Discussion

This study aimed to investigate the potential of pharmacokinetic parameters derived from the Ex-Tofts model and the DP model as biomarkers for identifying *IDH* mutation, *1p/19q* codeletion status, and tumor cell proliferation (*Ki-67* LI) in gliomas. The results of this study revealed that there was no significant difference in the diagnostic efficacy between the two models for predicting *IDH* mutation status and *Ki-67* expression. In predicting the *1p/19q* status, the DP model demonstrated a substantial increase in the parameter F and exhibited favorable diagnostic performance (AUC = 0.793), while the Ex-Tofts model did not effectively predict the *1p/19q* status. This suggests that the DP model holds greater potential than the Ex-Tofts model in predicting the *1p/19q* status with the exclusive perfusion parameter F.

The measurement of F in predicting the *1p/19q* status was made possible by the DP model, which separately describe intravascular perfusion and exchange between the intravascular and extravascular spaces. These processes are characterized by two distinct parameters, namely F and PS. Conversely, the Ex-Tofts model combines these two processes into a single parameter, K^{trans} (15). The use of appropriate pharmacokinetic models is crucial for the analysis of DCE-MRI data. Developing advanced pharmacokinetic models may be an important avenue to address the limitations of DCE in predicting *1p/19q* status. Higher F values observed in 2021 WHO oligodendrogliomas compared to astrocytomas may be related to their higher perfusion characteristics (18). An arterial spin labeling (ASL) study (19) has revealed that the cerebral blood flow (CBF) is significantly higher in oligodendrogliomas than astrocytomas, attributed to higher vascular density and gray matter involvement in oligodendrogliomas. Although CBF in ASL and F in DCE are not completely comparable, changes in this hemodynamic parameter indicate that the high perfusion characteristics of oligodendrogliomas can be used to predict the *1p/19q* status, which corroborates our results. Another study (20) as also highlighted the higher perfusion characteristics of oligodendrogliomas compared to astrocytomas, utilizing dynamic susceptibility contrast-enhanced (DSC) MRI. This study indicated that oligodendrogliomas revealed significantly higher cerebral

TABLE 4 ROC Analysis of kinetic parameters with significant difference in predicting *IDH* genotype.

	AUC (95%CI)	P	SEN	SPC	ACC	Cut-off
Ex-Tofts_ K^{trans}	0.651 (0.488, 0.814)	0.035	0.583	0.792	0.688	0.016
Ex-Tofts_ V_e	0.828 (0.706, 0.950)	< 0.001	0.667	1	0.833	1.670
Ex-Tofts_ V_p	0.741 (0.591, 0.891)	< 0.001	0.583	0.917	0.750	0.200
Ex-Tofts_ K_{ep}	0.785 (0.646, 0.923)	< 0.001	0.583	0.958	0.771	0.640
DP_F	0.472(0.302,0.642)	0.626	0.417	0.417	0.417	7.863
DP_ V_p	0.726 (0.574, 0.877)	0.002	0.750	0.750	0.750	0.600
DP_ V_e	0.818 (0.691, 0.945)	< 0.001	0.708	0.958	0.833	1.925
DP_PS	0.752 (0.608, 0.895)	< 0.001	0.708	0.792	0.750	1.535
DP_E	0.750 (0.609, 0.891)	< 0.001	0.500	0.958	0.729	8.805

10.3389/fonc.2024.1333798

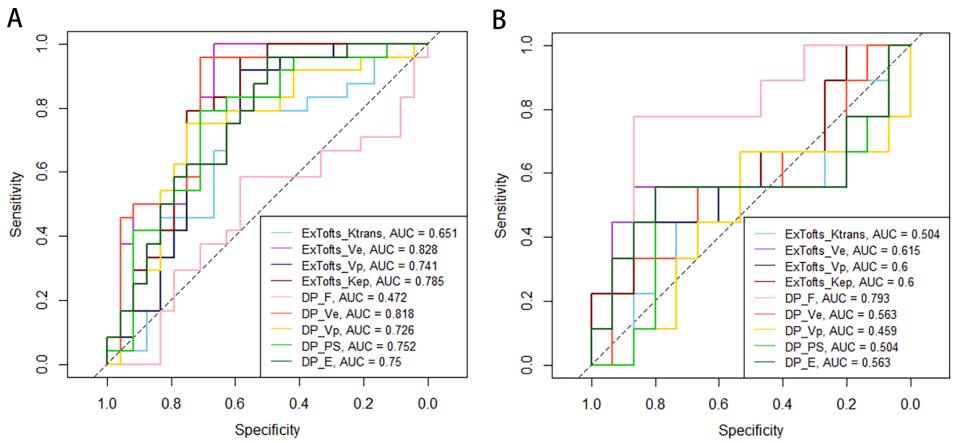

FIGURE 3
Receiver operating characteristic (ROC) plots and areas under ROC curve (AUCs) of Ex-Tofts and DP model parameters in differentiating of *IDH* mutation status **(A)** and *1p/19q* codeletion status **(B)**.

blood volume (CBV) when compared to astrocytomas. In DCE, the parameter V_p exhibits physiological similarity to CBV. V_p is a perfusion parameter that measures the fractional volume of the intravascular space and may be correlated with tissue microvascular density. Correlation analysis demonstrated that there was a relatively weak positive correlation between V_p and F (ρ = 0.56). This indicates that while both parameters represent tissue perfusion, they also possess a certain degree of independence from each other, suggesting that they characterize different aspects of tumor perfusion. Our results failed to found any significant difference in V_p between astrocytomas and oligodendrogliomas, which is consistent with Gupta's (21) conclusion. However, Lee et al. (22) have found a significant increase in V_p in oligodendrogliomas. Currently, there is limited literature on the use of perfusion imaging for identifying *1p/19q* codeletion status in gliomas, and most studies focus on DSC-MRI

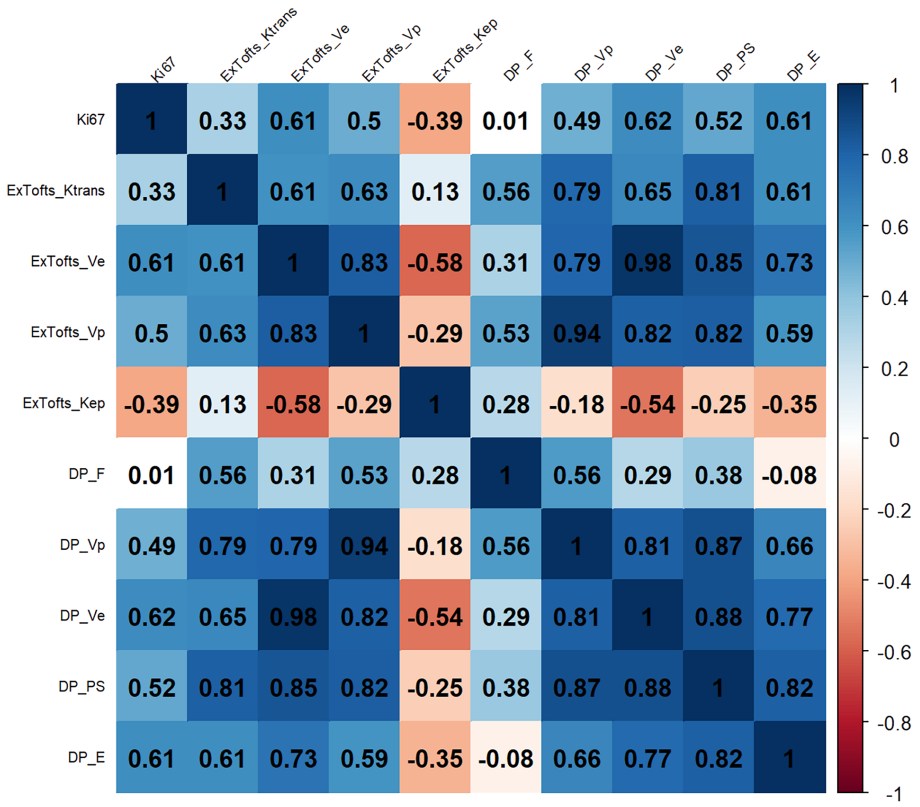

FIGURE 4
Heat map of correlations between the DCE parameters and *Ki-67* index.

10.3389/fonc.2024.1333798

TABLE 5 ROC Analysis of kinetic parameters with significant difference in predicting *1p/19q* status.

	AUC (95%CI)	P	SEN	SPC	ACC	Cut-off
Ex-Tofts_ K^{trans}	0.504(0.245,0.762)	0.489	0.733	0.333	0.583	0.010
Ex-Tofts_ V_e	0.615(0.344,0.885)	0.203	0.867	0.556	0.75	0.222
Ex-Tofts_ V_p	0.600(0.342,0.858)	0.223	0.867	0.444	0.708	0.022
Ex-Tofts_ K_{ep}	0.600(0.350,0.850)	0.216	0.667	0.556	0.625	1.342
DP_F	0.793 (0.595, 0.99)	0.002	0.867	0.778	0.833	7.154
DP_ V_p	0.459(0.194,0.724)	0.618	0.467	0.333	0.417	0.296
DP_ V_e	0.563(0.303,0.823)	0.318	0.933	0.333	0.708	0.197
DP_PS	0.504(0.226,0.782)	0.490	0.200	0.444	0.292	1.363
DP_E	0.563(0.274,0.851)	0.334	0.800	0.556	0.708	19.717

(12). The role of DCE in predicting *1p/19q* codeletion status remains controversial, and selecting appropriate pharmacokinetic models may be crucial for improving its clinical utility. Our study suggested one of the limitations of the Ex-Tofts model in characterizing perfusion is its inability to describe tissue blood flow velocity, thus necessitating the development of advanced pharmacokinetic models that factor in the transport of contrast agent molecules within the vasculature.

In predicting the *IDH* genotype, both Ex-Tofts and DP models have existing research (23, 24), and our findings regarding the comparison of parameter magnitudes align with previous studies. We identified V_e as the most distinguishing feature in discriminating between *IDH*-mutation and *IDH*-wild-type gliomas. V_e refers to the fractional volume of the extravascular extracellular space. As tumor cells proliferate excessively, the interstitial space decreases, resulting in a smaller V_e. Compared to *IDH* wild-type, *IDH* mutation could inhibit proliferation in glioma (25). However, unlike other solid tumors (16), a decrease in V_e suggests elevated vessel permeability rather than higher cell proliferation. The blood-brain barrier restricts the leakage of contrast agent molecules from the vasculature, leading to smaller measured V_e values. In *IDH* wild-type gliomas, we observed a significant increase in V_e, indicating a greater tendency for contrast agent molecules to leak out. This can be attributed to the presence of newly formed immature blood vessels in *IDH* wild-type gliomas, along with the irregular arrangement of endothelial cells and detachment of pericytes and astrocytes from microvascular walls (26), which increase the permeability of the blood-brain barrier and promote microvascular leakage. Conversely, *IDH*-mutation gliomas have been shown to exhibit decreased activation of hypoxia-inducible factor 1α (HIF-1α), leading to a reduction in hypoxia-induced angiogenesis (27). DCE-MRI can indirectly predict these genetic alterations by describing changes in tissue permeability.

Ki-67 LI showed the highest correlation coefficient with V_e of DP model among the DCE parameters with a moderate positive correlation observed ($\rho = 0.62$). The positive correlation between V_e and *Ki-67* may be related to the compromised integrity of the blood-brain barrier. The elevated proliferative activity of tumor cells requires a substantial amount of energy to sustain their rapid growth and division. In response to this increased energy demand, tumors activate various adaptive mechanisms, including the upregulation of HIF-1α, leading to an increase in tumor angiogenesis and a more abundant tumor microcirculation (28). The presence of newly formed and immature blood vessels increases tumor vascular permeability, facilitating the extravasation of contrast agents and subsequently resulting in elevated V_e values. This finding is consistent with Jiang et al. (29). However, we were unable to confirm a significant correlation between K^{trans} and *Ki-67*, as they did. This discrepancy may be due to the fact that Jiang et al. measured the maximum values of tumor hemodynamic parameters, while we focused on the median values within the ROI. In future studies, we may consider employing histogram analysis of DCE data to further explore this correlation.

Several limitations should be acknowledged in our study. Firstly, the sample size was relatively small, potentially introducing chance correlations when predicting *1p/19q* status, and the single-center design mean that the thresholds we identified may not be generalizable to other centers, limiting their applicability. Therefore, a prospective study with a larger sample size and multi-center is warranted to validate these findings. Secondly, the ROI delineation in our study was manually performed, and the adoption of machine learning algorithms for automated delineation holds promise in improving the objectivity of our research. Lastly, due to the update of the 2021 WHO CNS glioma classification, glioma grading is now categorized within pathological subtypes. The sample size in our study cohort was insufficient to conduct predictive research on glioma grading. We plan to further expand the sample size to explore the role of various DCE models in predicting glioma grading in future research.

5 Conclusion

DP model provided additional information on blood flow rate compared to the Ex-Tofts model, and it demonstrated a clear

advantage in predicting *1p/19q* status. However, it did not show a significant difference in predicting *IDH* and *Ki-67* compared to the Ex-Tofts model.

Data availability statement

The original contributions presented in the study are included in the article/supplementary material. Further inquiries can be addressed to the corresponding author.

Ethics statement

The studies involving humans were approved by Ethics Committee of the First Affiliated Hospital of Zhengzhou University. The studies were conducted in accordance with the local legislation and institutional requirements. The participants provided their written informed consent to participate in this study.

Author contributions

KZ: Writing – original draft, Writing – review & editing. HH: Writing – original draft. EG: Writing – original draft. JQ: Writing – original draft. TC: Writing – original draft. GYZ: Writing – original draft. GZ: Writing – original draft. YuZ: Writing – original draft. PW: Writing – original draft. JB: Writing – review & editing. YoZ: Writing – review & editing. ZH: Writing – review & editing. JC: Writing – review & editing. XM: Writing – review & editing.

Funding

The author(s) declare financial support was received for the research, authorship, and/or publication of this article. This study has received funding from the Youth Project of Henan Medical Science and Technology Research Project (grant numbers SBGJ202103078).

Conflict of interest

The authors declare that the research was conducted in the absence of any commercial or financial relationships that could be construed as a potential conflict of interest.

Publisher's note

Supplementary material

The Supplementary Material for this article can be found online at: https://www.frontiersin.org/articles/10.3389/fonc.2024.1333798/full#supplementary-material

References

1. Weller M, van den Bent M, Preusser M, Le Rhun E, Tonn JC, Minniti G, et al. EANO guidelines on the diagnosis and treatment of diffuse gliomas of adulthood. *Nat Rev Clin Oncol*. (2021) 18:170–86. doi: 10.1038/s41571-020-00447-z

2. Louis DN, Perry A, Wesseling P, Brat DJ, Cree IA, Figarella-Branger D, et al. The 2021 WHO classification of tumors of the central nervous system: a summary. *Neuro Oncol*. (2021) 23:1231–51. doi: 10.1093/neuonc/noab106

3. Xing Z, Huang W, Su Y, Yang X, Zhou X, Cao D. Non-invasive prediction of p53 and Ki-67 labelling indices and O-6-methylguanine-DNA methyltransferase promoter methylation status in adult patients with isocitrate dehydrogenase wild-type glioblastomas using diffusion-weighted imaging and dynamic susceptibility contrast-enhanced perfusion-weighted imaging combined with conventional MRI. *Clin Radiol*. (2022) 77:e576–e84. doi: 10.1016/j.crad.2022.03.015

4. Weller M, Tabatabai G, Kastner B, Felsberg J, Steinbach JP, Wick A, et al. MGMT promoter methylation is a strong prognostic biomarker for benefit from dose-intensified temozolomide rechallenge in progressive glioblastoma: the DIRECTOR trial. *Clin Cancer Res*. (2015) 21:2057–64. doi: 10.1158/1078-0432.CCR-14-2737

5. Cairncross G, Wang M, Shaw E, Jenkins R, Brachman D, Buckner J, et al. Phase III trial of chemoradiotherapy for anaplastic oligodendroglioma: long-term results of RTOG 9402. *J Clin Oncol*. (2013) 31:337–43. doi: 10.1200/JCO.2012.43.2674

6. Mellinghoff IK, Ellingson BM, Touat M, Maher E, de la Fuente MI, Holdhoff M, et al. Ivosidenib in isocitrate dehydrogenase 1-mutated advanced glioma. *J Clin Oncol*. (2020) 38:3398–406. doi: 10.1200/JCO.19.03327

7. Karpel-Massler G, Nguyen TTT, Shang E, Siegelin MD. Novel IDH1-targeted glioma therapies. *CNS Drugs*. (2019) 33:1155–66. doi: 10.1007/s40263-019-00684-6

8. Tanboon J, Williams EA, Louis DN. The diagnostic use of immunohistochemical surrogates for signature molecular genetic alterations in gliomas. *J Neuropathol Exp Neurol*. (2016) 75:4–18. doi: 10.1093/jnen/nlv009

9. Jackson RJ, Fuller GN, Abi-Said D, Lang FF, Gokaslan ZL, Shi WM, et al. Limitations of stereotactic biopsy in the initial management of gliomas. *Neuro Oncol*. (2001) 3:193–200. doi: 10.1093/neuonc/3.3.193

10. Lu J, Li X, Li H. Perfusion parameters derived from MRI for preoperative prediction of IDH mutation and MGMT promoter methylation status in glioblastomas. *Magn Reson Imaging*. (2021) 83:189–95. doi: 10.1016/j.mri.2021.09.005

11. Arzanforoosh F, van der Voort SR, Incekara F, Vincent A, Van den Bent M, Kros JM, et al. Microvasculature features derived from hybrid EPI MRI in non-enhancing adult-type diffuse glioma subtypes. *Cancers (Basel)*. (2023) 15(7):2135. doi: 10.3390/cancers15072135

12. Siakallis L, Topriceanu CC, Panovska-Griffiths J, Bisdas S. The role of DSC MR perfusion in predicting IDH mutation and 1p19q codeletion status in gliomas: meta-analysis and technical considerations. *Neuroradiology*. (2023) 65:1111–26. doi: 10.1007/s00234-023-03154-5

13. Stumpo V, Guida L, Bellomo J, Van Niftrik CHB, Sebok M, Berhouma M, et al. Hemodynamic imaging in cerebral diffuse glioma-part B: molecular correlates, treatment effect monitoring, prognosis, and future directions. *Cancers (Basel)*. (2022) 14(5):1342. doi: 10.3390/cancers14051342

14. van Santwijk L, Kouwenberg V, Meijer F, Smits M, Henssen D. A systematic review and meta-analysis on the differentiation of glioma grade and mutational status by use of perfusion-based magnetic resonance imaging. *Insights Imaging*. (2022) 13:102. doi: 10.1186/s13244-022-01230-7

15. Sourbron SP, Buckley DL. Classic models for dynamic contrast-enhanced MRI. *NMR Biomed*. (2013) 26:1004–27. doi: 10.1002/nbm.2940

16. Wang X, Li S, Lin X, Lu Y, Mao C, Ye Z, et al. Evaluation of tracer kinetic parameters in cervical cancer using dynamic contrast-enhanced MRI as biomarkers in terms of biological relevance, diagnostic performance and inter-center variability. *Front Oncol*. (2022) 12:958219. doi: 10.3389/fonc.2022.958219

17. Koh TS, Cheong LH, Tan CK, Lim CC. A distributed parameter model of cerebral blood-tissue exchange with account of capillary transit time distribution. *Neuroimage*. (2006) 30:426–35. doi: 10.1016/j.neuroimage.2005.09.032

18. Yamashita K, Togao O, Kikuchi K, Kuga D, Sangatsuda Y, Fujioka Y, et al. The cortical high-flow sign of oligodendroglioma, IDH-mutant and 1p/19q-codeleted: comparison between arterial spin labeling and dynamic susceptibility contrast methods. *Neuroradiology*. (2024) 66:187–92. doi: 10.1007/s00234-023-03267-x

19. Brendle C, Hempel JM, Schittenhelm J, Skardelly M, Tabatabai G, Bender B, et al. Glioma grading and determination of IDH mutation status and ATRX loss by DCE and ASL perfusion. *Clin Neuroradiol*. (2018) 28:421–8. doi: 10.1007/s00062-017-0590-z

20. Latysheva A, Emblem KE, Brandal P, Vik-Mo EO, Pahnke J, Roysland K, et al. Dynamic susceptibility contrast and diffusion MR imaging identify oligodendroglioma as defined by the 2016 WHO classification for brain tumors: histogram analysis approach. *Neuroradiology*. (2019) 61:545–55. doi: 10.1007/s00234-019-02173-5

21. Gupta M, Gupta A, Yadav V, Parvaze SP, Singh A, Saini J, et al. Comparative evaluation of intracranial oligodendroglioma and astrocytoma of similar grades using conventional and T1-weighted DCE-MRI. *Neuroradiology*. (2021) 63:1227–39. doi: 10.1007/s00234-021-02636-8

22. Lee JY, Ahn KJ, Lee YS, Jang JH, Jung SL, Kim BS. Differentiation of grade II and III oligodendrogliomas from grade II and III astrocytomas: a histogram analysis of perfusion parameters derived from dynamic contrast-enhanced (DCE) and dynamic susceptibility contrast (DSC) MRI. *Acta Radiol*. (2018) 59:723–31. doi: 10.1177/0284185117728981

23. Li Z, Zhao W, He B, Koh TS, Li Y, Zeng Y, et al. Application of distributed parameter model to assessment of glioma IDH mutation status by dynamic contrast-enhanced magnetic resonance imaging. *Contrast Media Mol Imaging*. (2020) 2020:8843084. doi: 10.1155/2020/8843084

24. Zhang HW, Lyu GW, He WJ, Lei Y, Lin F, Wang MZ, et al. DSC and DCE histogram analyses of glioma biomarkers, including IDH, MGMT, and TERT, on differentiation and survival. *Acad Radiol*. (2020) 27:e263–e71. doi: 10.1016/j.acra.2019.12.010

25. Gao A, Zhang H, Yan X, Wang S, Chen Q, Gao E, et al. Whole-tumor histogram analysis of multiple diffusion metrics for glioma genotyping. *Radiology*. (2022) 302:652–61. doi: 10.1148/radiol.210820

26. Guo H, Kang H, Tong H, Du X, Liu H, Tan Y, et al. Microvascular characteristics of lower-grade diffuse gliomas: investigating vessel size imaging for differentiating grades and subtypes. *Eur Radiol*. (2019) 29:1893–902. doi: 10.1007/s00330-018-5738-y

27. Kickingereder P, Sahm F, Radbruch A, Wick W, Heiland S, Deimling A, et al. IDH mutation status is associated with a distinct hypoxia/angiogenesis transcriptome signature which is non-invasively predictable with rCBV imaging in human glioma. *Sci Rep*. (2015) 5:16238. doi: 10.1038/srep16238

28. Shin JK, Kim JY. Dynamic contrast-enhanced and diffusion-weighted MRI of estrogen receptor-positive invasive breast cancers: Associations between quantitative MR parameters and Ki-67 proliferation status. *J Magn Reson Imaging*. (2017) 45:94–102. doi: 10.1002/jmri.25348

29. Jiang JS, Hua Y, Zhou XJ, Shen DD, Shi JL, Ge M, et al. Quantitative assessment of tumor cell proliferation in brain gliomas with dynamic contrast-enhanced MRI. *Acad Radiol*. (2019) 26:1215–21. doi: 10.1016/j.acra.2018.10.012

frontiers | Frontiers in Oncology

TYPE Case Report
PUBLISHED 27 November 2024
DOI 10.3389/fonc.2024.1464362

OPEN ACCESS

EDITED BY
Tanmay Abhay Kulkarni,
Mayo Clinic, United States

REVIEWED BY
Ruth Prieto,
Puerta de Hierro University Hospital Majadahonda, Spain
Alpana Mukhuty,
University of Burdwan, India

*CORRESPONDENCE
Paul Hanona
paulhano63@gmail.com

RECEIVED 13 July 2024
ACCEPTED 21 October 2024
PUBLISHED 27 November 2024

CITATION
Hanona P, Ezekwudo D and Anderson J (2024) Clinical response to dabrafenib plus trametinib in BRAF V600E mutated papillary craniopharyngiomas: a case report and literature review.
Front. Oncol. 14:1464362.
doi: 10.3389/fonc.2024.1464362

Clinical response to dabrafenib plus trametinib in BRAF V600E mutated papillary craniopharyngiomas: a case report and literature review

Paul Hanona*, Daniel Ezekwudo and Joseph Anderson

Beaumont Hospital, Beaumont Health, Royal Oak, MI, United States

Papillary craniopharyngiomas are rare tumors prevalent to the precision oncology world due to their high rate of BRAF V600E mutations. Symptoms include vision loss, neuroendocrine dysfunction, and cognitive dysfunction. Treatment involves an interdisciplinary approach with surgery, radiation, and systemic treatment. Recent attention has been directed toward targeted therapy in this space, especially with targets to the BRAF V600E mutated pathway. Focusing on this pathway could solidify future standards of care treatment. A 61-year-old male came in with bilateral homonymous hemianopsia. This prompted a brain MRI that showed a bilobed centrally cystic peripherally enhancing sellar and suprasellar mass with mass effect on the left greater than right optic chiasm and nerves. He underwent a primary resection of the suprasellar cystic tumor, and it was revealed that he had papillary craniopharyngioma. Three months later, he represented with visual defects, and repeat MRI showed cystic recurrence with compression of the optic chiasm. He underwent an endonasal resection of the middle fossa tumor; pathology, this time, showed a BRAF V600E mutated papillary craniopharyngioma. Nine months later, another recurrence happened, and the patient was started on BRAF and MEK inhibitors: dabrafenib (75 mg BID) and trametinib (2 mg daily). The patient has had clinical improvement of visual symptoms and is currently continuing this treatment. He was last seen in October of 2024, and he is clinically stable. The use of targeted therapies is an evolving space for BRAF V600E mutated papillary craniopharyngiomas. This is a case showing improvement of a craniopharyngioma after treatment with BRAF and MEK inhibitor combinations. The role of BRAF and MEK inhibitor combinations continues to evolve in this space.

KEYWORDS

papillary, craniopharyngioma, BRAF mutation V600E, dabrafenib, trametinib

Introduction

Craniopharyngiomas are slow-growing brain tumors that originate from Rathke's pouch remnants. They are incredibly rare with only 350 cases a year in the United States (1). They have a bimodal age distribution and occur equally in both men and women (2). They can arise near the pituitary stalk, within the sella, the third ventricle, and optic chiasm (3). Tumor topography, especially in regards to its relationship with the hypothalamus, can indicate tumor recurrence rates (4). They break down into two types, either adamantinomatous or papillary. Adamantinomatous types have mutations in CTNNB1, while papillary types have mutations in BRAF. Both types are overwhelmingly mutated with 96% of adamantinomatous types having CTNNB1 mutations and 94% of papillary types having BRAF V600E mutations. They have similar overall survival. The 10-year overall survival ranges between 80% and 96% (5).

Symptoms are challenging to identify due to the slow-growing nature of craniopharyngiomas. The most common symptoms include headaches, visual field deficits, endocrine alternations, and mental distrubances (6). Diagnosis involves MRI of the brain and or CT of the brain. A mass is usually seen that compresses nearby structures.

Calcifications are often seen (7). Endocrine testing for abnormalities in pituitary hormones is also crucial (6).

Treatment has traditionally involved surgery and radiation, with a more recent addition of targeted therapy. Neuroimaging alone can suggest BRAF mutant papillary types with a representative feature like lack of calcification. In these cases, biopsy, instead of aggressive surgery, is preferred, and the patient can be put on first-line targeted therapy with BRAF/MEK inhibitors. If neuroimaging suggests an adamantinomatous types, aggressive resection is preferred due to mass effect causing symptoms commonly being the presenting sign (8). Monitoring of endocrine function, edema, and hydrocephalus is also crucial during this period.

Targeted therapy is a fundamental tenet in the treatment of papillary craniopharyngiomas. All papillary craniopharyngiomas should be tested for BRAF V600E. Surgical resection of the tumor is the gold standard. First-line treatment of newly diagnosed craniopharyngiomas after resection is BRAF/MEK inhibition. This involves four to six cycles of targeted therapy and then reassessment for the need for RT, surgery, or continued therapy with BRAF/MEK inhibition. These agents usually include dabrafenib plus trametinib or vemurafenib plus cobimetinib (9). This is an ongoing area of research. This case report seeks to add to the literature that shows clinical improvement of craniopharyngiomas with BRAF/MEK inhibition.

Case description

This is a case of a 61-year-old male who first presented with changes in his vision in May 2022. A summary timeline of the patient's case can be found in Table 1. He has a history of hypertension, sarcoidosis, prediabetes, and sinus bradycardia. He had no surgeries up until this point. He is a never smoker and a never drinker. He had no relevant family history. Physical exam signs were largely remarkable for bilateral homonymous hemianopsia. Examination revealed visual acuity of 20/25 + 2 in the right eye and 20/200 + 1 with pinhole to 20/80–2 in the left eye. Brain MRI showed a bilobed centrally cystic peripherally enhancing sellar and suprasellar mass with mass effect on the left greater than right optic chiasm and nerves. He underwent an endonasal resection of the middle fossa tumor. Pathological results were indeterminant. His vision improved following his surgery.

In August 2022, the patient presented again with visual deficits. Repeat MRI showed a 10.3 mm × 14.6 mm × 17 mm cystic mass in the suprasellar area with enhancing mural nodules, most likely related to craniopharyngioma that is causing mass effect on the optic chiasma (Figures 1, 2). He underwent an endoscopic endonasal transplanum transtuberculum approach to the middle fossa skull base with a resection of the middle cranial fossa skull base tumor. Pathology revealed papillary craniopharyngioma, CNS WHO grade 1. BRAF V600E mutation was identified. Subsequently, a CSF leak was present, and he underwent a CSF leak repair. He followed up with the surgical team who monitored for symptoms of clinical relapse. Importantly, the patient never went for radiation.

Eight months after this second surgery, he had his first visit with an oncologist in June 2023. He again was having visual deficits, and he had an MRI that showed recurrence of the craniopharyngioma. At the time, it felt too risky to go back for a third neurosurgical resection; thus, a joint decision was made to have the patient undergo trial on targeted therapy with dabrafenib and trametinib. He started on dabrafenib 150 mg twice daily and trametinib 2 mg once daily. The plan was to keep him on this targeted therapy until progression. One month later, his vision improved, but his symptoms had not completely resolved. He did develop myalgia

FIGURE 1
Sagittal brain MRI showing a 10.3 mm × 14.6 mm × 17 mm cystic mass in the suprasellar area with enhancing mural nodules, most likely related to craniopharyngioma, causing mass effect on the optic chiasma.

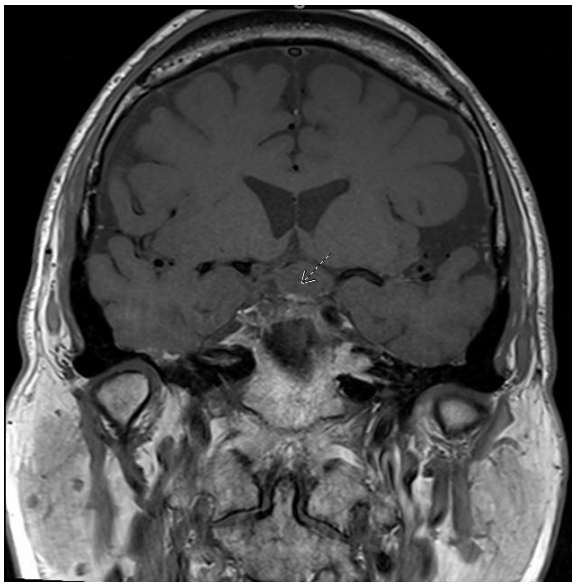

FIGURE 2
MRI coronal-transinfundibular showing a cystic mass (white arrow) in the suprasellar area with enhancing mural nodules, most likely related to craniopharyngioma, causing mass effect on the optic chiasma.

and fatigue while on targeted therapy, but otherwise, he was tolerating the therapy well. A follow up visit in August 2023 showed that his visual symptoms had gotten worse in the right eye. A brain MRI at that time was repeated and showed growth in the suprasellar region with a cystic mass (Figure 3). Thus, he underwent a third neurosurgical revision with an endonasal resection of the tumor. His vision again improved almost back to normal after this third surgery. After recovery from his surgery, the patient resumed targeted therapy with dabrafenib and trametinib. Since his third surgery, he has been back on dabrafenib and trametinib. He complains of fatigue but, otherwise, is tolerating the combination well. He continues to take these medications and follows with an oncologist regularly. Recently, as of June 2024, he was working with a physical therapist for an unrelated lumbar radiculopathy. Otherwise, the patient is faring well.

FIGURE 3
Brain MRI in August 2023 showing a suprasellar cystic brain mass consistent with a craniopharyngioma.

Discussion

Craniopharyngiomas are tumors that arise along the craniopharyngeal duct. Two key mutations in the CTNNB1 and BRAF V600E mutations lead to two different histological types being the adamantinomatous and papillary types, respectively. Symptoms include visual impairment, endocrine deficiencies, and other neurological abnormalities. MRI is proven to be one of the gold diagnostic standards for craniopharyngiomas. Treatment involves neurosurgery, radiotherapy, and now an evolving role for targeted treatment. Long-term survival is common; however, quality of life continues to be a challenge with common side effects of treatment including fatigue and psychosocial deficits (10). Patients commonly complain about reduction in social and emotional functioning citing that their psychosocial status is worse than their physical health. This includes patients going through anxiety, depression, and withdrawal. Patients also complained of reduced mobility (11).

The first step of the BRAF/MEK pathway involves a growth factor binding to a cell receptor. This activates the RAS protein, which activates the BRAF protein. This active BRAF protein phosphorylates and activates the MEK protein, and activated MEK protein phosphorylates and activates the ERK protein. ERK then moves into the nucleus and activates genes that help cells proliferate. When the BRAF gene is mutated, a mutated BRAF protein results. This mutated BRAF protein is constitutively activated leading to uncontrolled cell growth per the mechanism just described (12). Drugs, like dabrafenib and vemurafenib, target this mutated BRAF protein. To avoid resistance, a drug targeting the downstream MEK protein like trametinib is also given. Currently, dabrafenib is approved for mutated BRAF V600E melanomas, non-small cell lung cancers, solid tumors that are unresectable or metastatic, and thyroid cancers (13). Trametinib has the same approvals as dabrafenib, except with the addition of ovarian carcinoma (14).

Treatments utilizing surgery and radiation both have substantial morbidity. Keeping in mind that the overwhelming majority of papillary craniopharyngioma carry a BRAF V600E mutation, efforts are made to target this pathway. New approaches with targeted therapy are being investigated. The CTNNB1 mutation pathway has no current targeted treatment. However, the BRAF V600E mutation can be either targeted with dabrafenib and trametinib or vemurafenib and cobimetinib. Our patient was treated with dabrafenib and trametinib. Several case reports suggest efficacy with dabrafenib and trametinib. One case report of a 39-year old showed that the tumor volume was reduced by 85% after only 35 days (15). Another case report also showed marked tumor reduction and even improvement in the patient's panhypopituitarism (16). A publication shows that a 35-year-old man also had his tumor reduced in size by 95% over 21 months without any side effects (17). One patient had a complete response over 2 years (18). Patients can also be kept on this treatment for

TABLE 1 Timeline of patient's clinical history.

Date	Clinical	Radiological	Treatment
May 2022	Bilateral hemianopsia	Brain MRI showing a suprasellar mass	Endoscopic resection of craniopharyngioma with pathology being indeterminant
September 2022	Bilateral hemianopsia	Brain MRI showing a mass resembling a craniopharyngioma	Endoscopic resection of craniopharyngioma with pathology showing papillary craniopharyngioma, CNS WHO grade 1 with a BRAF V600E mutation
June 2023	Bilateral hemianopsia	Brain MRI showing recurrence of the craniopharyngioma	Patient is started on dabrafenib and trametinib
August 2023	Bilateral hemianopsia worsening	Brain MRI showing slight increase in the size of the craniopharyngioma	Third revision endonasal resection with residual mass remaining
September 2023	Stable bilateral hemianopsia	Not available	Resumed dabrafenib and trametinib
October 2024	Stable bilateral hemianopsia	Not available	Continuing dabrafenib and trametinib

more than 2 years especially since one case report showed that the patient continued to have clinical improvement 2 years after starting the dabrafenib and trametinib (19).

Since the tumors are benign in nature, targeting them with surgery and radiation can often lead to more morbidity than necessary. A summary of various studies pertaining to treatment of BRAF mutated craniopharyngiomas can be found in Table 2. If there was a way to introduce targeted treatment with BRAF and MEK inhibitors early on as neoadjuvant treatment, that could potentially reduce the morbidity from ensuing surgery and radiation (20). One case report showed that a 39-year old with a BRAF V600E mutated craniopharyngioma first received neoadjuvant dabrafenib and trametinib, then received definitive radiosurgery. The authors theorize that neoadjuvant targeted treatment could take patients who are poor surgical candidates and turn them into a better surgical candidate if the original tumor size shrinks (21).

Data are stronger regarding the vemurafenib and cobimetinib combination. A recent phase 2 study was done with 16 patients who had BRAF V600E mutations. BRAF/MEK inhibitor combination with vemurafenib and cobimetinib was administered in 28-day cycles. Fifteen out of those 16 patients had a durable objective partial response or better. The median reduction of tumor was 91%. Progression-free survival at 12 months was 87% and at 24 months 58%. The median number of cycles was eight cycles. Notable adverse events were rashes, hyperglycemia, and dehydration (9). Some patients have more pyrexia on dabrafenib and trametinib, and thus, switching over to vemurafenib and cobimetinib may be a better option (22). Our patient had pyrexia early with dabrafenib and trametinib, and thus, we may switch him over to vemurafenib and cobimetinib if it persists as a problem.

Regarding this patient's case specifically, he was treated with surgery multiple times before he started on targeted treatment with dabrafenib and trametinib. The patient himself remarked on the challenges of recovering from surgery multiple times. This also had a considerable

TABLE 2 Literature review with primary results of cases analyzed for this manuscript.

Studies	Demographics	Context	Dosage	Primary result
Brastianos et al.	39-Year-old male	Stage IV	Dabrafenib 150 mg BID, trametinib 2 mg BID	Combination BRAF and MEK inhibition reduced the tumor by 85% after 35 days
Roque et al.	47-Year-old female	Unresectable tumor proved refractory to radiation	Dabrafenib 150 mg BID, trametinib 2 mg BID	Combination BRAF and MEK inhibition reduced the tumor by more than 75% by 5 months; however, the patient had permanent panhypopituitarism
Nussbaum et al.	35-Year-old male	Post subtotal resection	Dabrafenib 75 mg BID, trametinib 2 mg BID	Combination BRAF and MEK inhibition reduced tumor by 95% over 21 months
Wu et al.	60-Year-old female and 60-year-old male	Post subtotal resection for both cases	Dabrafenib 150 mg BID, trametinib 2 mg BID	Combination BRAF and MEK inhibition in the 60-year-old female leads to a complete response for 2 years; in the male, the same combination showed a 20% reduction in tumor size over 1 month
Rao et al.	35-Year-old male	Post subtotal resection	Dabrafenib 150 mg BID	Single-agent BRAF inhibition led to a continued response over 2 years; however, patient had a remnant of panhypopituitarism
Khaddour et al.	39-Year-old male	Post subtotal resection	Dabrafenib 150 mg BID, trametinib 2 mg BID	Combination BRAF and MEK inhibition showed a 70% tumor reduction at 9 months; patient has been in remission for 2 years
Brastianos et al.	16 Total patients	NA	Vemurafenib 960 mg BID for 28 days, cobimetinib 60 mg daily for 21 days	Median reduction in volume of tumor was 91% over 22 months. PFS was 87% at 12 months and 58% at 24 months

NA, Not available.

effect on his quality of life. An argument could be made that the patient could have started on targeted treatment with dabrafenib and trametinib in the neoadjuvant setting before surgery, to perhaps make surgery a one-time event as opposed to multiple surgeries being necessary. Neoadjuvant dabrafenib and trametinib as a neoadjuvant could have reduced tumor volume leading to a less morbid surgery. When the patient was finally started on the dabrafenib and trametinib, one of the limitations was the ability to only assess the patient clinically and not with more frequent imaging. For example, the patient started on targeted treatment and clinically improved for 2 months before he felt that his vision was getting worse. It could have been beneficial to see what a brain MRI would have shown after 2 months of treatment, but a brain MRI would not have been approved by his insurance. Likewise, the patient had surgery after only 2 months of being treated with targeted therapy and resumed on targeted therapy after this surgery. The question could be asked if the patient is in remission because of the targeted treatment or the surgery. Limited publications are available discussing dabrafenib and trametinib in the neoadjuvant setting. Ultimately, more research is required to address this paradigm of using targeted treatment as a neoadjuvant treatment and then deciding whether or not the patient even needs surgery or radiation.

Data availability statement

The original contributions presented in the study are included in the article/Supplementary Material. Further inquiries can be directed to the corresponding author.

Ethics statement

Written informed consent was obtained from the individual(s) for the publication of any potentially identifiable images or data included in this article.

Author contributions

PH: Writing – original draft, Writing – review & editing. DE: Writing – review & editing. JA: Writing – review & editing.

Funding

The author(s) declare that no financial support was received for the research, authorship, and/or publication of this article.

Conflict of interest

The authors declare that the research was conducted in the absence of any commercial or financial relationships that could be construed as a potential conflict of interest.

Publisher's note

Supplementary material

The Supplementary Material for this article can be found online at: https://www.frontiersin.org/articles/10.3389/fonc.2024.1464362/full#supplementary-material

References

1. Ostrom QT, Cioffi G, Waite K, Kruchko C, Barnholtz-Sloan JS. CBTRUS statistical report: primary brain and other central nervous system tumors diagnosed in the United States in 2014-2018. *Neuro Oncol.* (2021) 23:iii1iii105. doi: 10.1093/neuonc/noab200

2. Bunin GR, Surawicz TS, Witman PA, Preston-Martin S, Davis F, Bruner JM. The descriptive epidemiology of craniopharyngioma. *J Neurosurg.* (1998) 89:547–51. doi: 10.3171/jns.1998.89.4.0547

3. Bollati A, Giunta F, Lenzi A, Marini G. Third ventricle intrinsic craniopharingioma. *Case Rep J Neurosurg Sci.* (1974) 18:216–9.

4. Prieto R, Barrios L, Pascual JM. Papillary craniopharyngioma: A type of tumor primarily impairing the hypothalamus - A comprehensive anatomo-clinical characterization of 350 well-described cases. *Neuroendocrinology.* (2022) 112:941–65. doi: 10.1159/000521652

5. Karavitaki N, Brufani C, Warner JT, Adams CB, Richards P, Ansorge O, et al. Craniopharyngiomas in children and adults: systematic analysis of 121 cases with long-term follow-up. *Clin Endocrinol (Oxf).* (2005) 62:397–409. doi: 10.1111/j.13652265.2005.02231.x

6. Garrè ML, Cama A. Craniopharyngioma: modern concepts in pathogenesis and treatment. *Curr Opin Pediatr.* (2007) 19:471–9. doi: 10.1097/MOP.0b013e3282495a22

7. Juratli TA, Jones PS, Wang N, Subramanian M, Aylwin SJB, Odia Y, et al. Targeted treatment of papillary craniopharyngiomas harboring BRAF V600E mutations. *Cancer.* (2019) 125:2910–4. doi: 10.1002/cncr.32197

8. Yamada S, Fukuhara N, Yamaguchi-Okada M, Nishioka H, Takeshita A, Takeuchi Y, et al. Therapeutic outcomes of transsphenoidal surgery in pediatric patients with craniopharyngiomas: a single-center study. *J Neurosurg Pediatr.* (2018) 21:549–62. doi: 10.3171/2017.10.PEDS17254

9. Brastianos PK, Twohy E, Geyer S, Gerstner ER, Kaufmann TJ, Tabrizi S, et al. BRAF-MEK inhibition in newly diagnosed papillary craniopharyngiomas. *N Engl J Med.* (2023) 389:118–26. doi: 10.1056/NEJMoa2213329

10. Müller HL, Merchant TE, Warmuth-Metz M, Martinez-Barbera JP, Puget S. Craniopharyngioma. *Nat Rev Dis Primers.* (2019) 5:75. doi: 10.1038/s41572-019-0125-9

11. Poretti A, Grotzer MA, Ribi K, Schönle E, Boltshauser E. Outcome of craniopharyngioma in children: long-term complications and quality of life. *Dev Med Child Neurol.* (2004) 46:2209. doi: 10.1017/s0012162204000374

12. Omholt K, Platz A, Kanter L, Ringborg U, Hansson J. NRAS and BRAF mutations arise early during melanoma pathogenesis and are preserved throughout tumor progression. *Clin Cancer Res.* (2003) 9:6483–8. doi: 10.1158/1078-0432.ccr-03-0884

13. Salama AKS, Li S, Macrae ER, Park JI, Mitchell EP, Zwiebel JA, et al. Dabrafenib and trametinib in patients with tumors with BRAFV600E mutations: results of the NCI-MATCH trial subprotocol H. *J Clin Oncol.* (2020) 38:3895–904. doi: 10.1200/JCO.20.00762

14. Gershenson DM, Miller A, Brady WE, Paul J, Carty K, Rodgers W, et al. Trametinib versus standard of care in patients with recurrent low-grade serous ovarian

cancer (GOG 281/LOGS): an international, randomised, open-label, multicentre, phase 2/3 trial. *Lancet*. (2022) 399:541–53. doi: 10.1016/S0140-6736(21)02175-9

15. Brastianos PK, Shankar GM, Gill CM, Taylor-Weiner A, Nayyar N, Panka DJ, et al. Dramatic response of BRAF V600E mutant papillary craniopharyngioma to targeted therapy. *J Natl Cancer Inst*. (2015) 108:djv310. doi: 10.1093/jnci/djv310

16. Roque A, Odia Y. BRAF-V600E mutant papillary craniopharyngioma dramatically responds to combination BRAF and MEK inhibitors. *CNS Oncol*. (2017) 6:95–9. doi: 10.2217/cns-20160034

17. Nussbaum PE, Nussbaum LA, Torok CM, Patel PD, Yesavage TA, Nussbaum ES. Case report and literature review of BRAF-V600 inhibitors for treatment of papillary craniopharyngiomas: A potential treatment paradigm shift. *J Clin Pharm Ther*. (2022) 47:826–31. doi: 10.1111/jcpt.13600

18. Wu ZP, Wang YL, Wang LC, Liu ZY, Fan RR, Zan X, et al. Case report: successful use of BRAF/MEK inhibitors in aggressive BRAF-mutant craniopharyngioma. *World Neurosurg*. (2023) 180: e117–26. doi: 10.1016/j.wneu.2023.08.137. ahead of print.

19. Rao M, Bhattacharjee M, Shepard S, Hsu S. Newly diagnosed papillary craniopharyngioma with BRAF V600E mutation treated with single-agent selective BRAF inhibitor dabrafenib: a case report. *Oncotarget*. (2019) 10:6038–42. doi: 10.18632/oncotarget.27203

20. Rostami E, Witt Nyström P, Libard S, Wikström J, Casar-Borota O, Gudjonsson O. Recurrent papillary craniopharyngioma with BRAFV600E mutation treated with neoadjuvant-targeted therapy. *Acta Neurochir (Wien)*. (2017) 159:2217–21. doi: 10.1007/s00701-017-3311-0

21. Khaddour K, Chicoine MR, Huang J, Dahiya S, Ansstas G. Successful use of BRAF/MEK inhibitors as a neoadjuvant approach in the definitive treatment of papillary craniopharyngioma. *J Natl Compr Canc Netw*. (2020) 18:1590–5. doi: 10.6004/jnccn.2020.7624

22. Garutti M, Bergnach M, Polesel J, Palmero L, Pizzichetta MA, Puglisi F. BRAF and MEK inhibitors and their toxicities: A meta-analysis. *Cancers (Basel)*. (2022) 15:141. doi: 10.3390/cancers15010141

frontiers | Frontiers in Oncology

TYPE Systematic Review
PUBLISHED 16 December 2024
DOI 10.3389/fonc.2024.1442612

OPEN ACCESS

EDITED BY
Ramcharan Singh Angom,
Mayo Clinic Florida, United States

REVIEWED BY
Christine Marosi,
Medical University of Vienna, Austria
Manuela Aramburu Berckemeyer,
Mayo Clinic Florida, United States

*CORRESPONDENCE
Jixuan Xu
xujixuan1995@outlook.com

†These authors have contributed equally to this work

RECEIVED 02 June 2024
ACCEPTED 26 November 2024
PUBLISHED 16 December 2024

CITATION
Chu X, Zhang T, Benghiat H and Xu J (2024) A systematic review of adult pineoblastoma. *Front. Oncol.* 14:1442612. doi: 10.3389/fonc.2024.1442612

A systematic review of adult pineoblastoma

Xiufeng Chu[1,2†], Ting Zhang[1†], Helen Benghiat[3] and Jixuan Xu[4,5*]

[1]Department of Oncology, The Fifth Affiliated Hospital of Zhengzhou University, Zhengzhou, China, [2]Marshall Medical Center, The Fifth Affiliated Hospital of Zhengzhou University, Zhengzhou, China, [3]Hall Edwards Radiotherapy Research Group, University Hospitals Birmingham, Birmingham, United Kingdom, [4]Department of Gastrointestinal & Thyroid Surgery, The Fifth Affiliated Hospital of Zhengzhou University, Zhengzhou, China, [5]Department of Cancer Studies, University of Birmingham, Birmingham, United Kingdom

Background: Adult pineoblastoma is an extremely rare central nervous system malignancy. Limitations of tumour databases, single institution retrospective analyses and a few case reports are not sufficient to clarify treatment options. Therefore, a systematic review of comprehensive research data provides referenceable treatment options.

Methods: A systematic review was performed using MEDLINE and Embase using the terms "pineoblastoma" and "adult". Relevant articles in the references were considered to supplement this systematic review. In addition, data were analysed using Kaplan-Meier survival curves, COX analysis, chi-square tests and log-rank tests.

Results: A total of 108 adult cases from 32 articles were included in this study and the median age at diagnosis was 30 years. The 5-year survival rate was 49.5% (95% confidence interval: 0.378-0.602) and the 10-year survival rate was 33.9% (95% confidence interval: 0.207-0.476). During the 10-year follow-up period, Kaplan-Meier survival curves highlighted that the gross total resection was more beneficial than subtotal resection and no surgery (P=0.018). The treatment modality of radiotherapy and chemotherapy was beneficial for survival (P<0.001; P=0.020). In addition, multivariate COX analysis showed that radiotherapy was an independent factor in the beneficial prognosis (P<0.001) and gross total resection tends to improve survival within five years (P=0.079).

Conclusion: For adult pineoblastoma, gross total excision and radiotherapy can be beneficial for survival.Systematic Review Registration: [website], identifier [registration number].

KEYWORDS

pineoblastoma, adult, surgery, radiotherapy, chemotherapy, survival

1 Introduction

Primary tumours of the pineal gland are rare and account for 0.1%-0.3% of intracranial malignancies (1). A variety of tumour subtypes can arise in the pineal gland. The recent World Health Organisation (WHO) Classification of Tumours of the Central Nervous System 2021 categorises primary pineal parenchymal tumours as: pineocytomas, pineal parenchymal tumours of intermediate differentiation (PPTID), pineoblastoma, papillary tumour of the pineal region and desmoplastic myxoid tumour of the pineal region, SMARCB1-mutant (2). Pineoblastoma (PB), accounts for approximately 45% of all pineal parenchymal tumour subtypes (3–5). It typically affects infants and young children with a slight female preponderance, although has been rarely reported in adults (3, 6). PB is classified as a WHO grade IV tumour and has a high rate of recurrence and propensity for spread via the cerebrospinal fluid (CSF) (7). Despite aggressive multimodality treatment, including surgery, radiotherapy and chemotherapy, the outcome of PB is poor with a 5-year survival of only 15% for patients < 5years of age (6).

Recent molecular characterisation has segregated PB into 5 molecular subgroups: PB-Group 1, PB-Group 2, PB-Group 3, RB and MYC; each with distinct clinico-pathologic and survival features (8, 9). Groups 1 to 3 PB arise in older children and adolescents and are associated with improved outcomes in contrast with patients with groups RB and MYC (9).

At present, management of adult PB is based on data extrapolated from paediatric practice. With small numbers of adult patients reported in multiple case reports and series; prognosis, as well as contribution of surgical resection and adjuvant chemo/radiotherapy on outcomes remain unclear.

1.1 Objectives

The objective of this study was to systematically review all adult cases of PB to determine patient characteristics as well as impact of surgical resection and adjuvant oncological therapy on prognosis from 1946 to 2021 in English journals.

2 Methods

This systematic review was reported as per the Preferred Reporting Items for Systematic Reviews and Meta-Analyses (PRISMA) guidelines. All articles reporting cases of pathologically confirmed adult PB were included. Using the terms "pineoblastoma" and "adult", MEDLINE and Embase databases were searched; with results limited to those written in English and published prior to June 2021. References from searched results were used in addition, and duplicate articles removed.

Data were collected on patient and tumour baseline characteristics, overall survival and treatment received. Kaplan-Meier survival curves were used to observe unadjusted survival, and log-rank test was used to compare survival outcomes in patients who received differing surgical procedures as well as adjuvant oncological therapies. A multivariate Cox model was used to determine which clinical variables were independently related to improved survival.

The Chi-square test was used to process categorical variables. Data were analysed using SPSS version 27.0 (IBM, Armonk, New York, USA). Kaplan-Meier curves were described by STATA 16.0 (STATA corporation, College Station, TX, USA) software.

3 Results

3.1 Study selection

As shown in Figure 1, a total of 169 articles were identified from the MEDLINE and Embase search. Besides, during the reading-through of the content and citations of these articles, additional 22 articles were found to contain retrievable original data of adult pineoblastoma cases. Among the above 191 articles, 61 were removed because of duplication, 94 were removed for lack of original data, and 4 were removed due to lack of patient survival. In summary, a total of 32 articles (3, 10–40) were included in this systematic review, which included case reports or series with an inherent risk of bias.

For eligible cases, we extract and analyse age, gender, surgery approach (GTR/STR), radiotherapy (RT) type, RT dose, CT, CT drugs, follow-up time and status. The detail regimen of chemotherapy was not analysed because of a lack of information from most patients. From a clinical perspective, total dose of radiotherapy to the pineal region (RTP) was analysed from RT dose data. The last follow-up time was defined as survival time.

3.2 Findings

From the selected 32 publications, 108 adult patients (age≥18 years) with pathologically confirmed PB were identified with demographic and treatment characteristics summarised in Table 1. Median age at diagnosis was 30 years (range 18-81). Of the 108 cases; 48 were male (44.4%) and 60 were female (55.6%). Forty-two patients (38.9%) had their presenting symptoms reported. The most common presenting symptoms included the following; alone or in combination: headache (n=31, 73.8%), visual disturbance including Parinaud's Syndrome (n=20, 47.6%), nausea and vomiting (n=10, 23.8%), dizziness (n=7, 16.7%), limb weakness (n=6, 14.3%) and deterioration in mobility (n=5, 11.9%). Information was available for 104 patients regarding extent of the disease at the time of diagnosis. Thirty-four patients (31.5%) were reported to have disseminated disease, and 70 (64.8%) had pineal disease only. Staging information was not available for 4 patients.

Of the 108 cases, 14 (13%) had gross total resection (GTR), 39 (36.1%) underwent subtotal resection (STR) and 54 (50%) had a biopsy. Extent of resection was not reported in one case (0.9%). The majority of patients [94 (87%)] received adjuvant radiotherapy following surgical resection or biopsy. Of the 94 patients who received adjuvant radiotherapy, 51 (54.3%) were treated with craniospinal irradiation (CSI). Seventeen (18%) patients received

focal radiotherapy, and for 26 (27.7%) no information was found regarding radiation technique.

Only 39 patients (36.1%) received adjuvant chemotherapy (CT). The chemotherapy regimen varied significantly, and prescription information was available for only 23 patients. Although the CT drug varied for almost every patient, a cisplatin-based schedule was used in the majority (60.8%). All of the 39 patients who received adjuvant CT had also received radiotherapy. No information was available regarding toxicity of therapy.

Of the 108 patients, 53 (49%) patients had died. Median overall survival (OS) was 59 months, with a 5- and 10- year OS of 49.5% and 33.9% respectively (Figure 2). Median length of follow up was 25.5 months (range 0.5-288 months).

A COX univariate analysis was used to observe and test which factors were associated with prognosis. Univariate variables that were statistically significant were included in the COX multivariate analysis model. Similar to the Kaplan–Meier curve, the COX analysis model evaluated prognostic factors in five-year and ten-year periods. Regarding the COX univariate analysis, factors including age, gender, surgery, RT, RT types, and CT were calculated (Figure 3). As shown in both figures, extent of resection, RT and CT are significantly associated with patient prognosis at both five and ten years.

As demonstrated in Figure 4, Cox multivariate analysis was used to determine which factors were associated with OS. There was a statistically significant benefit in OS at both 5 and 10 years for patients who received radiotherapy. (HR 0.16; $p < 0.001$). A trend towards improved OS at 5 years was seen for patients who had undergone a GTR (HR 0.16; $p = 0.079$). There was no statistically significant relationship demonstrated between the use of chemotherapy and OS.

According to the results of COX analysis, Kaplan-Meier univariate analysis focussed on these variables: choice of surgery, RT and CT. The Kaplan-Meier survival curve demonstrated that patients who underwent surgery (whether GTR or STR) had superior overall survival at 5 and 10 years ($p = 0.009$, $p = 0.018$) (Figure 5).

The Kaplan-Meier survival curve demonstrated that patients who received CT achieved better survival compared with patients who had no CT in both five-year and ten-year period time (Figure 6). Log-rank test P value presented that there was a statistical difference between the CT and no CT groups in two time periods (P value=0.007, P value=0.020).

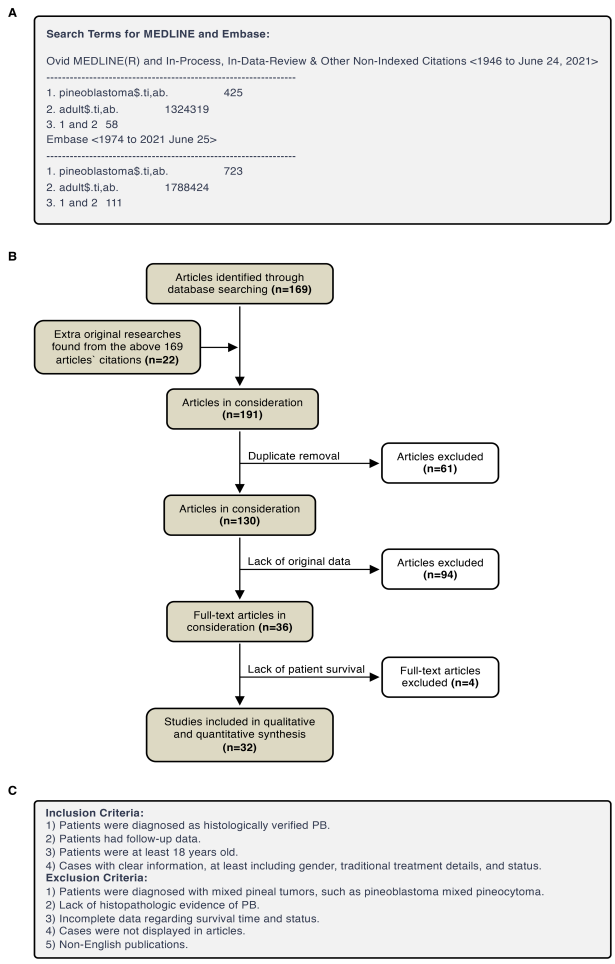

FIGURE 1
PRISMA flow diagram. **(A)** Search Terms for MEDLINE and Embase. **(B)** Eligibility assessment of papers for inclusion. **(C)** Eligibility assessment of cases for inclusion.

TABLE 1 Study population (n=108).

Patient characteristics	
Median age (range)	30 years (18-81)
Male	48 (44.4%)
Surgery	
GTR	14 (13%)
STR	39 (36.1%)
Biopsy	54 (50%)
Not reported	1 (0.9%)
Adjuvant RT	
Yes	94 (87%)
No	14 (13%)
RT type	
CSI	51 (54.3%)
Focal	17 (18%)
Unknown	26 (27.7%)
CT	
Yes	39 (36.1%)
No	63 (58.3%)
Unknown	6 (5.6%)
Median OS (range)	59 months (25.7-176)
Median FLUT	25.5 months

n, number of patients; GTR, gross-total resection; STR, subtotal resection; RT, radiotherapy; CSI, craniospinal irradiation; CT, chemotherapy; FLUT, follow-up time; OS, overall survival.

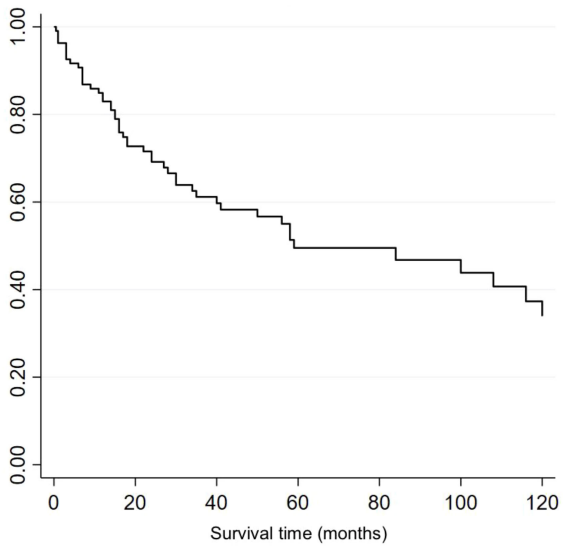

FIGURE 2
Kaplan-Meier survival curve for all patients regardless of treatment received.

The Kaplan-Meier survival curve demonstrated that patients who received RT got the better survival compared with those patients who had no RT in both five-year and ten-year period time (Figure 7).

4 Discussion

4.1 Survival

In our study, the median survival time for this series is 59 months (range: 25.7 months – 176 months). The lowest median survival from Lee et al. was 25.7 months and the highest median survival was 176 months from Selvanathan et al. (1, 41). The large difference between the two series regarding median survival could not be analysed as neither Lee et al. nor Selvanathan et al. presented complete case data (1, 41). As the series containing the largest number of cases, Jing et al. did not provide clear survival data (42). The rest of the reference median survival range is 35-105 months (3, 10–12, 43).

However, this study is not confined to one institutional or local database and the median survival of 59 months reflects the general level of overall survival of adults with PB over the last 50 years. The 5-year survival rate for patients in this study is 49.5%, which is similar to the 5-year survival rate of 51% reported by Lutterbach et al. (12). However, Selvanathan et al. reported a 5-year survival rate of 62.8% (1). This is most likely due to the inclusion of 16- to 17- years old patients in his cases, and therefore has a greater impact on the 5-year survival rate. On every account, the prognosis for adult patients themselves is better compared to the 5-year survival rate of 15% for children aged ≤5 years (6). For this reason, younger patients with PB are more likely to develop metastases (3). Although there is currently no clear clarification of the worse prognosis in paediatric PB patients, we believe that factors such as the lack of ability to self-assess and self-care, poor medical compliance, and a weaker immune system may greatly contribute to the worse prognosis in paediatric patients compared to adults.

4.2 Age

Adults are defined in this study as 18 years of age or older. Furthermore, age is not a factor in the prognosis of adult PB patients. Prior to 2014, retrospective analyses of adult PB had different definitions of adult age, with some articles defining 16-year-old as adults (1, 41). Two retrospective analyses after 2015 set the age at 18 years or older and noted the difficulty of comparing clinical factors in some of the retrospective analyses because the data for patients aged 16-17 years were unclear (10, 43). In contrast, Jing et al. only included patients over 20 years of age and did not explain the specific reasons.

On the other hand, stratifying this cohort of 108 patients based on a median age of 30 years, the Kaplan-Meier curve did not find an effect of age differences on survival. Lee et al. noted that age was not a statistically significant predictor of survival (41). However, Selvanathan et al. reported that the prognosis of patients deteriorated with increasing age (1). A review of Huo et al. study found that in an overall analysis of age in 64 patients including paediatric and adult patients, the risk of survival increased with each additional year of patient age. However, when Huo et al. validated the paediatric and adult groups (age≥18 years) of the cohort separately, COX regression analysis showed that age was no longer a risk factor for both groups of patients (43). In addition, a small series of retrospective analysis of Gener et al. pointed out that age was not a risk factor for prognosis (10). Thus, Selvanathan et al. found that age was associated with prognosis, most likely because the cohort included patients under 18 years of age (1).

4.3 Gender

Males and females comprised 44.4% and 55.6% of the total cohort in this study, respectively. Although there were slightly more female patients than male, no gender differences were found to have an impact on improving survival rates. Most of the adult PB series display a higher proportion of female patients and no statistically significant effect of gender on prognosis (1, 10, 42, 43). Only Lee et al. stated that there was a statistical trend for gender to improve survival (41). The interpretation of this finding needs to be considered in two ways. One is that in the Lee et al. cohort, the sample size was small and predominantly male, which is not consistent with the findings of most studies. The second is that a statistical trend cannot be equated with statistical significance, and it is likely that the trend would disappear after adjusting for other factors.

4.4 Surgery

The prevailing surgical approach is gross total resection (GTR) and subtotal resection (STR), with GTR being the recommended

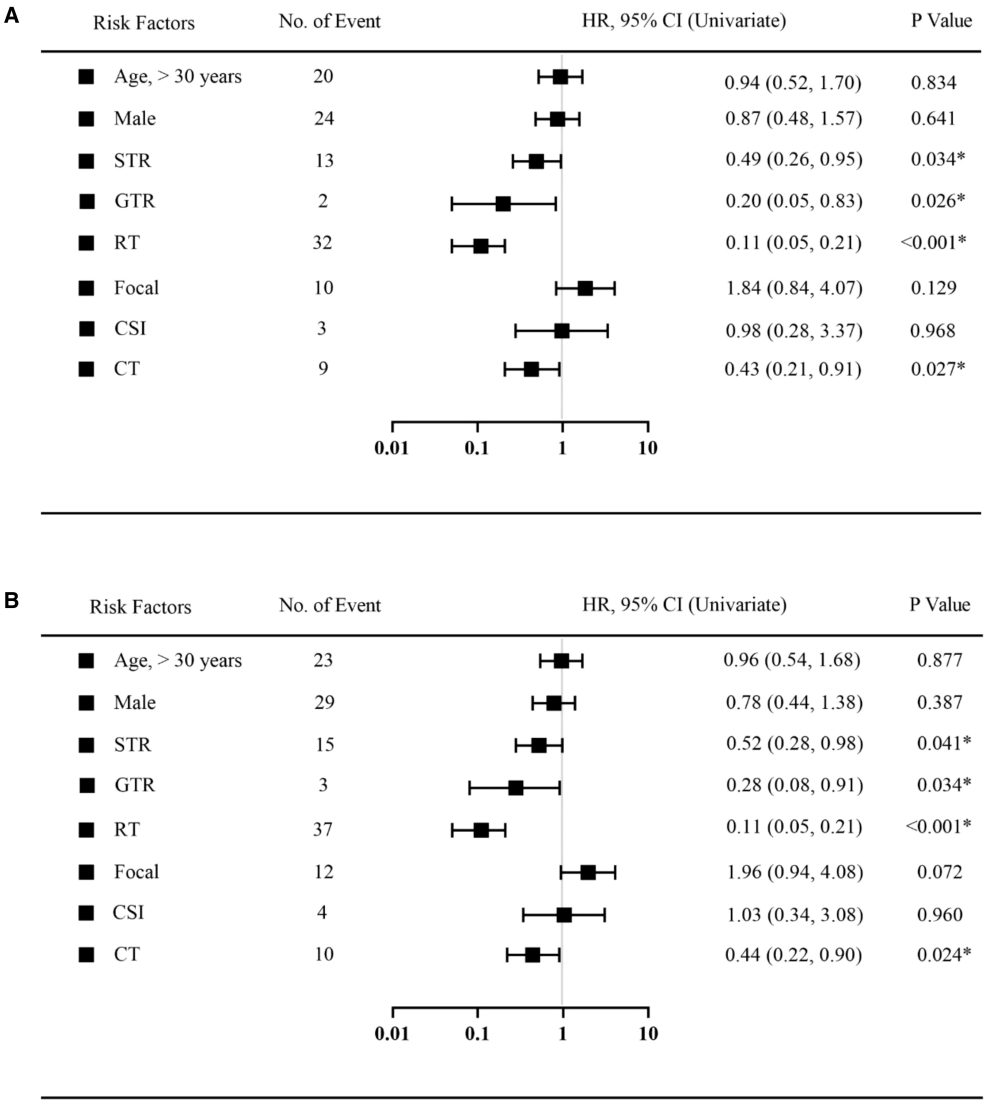

FIGURE 3
Univariate Cox regression analysis was used to estimate the prognostic factors in 5 years follow-up **(A)** or 10 years follow-up **(B)**. Black squares indicate the hazard ratio (HR). *Statistically significant. HR, hazard ratio; CI, Confidence Interval. STR, subtotal resection; GTR, gross-total resection; RT, radiotherapy; CSI, craniospinal irradiation; CT, chemotherapy.

approach on adult PB (44). According to the Kaplan-Meier curve, there is a significant difference in the effect of GTR, STR and no surgery on the survival rate in this study. Moreover, the effect of GTR is the best, and the effect of STR is the second. Although both GTR and STR were statistically significant in the univariate COX analysis, both lost statistical significance after the multivariate COX analysis. However, it is worth noting that the results of the multivariate COX analysis, which limited the five-year follow-up time, showed a statistical trend in GTR (P=0.079). Perhaps with an expanded sample size, GTR could be an independent variable in improving the prognosis of adult PB patients over the five years that they undergo GTR surgery. Multivariate COX analysis showed a disappearance of the tendency for GTR to improve prognosis within ten years (P=0.106), which may be related to the short survival period of the malignancy.

From a theoretical point of view, the relatively conservative approach to early surgery, such as STR, is due to the need to avoid surgical complications. With the development of clinical technology, microsurgery and neuronavigation technology can better support clinicians to choose a wider range of resection operations (6, 45). Moreover, studies have demonstrated that GTR is associated with better local control and a reduced rate of local recurrence (46, 47). Although Selvanathan et al. did not find a benefit from surgery, Tate et al. claimed that the role of GTR in the treatment of PB could not be ignored (1, 6).

4.5 Radiotherapy

In this study, RT not only demonstrated statistical significance in the Kaplan-Meier curve and univariate COX analysis (P<0.001),

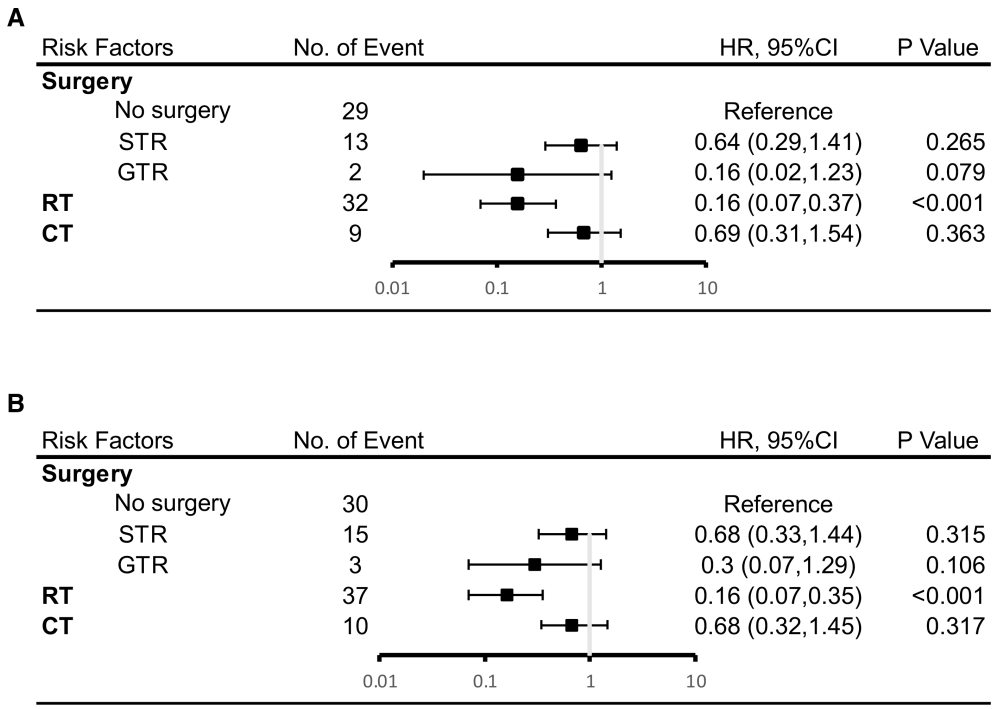

FIGURE 4
Results of multivariate analysis on overall survival at 5 years **(A)** or 10 years **(B)**. HR, hazard ratio; CI, Confidence Interval. *Statistically significant. STR, subtotal resection; GTR, gross-total resection; RT, radiotherapy; CT, chemotherapy.

but also emerged as the only independent prognostic factor in the multivariate COX analysis. In Selvanathan et al. cohort, there was no statistical difference in survival between patients who received RT and those who did not. However, he also found that patients who received RT may have prolonged survival, acknowledging that the lack of statistical significance was due to the limitations of the sample size (1). Similarly, this issue arose in the study by Huo et al. The risk factor for RT in 14 adults with PB was protective, but not statistically significant. After he had combined the adult and paediatric samples, the prognostic impact of RT was statistically significant (43).

For the impact of the type of RT, this study attempted to explore the effect of CSI, Focal and CSI + boost on survival. Although RT type was not found a statistical difference, CSI+boost demonstrated

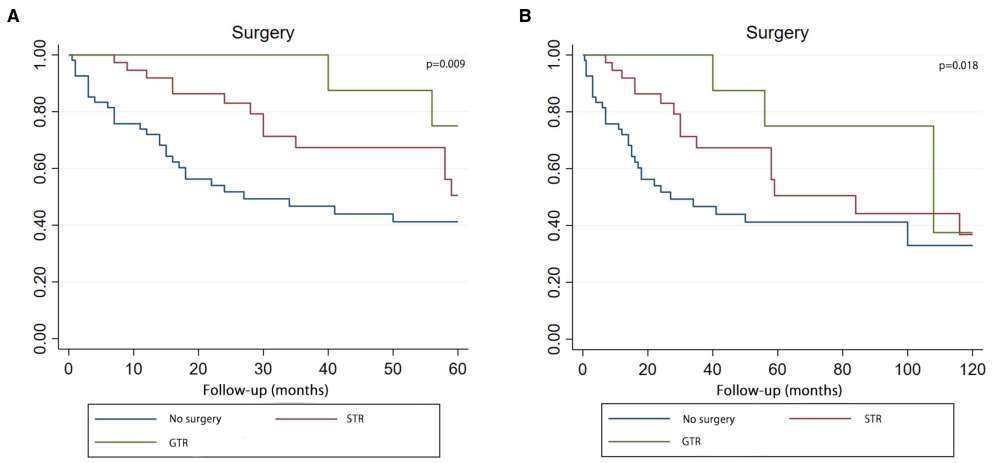

FIGURE 5
Kaplan–Meier curve analysis (Log-rank test) illustrating the survival rates of patients (n=107) between GTR, STR and no surgery for 5 years **(A)** or 10 years **(B)**. STR, subtotal resection; GTR, gross-total resection.

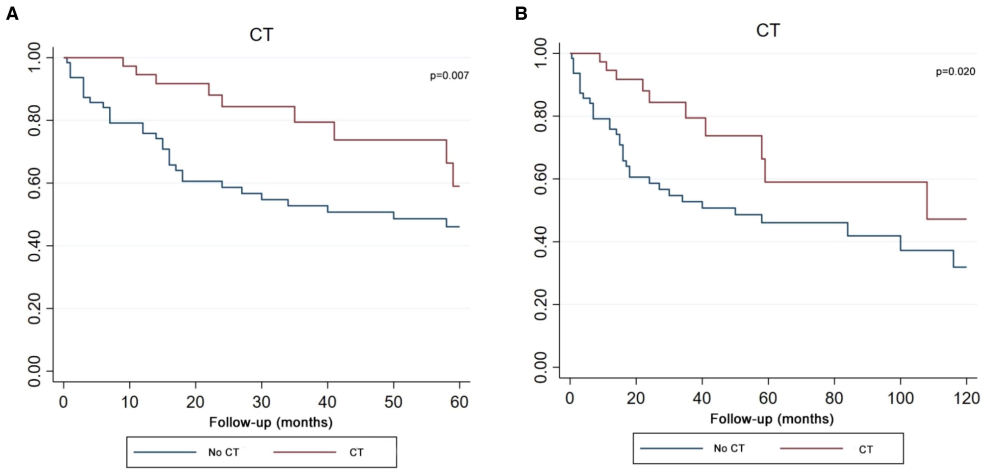

FIGURE 6
Kaplan–Meier curve analysis (Log-rank test) illustrating the survival rates of patients (n=102) between CT and no CT for 5 years **(A)** or 10 years **(B)**. CT, chemotherapy.

a trend towards improved survival. In fact, there is no retrospective analysis of adult PB that explores this factor. Therefore, it is difficult to compare and validate this result. In conclusion, the prognostic impact of radiotherapy may become clearer as the sample size of future studies is expanded and more prospective trials are explored.

4.6 Chemotherapy

In this study, the Kaplan-Meier curve and univariate COX analysis showed that CT was beneficial and statistically significant for survival. However, a multivariate COX analysis revealed that CT could not be used as an independent prognostic variable. This may indicate that CT in combination with surgery and RT can improve survival rates. In the Tate et al. cohort, the combination of RT and CT after surgery was more beneficial to survival than the CT after surgery. However, he did not analyse the effects of CT separately nor did he distinguish between adults and children in the cohort (6). Huo et al. distinguished between adults and children and studied the prognostic impact of CT, but he did not find it to be statistically significant (43). Jing et al. found that the combination of postoperative RT and CT significantly improved survival rates (42). In clinic, one case report supported that CT was effective in clinical practice (14).

5 Limitations

This systematic review summarises published cases with specific data, including institutional studies and case reports. This study

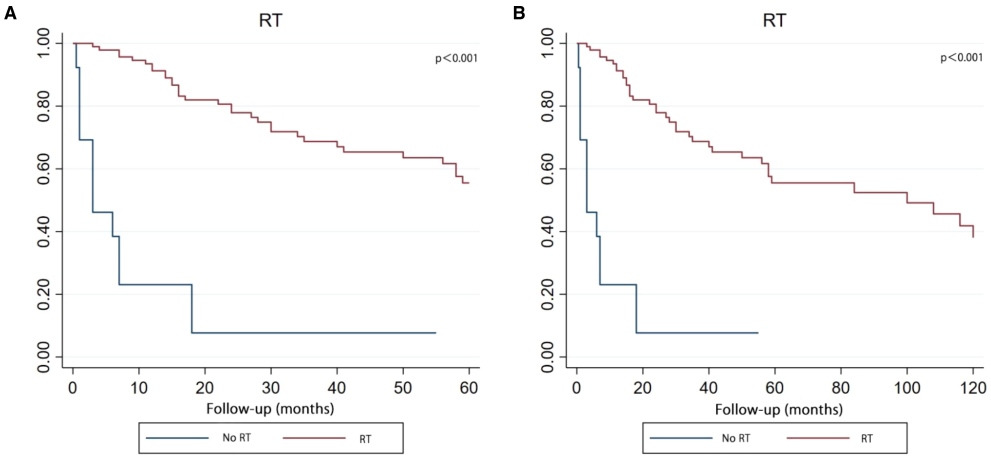

FIGURE 7
Kaplan–Meier curve analysis (Log-rank test) illustrating the survival rates of patients (n=108) between RT and no RT for 5 years **(A)** or 10 years **(B)**. RT, radiotherapy.

contains the most comprehensive number of adult PB cases available and is also the first systematic review of adult PB to provide evidence for the determination of treatment options. However, access to the database to retrieve the data was not achieved. It was also not possible to contact authors who did not provide specific data. In the study of the relationship between treatment and prognosis, the data of chemotherapeutic drugs are insufficient and cannot be statistically analysed. Sample size limitations did not allow for analysis of combination treatments. In addition, heterogeneity in tests, diagnosis and treatment modalities is objective due to differences in the year in which each patient is diagnosed. The operation of the treatment and the choice of medication are uncontrollable. However, the use of regression analysis to correct for covariates of confounding factors helped to reduce the effect of heterogeneity.

6 Conclusion

PB is a rare tumour of the pineal region. In adults, age and gender do not influence the overall survival of PB patients. Gross-total resection and radiotherapy are favourable factors for prognosis. Surgery combined with radiotherapy and chemotherapy is likely to be even more effective. In the future, further studies are needed to explore the contributions of radiotherapy methods, radiation doses, and chemotherapy regimens. Additionally, we advocate for the standardisation of follow-up intervals, the extension of the total duration of follow-up as well as the recording of professional activities and quality of life in original studies. Prospective studies with more restrictive selection criteria are more likely to identify the key factors that affect the survival of adult PB patients.

Data availability statement

The original contributions presented in the study are included in the article/Supplementary Material. Further inquiries can be directed to the corresponding authors.

Author contributions

XC: Writing – original draft, Writing – review & editing. TZ: Writing – review & editing, Data curation. HB: Writing – review & editing, Conceptualization. JX: Writing – original draft, Conceptualization.

Funding

The author(s) declare financial support was received for the research, authorship, and/or publication of this article. This project was supported by Research fund for the Doctoral program of the Fifth Affiliated Hospital of Zhengzhou University (pb2024kyqdj03), Supporting Program for Young Talent Innovation Teams of Zhengzhou University (32320688), Henan Medical Key Technologies R & D Program (LHGJ20220570).

Conflict of interest

The authors declare that the research was conducted in the absence of any commercial or financial relationships that could be construed as a potential conflict of interest.

Publisher's note

Supplementary material

The Supplementary Material for this article can be found online at: https://www.frontiersin.org/articles/10.3389/fonc.2024.1442612/full#supplementary-material

References

1. Selvanathan SK, Hammouche S, Smethurst W, Salminen HJ, Jenkinson MD. Outcome and prognostic features in adult pineoblastomas: analysis of cases from the SEER database. *Acta Neurochir (Wien)*. (2012) 154:863–9. doi: 10.1007/s00701-012-1330-4

2. Louis DN, Perry A, Wesseling P, Brat DJ, Cree IA, Figarella-Branger D, et al. The 2021 WHO classification of tumors of the central nervous system: a summary. *Neuro-Oncology*. 23:1231–51. doi: 10.1093/neuonc/noab106

3. Farnia B, Allen PK, Brown PD, Khatua S, Levine NB, Li J, et al. Clinical outcomes and patterns of failure in pineoblastoma: a 30-year, single-institution retrospective review. *World Neurosurg*. (2014) 82:1232–41. doi: 10.1016/j.wneu.2014.07.010

4. Mynarek M, Pizer B, Dufour C, van Vuurden D, Garami M, Massimino M, et al. Evaluation of age-dependent treatment strategies for children and young adults with pineoblastoma: analysis of pooled European Society for Paediatric Oncology (SIOP-E) and US Head Start data. *Neuro Oncol*. (2017) 19:576–85. doi: 10.1093/neuonc/now234

5. Tate MC, Rutkowski MJ, Parsa AT. Contemporary management of pineoblastoma. *Neurosurg Clin N Am*. (2011) 22:409–12, ix. doi: 10.1016/j.nec.2011.05.001

6. Tate M, Sughrue ME, Rutkowski MJ, Kane AJ, Aranda D, McClinton L, et al. The long-term postsurgical prognosis of patients with pineoblastoma. *Cancer*. (2012) 118:173–9. doi: 10.1002/cncr.v118.1

7. Tamrazi B, Nelson M, Blü ml S. Pineal region masses in pediatric patients. *Neuroimaging Clin N Am*. (2017) 27:85–97. doi: 10.1016/j.nic.2016.08.002

8. Pfaff E, Aichmü ller C, Sill M, Stichel D, Snuderl M, Karajannis MA, et al. Molecular subgrouping of primary pineal parenchymal tumors reveals distinct subtypes correlated with clinical parameters and genetic alterations. *Acta Neuropathol*. (2020) 139:243–57. doi: 10.1007/s00401-019-02101-0

9. Li BK, Vasiljevic A, Dufour C, Yao F, Ho BLB, Lu M, et al. Pineoblastoma segregates into molecular sub-groups with distinct clinico-pathologic features: a Rare Brain Tumor Consortium registry study. *Acta Neuropathol*. (2020) 139:223–41. doi: 10.1007/s00401-019-02111-y

10. Gener MA, Conger AR, Van Gompel J, Ariai MS, Jentoft M, Meyer FB, et al. Clinical, pathological, and surgical outcomes for adult pineoblastomas. *World Neurosurg*. (2015) 84:1816–24. doi: 10.1016/j.wneu.2015.08.005

11. Chang SM, Lillis-Hearne PK, Larson DA, Wara WM, Bollen AW, Prados MD. Pineoblastoma in adults. *Neurosurgery*. (1995) 37:383–90; discussion 90-1. doi: 10.1227/00006123-199509000-00003

12. Lutterbach J, Fauchon F, Schild SE, Chang SM, Pagenstecher A, Volk B, et al. Malignant pineal parenchymal tumors in adult patients: patterns of care and prognostic factors. *Neurosurgery*. (2002) 51:44–55; discussion -6. doi: 10.1097/00006123-200207000-00006

13. Fauchon F, Jouvet A, Paquis P, Saint-Pierre G, Mottolese C, Ben Hassel M, et al. Parenchymal pineal tumors: a clinicopathological study of 76 cases. *Int J Radiat Oncol Biol Phys*. (2000) 46:959–68. doi: 10.1016/S0360-3016(99)00389-2

14. Gaito S, Malagoli M, Depenni R, Pavesi G, Bruni A. Pineoblastoma in adults: A rare case successfully treated with multimodal approach including craniospinal irradiation using helical tomotherapy. *Cureus*. (2019) 11:e5852. doi: 10.7759/cureus.5852

15. Cuccia F, Mortellaro G, Cespuglio D, Valenti V, DE Gregorio G, Quartuccio E, et al. A case report of adult pineoblastoma occurring in a pregnant woman. *Anticancer Res*. (2019) 39:2627–31. doi: 10.21873/anticanres.13386

16. Neuwelt EA, Glasberg M, Frenkel E, Clark WK. Malignant pineal region tumors. A clinico-pathological study. *J Neurosurg*. (1979) 51:597–607. doi: 10.3171/jns.1979.51.5.0597

17. Borit A, Blackwood W, Mair WG. The separation of pineocytoma from pineoblastoma. *Cancer*. (1980) 45:1408–18. doi: 10.1002/1097-0142(19800315)45:6<1408::AID-CNCR2820450619>3.0.CO;2-0

18. Jooma R, Kendall BE. Diagnosis and management of pineal tumors. *J Neurosurg*. (1983) 58:654–65. doi: 10.3171/jns.1983.58.5.0654

19. Lesnick JE, Chayt KJ, Bruce DA, Rorke LB, Trojanowski J, Savino PJ, et al. Familial pineoblastoma. Report of two cases. *J Neurosurg*. (1985) 62:930–2. doi: 10.3171/jns.1985.62.6.0930

20. Uematsu Y, Itakura T, Hayashi S, Komai N. Pineoblastoma with an unusually long survival. Case report. *J Neurosurg*. (1988) 69:287–91. doi: 10.3171/jns.1988.69.2.0287

21. Jacobs JJ, Rosenberg AE. Extracranial skeletal metastasis from a pinealoblastoma. A case report and review of the literature. *Clin Orthop Relat Res*. (1989) 247:256–60. doi: 10.1097/00003086-198910000-00035

22. Vaquero J, Ramiro J, Martí nez R, Bravo G. Neurosurgical experience with tumours of the pineal region at Clinica Puerta de Hierro. *Acta Neurochir (Wien)*. (1992) 116:23–32. doi: 10.1007/BF01541249

23. Linggood RM, Chapman PH. Pineal tumors. *J Neurooncol*. (1992) 12:85–91. doi: 10.1007/BF00172460

24. Fuller BG, Kapp DS, Cox R. Radiation therapy of pineal region tumors: 25 new cases and a review of 208 previously reported cases. *Int J Radiat Oncol Biol Phys*. (1994) 28:229–45. doi: 10.1016/0360-3016(94)90162-7

25. Mena H, Nakazato Y, Jouvet A, Scheithauer BW. Pineoblastoma. In: Kleihues P, Cavenee WK, editors. *Pathology and Genetics of Tumours of the Nervous System*. IARC Press, Lyon (2000). p. 115–22.

26. Matsumoto K, Higashi H, Tomita S, Ohmoto T. Pineal region tumours treated with interstitial brachytherapy with low activity sources (192-iridium). *Acta Neurochir (Wien)*. (1995) 136:21–8. doi: 10.1007/BF01411431

27. Ashley DM, Longee D, Tien R, Fuchs H, Graham ML, Kurtzberg J, et al. Treatment of patients with pineoblastoma with high dose cyclophosphamide. *Med Pediatr Oncol*. (1996) 26:387–92. doi: 10.1002/(SICI)1096-911X(199606)26:6<387::AID-MPO3>3.0.CO;2-D

28. Brockmeyer DL, Walker ML, Thompson G, Fults DW. Astrocytoma and pineoblastoma arising sequentially in the fourth ventricle of the same patient. Case report and molecular analysis. *Pediatr Neurosurg*. (1997) 26:36–40. doi: 10.1159/000121159

29. Fujita A, Asada M, Saitoh M, Nakamura H, Kamikawa S, Kokunai T, et al. Pineoblastoma showing unusual ventricular extension in a young adult–case report. *Neurol Med Chir (Tokyo)*. (1999) 39:612–6. doi: 10.2176/nmc.39.612

30. Paulino AC, Melian E. Medulloblastoma and supratentorial primitive neuroectodermal tumors: an institutional experience. *Cancer*. (1999) 86:142–8. doi: 10.1002/(SICI)1097-0142(19990701)86:1<142::AID-CNCR20>3.0.CO;2-Y

31. Barlas O, Bayindir C, Imer M, Ayan I, Darendeliler E. Non-resective management of pineoblastoma. *Minim Invasive Neurosurg*. (2000) 43:163–70. doi: 10.1055/s-2000-14509

32. Nakamura M, Saeki N, Iwadate Y, Sunami K, Osato K, Yamaura A. Neuroradiological characteristics of pineocytoma and pineoblastoma. *Neuroradiology*. (2000) 42:509–14. doi: 10.1007/s002349900243

33. Charafe-Jauffret E, Lehmann G, Fauchon F, Michiels JF, Paquis P, Maraninchi D, et al. Vertebral metastases from pineoblastoma. *Arch Pathol Lab Med*. (2001) 125:939–43. doi: 10.5858/2001-125-0939-VMFP

34. Schild SE, Scheithauer BW, Haddock MG, Wong WW, Lyons MK, Marks LB, et al. Histologically confirmed pineal tumors and other germ cell tumors of the brain. *Cancer*. (1996) 78:2564–71. doi: 10.1002/(SICI)1097-0142(19961215)78:12<2564::AID-CNCR16>3.0.CO;2-U

35. Schild SE, Scheithauer BW, Schomberg PJ, Hook CC, Kelly PJ, Frick L, et al. Pineal parenchymal tumors. Clinical, pathologic, and therapeutic aspects. *Cancer*. (1993) 72:870–80. doi: 10.1002/1097-0142(19930801)72:3<870::AID-CNCR2820720336>3.0.CO;2-X

36. Ito T, Kanno H, Sato K, Oikawa M, Ozaki Y, Nakamura H, et al. Clinicopathologic study of pineal parenchymal tumors of intermediate differentiation. *World Neurosurg*. (2014) 81:783–9. doi: 10.1016/j.wneu.2013.02.007

37. Mena H, Rushing EJ, Ribas JL, Delahunt B, McCarthy WF. Tumors of pineal parenchymal cells: a correlation of histological features, including nucleolar organizer regions, with survival in 35 cases. *Hum Pathol*. (1995) 26:20–30. doi: 10.1016/0046-8177(95)90110-8

38. Ai P, Peng X, Jiang Y, Zhang H, Wang S, Wei Y. Complete regression of adult pineoblastoma following radiotherapy: A case report and review of the literature. *Oncol Lett*. (2015) 10:2329–32. doi: 10.3892/ol.2015.3574

39. Stoiber EM, Schaible B, Herfarth K, Schulz-Ertner D, Huber PE, Debus J, et al. Long term outcome of adolescent and adult patients with pineal parenchymal tumors treated with fractionated radiotherapy between 1982 and 2003–a single institution's experience. *Radiat Oncol*. (2010) 5:122. doi: 10.1186/1748-717X-5-122

40. Gadish T, Tulchinsky H, Deutsch AA, Rabau M. Pinealoblastoma in a patient with familial adenomatous polyposis: variant of Turcot syndrome type 2? Report of a case and review of the literature. *Dis Colon Rectum*. (2005) 48:2343–6. doi: 10.1007/s10350-005-0201-y

41. Lee JY, Wakabayashi T, Yoshida J. Management and survival of pineoblastoma: an analysis of 34 adults from the brain tumor registry of Japan. *Neurol Med Chir (Tokyo)*. (2005) 45:132–41; discussion 41-2. doi: 10.2176/nmc.45.132

42. Jing Y, Deng W, Zhang H, Jiang Y, Dong Z, Fan F, et al. Development and validation of a prognostic nomogram to predict cancer-specific survival in adult patients with pineoblastoma. *Front Oncol*. (2020) 10:1021. doi: 10.3389/fonc.2020.01021

43. Huo XL, Wang B, Zhang GJ, Ma JP, Wang L, Zhang LW, et al. Adverse factors of treatment response and overall survival in pediatric and adult patients with pineoblastoma. *Cancer Manag Res*. (2020) 12:7343–51. doi: 10.2147/CMAR.S258476

44. Palled S, Kalavagunta S, Beerappa Gowda J, Umesh K, Aal M, Abdul Razack T, et al. Tackling a recurrent pinealoblastoma. *Case Rep Oncological Med*. (2014) 2014:135435. doi: 10.1155/2014/135435

45. Reddy AT, Janss AJ, Phillips PC, Weiss HL, Packer RJ. Outcome for children with supratentorial primitive neuroectodermal tumors treated with surgery, radiation, and chemotherapy. *Cancer*. (2000) 88:2189–93. doi: 10.1002/(SICI)1097-0142(20000501)88:9<2189::AID-CNCR27>3.0.CO;2-G

46. Tomita T, McLone DG, Yasue M. Cerebral primitive neuroectodermal tumors in childhood. *J Neurooncol*. (1988) 6:233–43. doi: 10.1007/BF00163707

47. Frost PJ, Laperriere NJ, Wong CS, Milosevic MF, Simpson WJ, Pintilie M. Medulloblastoma in adults. *Int J Radiat Oncol Biol Phys*. (1995) 32:951–7. doi: 10.1016/0360-3016(94)00612-o

frontiers | Frontiers in Oncology

TYPE Original Research
PUBLISHED 30 January 2025
DOI 10.3389/fonc.2025.1451156

OPEN ACCESS

EDITED BY
Ramcharan Singh Angom,
Mayo Clinic Florida, United States

REVIEWED BY
Gabriele Multhoff,
Technical University of Munich, Germany
Imran Khan,
University of Nebraska Medical Center, United States
Vishal Singh,
Rutgers University, Newark, United States

*CORRESPONDENCE
Diana Spiegelberg
diana.spiegelberg@uu.se

†These authors have contributed equally to this work

RECEIVED 18 June 2024
ACCEPTED 06 January 2025
PUBLISHED 30 January 2025

CITATION
Uffenorde J, Hariri M, Papalanis E, Staffas A, Berg J, Stenerlöw B, Berglund H, Malmberg C and Spiegelberg D (2025) Enhancing glioblastoma therapy: unveiling synergistic anticancer effects of Onalespib - radiotherapy combination therapy.
Front. Oncol. 15:1451156.
doi: 10.3389/fonc.2025.1451156

Enhancing glioblastoma therapy: unveiling synergistic anticancer effects of Onalespib - radiotherapy combination therapy

Julia Uffenorde[1†], Mehran Hariri[2†], Eleftherios Papalanis[2], Annika Staffas[2], Josefine Berg[2], Bo Stenerlöw[2], Hanna Berglund[2], Christer Malmberg[3] and Diana Spiegelberg[1,2*]

[1]Department of Surgical Sciences, Uppsala University, Uppsala, Sweden, [2]Department of Immunology, Genetics and Pathology, Uppsala University, Uppsala, Sweden, [3]Department of Medical Sciences, Uppsala University, Uppsala, Sweden

Background: Glioblastoma (GBM) is the deadliest form of brain cancer, impacting both adults and children, marked by exceptionally high morbidity and mortality rates, even with current standard treatments such as surgery, radiation therapy, and chemotherapy. Therefore, there is a pressing need for new therapeutic strategies to improve survival and reduce treatment side effects. In this study, we investigated the effect of HSP90 inhibition in combination with radiotherapy in established and patient-derived glioblastoma cell lines.

Methods: Potential radiosensitizing effects of the HSP90 inhibitor Onalespib were studied in XTT and clonogenic survival assays as well as in tumor-mimicking multicellular spheroid models. Further, migration capacity and effects on protein expression were studied after exposure to Onalespib and radiation using Proximity Extension Assay analysis.

Results: HSP90 inhibition with Onalespib synergistically enhanced the radiosensitivity of glioblastoma cells grown in 2D and 3D models, resulting in increased cell death, reduced migration capacity and activation of the apoptotic signaling pathway. The proteomic analysis of glioblastoma cells treated with Onalespib, radiation, and their combination revealed significant alterations in protein expression profiles, involved in growth signaling, immune modulation pathways and angiogenesis. Moreover, the combination treatment indicated potential for enhancing cell cycle arrest and apoptosis, suggesting promising anti-tumor effects.

Conclusion: These findings demonstrate that HSP90 inhibition may be a promising strategy to enhance the efficacy of radiotherapy in the treatment of GBM, potentially leading to improved outcomes for patients battling this challenging disease.

KEYWORDS

CNS tumors, synergy, heat shock protein, radiotherapy, combination therapy, proteomics, proximity extension assay

1 Introduction

Glioblastoma (GBM) is the most frequent primary brain tumor in adults, with a median survival of less than 15 months despite aggressive treatment (1). Its occurrence in children remains relatively rare, constituting 3–15% of primary central nervous system (CNS) tumors. Despite the relative rarity, pediatric GBM exacts a significant toll with high morbidity and mortality rates, and with a 5-year survival of less than 20% (2, 3). The therapeutic strategies of GBM include open surgery and a combination of radiotherapy (60 Gy), typically given over 6 weeks (in 30 fractions of 2 Gy) with concurrent administration of the oral alkylating agent temozolomide (TMZ) (4, 5). There are indications that patients with epigenetic silencing of the DNA-repair protein MGMT in the tumor tissue benefit the most from TMZ, however, pediatric GBMs seldom display methylated MGMT promoters (5, 6). Unfortunately, TMZ treatment often leads to emergent tumor resistance (7), with multiple studies indicating that inactivation of the mismatch repair function (MMR) may be an important mechanism underlying acquired resistance. TMZ produces O6-methylguanine (O6-MG) lesions, which leads to base mispairing with thymine instead of cytosine during DNA replication, triggering DNA repair, cell cycle arrest, and ultimately cell death. In the case of MMR inactivation in post-treatment GBM patients, O6-MG is not recognized by MMR proteins and bypasses apoptosis, resulting in the survival of cancer cells and the proliferation of "cytidine to thymidine" hypermutator phenotypes (8, 9). Despite these insights, many aspects involved in GBM resistance to treatment are still poorly understood. The inadequate killing of cancer stem cells and the upregulation of DNA damage response (DDR) have been described as important contributors to low cancer survival (10).

New treatment approaches are needed to increase therapy success rates and improve clinical outcomes for patients with GBM. Based on the current understanding of the mechanisms underlying radiotherapy resistance, this may involve specific targeting of the resistant cancer cell subpopulations, as well as DDR mechanisms.

Recent research has identified the molecular chaperone heat shock protein 90 (HSP90) as a promising target for improving radiation treatment, including GBM (11–16). HSP90 is a member of the heat-shock protein family with a molecular mass of 90 kD. HSP90 is often overexpressed in human tumors, having a central role in buffering cellular stress and protein folding in an ATP-dependent manner. For this, HSP90 stabilizes multiple DDR proteins and oncoproteins which helps ensuring tumor cell survival and proliferation (17). HSP90 inhibitors exhibit higher affinity for the intertumoral HSP90 compared to the HSP90 in normal cells. This is due to the increased ATPase activity of HSP90 in tumor cells, which results from mutations or deregulation that are commonly present in cancerous cells (18). Therefore, HSP90 inhibitors have received interest as potentially attractive and potent cancer treatment agents. In our study, we used Onalespib, a second-generation HSP90 inhibitor with favorable toxicity profile (19) and the benefit of penetrating the blood-brain barrier (20). Onalespib already has undergone phase I studies with solid tumors with acceptable toxicity profiles and has shown antitumor activity in combination treatment (19, 21). Furthermore, long-acting effects of Onalespib against gliomas with a decrease in proliferation, migration, and angiogenesis of the tumor cells and an effective blood-brain barrier cross as a single agent or as a combination treatment with TMZ have been demonstrated *in vitro* and *in vivo* (20). Previous studies have demonstrated that Onalespib significantly impairs DNA repair by depleting homologous recombination (HR) proteins such as CHK1 and RAD51, reducing HR repair and increasing glioma stem cell sensitivity to radiation and TMZ (15). It also modulates DDR proteins, including ATM and DNA-PKcs, further compromising repair mechanisms (13). While its impact on MMR proteins is limited, with minor effects on MSH2 and downregulation of MSH4, MSH6, and EXO1, Onalespib's ability to target multiple DNA repair pathways underscores its potential to overcome treatment resistance (15).

Our study aims to investigate the efficacy and underlying molecular mechanisms of the combining the HSP90 inhibitor Onalespib with external beam radiotherapy in four glioblastoma cell lines *in vitro*, providing a comprehensive model for studying GBM's genetic diversity. U343 MG and U87 MG, widely used, feature wild-type p53, aiding radiation resistance studies and modeling invasiveness. However, the long-term culturing of these well-established cell lines may have reduced their molecular complexity. In contrast, the patient-derived lines U3013MG and U3024MG retain genetic heterogeneity (22), with sensitivity to certain therapies and exhibiting unique DNA repair defects. This combination supports the development of personalized GBM therapies while ensuring comparability with prior research.

By exploring the combination treatment of Onalespib and radiotherapy, we aim to contribute to the development of more effective therapeutic strategies for GBM and ultimately improve patient outcomes in this challenging disease.

2 Materials and methods

2.1 Cell lines

The glioblastoma cell lines were purchased from the American Type Culture Collection ATCC (Manassas, VA, United States). U87 MG (HTB-14) cells were grown in Dulbecco's Modified Eagle's Medium (DMEM (Biowest, MO, USA)) and was supplemented with 10% Fetal Bovine Serum (FBS, Sigma-Aldrich, Darmstadt, Germany) and 1% antibiotics (100 IU penicillin and 100 µg/ml streptomycin, Biochrom GmbH). The U343 were grown in MEM containing Earle's salts (Biochrom, Berlin, Germany or Sigma-Aldrich, Darmstadt, Germany) supplemented with 10% FBS (Sigma Aldrich, Darmstadt, Germany), 1% antibiotics (100 IU penicillin and 100 µg/ml streptomycin, (Biochrom GmbH, Berlin, Germany) and 1% sodium pyruvate (Thermo Fisher, Waltham, MA, USA). Both cell lines were grown in an incubator at 37° C and 5% CO_2. The human patient-derived GBM cell lines U3013MG and U3024MG, were obtained from the HGCC collection (22), and maintained in culture according to HGCC guidelines. Cells were maintained on laminin-coated tissue culture dishes (Primaria, Cat. No. 353802, Corning; laminin Cat. No. L2020, Sigma Aldrich) in a

serum-free medium composed of a 1:1 mixture of Neurobasal Medium (Cat. No. 21103-049, Thermo Fisher) and DMEM/F-12, GlutaMAX™ (Cat. No. 10565-018, Thermo Fisher). The medium was supplemented with 10 ng/ml FGF-2 (Cat. No. 100-18B, Peprotech), 10 ng/ml rhEGF (Cat. No. AF-100-15, Peprotech), N-2 (Cat. No. 17502048, Thermo Fisher), and B-27 solution (Cat. No. 17504044, Thermo Fisher).

2.2 Drug preparation

Onalespib (AT13387, Selleck Chemicals, Germany) was dissolved in DMSO and stored in aliquots at -20°C. Onalespib was further diluted in complete media for the desired assay concentrations.

2.3 Irradiation

For cell viability studies (XTT), migration and multicellular spheroid assays, Proximity Extension analysis and flow cytometry, cells were irradiated 24 h after drug incubation with 225 kV X-rays (X-RAD iR225, Precision X-Ray Inc., North Branford, CT, USA) at a dose-rate of 1.5 Gy/min using an inherent Ba filter (0.8 mm) and an external Cu filter (0.3 mm). For clonogenic survival (24 h after drug incubation), the irradiation was either performed as described above or with an Elekta Versa HD linear accelerator at the Uppsala University Hospital. The X-ray beam was set to 6 MV and the cells were placed at a water-equivalent depth of 10 cm using water-equivalent plastic attenuators. Cells were irradiated using a vertical beam (irradiation from above). The dose rate was approximately 4-5 Gy per minute. All irradiations were performed at room temperature.

2.4 XTT assays

The XTT assay was performed to assess the cell viability. U343 MG, U87 MG, U3013MG and U3024MG cells were seeded per well in 96-well plates (VWR, Pennsylvania, USA, laminin-coated for patient-derived cultures) and incubated at 37°C and 5% CO_2 for 48 h. Cell media was then removed and replaced by fresh media containing 0, 10, 25, 50 and 100 nM of Onalespib, followed by irradiation with 1, 2, 4, or 6 Gy. 72 hours after treatment, an XTT assay (ATCC, Manassa, VA) was performed according to the manufacturer's protocol. Briefly, XTT activation reagent, XTT reagent and cell media were mixed and 150 µl were added to the 60 inner wells (excluding the outer wells) of the plate, and then the plate was incubated at 37°C and 5% CO_2 in the dark. The absorbance was measured at 490 and 650 nm in a spectrophotometer 4 hours after incubation (Biorad, iMarkTM Microplate Absorbance Reader). The software used for the measurements was Microplate Manager Software 6 (Biorad). Each measurement was replicated at least six times.

2.5 Clonogenic assays

Clonogenic survival assays were performed as described previously (23) to assess the cell's ability to grow into a colony. In short, 100-4600 U343 cells were seeded in 6-well plates (VWR, Pennsylvania, USA) and incubated at 37°C and 5% CO_2 for 24 hours. 24 hours later, cells were treated with 2 ml of media-containing Onalespib (5-50 nM). After 24 hours, the cells were irradiated with 2-6 Gy of X-rays and incubated until colonies of more than 50 cells/colony were formed. Then, the medium was removed, followed by washing with cold PBS and the cells were fixated by adding 96% cold ethanol for 20 minutes. and stained with crystal violet (1% solution, Sigma-Aldrich, Darmstad, Germany). Colonies containing more than 50 cells were counted manually and the plating efficiency (PE) and the survival fraction (SF) were calculated. A linear quadratic curve fit ($S = \exp(-\alpha D - \beta D\ 2)$, where D = radiation dose in Gray, and α and β are fitting parameters) was calculated by using GraphPad Prism 9 software (San Diego, CA, USA).

One-way ANOVA followed by Tukey's multiple comparison's test determined significance. Data were expressed as mean SD and $p < 0.05$ considered to be statistically significant. The number of replicates within each experimental group was 3. Each experiment was repeated at least three times.

2.6 Multicellular tumor spheroids

96-well flat bottom plates (VWR, PA, USA) were coated with 50 µl of 1.5% agarose (Sigma Aldrich, Darmstad, Germany) dissolved in PBS (Biowest, MO, USA) according to (24).4500 U343 MG cells and 1500 U87 MG cells were seeded in 200 µl cell media/well and incubated at 37°C and 5% CO_2 for 72 hours until 3D spheroids formed. Twelve spheroids/group were treated with increasing Onalespib concentrations (50 nM-250 nM). The spheroids were incubated for 24 hours and then irradiated with 2-6 Gy of X-rays. Day 0 was considered to be the treatment day. Media was renewed (100 µl out, 100 µl in) every fourth day. After the treatment, spheroids were followed by photography every 3-4 days for 2 weeks. The images of the cell spheroids were obtained using a 4x magnification with a Canon EOS 700D digital camera (Canon, Tochigi, Japan) mounted on an inverted Nikon Diaphot-TMD microscope (Nikon, Tokyo, Japan). Assuming a spherical spheroid shape, the area of the spheroids was determined using a custom-made macro-command on ImageJ and the volume of the spheroids was calculated. Comparison between groups was performed using one-way ANOVA followed by Tukey's *post hoc* test. Data were expressed as mean SD and $p < 0.05$ considered to be statistically significant. The number of replicates within each experimental group was 12. Each experiment was repeated at least three times.

For live/dead cell count, U87 MG, U3013MG, and U3024MG spheroids were treated with 25, 50, and 100 nM Onalespib, as well as 2 or 4 Gy radiation. Three days post-treatment, live/dead cell counts were performed using trypan blue (BioRad) staining according to the manufacturer's instructions. For the limiting dilution assays, U87 MG cells were trypsinized (accutase was used for patient derived cell lines), and 50, 100, 250, 500, and 1,000 cells were seeded into 96-well round-bottom, ultra-low attachment plates (VWR, PA, USA). Spheroid-forming efficiency was assessed

three days later, and the data were analyzed using ELDA software, according to (25).

2.7 Migration/proliferation assay

The cell migration and proliferation ability of U343 MG and U87 MG cells was studied using a wound healing assay (also called scratch assay), as previously reported (35). In short, cells were grown at confluence in 6 well plates and a narrow area on the monolayer was scratched off with a p10 pipette tip. Afterwards, wells were washed and incubated with normal cell medium, 5-50 nM Onalespib and radiation of 2-6 Gy. Images from the same scratch location were obtained directly after scratching, 6, 12 and 24 h of incubation using an inverted microscope Nikon Diaphot (Nikon, Japan) mounted with Canon EOS 700D camera (Canon, Tochigi, Japan). Migration distance was measured and analyzed using ImageJ 2.0.0 software (NIH, Bethesda, MD, United States). The experiments were repeated 3 times.

2.8 Immunofluorescent biomarker for chromosomal double-strand breaks

The process of preparing slides and quantifying DNA double-strand break (DSB) repair foci was conducted following procedures previously described in (26). Briefly, U343 MG, and U87 MG cells were seeded in 4-well cell culture chamber slides (Nunc A/S, Roskilde, Denmark) to achieve approximately 70% confluency after incubation at 37°C for 24 h. Subsequently, cells were treated with DMSO, and 100 nM Onalespib for 24 h before irradiation with and without 2 and 6 Gy X-rays. Subsequently, samples were washed and replaced with fresh pre-warmed medium. The slides were then incubated at 37°C for 24 h. Afterward, cells underwent a washing step and were fixed with 1X PBS and 99% methanol (-20°C), respectively. Cell membranes were permeabilized with ice-cold acetone (Millipore, Merck, United States) for 10 seconds. Blocking of non-specific proteins was achieved by incubating the cells in 10% FBS PBS for 1 h at room temperature. Following this, the slides were exposed to Rabbit anti53BP1 (1:1000, ab36823, Abcam, Cambridge, United Kingdom) and mouse anti-γH2AX (1:100, JBW301, EMD Millipore Merck Darmstadt, Germany) antibodies overnight at 4°C. The next morning, the slides were incubated with Alexa fluor 555 (1:400, ab150086, Abcam, Cambridge, United Kingdom) and Alexa fluor 488 (1:400, ab150117, Abcam, Cambridge, United Kingdom) for 1 hour in the dark. Nuclei were stained with DAPI (ThermoFisher Scientific, Sweden) in the dark for approximately 2 minutes, followed by washing with 1X PBS and MQ water. The slides were air-dried before mounting with VECTASHIELD® antifade media (part of Maravai LifeSciences, USA). High-resolution images with a 20X NA 0.8 objective were captured using a Zeiss LSM 700 point scanning confocal microscope (Zeiss, Oberkochen, Germany). Foci quantification was performed on maximum intensity projection images using ImageJ software (Fiji Is Just ImageJ). The number of 53BP1 and γH2AX foci were counted for approximately 200 nuclei in each condition.

2.9 Flow cytometry

To assess the cell cycle distribution after treatment, flow cytometry was performed. Cells were seeded in T-25 flasks (purchased from VWR) and incubated at 37°C and 5% CO_2 until confluency was reached. Once confluent, cells were treated with 5 ml of media-containing 500 nM of Onalespib and irradiated with 2 and 4 Gy after 1 hour of drug incubation. After 48 hours, cells were trypsinized followed by washing with PBS and centrifuging (performed twice). Single cell suspensions were prepared by resuspension in PBS. Cold Ethanol was added to fixate the cells. Samples were kept at –20°C for a minimum of one week to ensure cell permeabilization. For flow cytometry analysis, the cells were centrifuged at 1200 rpm for 10 min and washed twice with ice-cold PBS, followed by adding 0.5 mL RNase (100 µg/mL) and 100 µL of PI (50 µg/mL). After 30 min of incubation time (at RT, in darkness) analysis was performed using a CytoFLEX (Beckman Coulter, Krefeld, Germany) flow cytometer. The data analysis and peaks recognition were done by FlowJoTM Software for Windows (Version 10.9 Becton, Dickinson and Company, Oregon, United States).

2.10 Western blot analysis

Whole-cell extracts were prepared according to the procedure described in (27). Briefly, the samples were separated using SDS-PAGE and then transferred onto a nitrocellulose membrane (Immobilon-P Transfer membrane, Millipore, Merck) through wet blotting. The membrane was blocked for 1 hour in PBS containing 5% BSA and incubated overnight at 4°C with a monoclonal p21 antibody (1:1000, ab109520, Abcam, Cambridge), an anti-γH2AX antibody (1:2000, ab11174, Abcam, Cambridge), and an anti-GAPDH antibody (1:500,000, ab8245, Abcam, Cambridge) as a protein loading control.

After three washes with PBS-Tween (1%), a secondary antibody conjugated with Horseradish Peroxidase specific to the primary antibody species was added for 1 hour at room temperature. This was followed by another three washing steps with PBS-Tween (1%). The immunoreactive bands were then visualized using an Amersham ImageQuant 800FL imaging system (Cytiva Life Science, Uppsala, Sweden) after applying an electrochemiluminescent reagent (Immobilon, Millipore). Uncropped Western blot membranes are shown in Supplementary Figure 5.

2.11 Proteomic analysis: proximity extension assay

U343 MG cell culture lysates were analyzed with Olinks Proximity Extension Assay using the Oncology II panel (v.7004, Olink Biosciences, Uppsala, Sweden), measuring expression of 96 proteins. Lysates taken at 24 h post-treatment of 500nM Onalespib or X-ray irradiation of 4 Gy or the combination of the two. Protein levels were expressed as normalized protein expression (NPX) on a log2-scale. Values below limit of detection (LOD) were truncated at the LOD. No values were above the upper limit of quantification.

All data analysis was performed with R (v4.3.1). In order to analyze expression signatures between treatments, hierarchical clustering was performed using the hclust function.

To identify important proteins, the standard deviation of each assay was used. A large standard deviation (big differences between treatments) corresponded to a high rank. This was performed on NPX values, normalized (by subtraction) to the control sample of the corresponding treatment, with the std function. Functional ontology analysis of the highly ranked proteins was performed using the clusterProfiler (v 4.0) package (28, 29), and the Reactome pathway knowledgebase (v87) as reference (30).

2.12 Statistical analysis, synergy analysis and tumor spheroid doubling time

The experimental data were analyzed using Microsoft Office Excel for Mac Version 16.8, and graphs were generated using GraphPad Prism 10 for Mac OS X. Statistical analysis of the viability, proliferation and migration assays was conducted using one-way ANOVA with Tukey's post-test in GraphPad Prism 9. Statistical analysis of cell cycle distribution was conducted using two-way ANOVA with Tukey's post-test in R (v4.3.1), using an interaction term between the cell cycle and treatment factors, independent of cell line effects (fraction ~ cycle * treatment + cell line), and the within treatment groups contrasts were compared in the *post-hoc* analysis. A p-value of ≤ 0.05 was considered statistically significant. The results are presented as means ± standard deviation (SD).

Synergy calculations for proliferation, clonogenic survival and migration assay data were performed using the SynergyFinder website (https://synergyfinder.org, accessed in February 2024). This analysis generated dose-response curves and provided Loewe synergy scores.

To evaluate the combined effects of Onalespib and external beam radiotherapy on multicellular tumor spheroid growth, the Loewe method was employed on day 14 of the experiment. A Loewe score ≥10 was considered synergistic, <10>-10 additive, and ≤ -10 antagonistic.

The tumor doubling time was determined using a modified Schwartz formula, expressed as follows: tumor doubling time = $[\ln 2 \times \Delta T]/[\ln (X_2/X1)]$, where X_1 represents the tumor size at the initial treatment day, X_2 represents the spheroid size at day 14 and ΔT denotes the time (in days) between the two measurements.

3 Results

3.1 Synergistic anticancer effects of combining Onalespib with radiotherapy on metabolic activity and cell viability

To determine cell viability of glioblastoma cells after exposure to various doses of the HSP90 inhibitor Onalespib and external radiation, metabolic activity was measured using XTT assay. The established glioblastoma cell lines U343 MG, U87 MG as well as the patient-derived glioblastoma lines U3013MG and U3024MG were exposed to Onalespib treatment at multiple doses followed by the application of radiation therapy 24 h after drug incubation, and absorbance measurement 72 h after drug treatment.

Results from both U343 MG and U87 MG revealed a significant dose-dependent decrease in cell viability and proliferation in following drug and radiation monotherapy (Figures 1A, B, D, E). Both glioblastoma cell models demonstrated a similar response to Onalespib treatment, e.g., inhibiting viability/proliferation by 47 and 44.5%, respectively, at a dose of 100 nM. U87 MG presented more sensitive to radiation, 46.4% survived a radiation dose of 4 Gy, while 68% of U343 MG cells were viable after the same dose. Furthermore, additional exposure of 25 nM resulted in a 13% and 24% reduction in the viability of U343 MG and U87 MG cells, respectively. In contrast, the patient-derived cell lines U3013MG and U3024MG showed no significant reduction in viability at low Onalespib concentrations, with only 100 nM causing a notable decrease (Figures 1G, J, left). However, both cell lines were highly sensitive to radiation, with 2 Gy reducing viability by 70.1% in U3013MG and 82% in U3024MG (Figures 1G, J, right).

The combined treatment was more effective for all established and patient-derived cell lines with the highest inhibition at the higher doses (Figures 1B, C, E, F, H, K). Synergistic combination effects, as evidenced by Loewe synergy values > 10, were observed at all drug doses >10 nM and 6 Gy of radiation. At lower radiation doses additive effects were observed except for drug concentrations ≥ 50 nM for U343 MG (Figure 1C). U87 MG demonstrated a similar pattern, with the highest synergistic values recorded at higher concentrations. However, synergistic effects were also observed at lower drug and radiation doses (Figure 1F). In patient-derived cell lines, U3013MG showed synergy at 10nM, 25 nM and 50 nM combined with 6 Gy (Figure 1I), while U3024MG exhibited synergy at 100 nM and 4Gy as well as 6 Gy (Figure 1L).

3.2 Synergistic anticancer effects of combining Onalespib with radiotherapy on clonogenicity (2D) and multicellular tumor spheroid growth (3D)

To further evaluate the effectiveness of combining radiation with Onalespib in glioblastoma clonogenic assay were performed (Figures 2A–D). Both radiation treatment and Onalespib treatment decreased cell survival in a concentration-dependent manner. Significant clonogenicity reduction was noted at 1, 2, 4, and 6 Gy. In line with the viability assays (see above), U87 MG showed an increased radiosensitivity compared to U343 MG. Further, monotreatment with 10 and 25 nM Onalespib significantly decreased to colony formation ability or U343 MG and 5,10 and 25 nM for U87 MG compared to DMSO-treated control samples (Figures 2A, B). A complete loss of colony formation was observed for 50 nM of Onalespib regardless of the delivered radiation dose (data not shown). Combination treatment of Onalespib and radiation decreased the clonogenicity even more, most pronounced at the highest drug and radiation doses (Figures 2C, D). However, even at low radiation doses, the combination treatment with 25nM

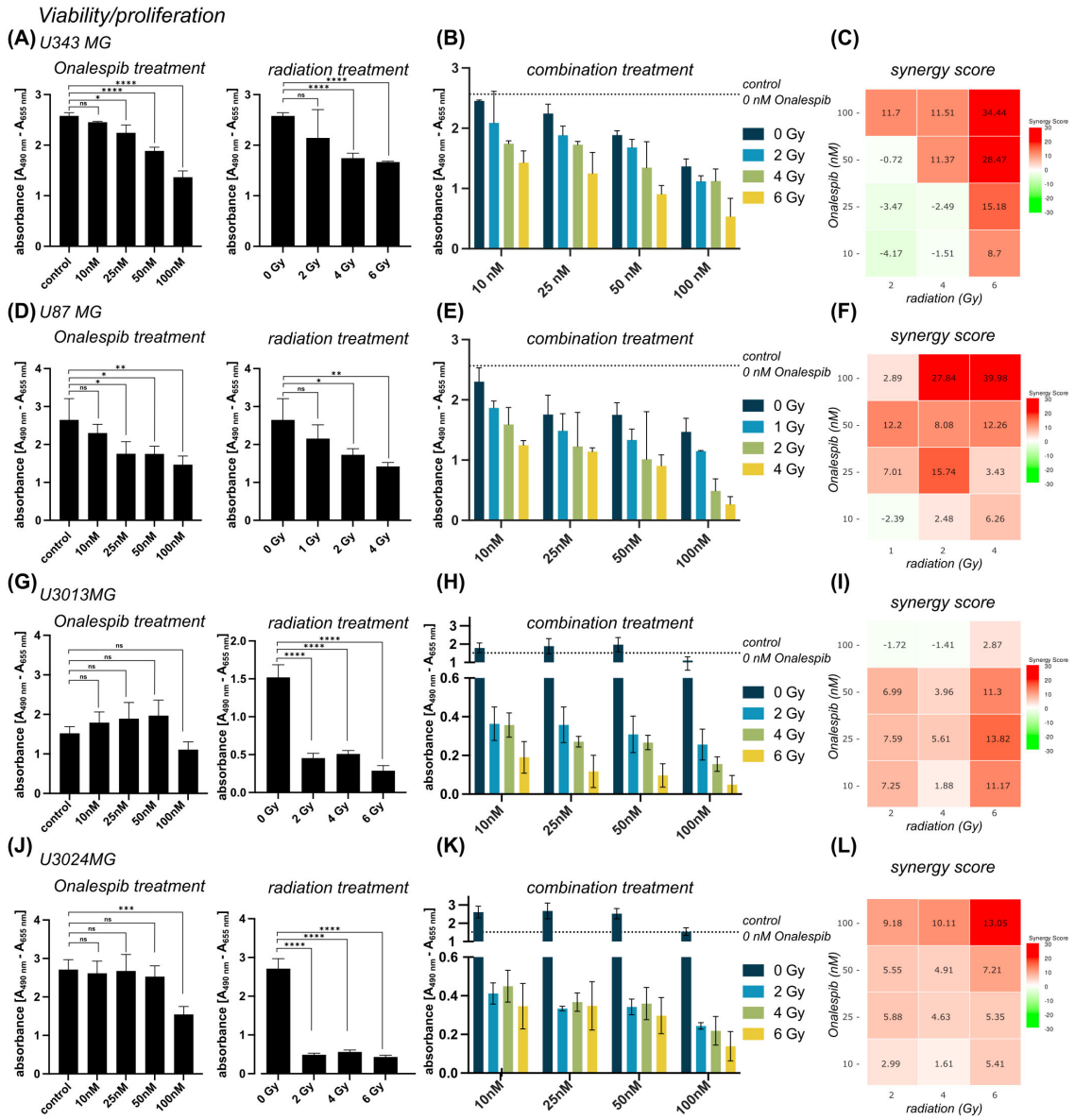

FIGURE 1
Viability of U343 MG **(A-C)**, U87 MG **(D-F)** U3013MG **(G-I)** and U3014MG **(J-L)** determined by XTT assay. **(A)** Viability (absorbance) after 0, 10, 25, 50 and 100 nM Onalespib treatment (left) and after radiotherapy with 0, 2, 4, 6 Gy (right) **(B)** combination effect of Onalespib and radiotherapy **(C)** LOEWE synergy scores **(D)** Viability (absorbance) after 0, 10, 25, 50 and 100 nM Onalespib treatment (left) and after radiotherapy with 0, 1, 2, 4 Gy (right) Right) **(E)** combination effect of Onalespib and radiotherapy **(F)** LOEWE synergy scores. **(G)** Viability (absorbance) after 0, 10, 25, 50 and 100 nM Onalespib treatment (left) and after radiotherapy with 0, 2, 4, 6 Gy (right) **(H)** combination effect of Onalespib and radiotherapy **(I)** LOEWE synergy scores **(J)** Viability (absorbance) after 0, 10, 25, 50 and 100 nM Onalespib treatment (left) and after radiotherapy with 0, 2, 4, 6 Gy (right) **(K)** combination effect of Onalespib and radiotherapy **(L)** LOEWE synergy scores. Data plotted as means ± standard deviation. One-way ANOVA with Tukey's post-test ns (not significant), *($p < 0.05$), **($p < 0.01$), ***($p < 0.001$) and ****($p < 0.0001$).

Onalespib was extremely potent. A clinically relevant radiation dose of 2 Gy in combination with 25nM Onalespib reduced the colony formation by 78.2% and 83.5% for U343 MG and U87 MG, respectively.

To mimic *in vivo* conditions, the efficacy of the drug and radiation treatment was tested in multicellular 3D tumor spheroid model (Figures 2E, F). Interestingly, the U343 MG and U87 MG glioblastoma spheroids exhibited less sensitivity compared to the previously evaluated 2D models. In line with the 2D models however, combined treatment with Onalespib and radiation resulted in concentration dependent additional inhibition of growth compared to individual treatments. The *in vitro* tumor spheroid doubling times for the different Onalespib treatments and radiation doses are summarized in Table 1. Untreated U343 MG and U87 MG tumor spheroids exhibited doubling times of 3.34 and 2.47 days, resulting in a volumetric increase of 1386% and 3720% after 14 days, respectively. Treatment with 250 nM Onalespib and 6 Gy radiation was able to significantly reduce proliferation and increase the doubling time to 67.31 and 26.23 days, respectively, corresponding to a volume increase of 14% and 41%.

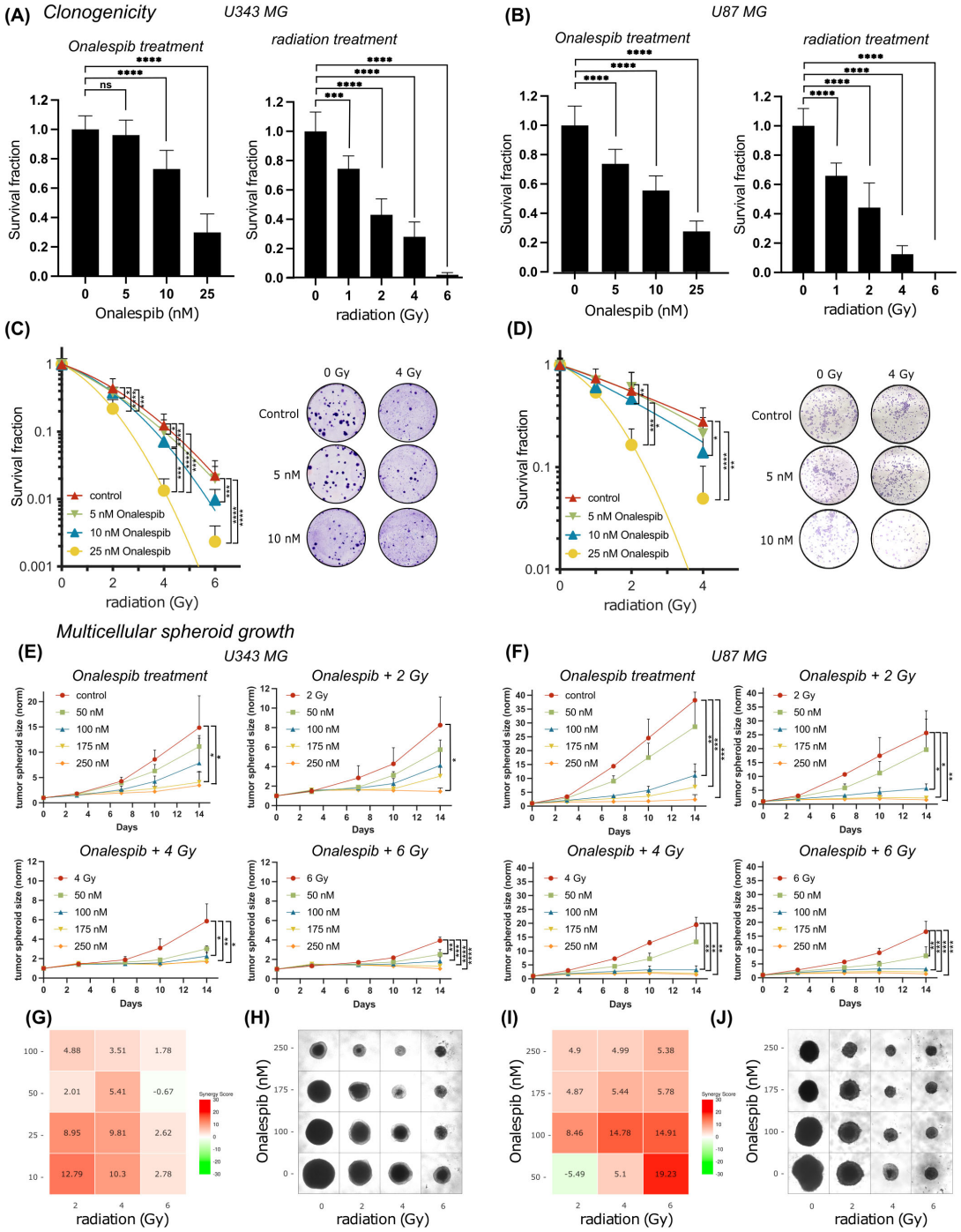

FIGURE 2
Colony formation and multicellular spheroid growth of U343 MG and U87 MG glioblastoma cells. Survival fraction of Onalespib and radiation treated U343 MG **(A)** and U87 MG **(B)** Survival fraction of Onalespib and radiation combination treatment of U343 MG **(C)** and U87 MG **(D)**. Representative images of the colonies of the monotreatments and the combined treatments of Onalespib and radiation. Onalespib monotherapy and combination therapy with radiation in 3D spheroid model of U434 MG **(E)** and U87 MG **(F)**. Graphs display the normalized spheroid volume (mm3) over time, (means ± standard deviation, n ≥ 3). LOEWE synergy scores for U34mg **(G)** and U87 MG **(I)**. Representative images of the U343 MG and U87 MG multicellular tumor spheroids at the endpoint of the assay are shown in **(H, J)**, respectively. Data plotted as means ± standard deviation, n ≥ 3. One-way ANOVA with Tukey's post-test ns (not significant), *($p < 0.05$), **($p < 0.01$), ***($p < 0.001$) and ****($p < 0.0001$).

Synergy calculations performed 14 days post treatment exposure, where a LOEWE synergy score of >10 indicated synergy, showed potentiating synergistic effects for several combinations of Onalespib (10 and 25 nM) and 4 and 6 Gy. This observation is also reflected in the glioblastoma spheroid images in Figures 2H, J.

To further characterize the multicellular tumor spheroids, we quantified live cells by labeling dead cells with trypan blue staining

10.3389/fonc.2025.1451156

TABLE 1 U343 MG and U87 MG tumor spheroid doubling time (TDT, days) and tumor spheroid volume (V) increase (%) after treatment with Onalespib (nM) and radiotherapy (Gy) on day 14.

	0 nM		50 nM		100 nM		175 nM		250 nM	
U343 MG	TDT (days)	V (%)	TDT (days)	V (%)	TDT (days)	V (%)	TDT (days)	V (%)	TDT (days)	V (%)
0 Gy	3.34	1386	3.74	1013	4.05	823	5.47	420	7.26	246
2 Gy	4.17	770	5.15	474	6.35	313	8.13	203	24.18	45
4 Gy	5.09	487	8.18	201	11.01	127	17.01	70	33.76	31
6 Gy	6.58	294	9.76	152	14.88	83	32.51	32	67.31	14
U87 MG	TDT (days)	V (%)	TDT (days)	V (%)	TDT (days)	V (%)	TDT (days)	V (%)	TDT (days)	V (%)
0 Gy	2.47	3720	2.68	2770	4.14	780	5.47	420	9.43	160
2 Gy	2.78	2460	2.83	2320	5.18	470	11.36	121	18.92	61
4 Gy	3.03	1850	3.48	1232	7.61	227	13.39	96	19.98	57
6 Gy	3.21	1560	4.35	693	7.77	219	15.33	80	26.23	41

three days after treatment with monotherapies of 25, 50, and 100 nM Onalespib and 2 or 4 Gy radiation on U87 MG, as well as patient-derived U3013MG and U3024MG tumor cell spheroids. No significant differences in spheroid size were observed across treatments at that timepoint. Interestingly, although the spheroid sizes remained comparable, the live cell/dead cell count within the spheroids varied. A strong correlation was observed between higher treatment doses and an increase in the dead cell population, Supplementary Figure 2A.

Additionally, we assessed spheroid-forming efficiency through limiting dilution assays using U87 MG, U3013MG, and U3024MG cells. These cell lines were treated with 25, 50, and 100 nM Onalespib, 2 or 4 Gy radiation, and combination therapies. All untreated controls of the three cell lines efficiently formed spheroids. However, increasing doses of both the drug and radiation led to a dose-dependent reduction in spheroid-forming capacity, Supplementary Figure 2B.

3.3 Interrupted migration potential of glioblastoma cells treated with Onalespib and radiotherapy

Wound healing assays (scratch assays) were performed to explore the impact of Onalespib and radiation treatment as well as their combination on the migratory capacity of U343 MG and U87 MG cells (Figure 3).

In both glioblastoma cell lines, monotreatment with Onalespib as well as radiation resulted in a concentration dependent reduction in cell migration compared to untreated control cells (Figures 3A, E). Generally, U343 MG cells (Figures 3A, B) migrated slightly slower as U87 MG (Figures 3E, F). Representative images of the U343 MG and U87 MG after the mono- and combination therapies are shown in Figures 3D, H, respectively. At the 12 h post treatment time point U343 MG had migrated and closed the wound by 72% while U87 MG had covered 86% of the induced wound. A radiation dose of 2 Gy reduced the migration potential significantly in U343 MG cells and augmented with increasing drug concentrations. Synergy scores for all drug and radiotherapy combinations are summarized in Figures 3C, G and Supplementary Figure 1. Surprisingly, 2 Gy had no significant effect on U87 MG cells measured at 12 and 24 h. The Onalespib and radiation combination effect was most clear in the higher combination treatment groups. While untreated control cells had closed the gap at 24 h, U343 MG cells treated with 50 nM Onalespib and 6 Gy radiation, had only migrated 44% and U87 MG 77% of that distance.

3.4 Accumulation of DNA double-strand breaks glioblastoma cells subjected to Onalespib and radiation combination treatments

We assessed DDR by measuring DNA double-strand breaks (DSBs) in U343 MG and U87 MG glioblastoma cells treated with Onalespib, radiation, or their combination using confocal microscopy (Figures 4A–C). The number of 53BP1 and γH2AX foci, both markers for DSBs, were counted in the cell nuclei. In both glioblastoma cell lines, untreated cells exhibited a low number of 53BP1 and γH2AX foci per nucleus, 2.5 53BP1 foci/cell and 0.4 γH2AX foci/cell for U343 MG and 2 53BP1foci/cell and 0.3 γH2AX foci/cell for U87 MG (Figure 4, Supplementary Figures 3A–F).

In U343 MG cells, both Onalespib and 2 Gy radiation monotherapies significantly increased the number of 53BP1 and γH2AX foci, with Onalespib alone inducing more foci than 2 Gy of radiation alone. The combination of 2 Gy radiation and Onalespib further increased the number of DNA damage foci. Increasing the radiation dose to 6 Gy in combination with Onalespib dramatically elevated 53BP1 and γH2AX foci expression, indicating extensive DSB accumulation and reduced repair efficiency. Notably, cells treated with 6 Gy radiation, both alone and in combination with Onalespib, exhibited a high number of foci with about 14 53BP1 foci/cell, reflecting unrepaired DSBs and an impaired repair capacity (Figures 4A, B). The minor difference observed between

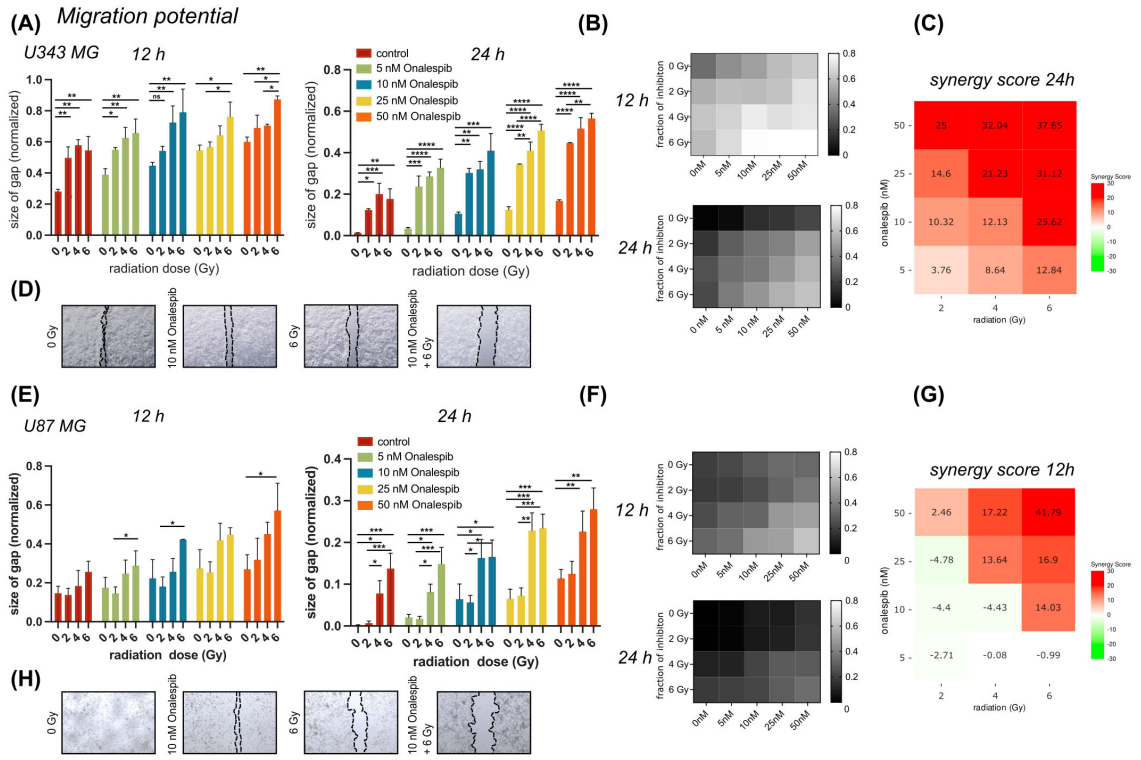

FIGURE 3
Wound healing/migration potential of U343 MG and U87 MG glioblastoma cells. **(A)** Effect of 0, 5,10, 25 or 50 nM of Onalespib combined with 0, 2, 4 or 6 Gy on U343 MG after 12 and 24 hours. **(B)** Heat map of mono- and combination treated U343 MG cells after 12 and 24 h. **(C)** 24 h U343 MG LOEWE synergy scores. **(D)** Representative images of scratched area. **(E)** Effect of 0, 5,10, 25 or 50 nM of Onalespib combined with 0, 2, 4 or 6 Gy on U87 MG after 12 and 24 hours. **(F)** Heat map of mono- and combination treated U343 MG cells after 12 and 24 h. **(G)** 12 h U87 MG LOEWE synergy scores. **(H)** Representative images of scratched area. Data plotted as means ± standard deviation, n ≥ 3. One-way ANOVA with Tukey's post-test ns (not significant), *(p < 0.05), **(p < 0.01), ***(p < 0.001) and ****(p < 0.0001).

the group treated with 6 Gy alone and the group treated with a combination of 6 Gy and Onalespib may be attributed to the U343 MG cells reaching their maximum threshold for DNA repair capacity, as reflected in both 53BP1 and γH2AX foci. When cells are exposed to high levels of radiation, their ability to repair damaged DNA can become overwhelmed.

In U87 MG cells, Onalespib monotherapy led to a minor increase in both γH2AX and 53BP1 foci. However, 2 Gy radiation significantly elevated the number of the foci compared to Onalespib treatment alone. The combination of 2 Gy radiation and Onalespib further enhanced the DSB repair response. Increasing the radiation dose to 6 Gy combined with Onalespib resulted in a dramatic increase in remaining 53BP1 foci (8 foci/cell), indicating a failure of U87 MG cells to effectively repair the extensive DNA damage caused by the combination therapy (Figures 4C, D). While generally lower γH2AX foci counts were observed across all treatment groups, the differences closely mirrored the variations in 53BP1 foci between groups in both cell lines. Representative images of the co-expression of 53BP1 and γH2AX are shown in Supplementary Figure 3 for both U343 MG and U87 MG cells. Both proteins were simultaneously activated by radiation and Onalespib, with foci appearing in close proximity within the nucleus, suggesting potential co-localization. However, some foci, mainly 53BP1, were also found in distinct nuclear regions.

To further substantiate the findings from confocal microscopy, we performed Western blot analysis of U343 MG cells to evaluate γH2AX levels in the control, radiotherapy, Onalespib, and combination treatment groups. The results, displayed in Supplementary Figure 3F (right), revealed that, as expected, γH2AX expression was significantly increased in the radiotherapy-treated group, indicating pronounced DNA damage. Treatment with Onalespib alone led to a rise in γH2AX levels compared to the control. The combination therapy also resulted in elevated γH2AX levels, albeit to a slightly lesser extent than the radiotherapy group alone.

Comparing U343 MG and U87 MG cells' DSB repair capacity in response to Onalespib and X-rays mono and combination therapy showed that, in both cell lines, Onalespib effectively decreased the cell DSB repair capacity in combinational treatment groups via inducing complex DSBs.

3.5 Alterations in cell cycle distribution of glioblastoma cells subjected to Onalespib and radiation combination treatments

We employed flow cytometric analysis to investigate alterations in cell cycle distribution of the cell lines U343 MG and U87 MG after exposure (48 h) to 100 nM Onalespib, 2 and 4 Gy radiation

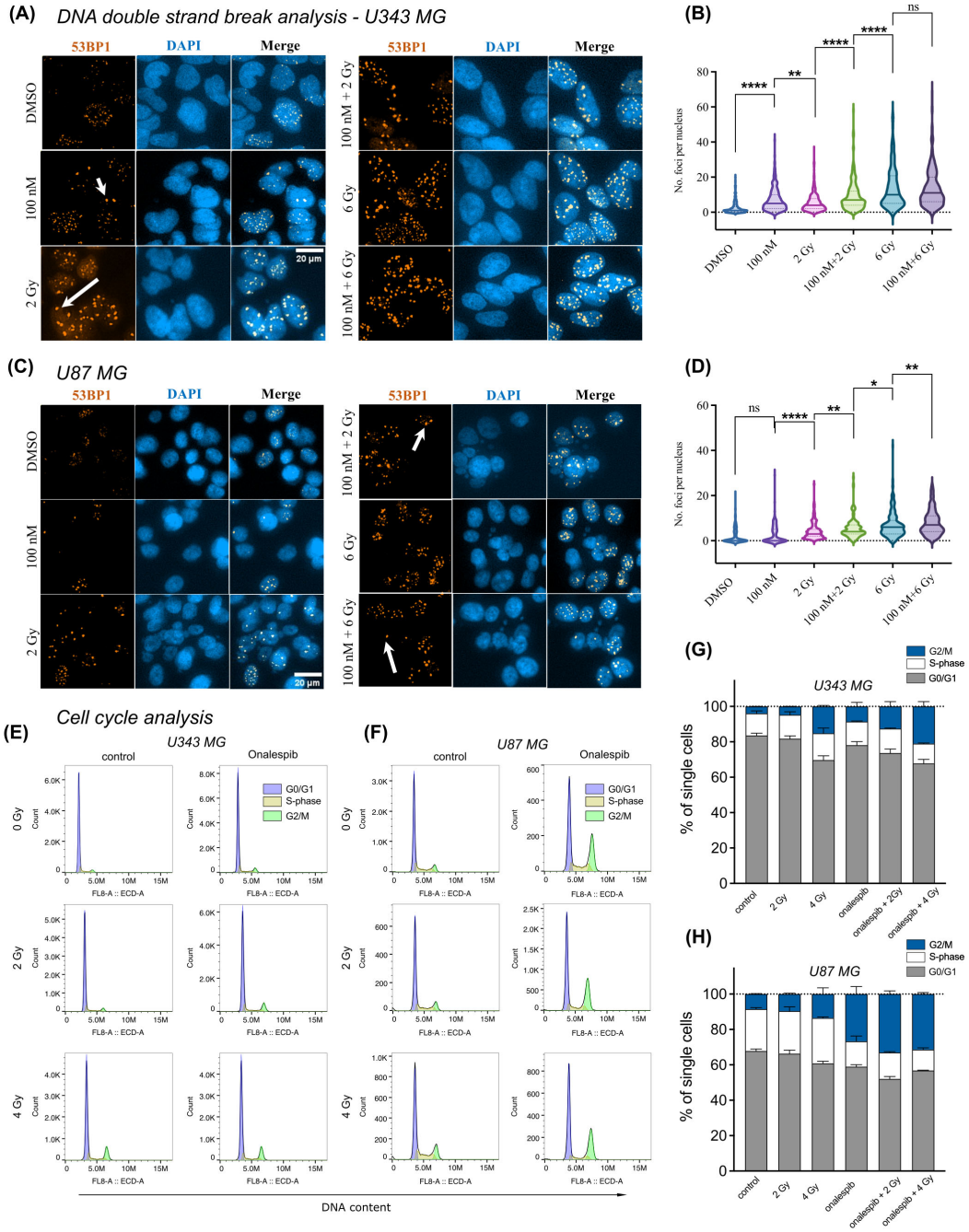

FIGURE 4
Distribution of 53BP1 foci analysis of U343 MG and U87 MG cells. **(A)** Confocal microscopy images of U343 MG cells treated with 100 nM Onalespib and 2 and 6 Gy radiation. Arrows indicate representative instances of counted 53PP1 foci. **(B)** Violin plots of U343 MG, number of 53BP1 foci per cell. **(C)** Confocal microscopy images of U87 MG cells treated with 100 nM Onalespib and 2 and 6 Gy radiation. Arrows indicate representative instances of counted 53BP1 foci. **(D)** Violin plots of U87 MG, number of 53BP1 foci per cells. Cell cycle analysis by flow cytometry of **(E)** U343 MG and **(F)** U87 MG cells 48 h after exposure of a single dose of 2 Gy, 4 Gy radiation and/or Onalespib, representative histograms. Average cell cycle distribution of **(G)** U343 MG and **(H)** U87 MG. Data plotted as means ± standard deviation, n = 2. ns (not significant), *($p < 0.05$), **($p < 0.01$) and ****($p < 0.0001$).

and their combinations (Figures 4E–H). Our findings show distinct changes in cell cycle phases compared to untreated controls. Specifically, a 4 Gy radiation dose reduced the percentage of cells in the G0/G1 phase from initially 83.5% to 70% in U343 MG cells and from 68% to 60% in U87 MG cells. At the same time, there was an increase in the number of cells in the G2/M phase for both investigated glioma cell lines. Combination treatment with Onalespib enhanced this effect, resulting in 21% of U343 MG cells and 31% of U87 MG cells being arrested in the G2/M phase. Additionally, we observed that combination of Onalespib and radiotherapy treatment reduced the percentage of cells in the S-phase compared to the untreated control samples, with the most

pronounced effect seen in U87 MG cells (Figure 4H), but not in U343 MG cells. These changes were statistically significant in a two-way ANOVA model (Supplementary Table 1).

We also studied p21 expression by Western blotting (Supplementary Figure 3F left), which confirmed the findings from the cell cycle flow analysis and aligned with the PEA analysis presented in the next paragraph. HSP90 inhibition by Onalespib suppressed the expression of CDKN1A (p21), a crucial regulator of cell cycle progression at G1 and S phase. However, both radiotherapy alone and in combination with Onalespib resulted in increased p21 expression, suggesting the initiation of cell cycle arrest following DNA damage and activation of cell death pathways.

3.6 Proteomic analysis of glioblastoma cells subjected to Onalespib and radiation combination treatments

The proteomic analysis conducted on U343 MG cells treated with Onalespib, radiation, and their combination revealed significant alterations in protein expression profiles. Hierarchical cluster analysis, shown in Figure 5 and Supplementary Figure 4, depicted distinct differences in protein expression among the treatment groups compared to control cells. Notably, Onalespib treatment primarily led to the downregulation of most tested proteins, while radiotherapy exhibited an overall inducing effect on protein expression. Combination therapy functionally resembled radiation therapy, except for proteins involved in necrosis, c-Flip, caspase and procaspase activity which were upregulated in comparison to radiation therapy alone.

Of particular interest were the changes in protein expression associated with cancer development, including pathways related to growth signaling, replicative potential, angiogenesis, metastasis, invasion, and resistance to cell death. In agreement with the Western blot analysis, Onalespib-mediated HSP90 inhibition decreased CDKN1A (p21) expression. However, when radiotherapy was administered, either on its own or together with Onalespib, there was an increase in p21 levels, indicating the induction of cell cycle arrest due to DNA damage and the activation of cell death mechanisms.

Additionally, FR-gamma (Folate receptor 3, FOLR3), a folate receptor essential for DNA synthesis, was suppressed by Onalespib. On the other hand, radiotherapy strongly induced its expression, potentially indicating an increased demand for folate during DNA damage response processes. However, the expression level within the combination treatment group was lower than with radiotherapy alone, suggesting that HSP90 downregulation by Onalespib reduces folate uptake. Folic acid can mitigate radiation-induced DNA damage by enhancing DNA synthesis and repair, as well as functioning as a radical scavenger. Similarly, FR_alpha (Folate receptor 1, FOLR1) was upregulated after exposure to radiation but decreased under HSP90 inhibition. This decrease may be beneficial, as elevated FOLR1 levels correlate with aggressive tumor characteristics, diminished response to chemoradiotherapy, and poorer overall survival rates.

VEGFA, a key regulator of angiogenesis, was strongly downregulated by HSP90 inhibition and further suppressed by radiotherapy. In line with these results, the combination treatment markedly decreased its expression, indicating a potential inhibition of tumor vascularization and growth.

Furthermore, TRAIL, a cytokine inducing apoptosis, was reduced by both HSP90 inhibition and radiotherapy individually. Apart from apoptotic cell death, TRAIL can mediate a programmed form of caspase-independent cell death known as necroptosis. Combination treatment significantly upregulated TRAIL expression, suggesting enhanced activation of tumor cell death mechanisms.

The functional analysis of the differentially expressed proteins (Figure 5B) identifies ontological pathways relevant to cancer development and treatment response which the proteins are involved in. Downregulation of proteins involved in growth factor-mediated signaling might indicate inhibition of cell proliferation and survival pathways, potentially impeding tumor progression. Conversely, upregulation of proteins involved in IL-4 and IL-13 signaling might indicate immune response modulation, possibly enhancing anti-tumor immunity or altering the tumor microenvironment. Induction of proteins involved in p53-induced cell cycle arrest pathways can imply activation of DNA damage response mechanisms, likely contributing to cell cycle arrest and inhibition of tumor cell proliferation. Additionally, upregulation of proteins involved in caspase activation suggests increased apoptotic cell death, potentially enhancing the anti-tumor effects of the treatments.

4 Discussion

GBM is characterized by HSP90 overexpression, aggressive growth, and poor prognosis (31). In cancer cells, the mechanisms of the HSP90 chaperone system differ significantly from those in normal cells. The rapid proliferation rate and reduced quality control in protein synthesis lead to increased and constant cellular stress. HSP90 stabilization has been developed as a coping mechanism, and HSP90 expression is 2- to 10-fold higher in cancer cells compared to normal cells, aiding in cell survival and function during tumorigenesis (20, 32). There is a connection between proliferation rate and expression level, and therefore high expression of HSP90 is associated with a poor prognosis in clinical treatment.

Due to the high innate resistance of GBM to standard treatments, it is crucial to find new agents that re-sensitize cancer cells to improve treatment efficacy. Combination therapy can enhance efficacy, reduce toxicity, and lower the incidences of drug resistance by exploiting the synergy of action (33). To date, the combination of HSP90 inhibitors with chemotherapy (27), targeted agents (34, 35), or immunotherapy (36) has demonstrated enhanced antitumor effects, summarized in (37).

In this study, we investigate the efficacy of Onalespib in combination with radiotherapy in two patient-derived glioblastoma cell lines U3013MG and U3024MG as well as the established cell lines U343 MG and U87 MG. Onalespib targets HSP90, overexpressed in cancer cells, suggesting selective targeting of tumor cells while sparing healthy brain tissue. Its ability to cross

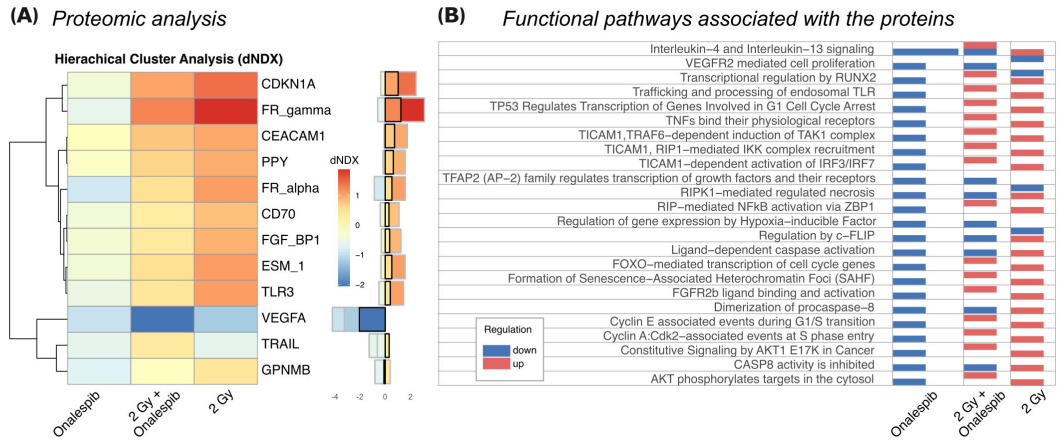

FIGURE 5
(A) The 12 most differentially expressed proteins between treatments (SD>0.5). Hierarchical clustering analysis illustrates the most prominent alterations in protein expression levels observed in U343 MG cells treated with radiation, Onalespib, and their combination, relative to untreated control cells. The difference in log(expression) to control (dNDX) is indicated, with positive values highlighted in red, indicating higher expression compared to control, and negative values shown in blue, indicating lower expression. Middle) Absolute dNDX values for each treatment group relative to the control are depicted using the same color scale as in panel **(A)**. The black square designates the combination treatment group. **(B)** Functional analysis indicating the main ontological pathways where the differentially expressed proteins are involved, and the overall direction of protein regulation. Note that up and down-regulation of specific proteins do not necessarily imply induction or suppression of the functional pathway which the protein is involved in.

the blood-brain barrier and achieve higher concentrations in brain tissue further supports its potential in brain cancer treatment.

While early clinical trials showed a favorable toxicity profile, with mild adverse events such as diarrhea, fatigue, and nausea, they did not focus on neurotoxicity or radiation therapy interactions (19, 21, 38, 39).

Our findings indicate that the combination of Onalespib with radiotherapy improves anti-tumor effects by decreasing cell viability, proliferation, and clonogenicity in the assessed cell lines grown in monolayer cell culture in a concentration-dependent manner (Figures 1, 2).

Further, multicellular tumor spheroid models, which mimic the *in vivo* microenvironment, such as hypoxic areas within avascular tumors, offer a valuable platform for pre-clinical drug and radiotherapy testing. This is a highly relevant model system in these investigations since lack of oxygen is associated with resistance to radiotherapy. HSP90 is upregulated in GBM spheroid models facilitating stem-like characteristics such as self-renewal, differentiation, tumorigenicity, and drug resistance. Our study shows that GBM tumor spheroids were more resistant to treatment, requiring higher concentrations compared to 2D experiments. However, the proliferation and doubling time of both U87 MG and U343 MG tumor spheroids were significantly reduced by Onalespib monotreatment, with combination treatment showing the most potent effects. Additionally, limiting dilution analysis and live/dead staining indicated a concentration-dependent decrease in spheroid formation capacity and an increased percentage of dead cells within the spheroids (Supplementary Figure 2). These findings are in line with other reports, where e.g., the HSP90 inhibitor (NVP) AUY922 shows radiosensitizing effects on GBM spheroid models (40). Also, the HSP90 inhibitor NXD30001, when combined with radiotherapy, significantly inhibited tumor growth and prolonged the median survival in an EGFR-driven genetically engineered mouse model of GBM (41).

In addition, our data demonstrate that combination therapy affects the rate of wound healing in a dose-dependent manner. Interestingly, HSP90 has previously been identified to efficiently decrease migration and invasion of human GBM cell lines by interaction with Ephrin type-A receptor 2 (EPHA2) (42, 43), a protein that was not affected in the performed PEA analysis.

One suggested mechanism for Onalespib's potentiation on the radiotherapy's effect could be the disruption of DNA repair. Radiation induces DNA double breaks (DSBs), followed by increased activation of DNA damage repair mechanisms. Counting γH2AX and 53BP1 foci in single cells serves as a sensitive biomarker for DSB presence and the cell's capacity for DSB repair after exposure to genotoxic agents. H2AX activation and 53BP1 recruitment to DSB sites, facilitated by its Tudor domain, plays a critical role in the DSB repair process by forming repair foci and activating cell cycle checkpoints to provide more time for repair. Quantifying these foci through nucleus immunofluorescence staining and microscopy reveals the extent of DNA damage and repair activity within individual cells.

Our finding demonstrates that Onalespib can increase the amount of DSBs as measured by γH2AX and 53BP1 foci in monotherapy, an effect that could be attributed to the inhibition of proteins involved in various DNA damage response pathways. These pathways include upstream checkpoint signaling, double-strand break repair by homologous recombination (HR), non-homologous end joining, as well as processes such as cross-link repair and DNA replication. Overall, the combination therapy led

to lower expression of proteins than in radiotherapy alone, among which several are involved in radiation damage response such as CDKN1A (p21).

The combination treatment of 6 Gy and 100 nM Onalespib resulted in a significant increase in 53BP1 foci in U343 MG but not in U87 MG cells, possibly due to differences in the DNA repair capacity. U87 MG has previously been described as resistant to TMZ treatment due to increased cell cycle arrest and DNA repair response. Notably, Onalespib has been found to effectively deplete key HR proteins, like CHK1 and RAD51, impairing HR repair and making patient-derived glioma stem cell lines more susceptible to radiation and TMZ (15). Studies in zebrafish bearing glioma xenografts have also shown the synergistic effects of Onalespib in combination with the GBM standard treatment, TMZ. Earlier *in vitro* and *in vivo* studies also showed that Onalespib can enhance the TMZ treatment (20). A significant limitation of radiation therapy is its reduced efficacy in hypoxic regions; however, HSP90 inhibition by NXD30001 and NVP-AUY922 has been shown to increase radiosensitivity in hypoxic CD133-positive subpopulations glioblastoma spheroids (10, 40), likely due to HIF-1α inhibition.

Proteomic analysis of U343 MG demonstrated Onalespib's association with downregulation of proteins involved in several functional pathways, whereas radiation therapy affected both up and down-regulation of these proteins.

Notably, CDKN1A (p21), which was found upregulated due to the combination treatment in our study, suggests interference with pathways critical for tumor suppression and may explain the synergetic effect of Onalespib to radiation. In literature, p21 remains still contradictory with the function either as an oncogene or as a tumor suppressor (44, 45). p21 acts as a regulatory checkpoint in cell division, leading to cell cycle arrest, increased levels of p53, and the activation of DNA repair mechanisms (46). It facilitates this arrest by binding to and inhibiting the activity of CDK1 and CDK2, thereby preventing progression from G1 to S phase and from G2 to mitosis. Downregulation of CDK1 contributes to G2 phase arrest and reduced cell proliferation, consistent with our findings of G2/M phase accumulation in the combination treatment groups. Interestingly, high LET radiation can induce CDKN1A foci at the DSB site that persist for several hours suggesting that CDKN1A can directly mediated interact with proteins involved in DDR (47).

Aggressive tumors are known to produce growth factors that promote the growth of blood vessels (angiogenesis), making endothelial cells proliferate and become more resistant to radiation. VEGFA, a critical factor in promoting angiogenesis, was significantly reduced by both HSP90 inhibition and radiotherapy alone. However, when used together, the combination treatment resulted in an even greater decrease in VEGFA expression, indicating a stronger inhibition of tumor blood vessel formation.

Additionally, TRAIL was slightly lowered by both HSP90 inhibition with Onalespib and radiotherapy independently. Yet, the combination treatment notably increased TRAIL expression. TRAIL plays a crucial role in regulating various biological responses in both cancer and normal cells, including the induction of programmed cell death mechanisms as apoptosis and necroptosis (48). The observed elevated levels of TRAIL in the combination group suggest a heightened activation of cell death pathways and might explain the observed synergistic effects. Previously, HSP90 inhibition by SNX-2112 was reported to enhance TRAIL-induced cytotoxicity on cervical cancer cells (49). This suggests that combining HSP90 inhibition with TRAIL could, besides of combination with radiotherapy, represent a novel treatment strategy, which would involve overcoming apoptosis resistance (49). Current research is directed towards developing anticancer agents that activate TRAIL, as it selectively targets cancer cells with minimal damage to normal cells (50).

The full list of altered protein expression in the Onalespib and combination treated groups (Supplementary Figure 4) may also reveal potential therapeutic targets for future investigation. For example, radiotherapy increased the expression of the immune checkpoint molecule CEACAM1. A recent study combining radiotherapy with CEACAM1 inhibitors resulted in strong and enduring immune responses against murine glioma, leading to extended survival in some mice (51). Consequently, targeting CEACAM1 could offer an effective immunotherapy strategy for the treatment of glioma.

The here presented *in vitro* analysis of Onalespib and radiotherapy demonstrated significant reductions in tumor cell growth, migration potential, and disruption of DNA double-strand break (DSB) damage response. These findings highlight the potential efficacy of this combination in treating GBM.

Despite the promising results, this study has several limitations. One significant limitation is the use of the U87 MG cell line obtained from ATCC, which has been shown to differ genetically from the original U87 MG line established at Uppsala University in the 1960s (52). Although the ATCC U87 MG line is likely to be a bona fide human glioblastoma cell line of unknown origin, it is widely used in glioma research due to its well-known characteristics and tumorigenic properties. However, the differences between ATCC U87 MG and the original glioma model suggest caution when comparing findings with studies that do not specify the origin of their U87 MG cells. Future studies should include additional, well-characterized glioma organoid models to strengthen the generalizability and applicability of the results. Additionally, while our OLINK proteomic analysis yielded valuable insights, it remains exploratory. Confirmation of key proteins, particularly those with potential as biomarkers or therapeutic targets, through more traditional methods like Western blotting, is essential for validation. Also, the proteomic investigation represents only a snapshot of the underlying processes and further studies are needed to elucidate the functional implications of these proteomic changes and their potential therapeutic implications for the treatment of GBM. In previous *in vivo* studies conducted by our group, the combination of Onalespib and radiation in models of colorectal, squamous cell carcinoma (12), and neuroendocrine (14) tumors did not result in adverse effects such as behavioral changes, loss of appetite, or weight loss. However, further investigation into Onalespib's impact on tumor growth and normal brain tissue is essential. Preclinical studies using neural stem or progenitor cells should assess survival, differentiation, and neurogenesis to evaluate potential neurotoxic effects. These studies are crucial to ensure

Onalespib's translational potential for brain cancer treatment, supported by a robust safety profile.

We are encouraged by our promising results, which suggest that the combination of radiation treatment and HSP90 inhibition could be an effective therapeutic option for patients with GBM, particularly those resistant to standard treatments. The synergistic effects of this combination hold promise for improving treatment efficacy and achieving better clinical outcomes. However, further investigations are required to determine optimal dosing and to identify the toxicity profile of Onalespib in a more clinically relevant setting.

Data availability statement

The datasets generated for this study are available on request to the corresponding author.

Ethics statement

The primary glioma cell lines used in this study were obtained from the HGCC sample collection which was approved by the Uppsala regional ethical review board (2007/353); informed consent was obtained from all subjects included.

Author contributions

JU: Data curation, Formal analysis, Investigation, Visualization, Writing – original draft, Writing – review & editing. MH: Data curation, Formal analysis, Investigation, Visualization, Writing – original draft, Writing – review & editing. EP: Data curation, Formal analysis, Investigation, Supervision, Visualization, Writing – original draft, Writing – review & editing. AS: Data curation, Formal analysis, Investigation, Writing – review & editing. JB: Data curation, Formal analysis, Writing – review & editing. BS: Writing – review & editing. HB: Data curation, Formal analysis, Investigation, Methodology, Writing – review & editing. CM: Conceptualization, Data curation, Formal analysis, Investigation, Methodology, Software, Visualization, Writing – review & editing. DS: Conceptualization, Data curation, Formal analysis, Funding acquisition, Investigation, Methodology, Project administration, Resources, Supervision, Validation, Visualization, Writing – original draft, Writing – review & editing.

Funding

The author(s) declare financial support was received for the research, authorship, and/or publication of this article. Funding support was received from the Swedish Childhood cancer foundation (PR2023-0111 and FT2023-0023), the Swedish Cancer society (21 0371 FE, 22 2365 Pj, 24 3787 Pj), Centre for Research & Development, Region Gävleborg, Åke Wibergs foundation and Erik, Karin och Gösta Selanders foundation.

Acknowledgments

Patient-derived glioblastoma cells were acquired from the Human Glioblastoma Cell Culture resource (www.hgcc.se) at the Dept. of Immunology, Genetics and Pathology, Uppsala University, Uppsala, Sweden. We thank Dr. Tobias Bergström for all practical advice and the help with the patient-derived cell line culture. Dosimetry and radiation treatment was performed by Medical Physicist Dr. Ulf Isacsson at the Uppsala University Hospital, and we thank him for his expertise and support. Confocal microscopy and flow cytometry was performed at the BioVis facility, Uppsala University. We thank Dr. Olga Vorontsova for the help with the Western blotting and Dr. Tabassom Mohajershojai for the help with preparing the Proximity Extension Assay lysates.

Conflict of interest

The authors declare that the research was conducted in the absence of any commercial or financial relationships that could be construed as a potential conflict of interest.

Generative AI statement

The authors declare that Generative AI was used in the creation of this manuscript. ChatGPT (version 4.0), a generative AI language model developed by OpenAI, was used for language editing.

Publisher's note

Supplementary material

The Supplementary Material for this article can be found online at: https://www.frontiersin.org/articles/10.3389/fonc.2025.1451156/full#supplementary-material

SUPPLEMENTARY FIGURE 1
Wound healing/migration potential of U343 MG and U87 MG glioblastoma cells. **(A)** 12 h U343 MG LOEWE synergy scores. **(B)** 24 h U343 MG LOEWE synergy scores. **(C)** 12 h U87 MG LOEWE synergy scores. **(D)** 24 h U87 MG LOEWE synergy scores.

SUPPLEMENTARY FIGURE 2
Live/dead cell percentage and limiting dilution assay. **(A)** U87 MG, U3013MG and U3024MG multicellular spheroids were exposed to Onalespib and radiation and their combination. Data plotted as means ± standard deviation. One-way ANOVA with Tukey's post-test *($p < 0.05$), **($p < 0.01$), ***($p < 0.001$) and ****($p < 0.0001$). **(B)** Limited dilution assay of U87 MG, U3013MG and U3024MG treated with a combination of 25nM,

50nM and 100nM Onalespib and 4 Gy radiation. Spheroid formation efficiency was elevated 3 days after plating. The natural log fraction of non-responding wells was plotted on a linear scale versus the cell density per well.

SUPPLEMENTARY FIGURE 3
Distribution of γH2AX foci analysis of U343 MG and U87 MG cells. **(A)** Confocal microscopy images of U343 MG cells treated with 100 nM Onalespib and 2 and 6 Gy radiation. Arrows indicate representative instances of counted γH2AX foci. **(B)** Violin plots of U343 MG, number of γH2AX foci per cell. **(C)** Representative images of co-expression 53BP1 and γH2AX foci of U343 MG cells treated with 100 nM Onalespib and 6 Gy radiation. **(D)** Confocal microscopy images of U87 MG cells treated with 100 nM Onalespib and 2 and 6 Gy radiation. Arrows indicate representative instances of counted γH2AX foci. **(D)** Violin plots of U87 MG, number of γH2AX foci per cells. **(F)** Representative images of co-expression 53BP1 and γH2AX foci of U87 MG cells treated with 100 nM Onalespib and 6 Gy radiation. **(G)** Western blot analysis of CDKN1A (p21) and γH2AX after exposure of Onalespib, radiation and their combination.

SUPPLEMENTARY FIGURE 4
Left: Hierarchical clustering analysis illustrates the most prominent alterations in protein expression levels observed in U343 MG cells treated with radiation, Onalespib, and their combination, relative to untreated control cells. The difference in log(expression) to control (dNDX) is indicated, with positive values highlighted in red, indicating higher expression compared to control, and negative values shown in blue, indicating lower expression. Middle: The standard deviation between treatments, where a large standard deviation indicates differentially expressed proteins of interest. The boxes delineate divergent clusters of interest of proteins with similar expression patterns. Right: Absolute dNDX for each treatment compared to control, using the same scale as left. Black square indicates the combination treatment group, with Onalespib positioned to the left and radiation with 2 Gy on the right-hand side.

SUPPLEMENTARY FIGURE 5
Uncropped Western blot membranes. Upper row: CDKN1A (p21) and corresponding loading control GAPDH. Lower row: γH2AX and corresponding loading control GAPDH. The dashed line shows the cropped image used in Supplementary Figure 3. The box with the solid line indicates a cut of the membrane (for separate incubation with the secondary antibody).

References

1. Hanif F, Muzaffar K, Perveen K, Malhi SM, Simjee Sh U. Glioblastoma Multiforme: A Review of its Epidemiology and Pathogenesis through Clinical Presentation and Treatment. *Asian Pac J Cancer Prev*. (2017) 18:3–9. doi: 10.22034/APJCP.2017.18.1.3

2. Singla AK, Madan R, Gupta K, Goyal S, Kumar N, Sahoo SK, et al. Clinical behavior and outcome in pediatric glioblastoma: current scenario. *Radiat Oncol J*. (2021) 39:72–7. doi: 10.3857/roj.2020.00591

3. Birbo B, Madu EE, Madu CO, Jain A, Lu Y. Role of HSP90 in cancer. *Int J Mol Sci*. (2021) 22. doi: 10.3390/ijms221910317

4. Bleeker FE, Molenaar RJ, Leenstra S. Recent advances in the molecular understanding of glioblastoma. *J Neuro Oncol*. (2012) 108:11–27. doi: 10.1007/s11060-011-0793-0

5. Schaff LR, Mellinghoff IK. Glioblastoma and other primary brain Malignancies in adults: A review. *Jama*. (2023) 329:574–87. doi: 10.1001/jama.2023.0023

6. Wyss J, Frank NA, Soleman J, Scheinemann K. Novel pharmacological treatment options in pediatric glioblastoma-A systematic review. *Cancers (Basel)*. (2022) 14. doi: 10.3390/cancers14112814

7. Teraiya M, Perreault H, Chen VC. An overview of glioblastoma multiforme and temozolomide resistance: can LC-MS-based proteomics reveal the fundamental mechanism of temozolomide resistance? *Front Oncol*. (2023) 13:1166207. doi: 10.3389/fonc.2023.1166207

8. Esteller M, Garcia-Foncillas J, Andion E, Goodman SN, Hidalgo OF, Vanaclocha V, et al. Inactivation of the DNA-repair gene MGMT and the clinical response of gliomas to alkylating agents. *N Engl J Med*. (2000) 343:1350–4. doi: 10.1056/NEJM200011093431901

9. Branch P, Aquilina G, Bignami M, Karran P. Defective mismatch binding and a mutator phenotype in cells tolerant to DNA damage. *Nature*. (1993) 362:652–4. doi: 10.1038/362652a0

10. Chen H, Gong Y, Ma Y, Thompson RC, Wang J, Cheng Z, et al. A brain-penetrating hsp90 inhibitor NXD30001 inhibits glioblastoma as a monotherapy or in combination with radiation. *Front Pharmacol*. (2020) 11:974. doi: 10.3389/fphar.2020.00974

11. Orth M, Albrecht V, Seidl K, Kinzel L, Unger K, Hess J, et al. Inhibition of HSP90 as a strategy to radiosensitize glioblastoma: targeting the DNA damage response and beyond. *Front Oncol*. (2021) 11:612354. doi: 10.3389/fonc.2021.612354

12. Spiegelberg D, Abramenkovs A, Mortensen ACL, Lundsten S, Nestor M, Stenerlöw B. The HSP90 inhibitor Onalespib exerts synergistic anti-cancer effects when combined with radiotherapy: an *in vitro* and *in vivo* approach. *Sci Rep*. (2020) 10:5923. doi: 10.1038/s41598-020-62293-4

13. Spiegelberg D, Dascalu A, Mortensen AC, Abramenkovs A, Kuku G, Nestor M, et al. The novel HSP90 inhibitor AT13387 potentiates radiation effects in squamous cell carcinoma and adenocarcinoma cells. *Oncotarget*. (2015) 6:35652–66. doi: 10.18632/oncotarget.v6i34

14. Lundsten S, Spiegelberg D, Raval NR, Nestor M. The radiosensitizer Onalespib increases complete remission in (177)Lu-DOTATATE-treated mice bearing neuroendocrine tumor xenografts. *Eur J Nucl Med Mol Imaging*. (2020) 47:980–90. doi: 10.1007/s00259-019-04673-1

15. Xu J, Wu PJ, Lai TH, Sharma P, Canella A, Welker AM, et al. Disruption of DNA repair and survival pathways through heat shock protein inhibition by onalespib to sensitize Malignant gliomas to chemoradiation therapy. *Clin Cancer Res*. (2022) 28:1979–90. doi: 10.1158/1078-0432.CCR-20-0468

16. Lundsten S, Spiegelberg D, Stenerlöw B, Nestor M. The HSP90 inhibitor onalespib potentiates 177Lu–DOTATATE therapy in neuroendocrine tumor cells. *Int J Oncol*. (2019) 55:1287–95. doi: 10.3892/ijo.2019.4888

17. Pratt WB, Morishima Y, Osawa Y. The Hsp90 chaperone machinery regulates signaling by modulating ligand binding clefts. *J Biol Chem*. (2008) 283:22885–9. doi: 10.1074/jbc.R800023200

18. Kamal A, Thao L, Sensintaffar J, Zhang L, Boehm MF, Fritz LC, et al. A high-affinity conformation of Hsp90 confers tumor selectivity on Hsp90 inhibitors. *Nature*. (2003) 425:407–10. doi: 10.1038/nature01913

19. Do K, Speranza G, Chang L-C, Polley EC, Bishop R, Zhu W, et al. Phase I study of the heat shock protein 90 (Hsp90) inhibitor onalespib (AT13387) administered on a daily for 2 consecutive days per week dosing schedule in patients with advanced solid tumors. *Invest New Drugs*. (2015) 33:921–30. doi: 10.1007/s10637-015-0255-1

20. Canella A, Welker AM, Yoo JY, Xu J, Abas FS, Kesanakurti D, et al. Efficacy of onalespib, a long-acting second-generation HSP90 inhibitor, as a single agent and in combination with temozolomide against Malignant gliomas. *Clin Cancer Res*. (2017) 23:6215–26. doi: 10.1158/1078-0432.CCR-16-3151

21. Williams NO, Quiroga D, Johnson C, Brufsky A, Chambers M, Bhattacharya S, et al. Phase Ib study of HSP90 inhibitor, onalespib (AT13387), in combination with paclitaxel in patients with advanced triple-negative breast cancer. *Ther Adv Med Oncol*. (2023) 15:17588359231217976. doi: 10.1177/17588359231217976

22. Xie Y, Bergström T, Jiang Y, Johansson P, Marinescu VD, Lindberg N, et al. The human glioblastoma cell culture resource: validated cell models representing all molecular subtypes. *EBioMedicine*. (2015) 2:1351–63. doi: 10.1016/j.ebiom.2015.08.026

23. Franken NA, Rodermond HM, Stap J, Haveman J, van Bree C. Clonogenic assay of cells *in vitro*. *Nat Protoc*. (2006) 1:2315–9. doi: 10.1038/nprot.2006.339

24. Friedrich J, Seidel C, Ebner R, Kunz-Schughart LA. Spheroid-based drug screen: considerations and practical approach. *Nat Protoc*. (2009) 4:309–24. doi: 10.1038/nprot.2008.226

25. Hu Y, Smyth GK. ELDA: extreme limiting dilution analysis for comparing depleted and enriched populations in stem cell and other assays. *J Immunol Methods*. (2009) 347:70–8. doi: 10.1016/j.jim.2009.06.008

26. Abramenkovs A, Hariri M, Spiegelberg D, Nilsson S, Stenerlöw B. Ra-223 induces clustered DNA damage and inhibits cell survival in several prostate cancer cell lines. *Transl Oncol*. (2022) 26:101543. doi: 10.1016/j.tranon.2022.101543

27. Mortensen ACL, Mohajershojai T, Hariri M, Pettersson M, Spiegelberg D. Overcoming limitations of cisplatin therapy by additional treatment with the HSP90 inhibitor onalespib. *Front Oncol*. (2020) 10:532285. doi: 10.3389/fonc.2020.532285

28. Wu T, Hu E, Xu S, Chen M, Guo P, Dai Z, et al. clusterProfiler 4.0: A universal enrichment tool for interpreting omics data. *Innovation (Camb)*. (2021) 2:100141. doi: 10.1016/j.xinn.2021.100141

29. Yu G, Wang LG, Han Y, He QY. clusterProfiler: an R package for comparing biological themes among gene clusters. *Omics*. (2012) 16:284–7. doi: 10.1089/omi.2011.0118

30. Milacic M, Beavers D, Conley P, Gong C, Gillespie M, Griss J, et al. The reactome pathway knowledgebase 2024. *Nucleic Acids Res*. (2024) 52:D672–d678. doi: 10.1093/nar/gkad1025

31. Kang X, Chen J, Hou J-F. HSP90 facilitates stemness and enhances glycolysis in glioma cells. *BMC Neurol*. (2022) 22:420. doi: 10.1186/s12883-022-02924-7

32. Liew HY, Tan XY, Chan HH, Khaw KY, Ong YS. Natural HSP90 inhibitors as a potential therapeutic intervention in treating cancers: A comprehensive review. *Pharmacol Res*. (2022) 181:106260. doi: 10.1016/j.phrs.2022.106260

33. Bayat Mokhtari R, Homayouni TS, Baluch N, Morgatskaya E, Kumar S, Das B, et al. Combination therapy in combating cancer. *Oncotarget*. (2017) 8:38022–43. doi: 10.18632/oncotarget.16723

34. Mortensen ACL, Berglund H, Hariri M, Papalanis E, Malmberg C, Spiegelberg D. Combination therapy of tyrosine kinase inhibitor sorafenib with the HSP90 inhibitor onalespib as a novel treatment regimen for thyroid cancer. *Sci Rep*. (2023) 13:16844. doi: 10.1038/s41598-023-43486-z

35. Modi S, Stopeck A, Linden H, Solit D, Chandarlapaty S, Rosen N, et al. HSP90 inhibition is effective in breast cancer: a phase II trial of tanespimycin (17-AAG) plus trastuzumab in patients with HER2-positive metastatic breast cancer progressing on trastuzumab. *Clin Cancer Res*. (2011) 17:5132–9. doi: 10.1158/1078-0432.CCR-11-0072

36. Mbofung RM, McKenzie JA, Malu S, Zhang M, Peng W, Liu C, et al. HSP90 inhibition enhances cancer immunotherapy by upregulating interferon response genes. *Nat Commun*. (2017) 8:451. doi: 10.1038/s41467-017-00449-z

37. Li ZN, Luo Y. HSP90 inhibitors and cancer: Prospects for use in targeted therapies (Review). *Oncol Rep*. (2023) 49:6. doi: 10.3892/or.2022.8443

38. Shapiro GI, Kwak E, Dezube BJ, Yule M, Ayrton J, Lyons J, et al. First-in-human phase I dose escalation study of a second-generation non-ansamycin HSP90 inhibitor, AT13387, in patients with advanced solid tumors. *Clin Cancer Res*. (2015) 21:87–97. doi: 10.1158/1078-0432.CCR-14-0979

39. Slovin S, Hussain S, Saad F, Garcia J, Picus J, Ferraldeschi R, et al. Pharmacodynamic and clinical results from a phase I/II study of the HSP90 inhibitor onalespib in combination with abiraterone acetate in prostate cancer. *Clin Cancer Res*. (2019) 25:4624–33. doi: 10.1158/1078-0432.CCR-18-3212

40. Tani T, Tojo N, Ohnishi K. Preferential radiosensitization to glioblastoma cancer stem cell-like cells by a Hsp90 inhibitor, N-vinylpyrrolidone-AUY922. *Oncol Lett*. (2022) 23:102. doi: 10.3892/ol.2022.13222

41. Zhu H, Woolfenden S, Bronson RT, Jaffer ZM, Barluenga S, Winssinger N, et al. The novel Hsp90 inhibitor NXD30001 induces tumor regression in a genetically engineered mouse model of glioblastoma multiforme. *Mol Cancer Ther*. (2010) 9:2618–26. doi: 10.1158/1535-7163.MCT-10-0248

42. Annamalai B, Liu X, Gopal U, Isaacs JS. Hsp90 is an essential regulator of EphA2 receptor stability and signaling: implications for cancer cell migration and metastasis. *Mol Cancer Res*. (2009) 7:1021–32. doi: 10.1158/1541-7786.MCR-08-0582

43. Gopal U, Bohonowych JE, Lema-Tome C, Liu A, Garrett-Mayer E, Wang B, et al. A novel extracellular Hsp90 mediated co-receptor function for LRP1 regulates EphA2 dependent glioblastoma cell invasion. *PloS One*. (2011) 6:e17649. doi: 10.1371/journal.pone.0017649

44. Manousakis E, Miralles CM, Esquerda MG, Wright RHG. CDKN1A/p21 in breast cancer: part of the problem, or part of the solution? *Int J Mol Sci*. (2023) 24:17488. doi: 10.3390/ijms242417488

45. Romanov VS, Pospelov VA, Pospelova TV. Cyclin-dependent kinase inhibitor p21(Waf1): contemporary view on its role in senescence and oncogenesis. *Biochem (Mosc)*. (2012) 77:575–84. doi: 10.1134/S000629791206003X

46. Engeland K. Cell cycle regulation: p53-p21-RB signaling. *Cell Death Differ*. (2022) 29:946–60. doi: 10.1038/s41418-022-00988-z

47. Jakob B, Scholz M, Taucher-Scholz G. Immediate localized CDKN1A (p21) radiation response after damage produced by heavy-ion tracks. *Radiat Res*. (2000) 154:398–405. doi: 10.1667/0033-7587(2000)154[0398:ILCPRR]2.0.CO;2

48. Montinaro A, Walczak H. Harnessing TRAIL-induced cell death for cancer therapy: a long walk with thrilling discoveries. *Cell Death Differ*. (2023) 30:237–49. doi: 10.1038/s41418-022-01059-z

49. Hu L, Wang Y, Chen Z, Fu L, Wang S, Zhang X, et al. Hsp90 inhibitor SNX-2112 enhances TRAIL-induced apoptosis of human cervical cancer cells via the ROS-mediated JNK-p53-autophagy-DR5 pathway. *Oxid Med Cell Longev*. (2019) 2019:9675450. doi: 10.1155/2019/9675450

50. Thang M, Mellows C, Mercer-Smith A, Nguyen P, Hingtgen S. Current approaches in enhancing TRAIL therapies in glioblastoma. *Neurooncol Adv*. (2023) 5:vdad047. doi: 10.1093/noajnl/vdad047

51. Li J, Chen Y, Fan Y, Wang H, Mu W, Liu X. Radiotherapy combined with anti-CEACAM1 immunotherapy to induce survival advantage in glioma. *Discovery Oncol*. (2023) 14:32. doi: 10.1007/s12672-023-00638-x

52. Allen M, Bjerke M, Edlund H, Nelander S, Westermark B. Origin of the U87MG glioma cell line: Good news and bad news. *Sci Transl Med*. (2016) 8:354re3. doi: 10.1126/scitranslmed.aaf6853

frontiers | Frontiers in Oncology

TYPE Case Report
PUBLISHED 20 March 2025
DOI 10.3389/fonc.2025.1477978

OPEN ACCESS

EDITED BY
Ramcharan Singh Angom,
Mayo Clinic Florida, United States

REVIEWED BY
Manabu Natsumeda,
Niigata University, Japan
Moatasem El-Ayadi,
Cairo University, Egypt

*CORRESPONDENCE
Merari Jasso
merarijjasso@hotmail.com

RECEIVED 08 August 2024
ACCEPTED 18 February 2025
PUBLISHED 20 March 2025

CITATION
Jasso M, Zhu JJ, Bhattacharjee MB and Hergenroeder GW (2025) Case Report: Rare intraventricular H3 K27-altered diffuse midline glioma in an adult. *Front. Oncol.* 15:1477978. doi: 10.3389/fonc.2025.1477978

Case Report: Rare intraventricular H3 K27-altered diffuse midline glioma in an adult

Merari Jasso[1]*, Jay-Jiguang Zhu[1], Meenakshi B. Bhattacharjee[2] and Georgene W. Hergenroeder[1]

[1]The Vivian L. Smith Department of Neurosurgery, McGovern Medical School at The University of Texas Health Science Center at Houston, Houston, TX, United States, [2]Department of Pathology & Laboratory Medicine, McGovern Medical School at The University of Texas Health Science Center at Houston, Houston, TX, United States

H3 K27-Altered Diffuse Midline Gliomas are commonly found in children and adolescents in midline locations such as the thalamus, brain stem, and spinal cord. It is rare for these tumors to affect adults and to occur in locations like the lateral ventricles. Despite aggressive treatment methodologies, there is no cure for this disease. The median survival is between 8-12 months. A 24-year-old white male presented to the emergency department due to severe headache refractory to pain medications with a 2-month history of progressive headaches and eventual memory problems. Computed tomography (CT) and magnetic resonance imaging (MRI) showed an intraventricular enhancing mass and hydrocephalus. The final diagnosis was an intraventricular H3 K27-Altered Diffuse Midline Glioma. The patient underwent two craniotomies, one laser interstitial thermal ablation (LITT), chemoradiotherapy, and bevacizumab and ONC206, through compassionate use. Despite a reduction in the tumor size, it continued to spread to other brain areas, leading to further complications and, eventually, his death, 10 months after initial diagnosis. From review of the literature, 21 cases were identified, and the median age was 24. Their median survival is 10.5 months (ranges 1 - 24 months). This case report presents the clinical, radiological, pathological, and molecular characteristics of a 24-year-old white man diagnosed with a ventricular H3 K27-Altered diffuse midline glioma, highlighting the rare presentation, management, and outcomes.

KEYWORDS

diffuse midline glioma (DMG), diffuse midline glioma H3 K27-altered, adult DMG, H3 K27, H3K27M mutation

Introduction

Diffuse midline gliomas (DMGs) characterized by the histone H3 K27M mutation are rare and aggressive high-grade tumors predominantly affecting children ages 5-10 years (1). The midline location defines this tumor type, diffuse growth pattern/infiltrating, and lysine-to-methionine substitution at position 27 on the H3 histone genes (2). This tumor type was first recognized in the 2016 World Health Organization (WHO) classification of central nervous system (CNS) tumors as DMG H3 K27M mutant. In 2021, WHO CNS tumor terminology

changed to DMG H3 K27-altered to include subtypes of DMG with alternative mechanisms for the loss of H3K27 methylation, such as EGFR mutant DMG or EZH inhibitory protein overexpression DMG. This classification is categorized as "pediatric-type diffuse midline glioma" and is subdivided into 4 subtypes (DMG H3 K27-altered; diffuse hemispheric glioma, H3 G34-mutant; diffuse pediatric-type high-grade glioma H3-wildtype and IDH-wildtype; and infant-type hemispheric glioma), each of which possess characteristic molecular profiles (3). DMGs commonly arise in the thalamus, brainstem, and spinal cord—regions critical for vital functions—making these tumors particularly challenging to treat. These tumors are typically diagnosed in children and are associated with a very poor prognosis. The 5-year survival rate for patients with DMGs is less than 1%, and the median overall survival ranges from eight to twelve months (4).

Ventricular tumors are also rare and represent 0.8-1.6% of intracranial tumors, but tend to be benign, such as central neurocytomas, choroid plexus papillomas or carcinomas, astrocytomas, meningiomas, ependymomas, colloid cysts, or craniopharyngiomas. This case report describes the clinical, radiological, pathological, and molecular characteristics of a 24-year-old white male diagnosed with a ventricular H3 K27-altered diffuse midline glioma, highlighting the challenges and complexities of management.

Case description

A 24-year-old white male firefighter with a history of asthma and attention deficit hyperactivity disorder (ADHD) presented with a 2-month history of nonspecific memory problems. He was described by family members as exhibiting forgetfulness of events and tasks. Developed progressive headaches that were alleviated by lying down and taking NASID medications with limited benefit. These headaches were subsequently accompanied by photophobia, phonophobia, nausea, and vomiting.

He presented to the emergency department due to a severe prolonged headache refractory to usual treatment, which led to a CT scan showing an intraventricular mass. A magnetic resonance image (MRI) of the brain with and without contrast revealed an irregular 6.4x7x4.5 cm (AP x Lat x CC) heterogeneous mass in the lateral ventricles appearing to be coming from the pineal region. This image did not identify involvement of midline structures like the thalamus. It occupied both lateral ventricles causing an 8 mm right midline shift (Figures 1A–D). The mass exhibited aggressive features, including restricted diffusion, necrosis, and heterogeneous contrast enhancement (Figures 1B, C) (5).

The following day, the patient underwent a left parietal craniotomy with a transparietal approach for mass resection and ventriculoperitoneal shunt (VPS) placement. The tumor location, firm and rubbery consistency, and similarity to adjacent brain tissue necessitated an initial partial resection. A postoperative MRI four days later showed expected surgical changes with a mass reduction to approximately 4.4x7x3.7 cm (AP x Lat x CC). Five days after the initial surgery, he underwent a second craniotomy with an interhemispheric approach focusing on the right lateral ventricle for further mass resection. MRI performed one day after the second surgery showed expected surgical changes and residual left intraventricular tumor of approximately 1.8x1.8x0.7cm with post-surgical periventricular enhancement of the thalamus.

The pathology report diagnosed a DMG H3 K27-Altered CNS WHO grade 4 with positive immunohistochemistry for H3K27M mutant nuclear expression, loss of H3K27me3 nuclear expression, (Figures 2A–C), weak to moderate nuclear expression of p53, strong expression of EGFR, and a Ki67 labeling index of 30-40%. The tumor was negative for IDH1 mutant protein expression and loss of ATRX expression. The Next Generation Sequencing (NGS) showed gene H3F3A K28M mutation, PTEN G132V – subclonal, RAD51B loss on exon 8, TSC2 E1344del, ATRX splice site 6849 + 2T>C.

Following discharge, the patient continued to experience memory difficulties and newly developed right side homonymous hemianopsia. On day 30, he began chemoradiotherapy, receiving fractionated external beam radiotherapy (54-60 Gy in 30 fractions) with concurrent temozolomide at 75 mg/m2 x 42 days. Throughout therapy, he experienced ongoing attention and memory difficulties, further visual field reduction at his right side, and seizures due to missed doses of anti-seizure medication. He completed chemoradiotherapy on Day 69.

On day 105, MRI evaluation revealed new enhancement within the splenium, left thalamus, and 3rd ventricle with dimensions of 2.6x3.2x2.2 cm, raising questions about regrowth versus radiation changes (Figures 1E–H). The treatment approach included laser interstitial thermal ablation (LITT) through the parietal lobes with intraoperative fluoroscopy for precise targeting and ventriculoperitoneal shunt (VPS) placement. The patient was subsequently treated under a compassionate use regimen with ONC206, a more potent analogue of ONC201, a selective dopamine receptor D2 (DRD2) antagonist and mitochondrial protease ClpP agonist, at 120mg once per week, oral, for approximately 3 months.

On Day 189, his VPS malfunctioned due to blockage causing gait instability and right hemiparesis, requiring the placement of new bilateral ventriculoperitoneal shunts. He began bevacizumab therapy at a dose of 10 mg/kg IV, (without 600mg) IV, every 14 days as a salvage therapy, experiencing side effects, such as nausea, vomiting, and asthenia. The last MRI, Day 199 showed a progression in FLAIR signal in basal ganglia and parietal lobes, most likely due to tumor infiltration, radiation changes with edema or likely a mixture all three components (Figures 1I–L).

On Day 314, the patient's condition deteriorated, leading to hospitalization. Despite intensive treatment efforts, he ultimately succumbed to his illness on the same day (Figure 3).

Discussion

Diffuse Midline Gliomas (DMGs) with the H3K27M mutation predominantly affect midline structures, such as the thalamus, brainstem, and spinal cord in children and adolescents. In adults, these tumors more commonly involve the diencephalic region, particularly the thalamus, with a mean age of onset around 42 years (1). This case report highlights the aggressive nature and complex management of an H3 K27-altered DMG in an adult with an unusual ventricular location, presenting significant clinical challenges.

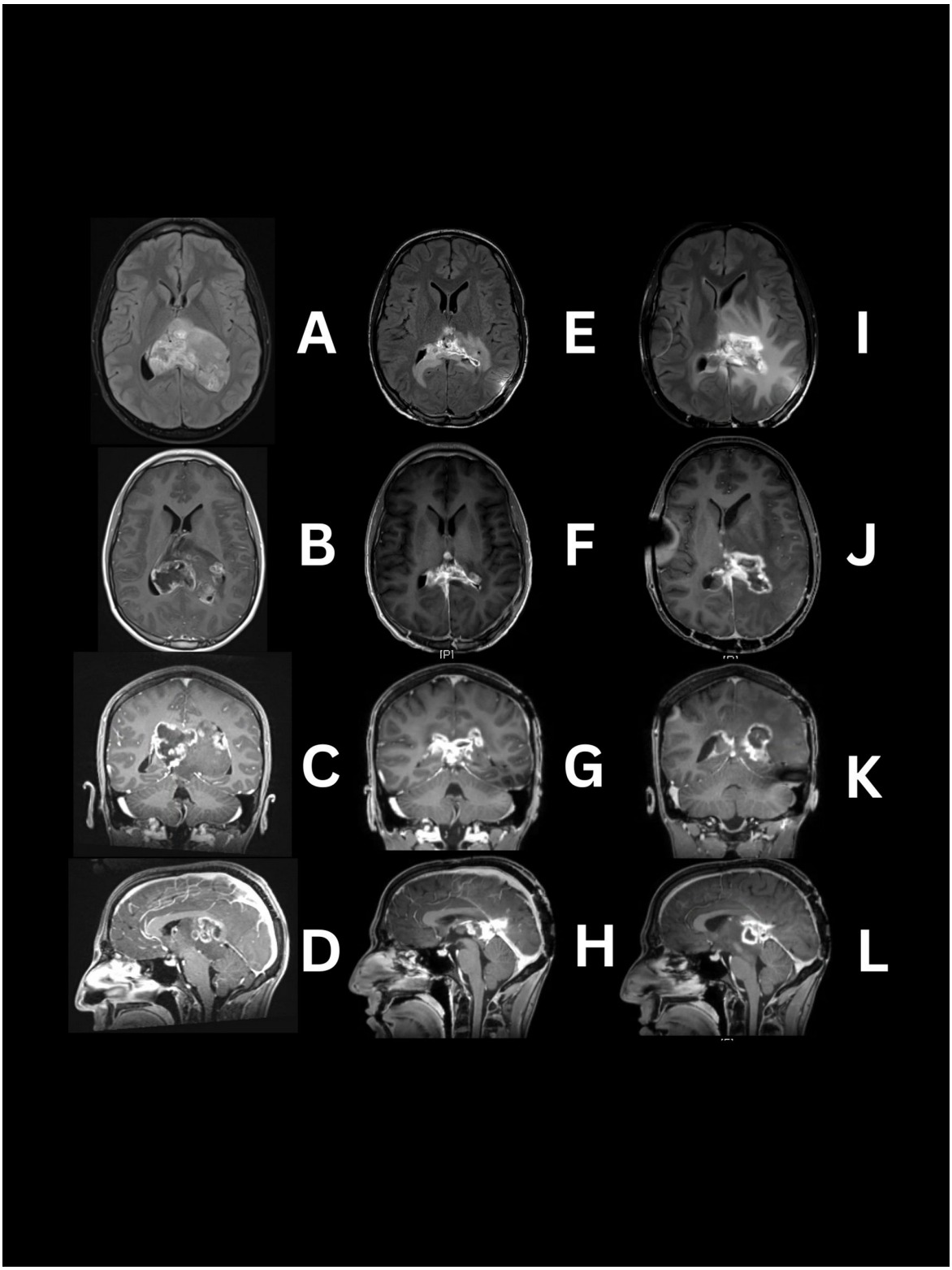

FIGURE 1
MRI images demonstrating serial progression of H3 K27-altered diffuse midline glioma. Preoperative **(A–D)** tumor located in lateral ventricles predominantly solid with patchy areas showing high intensity and central necrosis on the right side on T2/FLAIR and T1W post contrast. Day 104 post operation and chemoradiotherapy **(E–H)** reduced intraventricular tumor with periventricular FLAIR signal abnormality and contrast enhancement extending to the surrounding structures in T1W post-contrast images. Day 199 post-final treatment, **(I–L)** Progression of FLAIR signal (which is most likely a mixture of tumor infiltration with edema and radiation change) extending to basal ganglia and parietal lobes, with enhancement and necrosis of the intraventricular tumor and adjacent structures.

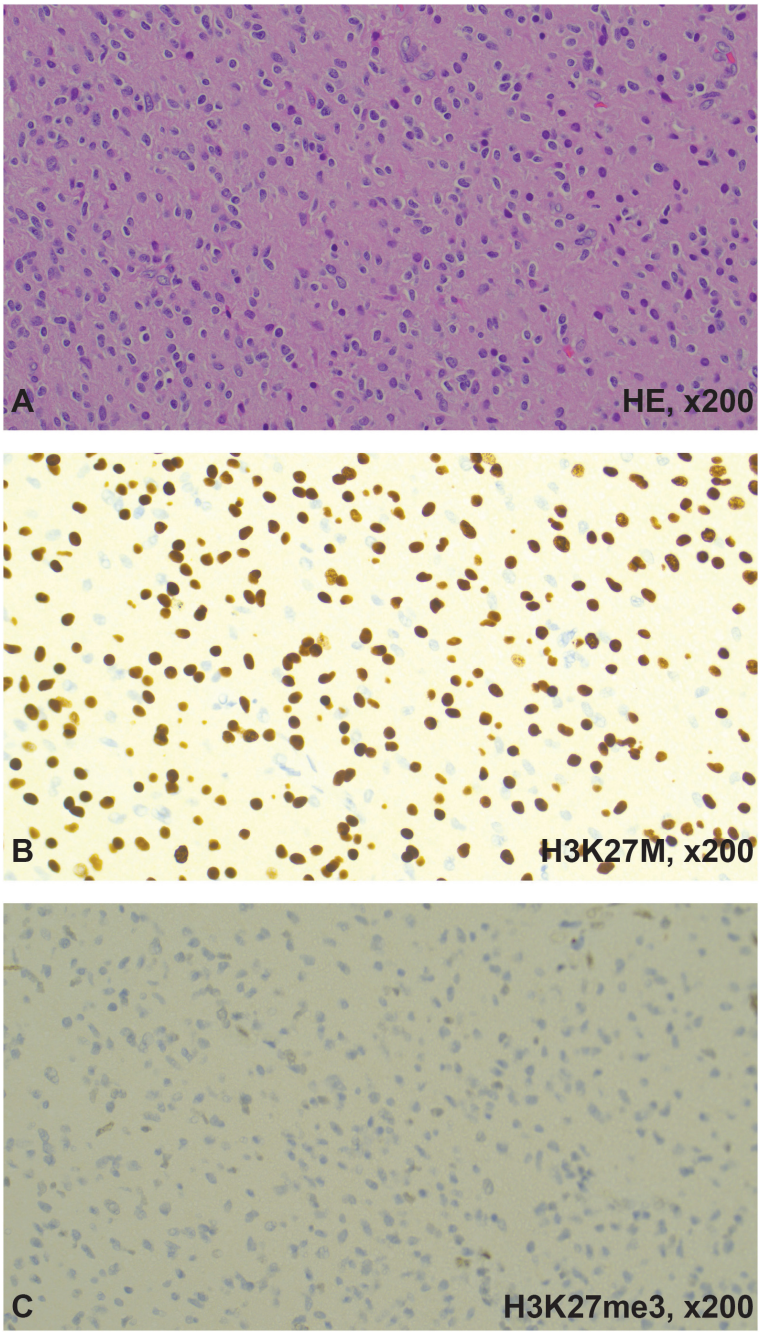

FIGURE 2
H&E and immunohistochemistry results. **(A)** Hematoxylin and Eosin (H&E) staining showed monomorphic to pleomorphic glial cells with high mitotic activity. **(B)** H3 K27M showed positive nuclear staining. **(C)** H3K27me3 showed loss of nuclear stain. The final diagnosis was DMG, H3 K27-altered, CNS WHO grade-4. Images were captured with the Leica Thunder imaging system (Danaher, Washington, DC).

Intraventricular tumors are rare and represent 0.8-1.6% of intracranial tumors. Intraventricular tumors are benign and are more common in childhood than adulthood. Some examples of these tumors are neoplasm of choroid plexus, ventricular wall and septum pellucid, and secondary malignant intraventricular tumors like glioblastoma multiforme. The most common clinical presentation is secondary to high ventricular pressure.

Table 1 presents a comparative analysis of 22 reported DMG cases with ventricular involvement. Most of these cases involve patients of Asian descent, suggesting a possible racial predisposition for ventricular involvement. The median age was 24, with a median survival of 10.5 months (1-24 months).

Clinical presentation varies depending on the anatomical area affected. In this case, the intraventricular mass caused headaches, attention, and memory problems for at least two months. These nonspecific symptoms, likely indicative of increased intracranial pressure, may have delayed diagnosis. However, given the aggressive nature of these tumors and the lack of highly effective

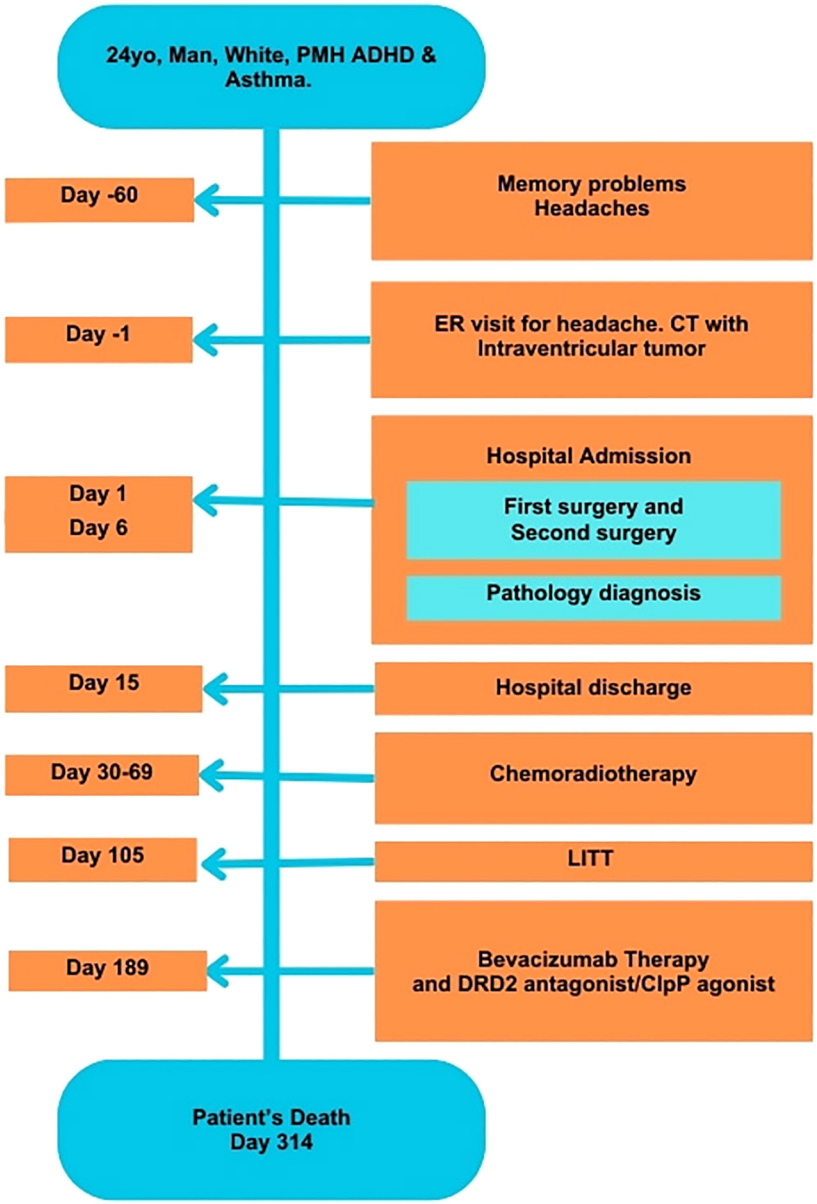

FIGURE 3
Timeline of development of symptoms and tumor treatments. ADHD, Attention Deficit Hyperactivity Disorder; ER, Emergency Room; CT, Computed tomography; LITT, Laser Interstitial Thermal ablation; PMH, Past Medical History.

treatments, it is unclear if an earlier diagnosis would have significantly altered the outcome.

The patient underwent two intraventricular surgeries, one-time LITT, fractionated external beam radiation (30 fractions) in combination with daily temozolomide, 3 sessions of monoclonal antibody therapy with bevacizumab at 10mg/kg every 14 days, and ONC206 drug through compassionate use. These therapies were based on the ASCO-SNO guidelines for diffuse astrocytic and oligodendroglial tumors in adults, encouraging radiotherapy and enrollment in clinical trials with this alteration (10).

The H3K27M mutation in DMG tumors is currently the primary negative prognostic factor in both adults and children. However, differentiation based on other genetic alterations could provide valuable targets for therapy, prognostication, and risk assessment. DMG tumors with H3K27M mutations in the midline region can also exhibit alterations, such as IDH negativity, ATRX loss, CDK2A deletion, TP53 overexpression, EGFR expression, and MGMT promoter methylation (11, 12).

In this case, the tumor exhibited the classic H3K27M protein expression alongside ATRX loss, moderate TP53 expression, EGFR overexpression by IHC, and H3F3A K28M mutation along with PTEN G132V – subclonal, RAD51B loss on exon 8, TSC2 E1344del, ATRX splice site 6849 + 2T>C by next generation sequencing (Foundation Medicine, Cambridge, MA). Immunohistochemical markers

TABLE 1 Comparison between Intraventricular DMG H3 K27-Altered cases.

Summary of Published Cases with Intraventricular DMG, H3 K27-Altered							
Reference	Age (years)	Sex	Race	Immunophenotype	No. of DMG H3 K27-Altered	Ventricle	Median survival (months)
Wang et al., 2018 (6).	Mean ± SD: 40.63 ± 21.82	Not Described	Asian	Not Described	3	Lateral	12.8
Luo et al., 2020 (7).	38	Male	Asian	GFAP, Olig2, Ki67 (+2%)	1	Lateral	24
Zhao et al., 2022 (8).	14	Female	Asian	GFAP, Olig2, S100	1	Lateral	1
Zheng et al., 2022 (9)	Median 24, Range 3 - 71	ND	Asian	Not Described	16	Not Described	10.5
Presenting case	24	Male	White	EGFR, P53, Ki67 (+30-40%), BRAF (V600E) negative	1	Lateral	10.5

EGFR, Epidermal growth factor receptor; GFAP, Glial fibrillary acidic protein; Ki67, Ki67 protein; Olig2, Oligodendrocyte transcription factor; S100, S100 protein; SD, Standard Deviation.

commonly observed in intraventricular DMG tumor case reports, were GFAP, Olig2, Ki67, and S100, were also expressed (Table 1).

Despite aggressive treatment, the primary ventricular tumor reduced in size by nearly 70%, yet continued to proliferate into adjacent areas like the thalamus and splenium. This progression might be linked to the tumor's immunophenotype, characterized by EGFR overexpression, loss of H3 K27 trimethylation, a high Ki67 proliferation index (30-40%), and weak P53 expression (13).

EGFR overexpression and loss of H3 K27 trimethylation are associated with increased migratory potential and greater propensity for thalamic invasion. Furthermore, TP53 loss, a common alteration in DMGs, is known to promote tumor self-renewal, induce epigenetic dysregulation, and confer resistance to radiotherapy (12, 13).

The molecular profile of this tumor likely played a critical role in its development, migration, and response or lack of response to treatment. Interestingly, the immunophenotype in this case differed from previously reported intraventricular DMG cases, aligning more closely with diffuse midline gliomas originating in the thalamus. This unique molecular profile may have facilitated the tumor's expansion from the ventricles into adjacent structures, including the thalamus, splenium, and third ventricle, contributing to its aggressive progression and resistance to conventional therapies.

Conclusion

The classification of DMG H3 K27-altered tumors was first designated in 2016 and was updated in 2021 to incorporate alternative mechanisms of H3K27 methylation loss. As such, documenting and analyzing atypical cases is vital to improving our understanding of this complex disease. These tumors are more frequently seen in children and primarily affect deep midline structures. Intracranial intraventricular tumors are rare, comprising less than 1.6% of all tumors, and typically have favorable outcomes when treated. However, this case presents a difficult-to-treat tumor with an unusual growth pattern from the ventricle to diencephalic structures.

Cases like the one presented here offer an opportunity to explore whether delayed diagnoses in adults are due to different growth rates, whether the tumor phenotype varies across age groups, or if molecular markers can predict tumor progression or indicate epigenetic alterations. Current treatment protocols are not specifically designed to target this mutation, leading to highly variable prognoses. Unfortunately, no single factor has yet been definitively identified as having a significant impact on outcomes, highlighting the ongoing need for research and the development of more effective, mutation based targeted therapies.

Data availability statement

The original contributions presented in the study are included in the article. Further inquiries can be directed to the corresponding author.

Ethics statement

The studies involving humans were approved by the Committee for the Protection of Human Subjects (CPHS). The studies were conducted in accordance with the local legislation and institutional requirements. However, the consent states that the patient will not be personally identified in any reports or publications that may result from this study. The content of this case report does not identify the patient. The patient is no longer alive to obtain consent for this specific publication.

Author contributions

MJ: Conceptualization, Data curation, Formal analysis, Investigation, Methodology, Writing – original draft, Writing – review & editing. JZ: Formal analysis, Investigation, Supervision, Validation, Writing – review & editing. MBB: Writing – review & editing, Data curation, Methodology, Supervision, Formal analysis, Validation, Investigation, Resources, Visualization. GH: Conceptualization, Formal analysis, Methodology, Resources, Supervision, Validation, Writing – original draft, Writing – review & editing.

Funding

The author(s) declare that no financial support was received for the research, authorship, and/or publication of this article.

Conflict of interest

The authors declare that the research was conducted in the absence of any commercial or financial relationships that could be construed as a potential conflict of interest.

Publisher's note

References

1. Bin-Alamer O, Ae J, Td A, Bettegowda C, Mukherjee D. H3K27-altered diffuse midline gliomas among adult patients: A systematic review of clinical features and survival analysis. *World Neurosurg.* (2022) 165:e251–64. doi: 10.1016/j.wneu.2022.06.020

2. Wang L, Li Z, Zhang M, Piao Y, Chen L, Liang H, et al. H3 K27M–mutant diffuse midline gliomas in different anatomical locations. *Hum Pathol.* (2018) 78:89–96. doi: 10.1016/j.humpath.2018.04.015

3. Louis D, Perry A, Wesseling P. The 2021 WHO classification of tumors of the central nervous system: a summary. *Neuro-Oncol.* (2021) 23:1231–51. doi: 10.1093/neuonc/noab106

4. van den Bent M, Saratsis AM, Geurts M, Franceschi E. H3 K27M-altered glioma and diffuse intrinsic pontine glioma: semi-systematic review of treatment landscape and future directions. *Neuro-oncol.* (2023) 26(Supplement_2):S110–S124. doi: 10.1093/neuonc/noad220

5. Daoud EV, Rajaram V, Cai C, Oberle R, Matin G, Raisanen J, et al. Adult brainstem gliomas with H3K27M mutation: radiology, pathology and prognosis. *J Neuropathol Exp Neurol.* (2018) 77:302–11. doi: 10.1093/jnen/nly006

6. Wang Y, Feng L, Ji P, Liu J, Guo S, Zhai Y, et al. Clinical features and molecular markers on diffuse midline gliomas with H3K27M mutations: A 43 cases retrospective cohort study. *Front Oncol.* (2021) 10:602553. doi: 10.3389/fonc.2020.602553

7. Luo Y, Zeng L, Xie XQ, Wang F, Li YZ, Wu DB, et al. H3K27M mutant diffuse midline glioma: a case report. *Eur Rev Med Pharmacol Sci.* (2020) 24:2579–84. doi: 10.26355/eurrev_202003_20527

8. Zhao B, Sun K, Zhang Z, Xu T, Zhao L, Liu C, et al. A rare presentation of primary lateral ventricle H3 K27-altered diffuse midline glioma in a 14-year-old girl: a case description. *Quantitative Imaging Med Surg.* (2022) 12:5288–95. doi: 10.21037/qims-22-339

9. Zheng L, Gong J, Yu T, Zou Y, Zhang M, Nie L, et al. Diffuse midline gliomas with histone H3 K27M mutation in adults and children: A retrospective series of 164 cases. *Am J Surg Pathol.* (2022) 46:863–71. doi: 10.1097/PAS.0000000000001897

10. Mohile NA, Messersmith H, Gatson NT, Hottinger A, Lassman A, Morton J, et al. Therapy for diffuse astrocytic and oligodendroglial tumors in adults: ASCO-SNO guideline. *J Clin Oncol.* (2022) 40:403–26. doi: 10.1200/JCO.21.02036

11. Schulte J, Buerki R, Lapointe S, Molinaro A, Zhang Y, Villanueva-Meyer J, et al. Clinical, radiologic and genetic characteristics of histone H3 K27M-mutant diffuse midline gliomas in adults. *Neuro-Oncol Adv.* (2020) 2:1–10. doi: 10.1093/noajnl/vdaa142

12. Gong X, Kuang S, Deng D, Wu J, Zhang L, Liu C. Differences in survival prognosticators between children and adults with H3K27M-mutant diffuse midline glioma. *CNS Neurosci Ther.* (2023) 29:3863–75. doi: 10.1111/cns.14307

13. Vallero S, Bertero L, Morana G, Sciortino P, Bertin D, Mussano A, et al. Pediatric diffuse midline glioma H3K27- altered: A complex clinical and biological landscape behind a neatly defined tumor type. *Front Oncol.* (2023) 12:1082062. doi: 10.3389/fonc.2022.1082062

Frontiers in Oncology

Advances knowledge of carcinogenesis and tumor progression for better treatment and management

The third most-cited oncology journal, which highlights research in carcinogenesis and tumor progression, bridging the gap between basic research and applications to imrpove diagnosis, therapeutics and management strategies.

Discover the latest Research Topics

See more →

Frontiers

Avenue du Tribunal-Fédéral 34
1005 Lausanne, Switzerland
frontiersin.org

Contact us

+41 (0)21 510 17 00
frontiersin.org/about/contact